GROUNDWATER - SURFACE WATER INTERACTIONS IN THE MABOU HARBOUR DRAINAGE BASIN AND POTENTIAL FOR HARBOUR CONTAMINATION

by

Raymond D. Craddock

Submitted in partial fulfilment of the requirements for the
degree of Master of Applied Science

at

Dalhousie University
Halifax, Nova Scotia
January 2021

© Copyright by Raymond D. Craddock, 2021

Table of Contents

LIST OF TABLES

APPENDIX

LIST OF FIGURES

APPENDIX

ABSTRACT

Groundwater-borne contamination to coastal waters is a growing risk in the Canadian Maritimes region. Groundwater contaminants can enter the marine environment directly as submarine groundwater discharge, or indirectly as groundwater-derived baseflow discharged through surface watercourses. In this study, the spatial patterns of groundwater-surface water interactions and the effects of direct and indirect groundwater discharge on nitrate and bacterial contamination of a natural harbour were assessed on a regional scale. The Mabou Harbour drainage basin in Cape Breton Island, Nova Scotia has a high density of agricultural land and a history of persistent microbial contamination. Shoreline and flood-plain piezometers were installed and continuously monitored to analyze temporal patterns in groundwater-surface water interactions (GSIs). Hydrograph analysis and evaluation of thermal regimes were used to assess the GSIs between the major rivers. Seepage meters were deployed at different locations to constrain direct submarine groundwater discharge fluxes. A 3D groundwater flow model was constructed using MODFLOW-NWT and calibrated to historic static well water levels in addition to the baseflow of major rivers in the drainage basin.

Model results, complemented by field data, yield important insights into the regional-scale groundwater flow and transport to surface waterbodies. Results suggest that direct groundwater discharge only accounts for 3% the of total catchment discharge, and residence times are substantially longer than survival times for most faecal coliform bacteria; therefore, it is not expected to be a significant contributor to the bacterial contamination frequently observed in the harbour. Conversely, the relatively deep flow paths associated with submarine groundwater discharge bypass the natural denitrification zones correlated with shallow flow through riparian zones and thus may pose nitrate contamination risks.

Model results indicate that indirect groundwater discharge represents the largest proportion of total groundwater discharge (~96%) and given the flushing rate of the harbour, contributes to a larger proportion of the total harbour water volume (~5%). Furthermore, the higher hydraulic gradients found in the fluvial valleys, in addition to the permeable alluvial aquifers, substantially reduce residence times to within the survival limits of certain microorganisms, such that groundwater-borne bacterial contamination via indirect groundwater discharge is plausible. Many of the fluvial valleys within the drainage basin present a deeply incised geomorphology where groundwater flow paths are deeper and bypass the denitrification processes associated with shallow flow through riparian zones. Additionally, the Mabou and NE Mabou rivers displayed direct-recharge river-aquifer system characteristics with little bank storage to assist in nitrate buffering.

Because natural harbours are commonplace for rural agricultural communities in coastal regions, these results may be applicable to similar environments and may be used to improve land-use planning (e.g., distribution of agricultural activities) in coastal watersheds. Given the research gap regarding submarine groundwater discharge in low-permeability environments, the findings of this case study can be used to better understand other Canadian coastlines that are dominated by glacial-till.

LIST OF ABBREVIATIONS AND SYMBOLS

A	Area
a	Tidal signal amplitude
β	Filter parameter
BFI	Baseflow index
CC	Correlation coefficient
CMZ	Coastal mixing zone
D	Diffusivity
DIN	Dissolved inorganic nitrate
ECCC	Environment and Climate Change Canada
ET	Evapotranspiration
f	Freshwater fraction
FFT	Fast Fourier transform analysis
h	Hydraulic head
H_o	Tidal signal amplitude
HSL	Hydrostratigraphic layer
HSU	Hydrostratigraphic unit
NSERC	Natural Sciences and Engineering Research Council
FSGD	Fresh submarine groundwater discharge
GIS	Geographical information system
GSI	Groundwater – surface water interaction
K	Hydraulic conductivity
K_R	Hydraulic conductivity of riverbed sediments
K_x	Hydraulic conductivity in the x-direction
K_y	Hydraulic conductivity in the y-direction
K_z	Hydraulic conductivity in the z-direction
l	Screen length
m	Meters
M	Bed thickness
masl	Meters above sea level
mbsl	Meters below sea level
MAR	Mean absolute residual
MR	Mean residual
NRMSE	Normalized root mean squared error
NSWLD	Nova Scotia Well Logs Database
p	Period
P	Precipitation
PET	Potential evapotranspiration
Q	Discharge
Q_A	Artificial abstractions
Q_F	Freshwater discharge
Q_G	Groundwater discharge
Q_Q	Quickflow
Q_R	Surface Runoff
Q_S	Tidal flushing

R^2	Coefficient of determination
r_s	Well-screen radius
r_w	Standpipe radius
RMSE	Root mean squared error
S	Storativity
S_H	Harbour salinity
S_O	Sea salinity
S_S	Specific storage
SGD	Submarine groundwater discharge
t	Time
T	Transmissivity
TDS	Total dissolved solids
T_o	Basic time lag
T_R	Harbour flushing rate
V	Volume
W	Volumetric flux of per unit volume of sources/sinks
z	Surface elevation

ACKNOWLEDGMENTS

First and foremost, I would like to thank my supervisor, Dr. Barret Kurylyk, for his guidance and support throughout my thesis. I am proud to be one of his first graduate students and will look back on this time fondly. I would also like to thank my supervisory committee, Dr. Rob Jamieson (Dalhousie University) and Gavin Kennedy (Department of Energy and Mines) who provided me with invaluable insight throughout my thesis. Dr. Jamieson's lab led the bacteria testing and microbial source tracking, which provided context and purpose to my groundwater research. Gavin Kennedy sourced secondary datasets from provincial records that were integral in model development. I would also like to thank Jonathan Keizer (Stantec Consulting Ltd.) and Dr. Aaron Mohammed (Dalhousie University) for their contributions to the numerical modeling exercises within this thesis. I am grateful to the members of the Dalhousie Coastal Hydrology Lab that have assisted with field activities in Mabou Harbour, and I wish that I were able to repay them fully throughout their future field campaigns.

I am thankful for Environment and Climate Change Canada (ECCC) for their funding of this research through the Atlantic Ecosystem Initiative program. I am also grateful to Natural Sciences and Engineering Research Council (NSERC) for supporting me with the Canada Graduate Scholarship. I would like to thank Lindy and Graham Pottinger, Nova Scotia Provincial Parks, and Inverness County for generously permitting the installation of equipment and allowing field research to be conducted on their property.

I would also like to thank my family, particularly Leah, for their love and support throughout my graduate studies. You have been invaluable at times when I needed perspective and motivation. I would also like to thank my brother, Sawyer, for his programming solution that was essential to the calibration phase of my numerical modelling.

Chapter 1: Introduction

1.1 Groundwater – Surface Water Interactions: Pathways for Groundwater – Borne Contaminants in Coastal Watersheds

Population density is approximately three times greater in coastal regions than in inland environments (Small & Nicholls, 2003), which creates a concentration of anthropogenic contamination in coastal watersheds. This is becoming increasingly evident in coastal waters (Windom et al., 1992; Chase et al., 2001), including in the Canadian Maritimes (Schafer, 1973; Menon, 1988; Siah et al., 2003;). Interactions between contaminated aquifers and surface waters are recognized to be important drivers of water quality and the health of marine ecosystems (Brunke and Gonser, 1997; Hayashi and Rosenberry, 2002; Conant et al., 2019). Groundwater contamination often occurs within shallow aquifers, which interacts with surface water bodies and thus have the potential to persistently transport significant contaminant loads to surface water (Winter et al., 1998).

Within a coastal watershed, groundwater-borne contaminants from polluted coastal aquifers are transported to the marine environment directly as submarine groundwater discharge (SGD; Burnett and Dulaiova, 2003), or indirectly as groundwater-derived baseflow discharged through surface watercourses that flow to the coast (Figure 1). Historically, coastal contamination was thought to only occur from surface contaminant loading via coastal rivers; however, in recent years a new paradigm is emerging in which coastal contamination is also acknowledged to be a subsurface phenomenon through SGD pathways (Sawyer et al., 2016; Michael et al., 2017). More investigation is required to

better understand SGD's role in coastal contamination, especially in Canada where there is a noted gap in research (Bobba et al., 2011).

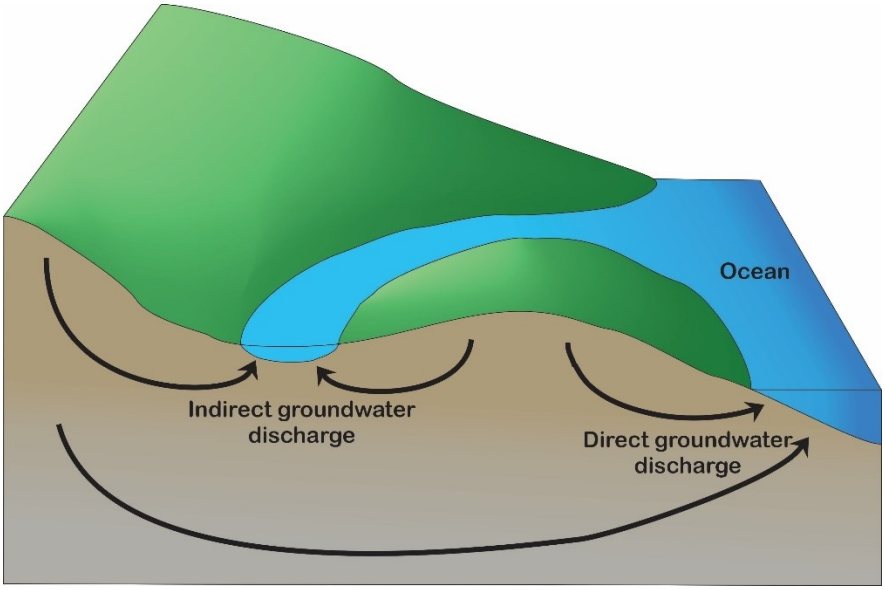

Figure 1: A conceptual model of how groundwater discharge within a coastal watershed is partitioned into direct and indirect groundwater discharge. Shallower flow paths (local flow regime) tend to discharge into the nearest downgradient discharge zone (e.g., streams, ocean), whereas deeper flow paths (i.e., regional flow) may bypass several recharge and discharge zones before discharging into a major discharge zone (e.g., major rivers, the ocean).

Common anthropogenic contaminant types found in groundwater include organics, synthetic organic chemicals, pharmaceuticals, heavy metals, excess nutrients, and carbon (Sawyer et al., 2016; Robinson et al., 2018), but there is evidence that biological contaminants in the coastal setting, particularly faecal bacteria, are also related to coastal groundwater discharge (Paul et al., 1997; Desmarais et al., 2002; Boehm et al., 2004). This thesis is focused on groundwater-surface water interactions in a coastal watershed and the effects they may have on nitrogen and bacterial fate and transport.

1.1.1 Ocean – Aquifer Interactions: Submarine Groundwater Discharge

SGD is defined as, "the flow of water through continental and insular margins from the seabed to the coastal ocean, regardless of fluid composition or driving force" (Burnett et al., 2003). Fluid composition is specifically addressed in this definition because there are both fresh and saline (circulated seawater) constituents in SGD. SGD is a global phenomenon and should occur in any place where the aquifer and sea are hydraulically connected (Burnett et al., 2003b) and where the hydraulic head in the adjacent aquifer or sediment is at least intermittently above sea level (Johannes, 1980). SGD has been observed since the Roman era (Kohout, 1966), but has only recently been investigated scientifically (Burnett and Dulaiova, 2003). Historically, geoscientists and oceanographers focused research efforts on the discharge of surface water into the ocean. When coastal water interactions with groundwater was considered, the focus was saltwater intrusion (Taniguchi et al., 2002). SGD was ignored because of the intrinsic investigation difficulty and the general lack of knowledge regarding its scientific importance (Taniguchi et al., 2019). However, SGD is gaining attention as it is now known to be a significant factor in the hydrological cycle, coastal biogeochemistry, and health of marine ecosystems (Taniguchi et al., 2002; Moore, 1999; Sawyer et al., 2016; Robinson et al., 2018).

There is some disagreement among scientists regarding the definition of SGD, which may lead to confusion when interpreting research. For instance, oceanographers consider any water seeping from the land into the ocean to be SGD, regardless of meteoric or oceanic origin. Conversely, hydrologists and hydrogeologists separate SGD into fresh and saline constituents. For example, the saline portion of this discharge is often referred

to as circulated sea water (e.g., Moore, 1999). Other researchers dispute the term circulated seawater as it may obscure the important changes to water chemistry that occur in the porous media (Taniguchi, 2019). Some researchers have suggested a nomenclature so that SGD fluxes can be compared between different studies (Taniguchi et al., 2002). Herein, the total SGD, containing both fresh and saline constituents, will be referred to as SGD, the freshwater component will be referred to as FSGD, and the saline component will be referred to as circulated SGD.

In general, SGD is driven by hydraulic, density, or thermal gradients (Kohout, 1967; Li, 1999; Taniguchi, 2002; Santos et al., 2012; Sawyer et al., 2016). Hydraulic gradients between the coastal aquifers and sea level are the driving force for FSGD. Alternatively, tidal pumping, and convection cycles (e.g., thermal and density driven) force the circulation of seawater through the subsurface. Tidal pumping refers to the infiltration of seawater associated with the localized oscillation of the hydraulic gradient during tidal cycles. The result of this tidal forcing across the beach face is the development of an upper saline plume (Figure 2 and Robinson et al., 2006). Research suggests that the primary constituent of SGD is circulated seawater indicating that these processes are significant drivers of SGD (Moore and Church, 1996; Li et al., 1999; Garrison et al., 2003). Tidal pumping can drive circulated SGD fluxes that are an order of magnitude higher than FSGD (Li et al., 1999), and in some situations it is the main factor controlling the SGD rate (Taniguchi, 2002). The residence time of circulated seawater due to tidal pumping ranges from days to several weeks (Michael et al., 2005; Robinson et al., 2007; Abarca et al., 2013; Heiss et al., 2014). Alternatively, the residence time of FSGD varies but can be many orders

of magnitude higher, depending on the flow path length and depth below the phreatic surface (Bratton et al., 2004; Tait et al., 2014).

Distance from the shore is the main control on SGD in addition to hydraulics and the flow domain geometry (Taniguchi et al., 2002). The magnitude of SGD is related to water depth, such that SGD appears to follow a decreasing power-law relationship with ocean depth (Taniguchi et al., 2002). As depth is related to distance from shore, the greatest SGD fluxes generally occur near the shore where seawater is shallower (Taniguchi et al., 2002). The majority of FSGD occurs within tens of meters (m) of the shoreline (Sawyer et al., 2016) and decreases exponentially with distance from the shoreline (Bokuniewicz, 1992). Under certain conditions, SGD may occur far offshore. For instance, volcanic or karstic bedrock channels may behave as conduits that can transfer fresh groundwater far offshore via submarine springs (Johnson et al., 2008). Additionally, confined aquifer conditions may result in SGD occurring kilometers offshore where the aquifer outcrops (Paldor et al., 2019).

FSGD rates depend on the coastal aquifer hydraulic conductivity (K) [m d^{-1}] and recharge patterns in the watershed (Sawyer et al., 2016). Recharge rates vary on storm, seasonal, and geological time scales, which will affect the hydraulic gradient that in turn drives the SGD flux. For example, there have been observable increases in the freshwater flux following hurricane seasons (Menning et al., 2015). On a longer timescale, SGD rates are strongly correlated with multi-year climate oscillations, such as El Niño, due to their impact on precipitation (Anderson and Emanuel, 2008). The FSGD flux varies greatly, often influenced by geology. For example, Darcy fluxes for fractured bedrock springs can

exceed meters per day (Bokuniewicz et al., 2008), but in diffuse discharge zones with lower hydraulic conductivity, Darcy fluxes may be orders of magnitude lower (Deming et al., 1992; Piekarek-Jankowska, 1996). SGD is also generally diffuse and heterogeneous with spatial patterns ranging in scale from meters to kilometers (Sawyer et al., 2016). On local scales, discharge may be focused into submarine springs by conduits, such as karsts, lava tubes, bedrock fractures, and buried paleochannels (Mulligan et al., 2007; Bokuniewicz et al., 2008; Johnson et al., 2008).

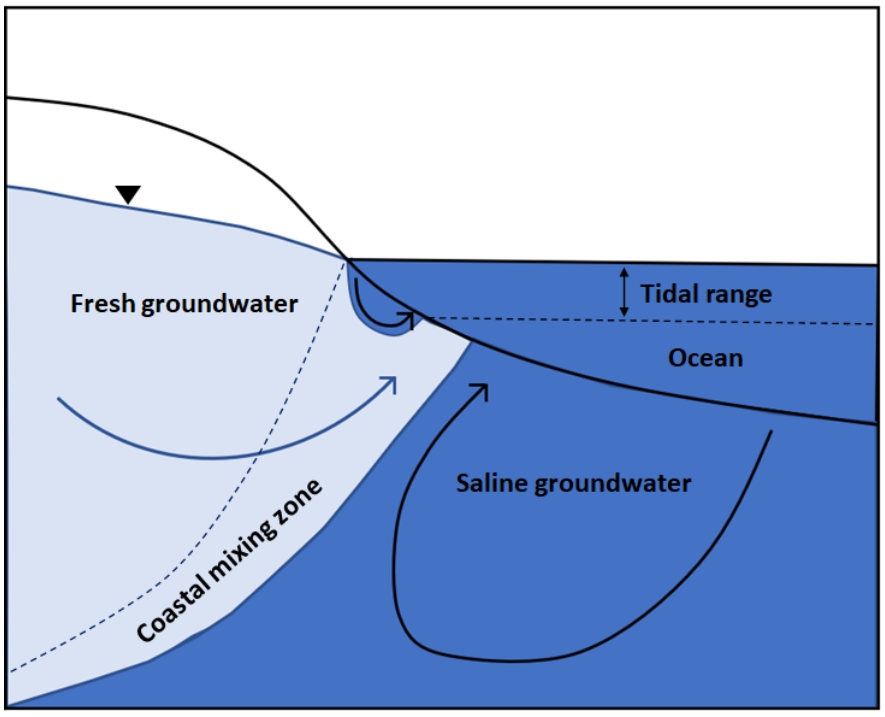

Figure 2: A conceptual model for FSGD, circulated SGD, and formation of the upper saline plume (modified from Robinson et al., 2018). The upper saline plume is represented by the smaller, semi-circular cycling of saline groundwater through the coastal mixing zone.

1.1.1.1 Importance to Ecology

SGD, both fresh and saline, plays an important role in coastal ecosystems and chemistry (Moore, 1999). Like riverine water, SGD transports solutes to the oceans, affecting biogeochemical processes and conditions (Moore, 2010). Once discharged into the ocean, solutes may be released to the atmosphere, deposit on the ocean floor, or be taken up by living organisms (Sawyer et al., 2016). As groundwater is transported from the continent to the ocean, it dissolves solids, and interacts with microorganisms, which alters the chemical composition (Sawyer et al., 2016). The chemistry of the groundwater at the discharge zone is a product of microbial interactions, geochemistry of the subsurface, and residence time (Sawyer et al., 2016). Groundwater is often enriched in nutrients relative to surface water, so SGD may have a dramatic effect on water quality and ecosystem health. For example, SGD-related nutrient fluxes have been shown to affect the production and health of marine fauna and flora (Fujita et al., 2019).

1.1.1.2 The Coastal Mixing Zone

The coastal mixing zone (CMZ), sometimes referred to as the subterranean estuary (Moore, 1999), describes a coastal aquifer where fresh and saline water and their different constituents mix. The CMZ is essentially the transition zone at the interface between meteoric groundwater and intruding seawater. Similar to fluvial estuaries, CMZs host the interactions between saline water, freshwater, and aquifer materials, which impose important modifications to fluid composition (Moore, 1999). CMZs are different then surficial mixing zones (i.e., estuaries) in that they have a much higher solid-fluid ratio, stable temperatures, and are enriched in reduced species such as NH_4^+ (Taniguchi et al.,

2019). Because the fresh and saline endmembers are so distinct, the CMZ is often marked by strong salinity, redox, and pH gradients that drive chemical reactions (Moore, 1999; Charette and Sholkovitz, 2002). These chemical reactions have been shown to affect contaminant loads, such as nitrate, prior to discharge into the marine environment (Slomp and Van Cappellen, 2004; Santos et al., 2008). Seasonal variations in the biogeochemical conditions of the CMZ can lead to variability in the transfer of nutrients and organic carbon to the marine environment (Santos et al., 2009). For example, Santos et al. (2009) found that SGD nutrient and dissolved organic carbon (DOC) fluxes into the Gulf of Mexico were respectively 60% and 40% higher in the summer relative to winter.

1.1.1.3 Importance to the Hydrologic Cycle

Regarding the seaward component of the hydrologic cycle, hydrologists have traditionally fixated on surface water discharge into the ocean; however, SGD is now gaining recognition as an important process (Burnett and Dulaiova, 2003). Even with a small flux per unit length of shoreline, SGD can be significant considering the shear immensity of total coastline and the fact that SGD is active in areas where large rivers are not present (Taniguchi et al., 2002). Researchers have used different methods to estimate the role of SGD in the global water flux, such as hydrograph separation (Zekster and Loaiciga, 1993), basic calculations with hydrogeological assumptions (Nace, 1970; Taniguchi et al., 2002), water balance (Zekster et al., 1973), and literature review (Church, 1996; Taniguchi et al., 2002). The resulting estimates are generally 6-10% of total surface water input into the ocean (Taniguchi et al., 2002). On a local/regional scale, water balance estimates are much more variable. For instance, while using Radium-226 mass balance, Moore (1996) estimated that SGD accounted for 40% of the freshwater flux to the South

Atlantic Bight during the study period. Furthermore, SGD may be more influential on the hydrologic cycle in an island setting, as it has been shown that the net discharge is generally greater per unit area of land for islands than for continents (Zekster and Everett, 2000; Moosdorf et al., 2015).

SGD estimates vary widely due to the spatially heterogeneous and temporally dynamic nature of SGD processes. Taniguchi et al. (2002) compiled available SGD data on an international scale in an attempt to quantify global SGD and found that global SGD rates are generally less then 0.1 m d^{-1}. Conversely, it is not uncommon to see that reported SGD rates from a coastal watershed exceed the local recharge rate, sometimes by more than two orders of magnitude (Taniguchi et al., 2002). There are two possible explanations for this discrepancy: 1) the areal extent of recharge zones is about two orders of magnitude greater than that for discharge zones; and 2) circulated saline groundwater discharge forms a significant component of the measured SGD (Taniguchi et al., 2002).

1.1.2 Stream – Aquifer Interactions

Surface water and groundwater systems are often perceived as disconnected entities and therefore studied separately (Kalbus et al., 2006); however, groundwater-surface water interactions (GSIs) between aquifers and surface water bodies can greatly influence the mass budget and quality of both subsurface and surface water (Sophocleous, 2002; Kalbus, 2006; Fleckenstein et al., 2010). For instance, the transition zone beneath the streams that host exchange processes is referred to as the hyporheic zone and has been recognized for its importance for flora, fauna, and stream metabolism (Hynes, 1983; Brunke and Gonser, 1997).

The history of GSI research is relatively recent, beginning in the 1960s (Fleckenstein et al., 2010). Seminal research by Tóth (1962; 1963; 1970) introduced links between topography, geology, and climate to form hydrogeologic environments and the different flow regimes (local, intermediate, and regional), which ultimately terminate at discharge zones. Tóth (1963) describes these flow systems as: the local flow regime which flows towards nearby discharge areas (Figure 1); the regional flow regime which flows great distances to major surface water bodies (Figure 1); and the intermediate flow regime which resides between local and regional flow systems and often bypasses several recharge and discharge areas. These flow regimes drive the spatial patterns of GSIs (Fleckenstein, 2010). Early work focused on the volumes of groundwater from a resource management perspective and have since shifted to near-channel and in-channel, process-oriented investigations addressing the influence groundwater exchange has on biogeochemistry and ecology (Sophocleous, 2002; Krause et al., 2009; Fleckenstein et al., 2010).

GSIs occur under four general conceptual models: 1) gaining streams where the aquifer has a higher hydraulic head than the stream stage driving groundwater discharge into the stream; 2) losing streams where the stream stage exceeds groundwater head causing surface water to recharge the aquifer; 3) flow-through channels where the aquifer hydraulic head is higher on one side of the stream and lower on the other resulting in groundwater discharge and recharge, respectively; and 4) disconnected streams where the aquifer and stream are separated by an unsaturated zone and the ephemeral streamflow infiltrates downwards toward the aquifer at a relatively constant rate (Sophocleous, 2002; Woessner, 2000). It is not uncommon for streams to have both gaining and losing sections

throughout the reach of a stream (Kalbus et al., 2006). Seasonal variations or precipitation events can alter the hydraulic head conditions within the aquifer and the stage within the stream thereby affecting the direction of fluid exchange (Kalbus et al., 2006). The flow and exchange of groundwater is controlled by the spatial distribution of *K* in the alluvial aquifer and channel, the stream stage relative to the hydraulic heads within the aquifer (Winter et al., 1998; Wroblicky et al., 1998), and the stream geomorphology (Woessner, 2000). The direction of flow and magnitude of the flux are governed by the hydraulic gradient and sediment *K*, respectively.

The exchanges between groundwater and streams vary with climatic conditions as described by (Brunke and Gonser, 1997). When precipitation is low, effluent conditions dominate, such that baseflow is the primary constituent of stream discharge. Conversely, during periods of heavy precipitation, resulting in high quickflow, the hydraulic gradient reverses and influent conditions dominate such that streamflow infiltrates banks and recharges the aquifer. The amount of this bank storage is controlled by the watershed characteristics, in addition to the transmissivity (*T*) [$m^2\ d^{-1}$] and storativity (*S*) [unitless] of the banks (Brunke and Gonser, 1997). The alternating periods of effluent and influent conditions help moderate the discharge variations of a river (Brunke and Gonser, 1997).

1.1.2.1 Importance to Ecology

The hyporheic zone is particularly important to stream and downstream ecology and is characterized by strong biogeochemical activity (Grimm and Fisher, 1984; Duff and Triska, 1990; Triska et al., 1993). Water exchange within the hyporheic zone facilitates solute transport, degradation, transformation, precipitation, sorption (Kalbus et al., 2006)

and material transformations (Sophocleous, 2002). The exchange between surface water and groundwater increases interaction between water and chemically reactive geologic materials, which can strongly influence water chemistry (Sophocleous, 2002). For example, rivers with less hyporheic exchange may not have a long enough residence time for significant nutrient mineralization to occur (Findlay, 1995). Hyporheic exchange increases residence times and dramatically influences the material transported from the catchment to the sea (Findlay, 1995). Similar to the denitrification that occurs in riparian zones, hyporheic exchange, including bank storage, buffers nitrate loads in stream systems (Duff and Triska, 1990; Triska et al., 1993).

1.1.2.2 Importance to Hydrological Cycle

Groundwater discharge into streams and other terrestrial surface water bodies acts as indirect groundwater discharge to the marine environment and is important to the hydrological cycle. On a global scale, baseflow accounts for approximately 10% and 30% of precipitation and total runoff, respectively, and displays great geographical variability (Zekster and Loaiciga, 1993). These estimates suggest that baseflow, or indirect groundwater discharge to the coast, constitutes approximately 83% of total groundwater discharge entering the marine environment. Other studies have shown the ratio between indirect and direct groundwater discharge to be lower for coastal watersheds (i.e., indirect groundwater is less dominant; e.g., Russoniello et al., 2016). Furthermore, the distribution of groundwater discharge between baseflow and SGD pathways has been shown to be sensitive to water table depth, such that baseflow pathways are dominant when high water tables are present (Russoniello et al., 2016).

1.1.3 Groundwater – Borne Nitrate in Coastal Watersheds

Nutrients, such as nitrate, can accumulate to high levels in groundwater and persist for decades (Nolan et al., 1988). Anthropogenic nitrate, which is a constituent of dissolved inorganic nitrogen (DIN) is generally sourced from fertilizer and sewage (Valiela et al., 1997), both of which excessively elevate DIN in coastal aquifers (Sawyer et al., 2016). Although it is difficult to quantify SGD and associated nutrient fluxes, it has been shown locally and regionally that SGD-related nutrient fluxes often rival or exceed river input to the ocean (Johannes, 1980; Johannes & Hearn, 1985; Oberdorfer et al., 1990; Valiela et al., 1990; Moore et al., 2002; Garrison et al., 2003; Slomp and Van Cappellen, 2004; Moore et al., 2008; Santos et al, 2008). Groundwater is also generally more concentrated in DIN relative to surface water, so the chemical flux ratio between SGD and fluvial input is disproportionate to the corresponding discharge rates (Moore, 1999). For example, FSGD accounts for half of the fluvial input in Tampa Bay, yet contributes equally to the nutrient load (Kroeger et al., 2007). Furthermore, SGD-related nutrient fluxes have important implications for the health of marine ecosystems and have been identified as a possible and substantial driver of eutrophication (LaRoche et al., 1997; Hu et al., 2006; Lee et al., 2010).

Nutrient contamination via coastal groundwater discharge, particularly SGD, is a legacy pollution issue due to the long residence time in coastal aquifers (Robinson et al., 2018). For instance, in Chesapeake Bay and Florida, it has been shown that nutrient contaminated groundwater in the coastal aquifer has multi-decadal residence time before being discharged to the sea (Hu et al., 2006; Sanford and Pope, 2013). Although fluvial nutrient fluxes into the marine environment are increasing (Diaz and Rosenberg, 2008), the

future implications for SGD-related DIN is still unknown, and it may take decades for the changes to present themselves.

There are natural nitrate buffers found in coastal watersheds that can influence nutrient loading to coastal water bodies. For instance, it has been well established that riparian zones are important buffers for nutrients originating from adjacent terrestrial anthropogenic activities (Haycock and Pinay, 1993; Gold et al., 2001; Burt et al., 2002; Rassam et al., 2008). Topography, hydraulic properties, and groundwater flow dynamics are important factors in the denitrification process. Maximum nitrate removal is associated with shallow groundwater flow (Simmons et al., 1992; Starr and Gillham, 1993; Nelson et al., 1995; Gold et al., 1998) through soils rich in organic carbon and roots (Gold et al., 2001). Additionally, a moderate *K* will support substantial flow while maintaining adequate residence time for denitrification to occur (Rassam et al., 2008). Areas where these conditions are met generally coincide with flat lowlands, such as alluvial plains (Rassam et al., 2006). Regarding nitrate buffers associated with SGD pathways, under certain redox conditions, the CMZ may also attenuate high nutrient levels in fresh groundwater prior to discharge. The nitrogen flux through the CMZ is greatly dependent on the residence time in the mixing zone and the redox conditions of the two water endmembers (Slomp and Van Cappellen, 2004).

The methods for determining groundwater-borne nitrate loads are different depending on the pathway for groundwater discharge (i.e., SGD or baseflow). There is more uncertainty associated with the quantification of SGD-associated nutrient fluxes as SGD is inherently difficult to quantify and the influence of the CMZ on nutrients is not

always constrained. Currently, the standard method of quantifying nutrient fluxes via SGD is to multiply the FSGD flux by the nutrient concentrations in the groundwater (Robinson et al., 2018). The issue with this method is that it neglects the influence that the CMZ has on nitrate loads. Conversely, the quantification of nutrient fluxes via groundwater-derived baseflow would be relatively easy, as watercourses can be sampled during baseflow conditions.

1.1.4 Groundwater – Borne Faecal Microbial Contaminants in Coastal Watersheds

Faecal microbes, including coliform bacteria, are another common contaminant within aquifers and are largely associated with sewage treatment and agriculture (Sinton et al., 1997; Goss et al., 1998; Jamieson et al., 2002). Bacteria survival in the subsurface is dependant on numerous variables including soil moisture, soil type, temperature, pH, manure application methods, nutrient availability, and microorganism competition (Jamieson et al., 2002). The survival of faecal coliform bacteria, including *Escherichia coli* (*E. coli)*, in the saturated zone is generally less than 55 days (McFeters et al., 1974; Keswick et al., 1982; Bitton et al., 1983; Pekdeger & Matthess, 1983; Dowd & Pillai, 1997; Taylor et al., 2004); however, some pathogenic bacteria such as *Enterococcus*, *Streptococcus*, and *Klebsiella pneumoniae* can persist for more than 200 days (McFeters et al., 1974; Keswick et al., 1982; Bitton et al., 1983; Dowd & Pillai, 1997). Other studies have shown that *E. Coli*, *Salmonella enterica* serovar Typhimurium, and other pathogenic bacteria survived up to 100 days or greater under saturated conditions at 10°C (Filip et al., 1988). Regardless of the relatively brief fate of faecal coliform bacteria in the phreatic zone, bacterial contamination of aquifers in agricultural watersheds is prevalent (Goss et

al., 1998). It should be noted that faecal coliform bacteria are not always good indicators for groundwater transport of other faecal pathogens, particularly viruses, that have the greatest transport potential due to their smaller size and greater persistence in the saturated zone (Yates et al., 1985; Bitton and Harvey, 1992). Microbial transport, particularly bacteria, is primarily controlled by macropores and secondary porosity where attenuating processes, such as adsorption and mechanical filtration, are bypassed (Smith et al., 1985; Jamieson et al., 2002; Beven and Germann, 2013) and where porewater velocities and solute advection may be very high.

Several studies have been conducted on microbial contamination of coastal environments associated with groundwater discharge, particularly SGD. A link between groundwater discharge and faecal indicator bacteria was established in Huntington Beach, CA, with the highest microbial loads detected during spring tides (Boehm et al., 2004). Similarly, the correlation between periods of high SGD and faecal indicator bacteria, sourced by sewage, have been observed (Yau et al., 2014). Faecal bacteria from waste injection wells to the marine environment has also been observed but required groundwater systems with high advective rates and very short residence times (Paul et al., 1996). Paul et al. (1996) also concluded that microbial transport was most rapid in areas where tidal pumping was influential.

1.2 SITE DESCRIPTION

Mabou Harbour, in Inverness County of Cape Breton Island, Nova Scotia, Canada was selected as the study site for this thesis (Figure 3). Mabou Harbour is representative of the many natural harbours throughout the Maritime region of Canada in that the surrounding landscape is overlain by glacial deposits, predominantly composed of till. Natural harbours are commonplace for rural agricultural communities in coastal regions, which is evident in the Mabou Harbour drainage basin. The Cape Breton Partnership & The Inverness/Victoria Federation of Agriculture (CBP and IVFA, n.d.) identified 58 agricultural operations within the drainage basin covering a range of commodities, with 36 of them specified as beef or dairy farms. Thirteen of these cattle-bearing farms are located immediately adjacent to the harbour, according to the harbour boundary defined in this thesis. The remainder are spread throughout the drainage basin and are often adjacent to major rivers or their tributaries. The harbour also hosts an aquaculture industry with nine oyster leases and one lease for seeding stock (CBP and IVFA, n.d.). Unfortunately, the harbour has a history of persistent faecal bacterial contamination resulting in frequent closures to aquaculture operations.

Mabou Harbour is located on the west coast of Cape Breton Island with the mouth of the harbour positioned at approximately 46°5'15"N and 61°28'24"W (Figure 3a). The harbour is approximately 6.7 km^2 in area including the tidal flats. Based on a spline-interpolation of bathymetric data, provided by the Applied Geomatics Research Group (AGRG, 2017), the harbour volume is approximately 2.84×10^7 m^3. The total drainage basin area is 363.1 km^2 (excluding the harbour) and is further broken down into three sub-

catchments for the Southwest Mabou, Northeast Mabou, and Mabou Rivers (herein referred to as the Mabou rivers), in addition to the harbour subcatchment containing the smaller tributaries that discharge directly into the harbour (Figure 3b; Table 1). For the purpose of this thesis, the boundary between the major rivers and the harbour was defined as the point where braided streams or significant pooling began over the tidally influenced mudflats. The sub-catchment delineations were derived from Nova Scotia Department of Environment (2018) and work completed for the CBP and IFVA (n.d.) by the Department of Natural Resources. The subcatchments were re-delineated from the locations of river mouths (as defined in this thesis) using the Enhanced Digital Elevation Model, Nova Scotia, Canada (herein referred to as DEM; Service Nova Scotia and Municipal Relations [SNSMR], 2003), which was converted into a topographic map. The harbour subcatchment, followed by the Mabou and NE Mabou River subcatchments, has the greatest agricultural density; however, the Mabou River subcatchment has the greatest agricultural coverage (Table 1 and Environment and Agriculture Technology Research Group of the Nova Scotia Community College [EAT], 2018).

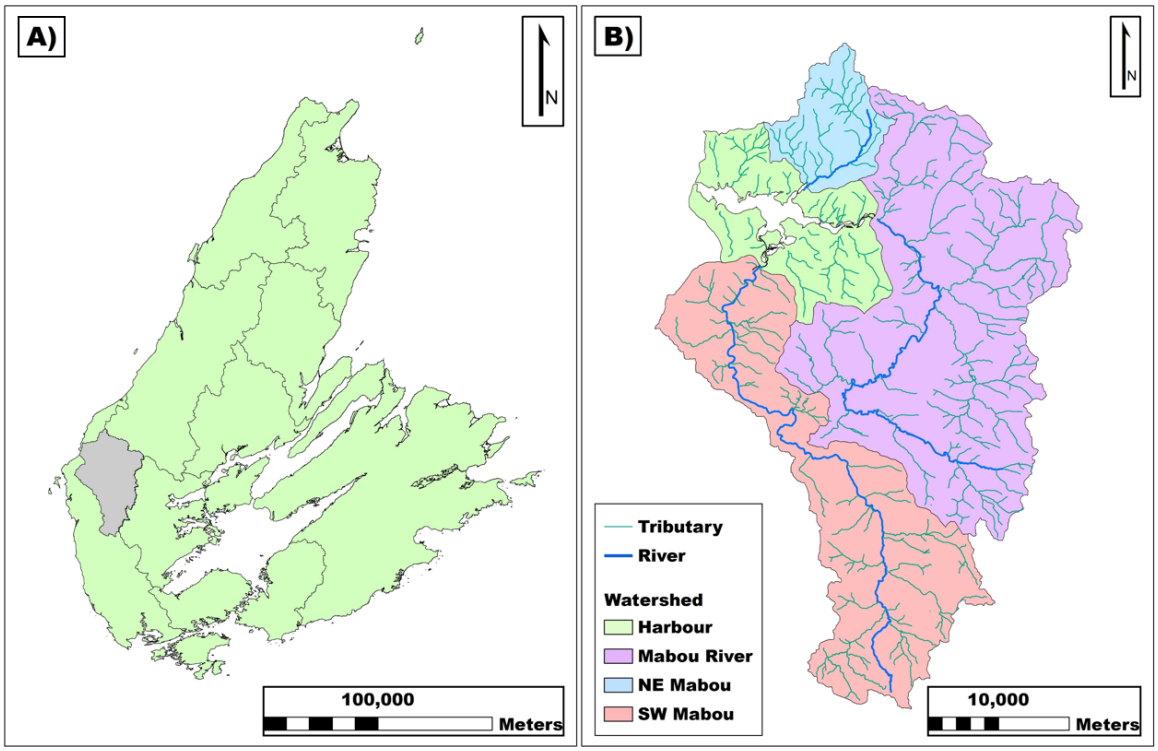

Figure 3: A) Map of Cape Breton Island primary watersheds and location of the Mabou Harbour drainage basin (grey); B) delineation of the Mabou Harbour drainage basin and included subcatchments. Catchment delineations were derived from Nova Scotia Department of Environment (2018) and a shapefile created by the Department of Natural Resources for CBP and IVFA (n.d.). Watercourses were adapted from Department of Lands and Forestry (2020) as described in Section 3.2.2.6.3.

Table 1: Drainage basin and subcatchment drainage areas, agricultural land coverage, and contribution to total agriculture in the Mabou Harbour drainage basin (EAT, 2018). Watershed boundaries derived from Nova Scotia Department of Environment (2018) and work completed for the CBP and IFVA (n.d.) by the Department of Natural Resources.

Catchment	Drainage area [km^2]	Agr. land [km^2]	[%]	Agr. contribution [% of total]
Harbour	46.4	9.5	20.5	30.8
Mabou River	175.0	14.6	8.3	47.4
NE Mabou River	25.5	2	7.8	6.5
SW Mabou River	116.2	4.7	4.0	15.3
Total	363.1	30.8	8.5	100

Mabou Harbour experiences a temperate/humid continental climate (Kottek et al., 2006; Amani et al., 2019) with a high annual precipitation. The closest and most representative climate stations with relatively complete precipitation data for 2019 are Port Hawkesbury (Environment and Climate Change Canada [ECCC] climate ID: 8204495) and Cheticamp Highlands National Park (ECCC climate ID: 8200828). Following corrections for missing data, the estimated 2019 annual precipitations are 1450 and 1587 mm, respectively. For the purpose of this study, the precipitation data will be averaged between the two climate stations as Mabou Harbour lies between them, resulting in an estimated 2019 annual precipitation of 1518 mm.

Mabou Harbour has a diverse and complex geology due to its location within an orogenic belt and a variety of depositional environments associated with a history of plate convergence, divergence, and glaciation (Baechler et al., 2019 and Figure 4). Furthermore, the drainage basin lies within the Hallow Fault System, which manifests as a complex system of low angle thrust and high angle strike-slip faults (Baechler, 2015). Barr et al. (2017) was used to analyze the bedrock geology of the Mabou Harbour drainage basin. Pre-Cambrian metamorphic basement rock is uplifted forming the Mabou Highlands in the north of the site, along with Silurian volcanics of variable compositions (Barr et al., 2017). The vast majority of the drainage basin is composed of Carboniferous siliciclastics, carbonates, and evaporites (Barr et al., 2017). Important lithostratigraphic units found within the drainage basin are displayed in Figure 4 and described in Table 2. Carbonates are often present as the primary lithology, or as intercalations, providing ample opportunity for karstification to occur. Karst landforms have been observed within the domain, with the majority of the area categorized as high or medium risk of encountering karst flow

systems and landforms (Drage and McKinnon, 2019). Baechler & Boehner (2014) estimated that approximately 23% of Cape Breton Island is comprised of some variation of glaciated meta-carbonates, carbonates, and evaporite lithostratigraphic units, which could potentially develop karst flow systems. Coal deposits are likely present in the domain with a former coal mine located immediately to the northwest. The drainage basin is characterized by high relief with elevations ranging from 335 m above sea level (masl) in the northern highlands to a bathymetric depth of 23 m below sea level (mbsl) in the deepest portion of the harbour (SNSMR, 2003; AGRG, 2017).

The overburden material in the Mabou Harbour drainage basin is heterogenous in both composition and thickness (Figure 5). Thickness varies from tens of meters in the lowlands to thin veneers overlaying outcropping bedrock. The majority of the study area is composed of low-permeability materials such as silty or stony glacial till, or mud-rich organic deposits (Cann et al., 1963; Stea et al., 2006). The overburden of the highlands and fluvial valleys are generally characterized by coarser, more permeable materials such as colluvium, residuum, and alluvium (Stea et al., 2006). Coarse-grained glaciofluvial and marine deposits are also present in the watershed, with the marine deposits represented by the sandy West Mabou Beach at the mouth of the harbour (Stea et al., 2006).

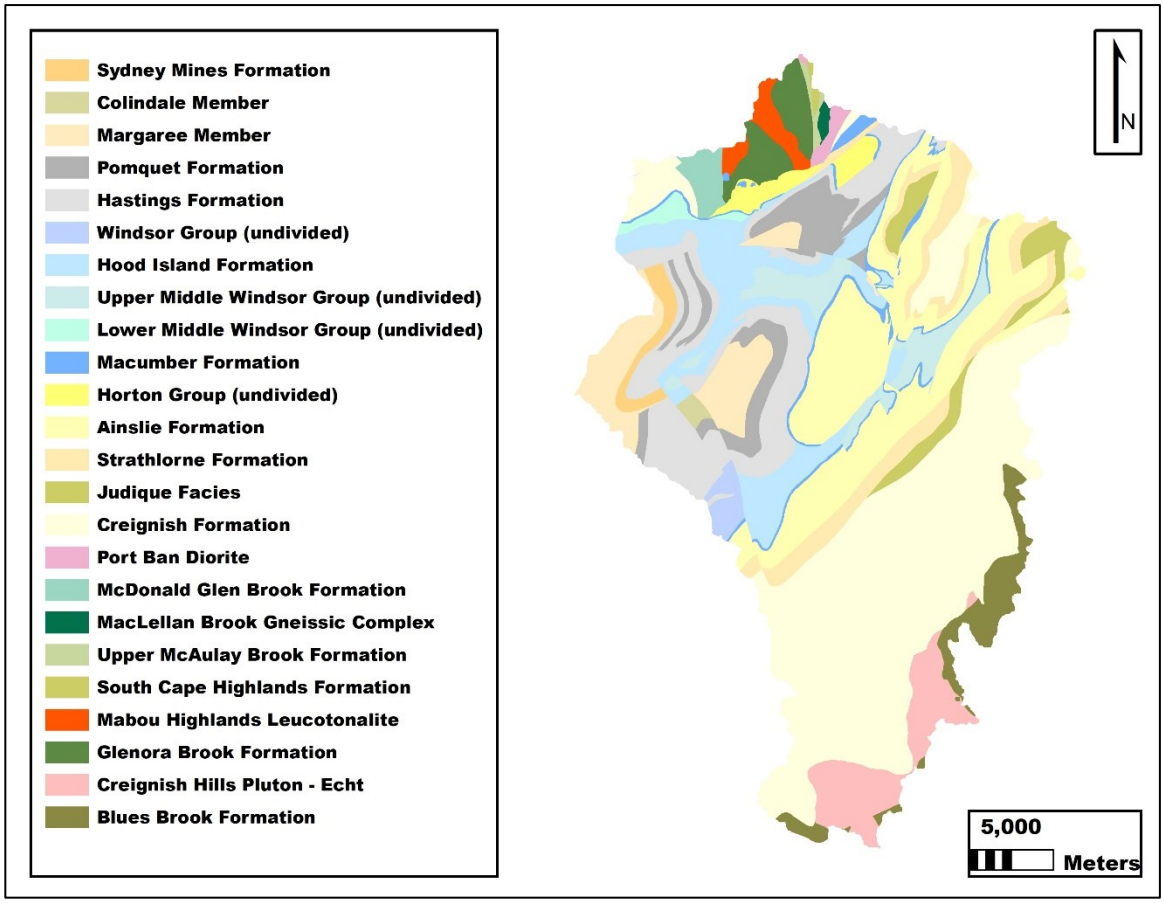

Figure 4: Bedrock geology of the Mabou Harbour drainage basin. Adapted from Barr et al. (2017).

Table 2: Important lithostratigraphic units in the Mabou Harbour drainage basin and unit descriptions taken verbatim from Barr et al. (2017). All units are Carboniferous in age.

Lithostratigraphic unit	Parent	Unit description
Margaree Member	Port Hood Formation	Fine-grained grey-brown sandstone with intercalated red-brown siltstone and shale.
Pomquet Formation	Mabou Group	Red-brown, minor grey siltstone and minor interbedded reddish-grey to grey-green fine-grained sandstone, typically ripple-marked.
Hastings Formation	Mabou Group	Grey and dark grey siltstone and shale with buff, thin stromatolitic limestone; minor anhydrite and gypsum in the subsurface; locally [*sic*] intervals of red siltstone and sandstone.
Hood Island Formation	Upper Windsor Group	Red-brown siltstone, intercalated limestone, dolostone, and gypsum.
Upper Middle Windsor Group	Middle Windsor Group	Limestone, variably dolomitic and fossiliferous with intercalated gypsum, fine-grained red sandstone, and siltstone.
Lower Middle Windsor Group	Middle Windsor Group	Anhydrite and gypsum, minor laminated carbonate rocks.
Ainslie Formation	Upper Horton Group	Grey-green and red-brown sandstone interbedded with red-brown and minor grey siltstone and shale.
Creignish Formation	Lower Horton Group	Grey and greenish-grey sandstone ranging to conglomerate; reddish-brown conglomerate, pebble sandstone and coarse sandstone; abundant gabbroic dykes and sills.

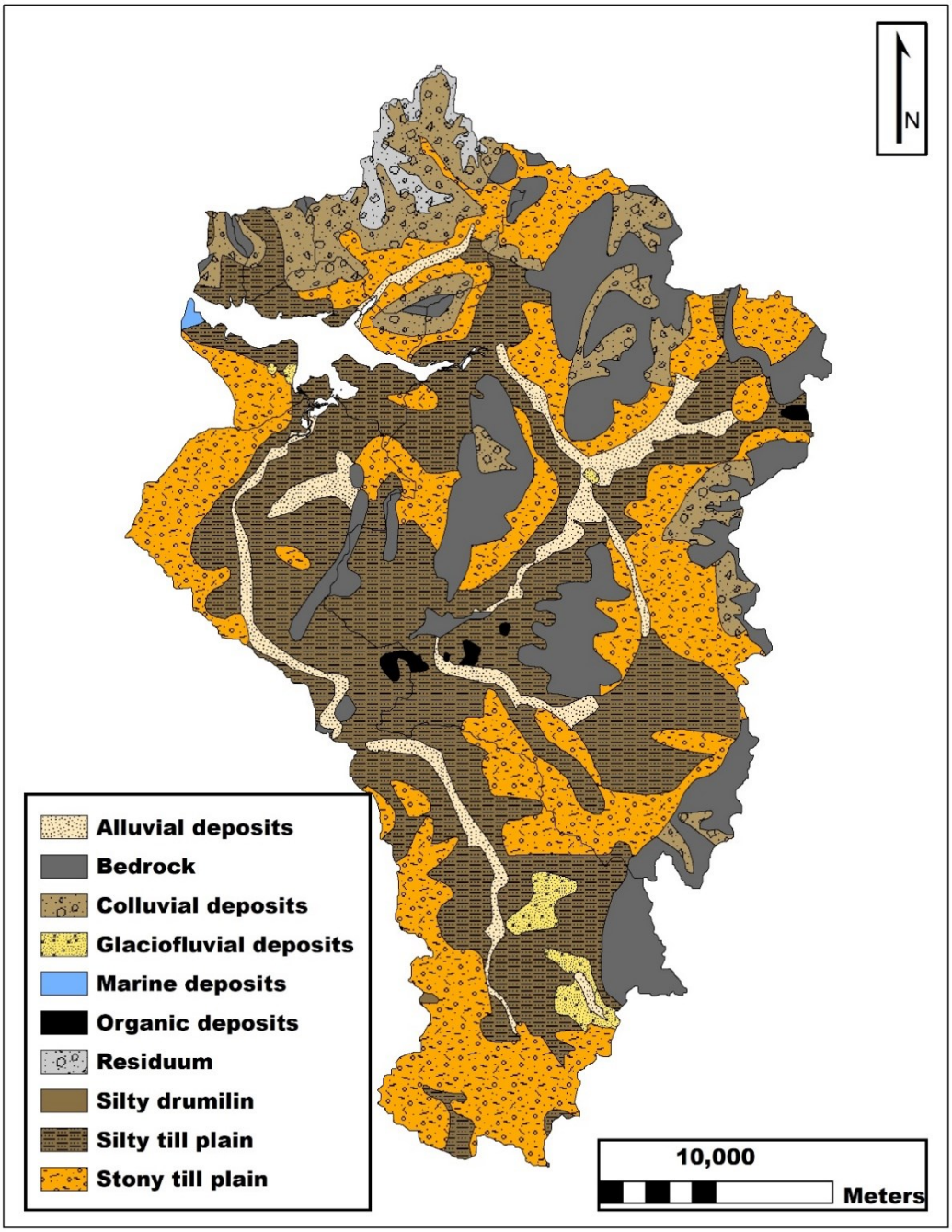

Figure 5: Surficial geology map for the Mabou Harbour Drainage Basin (Stea et al., 2006).

1.3 RESEARCH OBJECTIVES

This thesis investigates the spatial patterns of GSIs within a coastal drainage basin and evaluates the potential risks associated with direct and indirect groundwater discharge on nitrate and microbial contamination of a natural harbour. Direct and indirect groundwater discharge are defined with respect to Mabou Harbour and are used herein to describe the mechanisms through which groundwater reaches the coastal body. Direct groundwater discharge is defined as SGD to the harbour, and indirect groundwater discharge is groundwater discharged into fluvial systems draining into the harbour. The following hypotheses are tested throughout this thesis:

i) indirect groundwater discharge is the dominant mechanism for groundwater to enter the harbour;

ii) indirect groundwater discharge is associated with the greatest risk for groundwater-borne contaminants to enter the harbour due to a presumably larger contribution relative to SGD; and

iii) provided SGD is adequately large, direct groundwater discharge will be a potential mechanism for nitrate contamination, and possibly microbial contamination if residence times are determined to be sufficiently short.

A combination of field methods and modeling was employed to test these hypotheses. Stilling wells, thermal sensors, seepage meters, and piezometers installed in floodplains and coastal zones were used to characterize GSIs and their spatiotemporal patterns. A simplified, steady-state, three-dimensional groundwater flow model was constructed to investigate flow paths and residence times in addition to the spatial

distribution and fluxes of GSIs on a regional scale. Model results were then used to identify hydrogeological and geomorphological conditions associated with risks of groundwater-borne contaminant transport to surface waters.

There are several potential sources of nitrate and microbial contamination of aquifers within the domain including manure application, septic systems, and raw sewage disposal predating regulation. Agriculture and manure spreading are common non-point sources for DIN and pathogenic microorganisms in groundwater (Reddy et al., 1981; Goss et al., 1988; Jamieson et al., 2002). Given the concentration of agriculture, particularly the 36 beef and dairy operations (CBP and IVFA, n.d.), the transport potential of agriculturally sourced groundwater-borne contaminants (i.e., nitrate and faecal coliform bacteria) to the harbour will be discussed.

1.4 ORGANIZATION OF THESIS

This thesis was prepared under the traditional format in accordance with the Dalhousie University Faculty of Graduate Studies guidelines. It is the author's intention to condense the four chapters of this document into a single manuscript for submission to *Hydrogeology Journal*.

The introductory chapter (Chapter 1) includes a comprehensive literature review for the fundamental concepts and processes related to the research objectives including GSIs, SGD, and groundwater-borne contaminant transport. The site description follows the literature review, covering physiography, climatology, hydrology, and geology. Chapter 1 concludes with a summary of research objectives and briefly discusses the methodology for testing the hypotheses.

Chapter 2 and 3 constitute the bulk of the thesis and follow the standard format for a scientific paper containing the following sections: introduction, methodology, results, discussion, and conclusion; however, the literature review is not reiterated from Chapter 1. Chapter 2 reports results from the field campaigns directed toward characterizing GSIs and their spatiotemporal patterns. Chapter 3 focuses on the simplified, steady-state, three-dimensional groundwater flow model which provides insight into the flow paths and residence times, in addition to the spatial distribution of GSIs on a regional scale. Most of the discussion on the effects of direct and indirect groundwater discharge on harbour contamination is found in Chapter 3 which provides a regional analysis.

REFERENCES: CHAPTER 1

Applied Geomatics Research Group. (2017). *Topo-bathymetric lidar research for aquaculture and coastal development in Nova Scotia: final report*. Technical report, NSCC Middleton, NS.

Anderson Jr, W. P., & Emanuel, R. E. (2010). Effect of interannual climate oscillations on rates of submarine groundwater discharge. *Water Resources Research, 46*(5).

Abarca, E., Karam, H., Hemond, H. F., & Harvey, C. F. (2013). Transient groundwater dynamics in a coastal aquifer: The effects of tides, the lunar cycle, and the beach profile. *Water Resources Research, 49*(5), 2473-2488.

Amani, M., Mahdavi, S., Afshar, M., Brisco, B., Huang, W., Mohammad Javad Mirzadeh, S., White, L., Banks, S., Montgomery, J. & Hopkinson, C. (2019). Canadian wetland inventory using Google Earth Engine: The first map and preliminary results. *Remote Sensing*, *11*(7), 842.

Baechler, F. (2015). The geology and hydrogoelogy of faults on Cape Breton Island, Nova Scotia, Canada: An overview. *Atlantic Geology*, *51*, 242.

Baechler, F., & Broehner, R. (2014). Karst geology and hydrogeology of Cape Breton Island, Nova Scotia: An overview. *Canadian Journal of Earth Sciences*, *51*(7), 701–714.

Baechler, F. E., Cross, H. J., & Baechler, L. (2019). The geology and hydrogeology of springs on Cape Breton island, Nova Scotia, Canada: An overview. *Atlantic Geology*, *55*, 137–161.

Barr, S. M., White, C. E., Fisher, B. E., McKinnon, J. S., Barras, A. L., & Hapgood, D. S. (2017). *DP ME 433, version 1, 2017. Digital geological data generated as part of the bedrock geological mapping compilation project for Cape Breton Island, Nova Scotia.* Nova Scotia Department of Natural Resources, Geoscience and Mines Branch.

Beven, K., & Germann, P. (2013). Macropores and water flow in soils revisited. *Water Resources Research*, *49*(6), 3071-3092.

Bitton, G., Farrah, S. R., Ruskin, R. H., Butner, J., & Choum, Y. J. (1983). Survival of pathogenic and indicator organisms in ground water. *Groundwater, 21*(4), 405–410.

Bitton, G., & Harvey, R. W. (1992). Transport of pathogens through soils and aquifers. *Environmental microbiology, 19*, 103-123.

Bobba, A., Chambers, G., & Wrona, P. (2012). Submarine groundwater discharge (SGWD): An unseen yet potentially important coastal phenomenon in Canada. *Natural Hazards, 60*(3), 991-1012.

Boehm, A. B., Shellenbarger, G. G., & Paytan, A. (2004). Groundwater discharge: Potential association with fecal indicator bacteria in the surf zone. *Environmental Science and Technology*, *38*(13), 3558–3566.

Bokuniewicz, H. J. (1992). Analytical descriptions of subaqueous groundwater seepage. *Estuarie*, *15*, 458–464.

Bokuniewicz, H., Taniguchi, M., Ishitoibi, T., Charette, M., Allen, M., & Kontar, E. A. (2008). Direct measurements of submarine groundwater discharge (SGD) over a fractured rock aquifer in Flamengo Bay Brazil. *Estuarine, Coastal and Shelf Science, 76*(3), 466-472.

Bratton, J. F., Böhlke, J. K., Manheim, F. T., & Krantz, D. E. (2004). Ground water beneath coastal bays of the Delmarva Peninsula : ages and nutrients. *Ground Water*, *42*(7), 1021–1034.

Brunke, M., & Gonser, T. (1997). The ecological significance of exchange processes between rivers and groundwater. *Freshwater Biology*, *37*(1), 1–33.

Burnett, W. C., & Dulaiova, H. (2003). Estimating the dynamics of groundwater input into the coastal zone via continuous radon-222 measurements, *Journal of Environmental Radioactivity, 69*(1-2), 21–35.

Burnett, W. C., Cable, J., & Corbett, D. (2003). Radon tracing of submarine groundwater discharge in coastal environments. In *Land and Marine Hydrogeology* (pp. 25–43).

Burnett, W. C., Bokuniewicz, H., Huettel, M., Moore, W. S., & Taniguchi, M. (2003b). Groundwater and pore water inputs to the coastal zone. *Biogeochemistry*, *66*(1), 3-33.

Burt, T. P., Bates, P. D., Stewart, M. D., Claxton, A. J., Anderson, M. G., & Price, D. A. (2002). Water table fluctuations within the floodplain of the River Severn, England. *Journal of Hydrology 262*, 1-20.

Cann, D. B., MacDougall, J. I., & Hilchey, J. D. (1963*). Soil survey of Cape Breton Island Nova Scotia*. Canada Department of Agriculture and Nova Scotia Department of Agriculture and Marketing.

Cape Breton Partnership & The Inverness/Victoria Federation of Agriculture. (n.d.). *Water resources program report: Mabou Harbour watershed*. Prepared for: Nova Scotia Federation of Agriculture.

Charette, M. A., & Sholkovitz, E. R. (2002). Oxidative precipitation of groundwater-derived ferrous iron in the subterranean estuary of a coastal bay. *Geophyical Research Letters*, *29*(10), 85.

Chase, M. E., Jones, S. H., Hennigar, P., Sowles, J., Harding, G. C. H., Freeman, K., Wells, P. G., Krahforst, C., Crawford, R., Pederson, J., & Taylor, D. (2001). Gulfwatch: Monitoring spatial and temporal patterns of trace metal and organic contaminants in the Gulf of Maine (1991–1997) with the blue mussel, Mytilus edulis L. *Marine Pollution Bulletin, 42*(6), 490-504.

Church, T. M. (1996). An underground route for the water cycle. *Nature*, *380*(6575), 579-580.

Conant Jr, B., Robinson, C. E., Hinton, M. J., & Russell, H. A. (2019). A framework for conceptualizing groundwater-surface water interactions and identifying potential impacts on water quality, water quantity, and ecosystems. *Journal of Hydrology, 574*, 609-627.

Deming, D., Sass, J. H., Lachenbruch, A. H., & De Rito, R. F. (1992). Heat flow and subsurface temperature as evidence for basin-scale ground-water flow, North Slope of Alaska. *Geological Society of America Bulletin, 104*(5), 528–542.

Desmarais, T. R., Solo-gabriele, H. M., & Palmer, C. J. (2002). Influence of soil on fecal indicator organisms in a tidally influenced subtropical environment. *Applied and Environmental Microbiology, 68*(3), 1165–1172.

Diaz, R. J., & Rosenberg, R. (2008). Spreading dead zones and consequences for marine ecosystems. *Science*, *321*(5891), 926–929.

Dowd, S. E., & Pillai, S. D. (1997). Survival and transport of selected bacterial pathogens and indicator viruses under sandy aquifer conditions. *Journal of Environmental Science and Health, 32*(8), 2245-2258,

Drage, J., & McKinnon, J. S., (2019). *DP ME 494, Version 1, 2019, Digital version of karst risk map of Nova Scotia.* Nova Scotia Department of Energy and Mines, Geological Survey Division.

Duff, J. H., & Triska, F. J. (1990). Denitrifications in sediments from the hyporheic zone adjacent to a small forested stream. *Canadian Journal of Fisheries and Aquatic Sciences, 47*(6), 1140-1147.

Environment and Agriculture Technology Research Group of the Nova Scotia Community College. (2018). *Agricultural Land Identification Project*. Nova Scotia Community College.

Findlay, S. (1995). Importance of surface-subsurface exchange in stream ecosystems: The hyporheic zone. *Limnology and Oceanography, 40*(1), 159-164.

Filip, Z., Kaddu-Mulindwa, D., & Milde, G. (1988). Survival of some pathogenic and facultative pathogenic bacteria in groundwater. *Water Science and Technology, 20*, 227-231.

Fleckenstein, J. H., Krause, S., Hannah, D. M., & Boano, F. (2010). Groundwater-surface water interactions: New methods and models to improve understanding of processes and dynamics. *Advances in Water Resources, 33*(11), 1291-1295.

Fujita, K., Shoji, J., Sugimoto, R., Nakajima, T., Honda, H., Takeuchi, M., Tominaga, O., Taniguchi, M. (2019). Increase in fish production through bottom-up trophic linkage in coastal waters induced by nutrients supplied via submarine groundwater. *Frontiers in Environmental Science*, *7*, 1–10.

Garrison, G. H., Glenn, C. R., & McMurtry, G. M. (2003). Measurement of submarine groundwater discharge in Kahana Bay, O'ahu, Hawai'i. *Limnology and Oceanography*, *48*(2), 920–928.

Gold, A. J., Jacinthe, P. A., Groffman, P. M., Wright, W. R., & Puffer, R. H. (1998). Patchiness in groundwater nitrate removal in a riparian forest. *Journal of Environmental Quality, 27*, 146-155.

Gold, A. J., Groffman, P. M., Addy, K., Kellogg, D. Q., Stolt, M., & Rosenblatt, A. E. (2001). Landscape attributes as controls on ground water nitrate removal capacity of riparian zones. *Water Resources*, *37*(6), 1457–1464.

Goss, M. J., Barry, D. A. J., & Rudolph, D. L. (1998). Contamination in Ontario farmstead domestic wells and its association with agriculture: 1. Results from drinking water wells. *Journal of Contaminant Hydrology, 32*(3–4), 267–293.

Grimm, N. B., & Fisher, S. G. (1984). Exchange between interstitial and surface water: Implications for stream metabolism and nutrient cycling. *Hydrobiologia, 111*(3), 219-228.

Hayashi, M., & Rosenberry, D. O. (2002). Effects of ground water exchange on the hydrology and ecology of surface water. *Groundwater, 40*(3), 309-316.

Haycock, N. E., & Pinay, G. (1993). Groundwater nitrate dynamics in grass and poplar vegetated riparian buffer strips during the winter. *Journal of Environmental Quality, 22*, 273-278.

Heiss, J. W., Ullman, W. J., & Michael, H. A. (2014). Swash zone moisture dynamics and unsaturated infiltration in two sandy beach aquifers. *Estuarine, Coastal and Shelf Science*, *143*, 20–31.

Hu, C., Muller-Karger, F. E., & Swarzenski, P. W. (2006). Hurricanes, submarine groundwater discharge, and Florida's red tides. *Geophysical Research Letters*, *33*(11), 1–5.

Hynes, H. B. N. (1983). Groundwater and stream ecology. *Hydrobiologia*, *100*(1), 93–99.

Jamieson, R. C., Gordon, R. J., Sharples, K. E., Stratton, G. W., & Madani, A. (2002). Movement and persistence of fecal bacteria in agricultural soils and subsurface drainage water: A review. *Canadian Biosystems Engineering / Le Genie Des Biosystems Au Canada*, 44, 1–9.

Johannes, R. E. (1980). The ecological significance of the submarine discharge of groundwater. *Marine Ecology Progress Series*, *3*, 365–373.

Johannes, R. E., & Hearn, C. J. (1985). The effect of subsurface groundwater discharge on nutrient and salinity regimes in a coastal lagoon off Perth, West Australia. *Estuarine Coastal and Shelf Science, 21*(6), 789–800.

Johnson, A. G., Glenn, C. R., Burnett, W. C., Peterson, R. N., & Lucey, P. G. (2008). Aerial infrared imaging reveals large nutrient-rich groundwater inputs to the ocean. *Geophysical Research Letters*, *35*(15), 1–6.

Kalbus, E., Reinstorf, F., Schirmer, M., & Measuring, M. S. (2006). Measuring methods for groundwater – surface water interactions: A review. *Hydrology and Earth System Sciences, 10*, 873-887.

Keswick, B. H., Gerba, C. P., Secor, S. L., & Cech, I. (1982) Survival of Enteric Viruses and Indicator Bacteria in Groundwater. *Journal of Environmental Science and Health, 17*(6), 903-912.

Kohout, F. A. (1966). Submarine springs: A neglected phenomenon of coastal hydrology. *Hydrology, 26*, 391-413.

Kohout, F. (1967). Groundwater flow and geothermal regime of Florida Plateau. *AAPG Bulletin*, *51*(10), 2165–2166.

Kottek, M., Grieser, J., Beck, C., Rudolf, B., & Rubel, F. (2006). World map of the Köppen-Geiger climate classification updated. *Meteorologische Zeitschrift, 6*(3), 259-263.

Krause, S., Hannah, D., Fleckenstein, J., & Krause, S. (2009). Hyporheic hydrology: Interactions at the groundwater-surface water interface. *Hydrological Processes, 23*(15), 2103-2107.

Kroeger, K. D., Swarzenski, P. W., Greenwood, W. J., & Reich, C. (2007). Submarine groundwater discharge to Tampa Bay: Nutrient fluxes and biogeochemistry of the coastal aquifer. *Marine Chemistry*, *104*(1–2), 85–97.

LaRoche, J., Nuzzi, R., Waters, R., Wyman, K., Falkowski, P., & Wallace, D. (1997). Brown tide blooms in Long Island's coastal waters linked to interannual variability in groundwater flow. *Global Change Biology, 3*(5), 397-410.

Lee, Y., Kim, G., Lim, W., & Hwangb, D. (2010). A relationship between Submarine groundwater-borne nutrients traced by Ra isotopes and the intensity of Dinoflagellate red-tides occurring in the southern sea of Korea. *Limnology and Oceanography*, *55*(1), 1–10.

Li, L., Barry, D. A., Stagnitti, F., & Parlange, J. Y. (1999). Submarine groundwater discharge and associated chemical input to a coastal sea. *Water Resources Research*, *35*(11), 3253–3259.

McFeters, G. A., Bissonnette, G. K., Jezeski, J. J., Thomson, C. A., Stuart, D. G. (1974). Comparative survival of indicator bacteria and enteric pathogens in well water. *Applied Microbiology, 27*(5):823-829.

Menning, D. M., Wynn, J. G., & Garey, J. R. (2015). Karst estuaries are governed by interactions between inland hydrological conditions and sea level. *Journal of Hydrology*, *527*, 718–733.

Menon, A. S. (1988). Molluscan shellfish and water quality problems in Atlantic Canada. *Toxicity Assessment, 3*(5), 679-686.

Michael, H. A., Mulligan, A. E., & Harvey, C. F. (2005). Seasonal oscillations in water exchange between aquifers and the coastal ocean. *Nature*, *436*(7054), 1145–1148.

Michael, H., Post, V., Wilson, A., & Werner, A. (2017). Science, society, and the coastal groundwater squeeze. *Water Resources Research, 53*(4), 2610-2617.

Moore, W. S. (1999). The subterranean estuary: A reaction zone of ground water and sea water. *Marine Chemistry*, *65*(1–2), 111–125.

Moore, W. S. (2010). The effect of submarine groundwater discharge on the ocean. *Annual Review of Marine Science*, 2, 59-88.

Moore, W. S., & Church, T. M. (1996). Submarine groundwater discharge. *Nature, 382*(6587), 122-122.

Moore, W. S., Krest, J., Taylor, G., Roggenstein, E., Joye, S., & Lee, R. (2002). Thermal evidence of water through a coastal aquifer: Implications for nutrient fluxes. *Geophysical Research Letters, 29*(14), 49-1.

Moore, W. S., Sarmiento, J. L., & Key, R. M. (2008). Submarine groundwater discharge revealed by 228Ra distribution in the upper Atlantic Ocean. *Nature Geoscience*, *1*(5), 309–311.

Moosdorf, N., Stieglitz, T., Waska, H., Durr, H. H., & Hartmann, J. (2015). Submarine groundwater discharge from tropical islands: A review. *Grundwasser*, *20*, 53–67.

Mulligan, A. E., Evans, R. L., & Lizarralde, D. (2007). The role of paleochannels in groundwater/seawater exchange. *Journal of Hydrology*, *335*(3–4), 313–329.

Nace, R. L. (1970). World hydrology: Status and prospects. *Symposium on World Water Balance*, *1*(92).

Nelson, W. M., Gold, A. J., & Groffman, P. M. (1995). Spatial and temporal variation in groundwater nitrate removal in a riparian forest. *Journal of Environmental Quality 24*, 691-699.

Nolan, B.T., Ruddy, B.C., Hitt, K.J., & Helsel, D.R. (1998). A national look at nitrate contamination of ground water. *Water Conditioning and Purification, 39* (12), 76-79.

Nova Scotia Department of Environment. (2018). *1:10,000 watersheds for Nova Scotia*.

Nova Scotia Department of Lands and Forestry. (2020). *Nova Scotia topographic database*.

Oberdorfer, J. A., Valentino, M. A., & Smith, S. V. (1990). Groundwater contribution to the nutrient budget of Tomales Bay, California. *Biogeochemistry, 10*(3), 199–216.

Paldor, A., Shalev, E., Katz, O., & Aharonov, E. (2019). Dynamics of saltwater intrusion and submarine groundwater discharge in confined coastal aquifers: a case study in northern Israel. *Hydrogeology Journal, 27*(5), 1611-1625.

Paul, J. H., Rose, J. B., Jiang, S. C., Zhou, X., Cochran, P., Kellogg, C., Kang, J. B., Griffin, D., Farrah, S., & Lukasik, J. (1997). Evidence for groundwater and surface marine water contamination by waste disposal wells in the Florida Keys. *Water Resources*, *31*(6), 1448–1454.

Pekdeger, A., & Matthess, G. (1983). Factors of bacteria and virus transport in groundwater. *Environmental Geology, 5*(2), 49–52.

Piekarek-Jankowska. (1996). Hydrochemical effects of submarine groundwater discharge to the Puck Bay (Southern Baltic Sea, Poland). *Geographia Polonica, 67*, 103-120.

Rassam, D.W., Fellows, C., S., I., De Hayr, R., Hunter, H., & Bloesch, P. (2006). The hydrology of riparian buffer zones; Two case studies in an ephemeral and a perennial stream. *Journal of Hydrology*, *325*(1–4), 308–324.

Rassam, D. W., Pagendam, D. E., & Hunter, H. M. (2008). Conceptualisation and application of models for groundwater-surface water interactions and nitrate attenuation potential in riparian zones. *Environmental Modelling and Software*, *23*(7), 859–875.

Reddy, K. R., Khaleel, R., & Overcash, M. R. (1981). Behavior and transport of microbial pathogens and indicator organisms in soils treated with organic wastes. *Journal of Environmental Quality*, *10*(3), 255-266.

Robinson, C., Gibbes, B., & Li, L. (2006). Driving mechanisms for groundwater flow and salt transport in a subterranean estuary. *Geophysical Research Letters, 33*(3).

Robinson, C., Li, L., & Barry, D. A. (2007). Effect of tidal forcing on a subterranean estuary. *Advances in Water Resources*, *30*(4), 851–865.

Robinson, C. E., Xin, P., Santos, I. R., Charette, M. A., Li, L., & Barry, D. A. (2018). Groundwater dynamics in subterranean estuaries of coastal unconfined aquifers: Controls on submarine groundwater discharge and chemical inputs to the ocean. *Advances in Water Resources*, *115*, 315–331.

Russoniello, C. J., Konikow, L. F., Kroeger, K. D., Fernandez, C., Andres, A. S., & Michael, H. A. (2016). Hydrogeologic controls on groundwater discharge and nitrogen loads in a coastal watershed. *Journal of Hydrology, 538*, 783–793.

Sanford, W. E., & Pope, J. P. (2013). Quantifying groundwater's role in delaying improvements to Chesapeake Bay water quality. *Environmental Science and Technology*, *47*(23), 13330–13338.

Santos, I. R., Burnett, W. C., Chanton, J., Mwashote, B., Suryaputra, N. A., Dittmar, T., … Suryaputra, I. G. N. A. (2008). Nutrient biogeochemistry in a Gulf of Mexico subterranean estuary and groundwater- derived fluxes to the coastal ocean. *Limnology and Oceanography*, *53*(2), 705–718.

Santos, I. R., Burnett, W. C., Dittmar, T., Suryaputra, I. G. N. A., & Chanton, J. (2009). Tidal pumping drives nutrient and dissolved organic matter dynamics in a Gulf of Mexico subterranean estuary. *Geochimica et Cosmochimica Acta*, *73*(5), 1325–1339

Santos, I. R., Eyre, B. D., & Huettel, M. (2012). The driving forces of porewater and groundwater flow in permeable coastal sediments: A review. *Estuarine, Coastal and Shelf Science*, *98*, 1–15

Sawyer, A. H., Michael, H. A., & Schroth, A. W. (2016). From soil to sea: The role of groundwater in coastal critical zone processes. *Wiley Interdisciplinary Reviews: Water*, *3*(5), 706–726.

Schafer, C. T. (1973). Distribution of foraminifera near pollution sources in Chaleur Bay. *Water, Air, and Soil Pollution, 2*(2), 219-233.

Service Nova Scotia and Municipal Relations. (2003). Enhanced digital elevation model, Nova Scotia, Canada. Service Nova Scotia and Municipal Relations, Registry and Information Management Services, Nova Scotia, Canada.

Shinn, E. A., Reich, C. D., & Hickey, T. D. (2002). Seepage meters and Bernoulli's revenge. *Estuaries*, *25*(1), 126–132.

Shum, K. T. (1992). Wave-induced advective transport below a rippled water-sediment interface. *Journal of Geophysical Research*, *92*(C1), 789–808.

Siah, A., Pellerin, J., Amiard, J. C., Pelletier, E., & Viglino, L. (2003). Delayed gametogenesis and progesterone levels in soft-shell clams (Mya arenaria) in relation to in situ contamination to organotins and heavy metals in the St. Lawrence River (Canada). *Comparative Biochemistry and Physiology Part C: Toxicology & Pharmacology, 135*(2), 145-156.

Simmons, R. C., Gold, A. J., and Groffman, P. M. (1992). Nitrate dynamics in riparian forests: Groundwater studies. *Journal of Environmental Quality, 21,* 656-665.

Sinton, L. W., Finlay, R. K., Pang, L., & Scott, D. M. (1997). Transport of bacteria and bacteriophages in irrigated effluent into and through an alluvial gravel aquifer. *Water, Air, and Soil Pollution*, *98*(1–2), 17–42.

Slomp, C. P., & Van Cappellen, P. (2004). Nutrient inputs to the coastal ocean through submarine groundwater discharge: Controls and potential impact. *Journal of Hydrology*, *295*(1–4), 64–86.

Small, C., & Nicholls, R. J. (2003). A global analysis of human settlement in coastal zones. *Journal of Coastal Resources*, *19*, 584–599.

Smith, M. S., Thomas, G. W., White, R. E., & Ritonga, D. (1985). Transport of Escherichia coli through intact and disturbed soil columns. *Journal of Environmental Quality, 14*, 87-91.

Sophocleous, M. (2002). Interactions between groundwater and surface water: The state of the science. *Hydrogeology Journal, 10*(1), 52-67.

Starr, R. C. and Gillham, R. W. (1993). Denitrification and organic carbon availability in two aquifers. *Groundwater,* 31, 934 - 947.

Stea, R. R., Conley, H., Brown, Y., & Fisher, B. E., (2006). *DP ME 36, version 2, 2006. Digital version of Nova Scotia Department of Natural Resources map ME 1992-3, surficial geology map of the province of Nova Scotia, 1:500 000*. Nova Scotia Department of Natural Resources, Mineral Resources Branch.

Tait, D. R., Erler, D. V., Santos, I. R., Cyronak, T. J., Morgenstern, U., & Eyre, B. D. (2014). The influence of groundwater inputs and age on nutrient dynamics in a coral reef lagoon. *Marine Chemistry*, *166*, 36–47.

Taniguchi, M. (2002). Tidal effects on submarine groundwater discharge into the ocean. *Geophysical Research Letters*, *29*(12).

Taniguchi, M., Burnett, W. C., Cable, J. E., & Turner, J. V. (2002). Investigation of submarine groundwater discharge. *Hydrological Processes, 16*(11), 2115-2129.

Taniguchi, M., Dulai, H., Burnett, K. M., Santos, I. R., Sugimoto, R., Stieglitz, T., Kim, G., Moosdorf, N., Burnett, W. C. (2019). Submarine groundwater discharge: Updates on its measurement techniques, geophysical drivers, magnitudes, and effects. *Frontiers in Environmental Science*, *7*, 1–26.

Taylor, R., Cronin, A., Pedley, S., Barker, J., & Atkinson, T. (2004). The implications of groundwater velocity variations on microbial transport and wellhead protection–review of field evidence. *FEMS Microbiology Ecology, 49*(1), 17-26.

Tóth, J. (1962). A theory of groundwater motion in small drainage basins in central Alberta, Canada. *Journal of Geophysical Research, 67*(11), 4375-4388.

Tóth, J. (1963). A theoretical analysis of groundwater flow in small drainage basins. *Journal of Geophysical Research, 68*(16), 4795-4812.

Tóth, J. (1970). A conceptual model of the groundwater regime and the hydrogeologic environment. *Journal of Hydrology, 10*(2), 164-176.

Triska, F. J., Duff, J. H., & Avanzino, R. J. (1993). The role of water exchange between a stream channel and its hyporheic zone in nitrogen cycling at the terrestrial—aquatic interface. In *Nutrient dynamics and retention in land/water ecotones of Lowland, Temperate Lakes and Rivers* (pp. 167-184). Springer, Dordrecht.

Valiela, I., Collins, G., Kremer, J., Lajtha, K., Geist, M., Seely, B., Brawley, J., & Sham, C. H. (1997). Nitrogen loading from coastal watersheds to receiving estuaries: New method and application. *Ecological Applications*, *7*(2), 358–380.

Valiela, I., Costa, J., Foreman, K., Teal, J. M., Howes, B., & Aubrey, D. (1990). Transport of groundwater-borne nutrients from watersheds and their effects on coastal waters. *Biogeochemistry, 10*(3), 177–197.

Windom, H. L. (1992). Contamination of the marine environment from land-based sources. *Marine Pollution Bulletin*, 25(1-4), 32-36.

Winter, T. C., Harvey, J. W., Franke, O. L., & Alley, W. M. (1998). *Ground water and surface water: A single resource* (Vol. 1139). US Geological Survey Circular 1139.

Woessner, W. W. (2000). Stream and fluvial plain ground water interactions: Rescaling hydrogeologic thought. *Ground Water*, *38*(3), 423-429.

Wroblicky, G. J., Campana, M. E., Valett, H. M., & Dahm, C. N. (1998). Seasonal variation in surface-subsurface water exchange and lateral hyporheic area of two stream-aquifer systems. *Water Resources Research, 34*(3), 317-328.

Yates, M. V., Gerba, C. P., & Kelley, L. M. (1985). Virus persistence in groundwater. *Applied and Environmental Microbiology*, *49*(4), 778-781.

Yau, V. M., Schiff, K. C., Arnold, B. F., Griffith, J. F., Gruber, J. S., Wright, C. C., Wade, T. J., Burns, S., Hayes, J. M., McGee, C., Gold, M., Cao, Y., Boehm, A. B., Weisberg, S. B., & Colford, J. M. (2014). Effect of submarine groundwater discharge on bacterial indicators and swimmer health at Avalon Beach, CA, USA. *Water Research, 59*, 23–36.

Younger, P. L. (1996). Submarine groundwater discharge. *Nature*, *382*, 121–122.

Zekster, I. S., Ivanov, V. A., & Meskheteli, A. V. (1973). The problem of direct groundwater discharge to the seas. *Journal of Hydrology*, *20*, 1–36.

Zektser, I. S., & Loaiciga, H. A. (1993). Groundwater fluxes in the global hydrologic cycle: Past, present and future. *Journal of Hydrology, 144*(1-4), 405-427.

Zektster, I. S., & Everett, L. G. (2000). *Groundwater and the environment: Applications for the global community.* CRC Press, Boca Raton.

Chapter 2: Investigation of Groundwater – Surface Water Interactions using Multiple Field Methods

2.1 Introduction

Throughout this investigation, numerous field methods were employed to evaluate the spatiotemporal patterns of groundwater-surface water interactions (GSIs) in the Mabou Harbour drainage basin, particularly around the harbour and floodplains of the major tributaries. Common techniques for assessing GSIs in marine and fluvial environments were used in this study, including hydrograph separation, piezometers, seepage meters, and water sampling (water quality sampling results presented in Appendix II). Although this chapter stands alone as an independent field-study, the baseflow separation and seepage meter data were also used to calibrate and validate the numerical modeling exercise in Chapter 3.

2.2 Methodology

2.2.1 Hydrograph Analysis

Hydrograph analysis is a commonly applied approach for estimating groundwater contributions to streams and rivers (Hiscock and Bense, 2014). In this method, streamflow is separated into the two direct runoff constituents, baseflow and quickflow. Quickflow consists of surface runoff and interflow that rapidly enters a watercourse following a precipitation or snowmelt event (Sophocleous, 2002; Brodie and Hostetler, 2005). Conversely, baseflow is a more persistent and consistent water source that feeds watercourses between precipitation or snowmelt events (Sophocleous, 2002; Brodie and

Hostetler, 2005). As the Mabou rivers are not sourced from lakes, it is assumed that the baseflow is directly derived from groundwater discharge into streams as demonstrated in the literature (e.g., Mau and Winter, 1997; Hannula et al., 2003).

Stilling wells were installed in the Mabou and NE Mabou Rivers towards their mouths as presented in Figure 6. Another stilling well was installed near the mouth of the SW Mabou River but was displaced during extreme streamflow. The stilling wells consisted of perforated 3" ABS pipes hose clamped to a 1" rebar stake that was driven into the deepest part of the channel (Figure 7). Water Level Data Loggers (HOBO, U20-001-004), with a <0.14 cm resolution and maximum water level error of 0.6 cm, were installed in the stilling wells, using a measured length of fishing line, to continuously gauge water levels. The level loggers were unvented and were therefore corrected with barometric data recorded using a Water Level Data Logger (HOBO, U20L-04) with a <0.14 cm resolution and a maximum water level error of 0.8 cm. The barometric logger was fastened to a tree, near the Mabou River hydrometric station, in a ventilated PVC casing. By delineating the gauged drainage areas using the DEM (SNSMR, 2003), it was determined that gauged drainage areas covered 87% and 98% of the total Mabou and NE Mabou watersheds, respectively. The Mabou rivers were gauged periodically during 2018-2020 (Figure 7); however, stilling wells were only present from May 6 – October 21, 2019 due to river-ice conditions. The data were only retrieved from the Mabou and NE Mabou Rivers, as the SW Mabou River stilling well was washed away during a heavy streamflow. The majority of the stream-gauging was completed using a Flowtracker2 Handheld-ADV (SonTek; Figure 7), except for the first stream-gauging exercises which were completed using a pygmy current-meter and the conventional current-meter method (Rantz, 1982).

The stream gauging results that were concurrent with continuous stage monitoring were used to construct rating curves as a method of estimating streamflow between stream gauging activities. As the stilling well elevation was surveyed relative to the elevation of the neighboring piezometers, it was possible to add stream gauging results to the rating curve following the removal of the stilling wells. In such cases, the river stage was surveyed using the neighboring piezometer (top of casing) as a datum and then applying a correction factor to convert the river stage to the corresponding stilling well measurement. Stream discharge was plotted against the stage measurements, relative to the pressure transducer depth within the stilling well, and a power-law trendline was fit to the observations to create rating curves. The use of power-law equations to create rating curves is a commonly applied approach in hydrology (Petersen-Øverleir, 2004; Di Baldassarre and Claps, 2011; Domeneghetti et al., 2012). The rating curves were then applied to convert the continuous data from the stilling wells into hydrographs.

The SWAT baseflow filter program (Bflow; Arnold et al., 1995) was used to separate baseflow from quickflow. Recursive filters, such as Bflow, separate high (quickflow) and low (baseflow) frequency signals from the hydrograph. The equation of the recursive filter is:

$$Q_{Q(t)} = \beta\, Q_{Q(t-1)} + \left(\frac{1+\beta}{2}\right) \times (Q_{(t)} - Q_{(t-1)}) \quad (1)$$

where $Q_{Q(t)}$ and $Q_{Q(t-1)}$ are quickflows [$m^3\ d^{-1}$] at the t and t-1 time-steps [d], respectively, $Q_{(t)}$ and $Q_{(t-1)}$ are stream discharges [$m^3\ d^{-1}$] at the t and t-1 time steps, respectively, and β is the filter parameter (Arnold et al., 1995). Previous studies have concluded that a β

value of 0.925 yields realistic results relative to manual techniques (Nathan and McMahon, 1990; Arnold and Allen, 1999) and is the default for Bflow. As the filter is setup to work with daily data, the hydrometric data, which had a time resolution of 15 minutes, were converted into daily average streamflow.

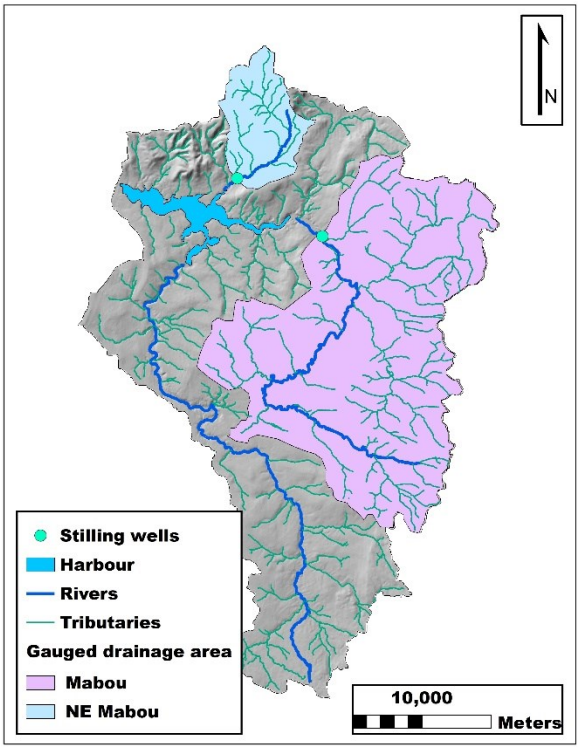

Figure 6: Stilling well locations and corresponding gauged drainage areas in the Mabou Harbour drainage basin. The Mabou Harbour drainage basin was derived from Nova Scotia Department of Environment (2018) and work completed for the CBP and IFVA (n.d.) by the Department of Natural Resources.

Figure 7: Installation of a stilling well in the Mabou River during May 2019 (left image). Stream gauging of the NE Mabou River in March 2020 (right image) using a Flowtracker2 Handheld-ADV (SonTek).

2.2.2 Piezometers

A series of floodplain and coastal zone piezometers were installed throughout the drainage basin (Figure 8) to investigate spatiotemporal patterns in groundwater flow dynamics and to facilitate groundwater sampling. The piezometers were completed into the overburden with depths presented in Table 3. Piezometer construction consisted of 2.54 cm (1") PVC casing with a 25 cm screened interval. Piezometers were installed using a combination of drilling with either a hand auger or Backpack Drill (Shaw), and driving with a sledgehammer. Piezometers were developed and sealed at the surface using bentonite to prevent flow along the borehole annulus. Level loggers were installed to collect continuous data over the majority of the 2019 field season (August 28 – October 21, 2019) to record temporal patterns in head and hydraulic gradients between floodplains or coastal zones and their respective rivers or coastline. Level Data Loggers (HOBO, U20-001-004), with a <0.14 cm resolution and maximum water level error of 0.6 cm, were

installed at all locations, except for the WWTP piezometer. For the WWTP piezometer, a Titanium Water Level Data Logger (HOBO, U20-001-01-Ti), with a <0.21 cm resolution and maximum water level error of 1 cm, was installed. The NE Mabou River piezometer was completed 1 m away from the riverbank, and the Mabou River piezometer 2.5 m away. The coastal piezometers are located 3.2 m, 7.1 m, and 17.5 m from normal high tide at the Lindy lower, south harbour, and Lindy upper stations, respectively (Figure 8; Figure 9). A Virtuoso tidal logger (RBR), with an accuracy and resolution of ±0.05% and 0.001% of full scale, respectively, was deployed near the mouth of the harbour (N46° 05.080' W61° 27.622'; Figure A1) to aid in the analysis of connectivity between the aquifer and ocean which may manifest as tidal signals propagating through the coastal aquifers (Abarca et al., 2013; Trglavcnik et al., 2018). Fast Fourier transform analysis (FFT), using the Matlab FFTW tool (Frigo and Johnson, 1998), was completed on the tidal logger's and coastal piezometer's time series to identify dominant periodic signals in the data and to facilitate comparison of signals between the harbour and aquifer.

Table 3: Piezometer screen interval depths measured with respect to the surface.

	Top of screen [m]	Bottom of screen [m]
Mabou river	1.360	1.610
NE River	1.650	1.900
WWTP	1.810	2.060
Lindy Lower	0.935	1.185
Lindy Upper	1.730	1.980
South Harbour	1.055	1.305

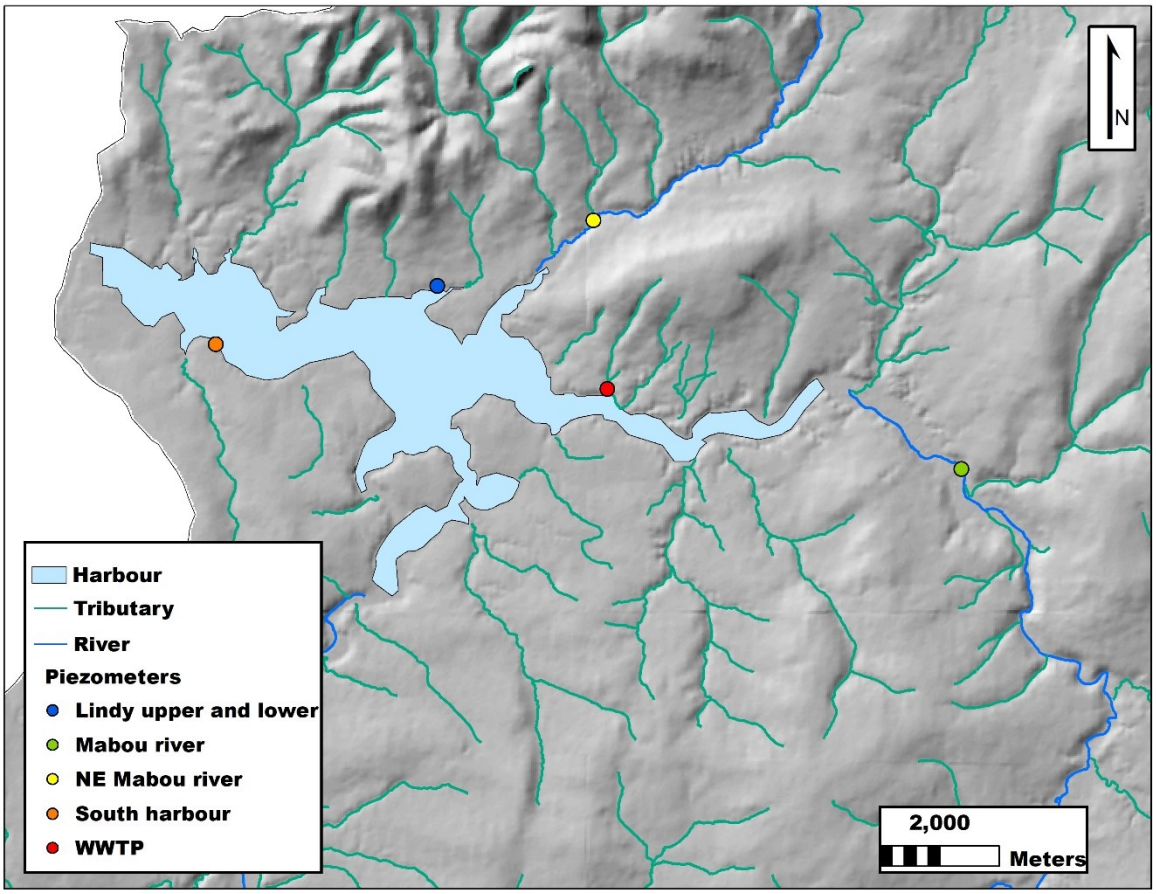

Figure 8: Piezometer distribution surrounding the Mabou Harbour, and NE Mabou and Mabou Rivers. Watercourses were adapted from Department of Lands and Forestry (2020) as described in Section 3.2.2.6.3.

Figure 9: The Lindy Lower piezometer located 3.2 m from the high tideline at the Pottinger residence within the MacEachern Bay of Mabou Harbour.

2.2.3 Hydraulic Conductivity Estimates

Developing an understanding of hydraulic properties, particularly hydraulic conductivity (*K)*, is an important step in the analysis of a groundwater system. Within the drainage basin, it is assumed that most of the GSIs are taking place within the surficial aquifers; therefore, it is vital to constrain the *K* for the two predominant overburden types associated with surface waterbodies, which are glacial till and alluvium. Slug or bail tests are commonly applied approaches for measuring *K* in single well installations due to the logistical simplicity (Butler Jr, 2019). Bail tests consist of rapidly removing water from a well, instantaneously changing the head, to which the well recovers at an exponential rate

dependent on factors such as screen length and aquifer properties. In this study, bail tests were conducted in both silty glacial till and alluvium at the Lindy lower and NE Mabou River piezometers, respectively. The Hvorslev method for partially penetrating unconfined wells was applied to well-recovery data to estimate *K* (Hvorslev, 1951). The Hvorslev method (1951) is a single-well test that can be applied to either slug or bail tests. This method estimates *K* based on well recovery as indicated at any point by drawdown and considers well geometry, such as standpipe radius (r_w) [m], screen length (l_s) [m] and screen radius (R_s) [m]. A simplified form of the Hvorslev solution (1951) is as follows:

$$K = \frac{r_w^2 \ln\left(\frac{l_s}{r_s}\right)}{2LT_o} \tag{2}$$

where the variable T_o is the basic time lag representing the time when the drawdown ratio equals 0.37 (Appendix IV).

The analysis of tidal signal propagation was also used to estimate *K* of silty glacial till, and results were compared to the bail test. The basis of this method is that groundwater levels in coastal aquifers fluctuate in response to tidal cycles, storm surges, and higher frequency forces such as waves (Ferris, 1952; Trglavcnik, 2018). The amplitude and lag of these aquifer responses are dependent on numerous factors including aquifer properties, and characteristics of the ocean forces (Jacob, 1950). The horizontal propagation of tidal signals through aquifers can also be used to estimate *K* using the equation for confined aquifers (Jacob, 1950):

$$h(x,t) = H_o e^{\left(-x\sqrt{\frac{\pi}{Dp}}\right)} sin\left(\frac{2\pi t}{p} - x\sqrt{\frac{\pi}{Dp}}\right) \tag{3}$$

where $h(x,t)$ is the head within the aquifer [m], H_o is the amplitude of the tidal signal [m], x is the distance between the well and sea [m], p is the tidal signal period [d], t is time [d] and D is diffusivity [$m^2\ d^{-1}$]. Diffusivity is equal to K/S_S, where S_S is specific storage [m^{-1}]. By isolating the amplitude component of the above analytical solution, a diurnal tidal signal observed at the Lindy lower piezometer was analyzed using the simplified equation:

$$a = H_o e^{\left(-x\sqrt{\frac{\pi}{Dp}}\right)} \quad (4)$$

where a is the amplitude of the tidal signal experienced within the aquifer [m]. Based on field measurements at different points during the tidal cycle, x was estimated to be 8.2 m and is relative to the mid-tideline. S_S was assumed to be 9.82×10^{-4} m^{-1} for silt based on a review of the literature (Younger, 1993) as S_S estimates from the bail tests are assumed to be unreliable due to the small sample volume of the aquifer. The use of Ss, rather than specific yield, as the storage parameter in Equation (4) is predicated on the assumption that the glacial till functions as a confined aquifer in terms of how it transmits tidal signals.

2.2.4 Thermal Analysis

Thermal analysis of streams is a relatively inexpensive and effective method for evaluating groundwater – surface water interactions. The thermal regime of a river is determined by a number of different factors that can generally be classified as: 1) atmospheric conditions; 2) topographical or geographical settings; 3) river hydraulics (e.g., inflows and outflows); and 4) streambed heat exchanges (Caissie, 2006). Other factors such as stream aspect, tree cover, stream size, and fluvial geomorphology have also been shown to impact stream temperatures (Macan, 1958; Mosley, 1983; Zwieniecki & Newton, 1999; Torgersen et al., 2001; Caissie, 2006; Dugdale et al., 2018). As this investigation involves

streams within the same drainage basin, topographical, geographical, and streambed variables are considered relatively constant; thus, the hydraulics, or mixing of groundwater and surface water sources, is considered to be the main driver for differences in thermal regimes between the Mabou rivers. It should be noted that although climatic conditions are similar between the different rivers, there may also be variations in atmospheric loading due to differing degrees of canopy shading.

TidbiT MX Temperature 400' Data Loggers (HOBO, MX2203), with a 0.01°C resolution and an accuracy of ±0.25°C, were attached to rebar-stakes and installed in the Mabou rivers. Stream-temperature measurements were taken every 30-minutes from June 20 – October 22, 2019. Simple regression models were used to qualitatively assess and compare the groundwater dominance between the major rivers within the drainage basin. Daily mean stream vs. daily mean air temperatures were plotted, and a linear regression line was fit to the points. Hourly air-temperature data were gathered and averaged from the Northeast Margaree (AUT) climate station (ECCC climate ID: 8204154). This exercise used daily timescales; however, it should be noted that different scales will yield different relationships (Caissie, 2006). The relationship between stream and air temperature is a function of groundwater dominance. The slope of this regression line is a qualitative indicator of groundwater control, with high slopes and low intercepts indicating quickflow-dominated conditions and low slopes and high intercepts indicating baseflow-dominated conditions (e.g., Smith, 1981; Mackey and Berrie, 1991; Kelleher et al., 2012; Mayer, 2012). Another temperature-related indicator of groundwater dominance in streamflow is the scale of daily variations in stream temperature. For instance, daily variations are

generally smaller for streams where groundwater discharge is dominant (Caissie, 2006). Diel-variations in stream temperature were plotted from June 20 – October 22, 2019 for the Mabou rivers and compared.

2.2.5 Seepage Meters

Seepage meters allow direct measurements of groundwater-surface water exchanges and facilitate water quality analysis of discharging water. The design originated in the 1940's (Duque et al., 2020) as a way of measuring groundwater discharge in lacustrine and fluvial settings; however, it was later proposed for marine use by Lee (1977) to investigate submarine groundwater discharge (SGD). Quantification of SGD to the marine environment, particularly the fresh component and associated solute loads, has driven the use and development of seepage meter studies (Johannes, 1980; Slomp and Van Cappellen, 2004; Wang et al., 2018). To date, seepage meters are the dominant methodology applied to the direct quantification of SGD fluxes (Duque et al., 2020), presumably for their simplicity and effectiveness. However, there are numerous disadvantages to seepage meters, including: 1) the logistical complexity and the large amount of time associated with seepage meter studies; 2) seepage meters yield a point estimate and do not account for the spatial heterogeneity in SGD (Michael, 2003); and 3) seepage meters measure total SGD rather than fresh SGD (FSGD). A solution to the latter issue is to analyze the SGD chemistry to distinguish the fresh and saline components.

The equipment used in this investigation consisted of the top portion of a poly 55-gallon container drum that is hydraulically connected to a plastic bag at the end of a hose. The drum is inserted deep enough into the submarine sediments to form an adequate seal

(Figure 10). As SGD discharges into the drum, an equal volume of water is forced into the plastic collection bag. The water within the collection bag was measured following a full tidal cycle using a graduated cylinder. To facilitate simple measurements, a quick-release connection and a shut-off valve separate the collection bag from the drum. Seepage meters were installed in four different locations to characterize the regional-scale heterogeneity in geological and hydrogeological conditions (Figure 11). Collection bags were sampled from October 6 – October 9, 2020 following each tidal cycle. Storm surges on October 8 resulted in a reduction of sample frequency. Due to logistical constraints related to site location and the implications of Covid-19 for the 2020 field season, seepage meters were not installed long enough to allow equilibration with SGD chemistry. Therefore, salinity and water chemistry were not analyzed from the collection bags and the FSGD component remains unknown.

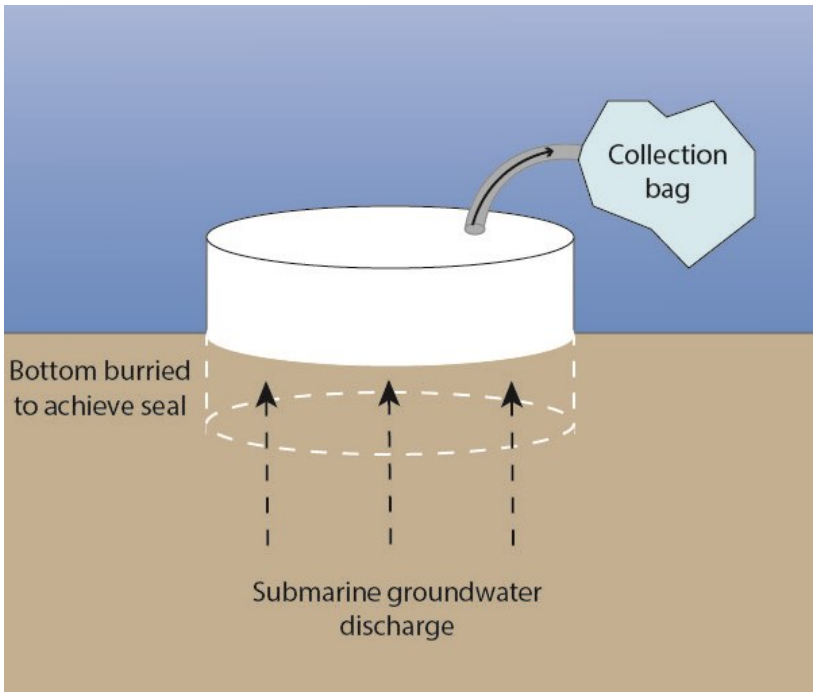

Figure 10: Installation and functioning of a seepage meter used in a marine environment.

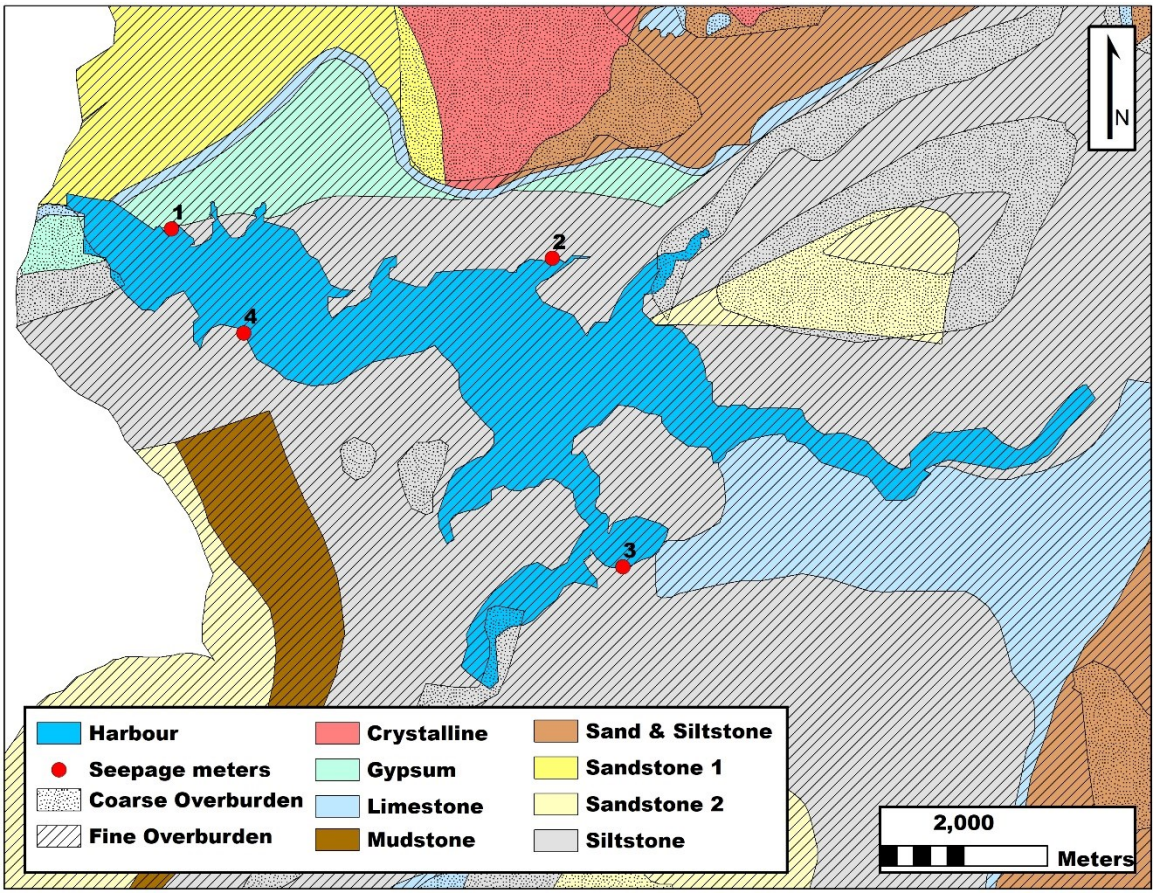

Figure 11: Seepage meter locations and hydrostratigraphic units (HSUs; as described in Section 3.2.2.4). HSUs are presented, rather than lithostratigraphic units, as a simplified geological model was employed for the numerical groundwater modeling described in Section 3.2.2. Bedrock HSUs are derived from Barr et al. (2017). Surficial HSUs are derived from Stea et al. (2006).

2.2.6 Water Balance Estimates

The baseflow estimates and precipitation data were used to estimate water budgets during the 2019 field season. Water balance components, such as evapotranspiration (*ET)*, were estimated using the water balance equation (Hiscock and Bense, 2014):

$$P - ET = Q_R + Q_G + Q_A \quad (5)$$

where P is precipitation [m yr^{-1}], ET is evapotranspiration [m yr^{-1}], Q_R is surface runoff and interflow [m yr^{-1}], Q_G is groundwater discharge [m yr^{-1}], and Q_A is artificial abstractions

[m yr^{-1}]. This equation assumes: 1) the groundwater divide corresponds with the drainage divide, which is a commonly applied assumption in groundwater studies (Hiscock and Bense, 2014; Han et al., 2019); 2) baseflow represents riverine groundwater discharge; and 3) that the change in storage between years is negligible (i.e., groundwater discharge is equal to groundwater recharge). Over longer timescales of multiple years, change in storage is considered to be negligible (Hiscock and Bense, 2014), but due to a lack of continuous data, this assumption was applied over a shorter time-period. To calculate the water balance, it was assumed that artificial abstractions and consumption in the drainage basin, such as pumped groundwater, are negligible. The municipal supply well VMa-P3 is currently approved for 396 m^3 d^{-1} which would have a small impact on the water balance for the full drainage basin (i.e., only 0.09% of the daily groundwater recharge estimated with numerical modeling [Section 3.3.4]). It was also assumed that groundwater recharge from regional flow outside of the drainage basin is negligible. A source of uncertainty in this model is that although baseflow is useful in the assessment of recharge conditions (Hiscock and Bense, 2014), it may actually comprise of a combination of both interflow and baseflow (Rivard et al, 2014). It should be acknowledged that the use of hydrograph analysis as a means of estimating the groundwater component of streamflow may overestimate groundwater discharge, thus impacting recharge estimates.

Annual water balance estimates are required for the calibration of a steady state, three-dimensional groundwater flow model (Section 3.2.3.3); however, hydrometric data could only be gathered during the period of May 6 – October 21, 2019 due to river-ice conditions. To address this issue, seasonal data was extrapolated into annual estimates based on temporal patterns observed in catchments with similar BFI, geology, topography,

and climate (Appendix I). The MacLennan's Cross River and River Inhabitants (Figure 12) were used to guide the extrapolation of the Mabou and NE Mabou Rivers, respectively. Analysis of two-year data shows that although precipitation, stream discharge, and baseflow/precipitation ratios vary between years, the proportion of annual baseflow and streamflow that occurs in the field season compared to the off-season appears to be relatively consistent within a catchment, regardless of differences in annual precipitation (Appendix I). Despite the similarities between the MacLennan's Cross River and River Inhabitants with the Mabou rivers, the extrapolation of seasonal data based on similar catchments introduces considerable uncertainty to annual water budget estimates.

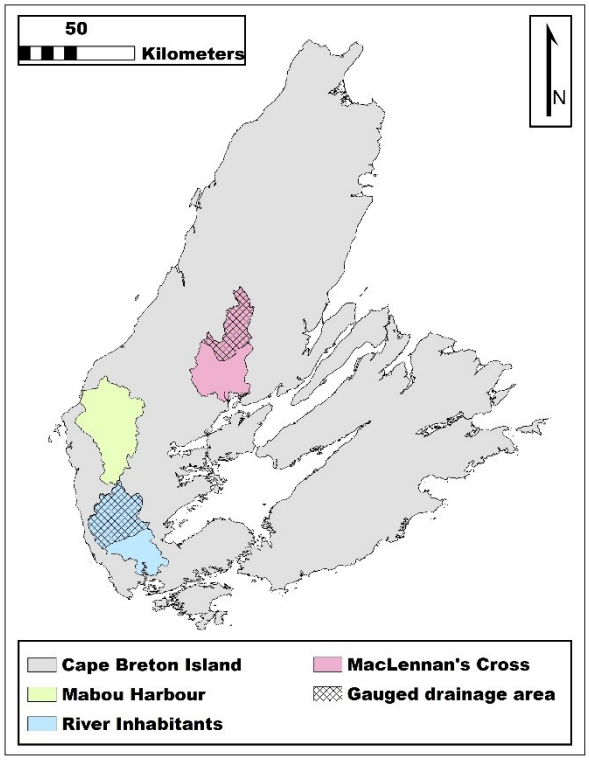

Figure 12: Location of the Mabou Harbour drainage basin and surrogate watersheds on Cape Breton Island, Nova Scotia. Surrogate watershed boundaries were taken from Nova Scotia Department of Environment (2018). Gauged drainage areas were delineated manually using the DEM (SNSMR, 2003). The Mabou Harbour drainage basin was derived from Nova Scotia Department of Environment (2018) and work completed for the CBP and IFVA (n.d.) by the Department of Natural Resources.

2.3 RESULTS

2.3.1 Hydrograph Analysis

The rating curves for the Mabou and NE Mabou Rivers are presented in Figure 13, and a full summary of the stream discharge measurements are presented in Appendix I. Correlation coefficients of 0.996 and 0.971 for the Mabou and NE Mabou Rivers were achieved, respectively, indicating a strong relationship between the discharge and relative stage. The high correlation coefficients indicate that rating curves are sufficiently accurate for low discharges; however, due to a lack of observations at high discharges, the rating curve is not constrained for high streamflow. For instance, the respective maximum gauged discharges for the Mabou and NE Mabou Rivers were 7% and 9% of the maximum discharges determined by the rating curves. During the greatest peak flow on August 28, 2019, quickflows determined by hydrograph separation were approximately 89% - 93% and 70% - 82% of total precipitation for the Mabou and NE Mabou Rivers, respectively. The lower and upper bounds of these ranges were determined using Port Hawkesbury (ECCC climate ID: 8204495) and Cheticamp Highlands National Park (ECCC climate ID: 8200828) precipitation data, respectively.

The stream and baseflow hydrographs for the Mabou and NE Mabou Rivers and their corresponding baseflow indexes (BFIs) are presented in Figure 14. The BFI is substantially higher in the NE Mabou River watershed (0.68 vs. 0.46), presumably due to coarse-grained overburden, including residuum, colluvium, and alluvium, dominating the surficial geology (Figure 5; Stea et al., 2006). The Mabou and NE Mabou River BFIs agree with 2017-2018 data for surrogate watersheds with similar topography and surficial

geology (i.e., River Inhabitants and MacLennan's Cross, respectively) to which the SWAT Bflow filter program (Arnold, 1995) was applied (Table A3; Table A2). Additionally, the BFI for NE Mabou River agrees with BFIs determined for the nearby April Brook watershed (0.65; Türker, 1969). Visual inspection suggests that baseflow separations are reasonable, such that baseflow curves meet the hydrograph approximately at the inflection point of recession curves (Figure 14 and Brodie and Hostetler, 2005). The convergence of the baseflow and stream hydrographs at the recession curve inflection point reduces the influence of peak flow uncertainties on baseflow estimates; however, there may be an impact on BFIs. Within the drainage basin, baseflow is considered to be completely groundwater-derived as the headwaters of watercourses do not originate from surface water bodies. Figure 14a shows that quickflow is more pronounced and prolonged in the Mabou River relative to the NE Mabou River, where quickflow is brief (Figure 14b). This is supported by the differences in BFIs, which suggests that groundwater-derived baseflow dominates quickflow in the NE Mabou River. During the field-season (168 d), the total baseflow discharge was respectively 2.24×10^{7} and 6.02×10^{6} m^3 for the Mabou and NE Mabou Rivers corresponding to mean daily discharges of 1.54 and 0.41 $m^3\ s^{-1}$, respectively.

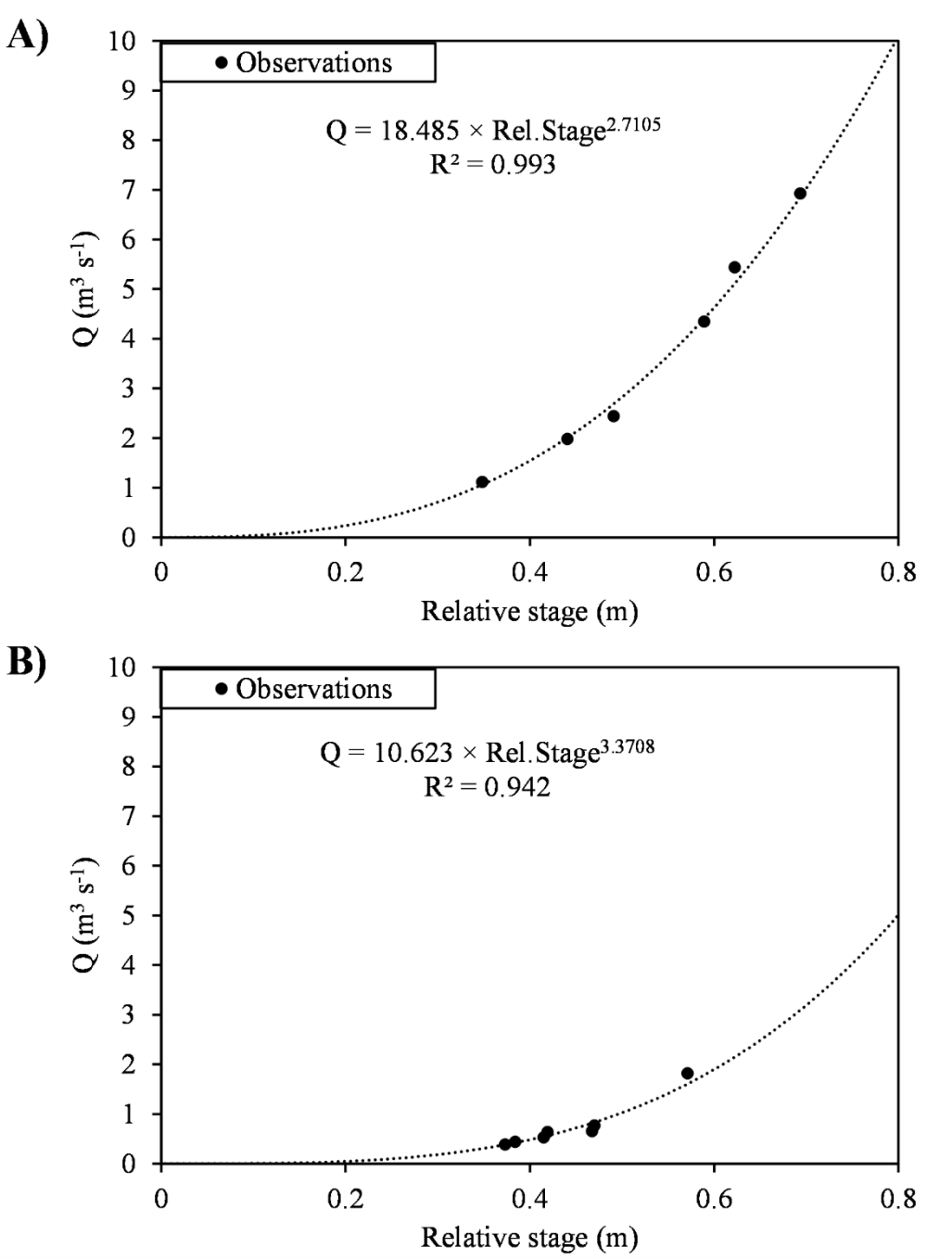

Figure 13: Rating curves for the Mabou River (A) and NE Mabou River (B). Stage is relative to the pressure transducer elevation within the stilling wells.

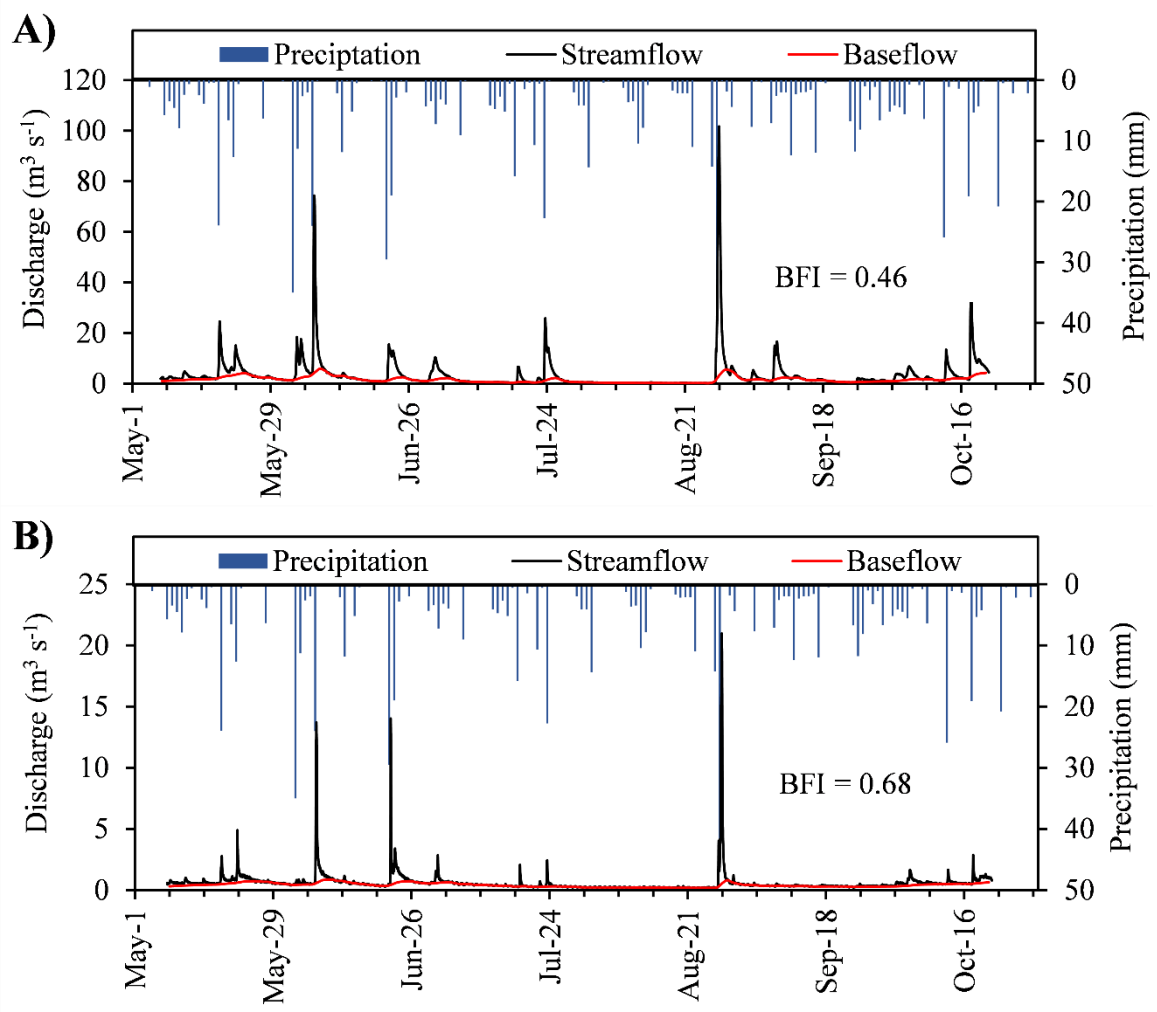

Figure 14: Stream and baseflow hydrographs for the Mabou River (A) and NE Mabou River (B) during the 2019 field season (May 6 – October 21) in addition to the mean daily precipitation data from the Port Hawkesbury (ECCC climate ID: 8204495) and Cheticamp Highlands National Park (ECCC climate ID: 8200828). Baseflow is obtained from SWAT Bflow filter program (Arnold et al., 1995).

2.3.2 Piezometers

2.3.2.1 River Piezometers

The time-series for river stages and floodplain heads at the Mabou and NE Mabou Rivers are presented in Figure 15. The stages of both rivers display strong correlations with their corresponding piezometer heads, indicating strong aquifer-stream connectivity. The river stage and floodplain head are more similar at the NE Mabou River than the Mabou river station; however, the distance between the piezometer and riverbank is 60% less (1 m vs. 2.5 m). Figure 16 presents the relationship between the hydraulic gradient (from river to floodplain) and river stage for the Mabou and NE Mabou rivers. The two rivers exhibit different temporal patterns in hydraulic gradients and responses to heavy precipitation events.

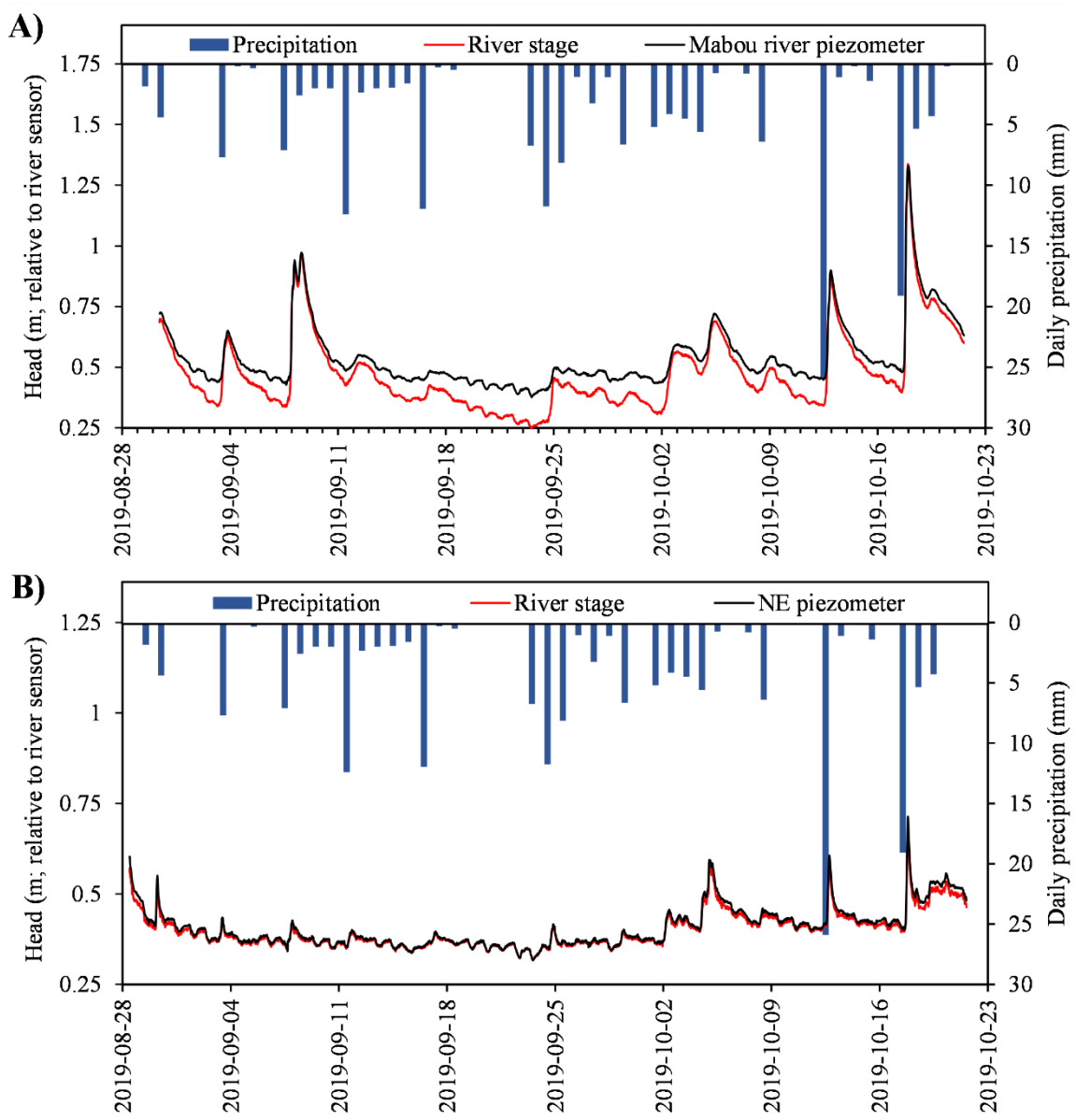

Figure 15: Floodplain piezometer and stage hydrographs for Mabou and NE Mabou rivers (A and B, respectively) in addition to the mean daily precipitation data from the Port Hawkesbury (ECCC climate ID: 8204495) and Cheticamp Highlands National Park (ECCC climate ID: 8200828). River stage is relative to the stilling well transducer and does not reflect the maximum depth within the channel. The depth to the floodplain water table is generally <1.25 m at Mabou River and <0.75 m at NE Mabou River.

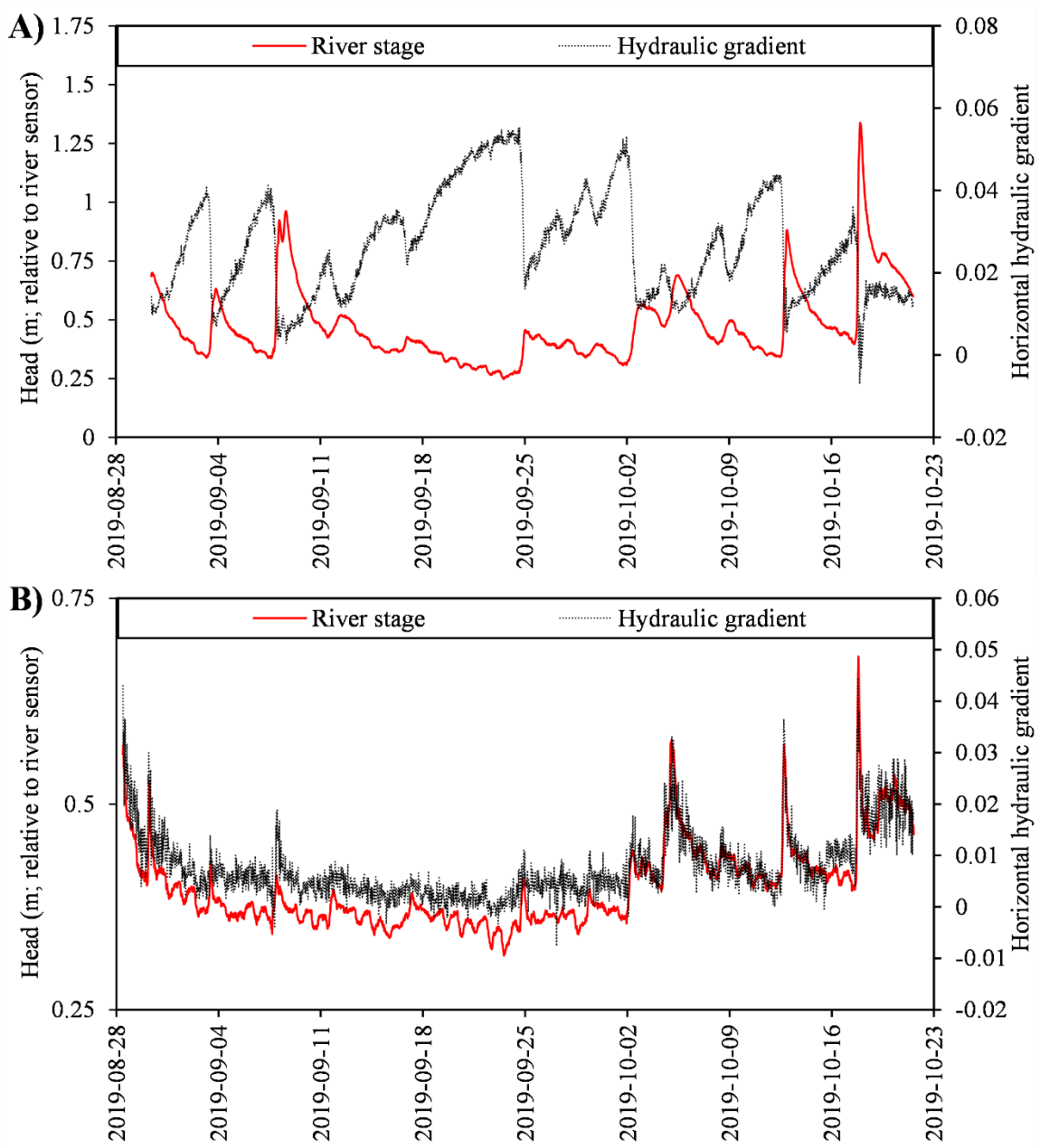

Figure 16: Hydraulic gradients relative to river stage for the Mabou and NE Mabou rivers (A and B, respectively). A positive hydraulic gradient indicates that piezometer head is higher than river stage. Distances between piezometer and riverbank are 2.5 m (A) and 1 m (B).

2.3.2.1.1 Mabou River – Aquifer System

The Mabou River station experienced marginal differences between river stage and floodplain head during heavy streamflow, with the difference increasing during dry periods (Figure 15a). The hydraulic gradient, from river to the floodplain, was steepest during periods of low streamflow (Sep. 18, 2019 – Oct. 2, 2019) and lowest during wet periods (remainder of 2019 data; Figure 16a) with a mean value of 2.7%. Following peak flows, hydraulic gradient increases logarithmically until baseflow conditions stabilize. Only on Oct. 17, 2019, did the hydraulic gradient reverse over the 2.5 m distance between the riverbank and piezometer; however, more frequent reversals may have occurred closer to the bank. For instance, the inflection point and rising limb of the stage-hydrograph slightly precedes that of the piezometer hydrograph suggesting that gradient reversals occur in closer proximity to the riverbank. A reversal in hydraulic gradients would indicate that the stream is temporarily recharging the flood-plain aquifer, also known as bank storage (Todd, 1955). This stream-derived groundwater is stored in the floodplain until stream stage subsides and the groundwater flow direction returns to normal conditions (Todd, 1955). Stream stage and head were approximately equal during heavy streamflows (Figure 15a), which may suggest that stream-derived recharge is the main driver in head changes under such conditions, rather than recharge from precipitation. Alternatively, during smaller precipitation events (e.g., Sep. 25, 2019), piezometer head exceeds the maximum river stage, indicating that recharge from precipitation dominates in these conditions.

2.3.2.1.2 NE Mabou River – Aquifer System

The NE Mabou River displays marginal differences between river stage and floodplain head during dry periods (baseflow conditions) with differences increasing

during high streamflow events (Figure 15b). These trends are opposite to those observed at the Mabou River station. The hydraulic gradient, from river to the floodplain, was highest during high streamflow events and lowest during periods of low streamflow (Sep. 14, 2019 – Sep. 25, 2019) with a mean value of 0.8%. Occasionally, during low streamflow periods, hydraulic gradient fluctuated between positive and negative (Figure 16b); however, the gradients were within the combined error from loggers, elevation surveys of piezometers and wells, and the ability of the stilling well to moderate high-frequency water fluctuations. The inflection point and rising limb of the piezometer hydrograph slightly precedes the river stage-hydrograph, and the maximum head exceeds the maximum stage at peak flow (Figure 15a). This observation in conjunction with the increased hydraulic gradient during high-discharge streamflows suggests that recharge from precipitation dominates over bank storage, such that recharge from precipitation is so rapid, it precedes runoff. Following a significant precipitation event and high discharge, pressure head in the piezometer decreases exponentially.

2.3.2.2 Coastal – Zone Piezometers

The temporal relationships between harbour levels and the coastal piezometers (Lindy lower, Lindy upper, and south harbour) are presented in Figure 17. There is a strong correlation between the hydrographs for south harbour and Lindy lower, which are located on the south and north shores, respectively. The hydrograph for Lindy upper exhibits an extremely slow recovery following well development and little fluctuation indicating that it was completed in a low-*K* material. Diurnal and semi-diurnal signals are most evident and consistent at Lindy lower (Figure 17a). South harbour and Lindy upper display diurnal signals predominantly during periods of mixed tidal patterns (Figure 17b and c,

respectively). It is possible that the periodic signals observed at the two wells furthest from the harbour are due to other forces (e.g., atmospheric).

During the study period, the harbour experienced a mixed tidal pattern where semi-diurnal tides dominate but display asymmetry between the tides (Figure 17). In some instances, the asymmetry was so great that the tidal pattern resembled a diurnal cycle. Although the harbour level, as measured with the Virtuoso tidal logger (RBR), never reaches the water table at the nearest well (Lindy lower), wave runup must be significant as head exceeds the surface elevation on Sep. 7 – 8, 2019 (post-tropical storm) indicating that the station was inundated by the storm surge.

The results from the FFT performed on tidal cycles and coastal piezometers are presented in Figure 18 and Figure 19, respectively. Although FFT results are in frequencies, the discussion of results will be regarding their associated periods, as it is more intuitive. The tides exhibited both semi-diurnal and diurnal tidal signals but did not align with the frequencies of the major tidal constituents (M2, S2, N2, K1, O1, P1, Q1, and S1; Figure 18). Instead, the harbour tides were dominated by 11.83, 12.30, and 12.55 hr semi-diurnal signals in addition to 23.24, and 25.1 hr diurnal signals. Overall, the frequencies detected in the harbour were higher than major tidal constituents defined in the literature (Figure 18; Wolanski and Elliott, 2015); however, this may be due to the sampling frequency of the tidal logger (30 minutes). The semi-diurnal and diurnal signals can also be seen in the harbour sea level trends (Figure 17). Furthermore, the 14-day spring/neap tides can be observed in the tidal data (Figure 17), which are based on the synchronicity of the M2 and S2 tidal constituents (Parker, 2007).

The FFT of the coastal piezometers shows a dominance of low-frequency (long-period) signals (Figure 19). The strongest semi-diurnal signal was detected at Lindy lower (12.28 hr; Figure 19a), suggesting propagation of semi-diurnal tidal signals. The semi-diurnal signals decayed progressively with increased distance to the south harbour and Lindy upper piezometers (Figure 19b and Figure 19c, respectively), both of which exhibited a period of 11.92 hr and do not correlate with the frequency for the dominant semi-diurnal tide in the harbour. Lindy lower also displays a 23.68 hr diurnal signal which is not observed in the other coastal piezometers (Figure 19). The diurnal signal periods detected in the further wells do not correlate with the tidal data suggesting that it may be due to another process. It is also possible that the slight differences between the frequencies obtained from the FFT and the theoretical frequencies associated with the tidal constituents are an artifact of the data sampling intervals (15 minutes and 30 minutes for the piezometers and tidal logger, respectively).

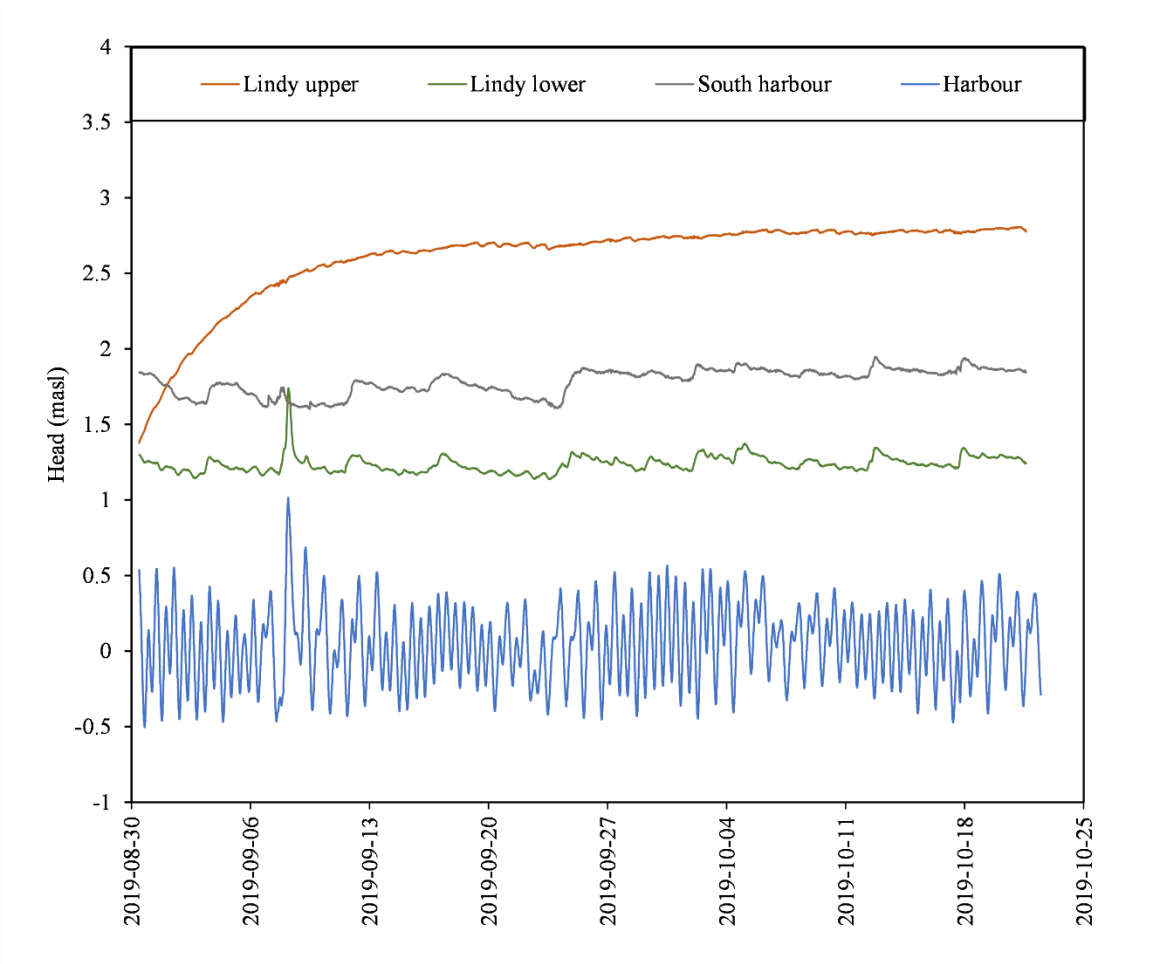

Figure 17: Coastal piezometer hydrographs (Lindy upper, Lindy lower, and south harbour; Figure 8) relative to mean sea level. Mean sea level was set to the mean stage observed in the Virtuoso tidal logger (RBR) during the study period. The effects of a post-tropical storm are evident on September 8, 2019, which resulted in the inundation of the Lindy lower piezometer.

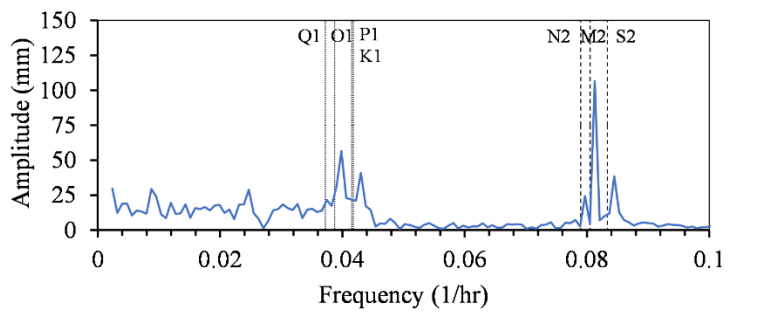

Figure 18: Results from fast Fourier transform analysis of tidal data over the piezometer instrumentation period (Aug. 30 - Oct. 21, 2019). Diurnal (Q1, O1, P1, K1) and semi-diurnal (N2, M2, and S2) tidal constituents (Wolanski and Elliot, 2015) do not align with the tidal signals observed in the harbour.

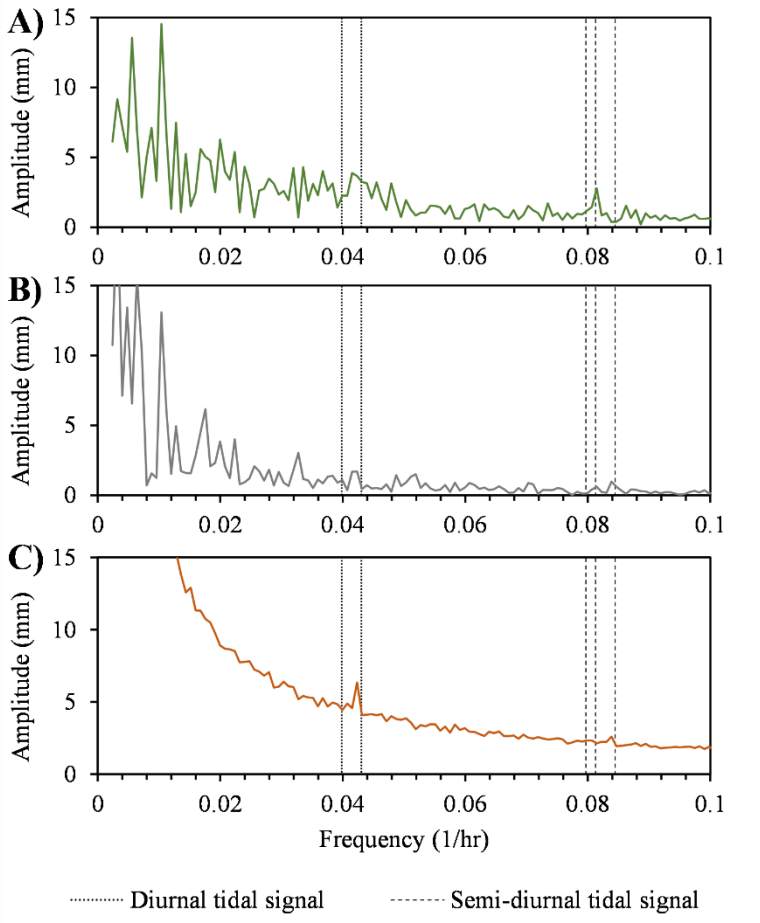

Figure 19: Results from fast Fourier transform analysis of the Lindy lower (A), south harbour (B), and Lindy upper (C) piezometers over the piezometer instrumentation period (Aug. 30 - Oct. 21, 2019). Diurnal and semi-diurnal signals observed in the tidal data are presented by dotted and dashed vertical lines, respectively.

2.3.3 Hydraulic Conductivity Estimates

A single bail test was conducted at Lindy lower and two at NE Mabou River. Figure A6 (Appendix IV) displays the fit between the straight-line method and the field data. The *K* estimates for silty glacial till and alluvium are presented in Table 4. The geometric mean was used to average the two NE Mabou River tests as *K* follows a log-normal distribution (i.e., *K*-distribution is bound by zero). As expected, the alluvium yielded a higher *K* estimate than the silty glacial till, but only by an order of magnitude. There was strong agreement between the Hvorslev and Jacob equations (Jacob, 1950; Hvorslev, 1951) for the glacial till (0.015 m d^{-1} vs. 0.021 m d^{-1}). Estimates for the silty glacial till are consistent with regional studies (Cann et al., 1963; Rivard et al., 2008; Rivard et al., 20012; SLR Consulting, 2015). The estimate for alluvium is relatively low within the generally accepted ranges cited in the literature (Domenico and Schwartz, 1990), but agrees with regional data (Rivard et al., 2008).

The *K* estimations from bail tests should be considered a lower bound due to the discrepancy commonly observed between slug/bail tests and larger scale tests (Butler Jr, 2019). This discrepancy may be due to numerous factors, including: 1) less well-development; 2) the influence of well construction on well recovery; 3) the small spatial coverage and sample volume may not capture larger scale features that influence *K*; and 4) the fact that common assumptions underlying conventional analysis techniques are often not adhered to with bail tests (Butler Jr, 2019). Well-construction is particularly important in moderate to high-*K* mediums because the recovery may be impeded if well radius or screen length is insufficient (Butler Jr, 2019). For instance, the 1” well-radius coupled with

a 7/8" datalogger could potentially have restricted flow to the upper portion of the well, resulting in an underestimation of *K* for the alluvium.

Table 4: K estimates for silty glacial till and alluvium based on the Hvorslev method for bail tests (1951) and the Jacob equation for tidal signal propagation (1950).

Piezometer	Overburden type	Estimated K [m d^{-1}]	Method
Lindy Lower	Silty glacial till	0.015	Hvorslev (1951)
Lindy Lower	Silty glacial till	0.021	Jacob (1950)
NE Mabou	Alluvium	0.38 ± 0.22	Hvorslev (1951)

2.3.4 Thermal Analysis

Figure 20a exhibits the simple regression models for the Mabou, NE Mabou, and SW Mabou Rivers based on air and water temperature data collected from June 20 to October 22, 2019. The simple regression models explain 81% - 83% of the variability in stream temperatures, as indicated by the coefficients of determinants (R^2). As indicated by the shallower slope (0.51), NE Mabou River has the greatest groundwater dominance, followed by the Mabou (0.77) and SW Mabou (0.99) Rivers. Similarly, the y-intercepts are 5.39°C, 4.12°C, and 3.27°C for the NE Mabou, Mabou, and SW Mabou Rivers, respectively, and are in agreement with the heirarchy of groundwater dominance inferred from the slopes of the simple regression models. Figure 20b exhibits the diel-variations in temperature between the three rivers. Based on the assumption that groundwater-dominated streams experience smaller diel-variation in temperature (Caissie, 2006), the trends presented in Figure 20b suggest the same heirarchy of groundwater-dominance between the three streams as indicated by the simple regression models.

Both the simple regression models and the diel-variations show that the SW Mabou River is strongly correlated with air temperature (slope = 0.99) indicating that the thermal regime is controlled by atmospheric heat fluxes. Although it is assumed that the regression relationship is controlled by groundwater inflows, it may be complicated by geomorpholigical conditions, such as the wider and shallower river channel observed in the SW Mabou River. For instance, wide, shallow channels would increase exposure to meteorological conditions. Conversely, the NE Mabou River has the most moderated temperature, presumably due to higher groundwater discharge. Limitations of assuming these different thermal characteristics are due exclusively to differing degrees of groundwater influence are discussed in section 2.4.1.2.

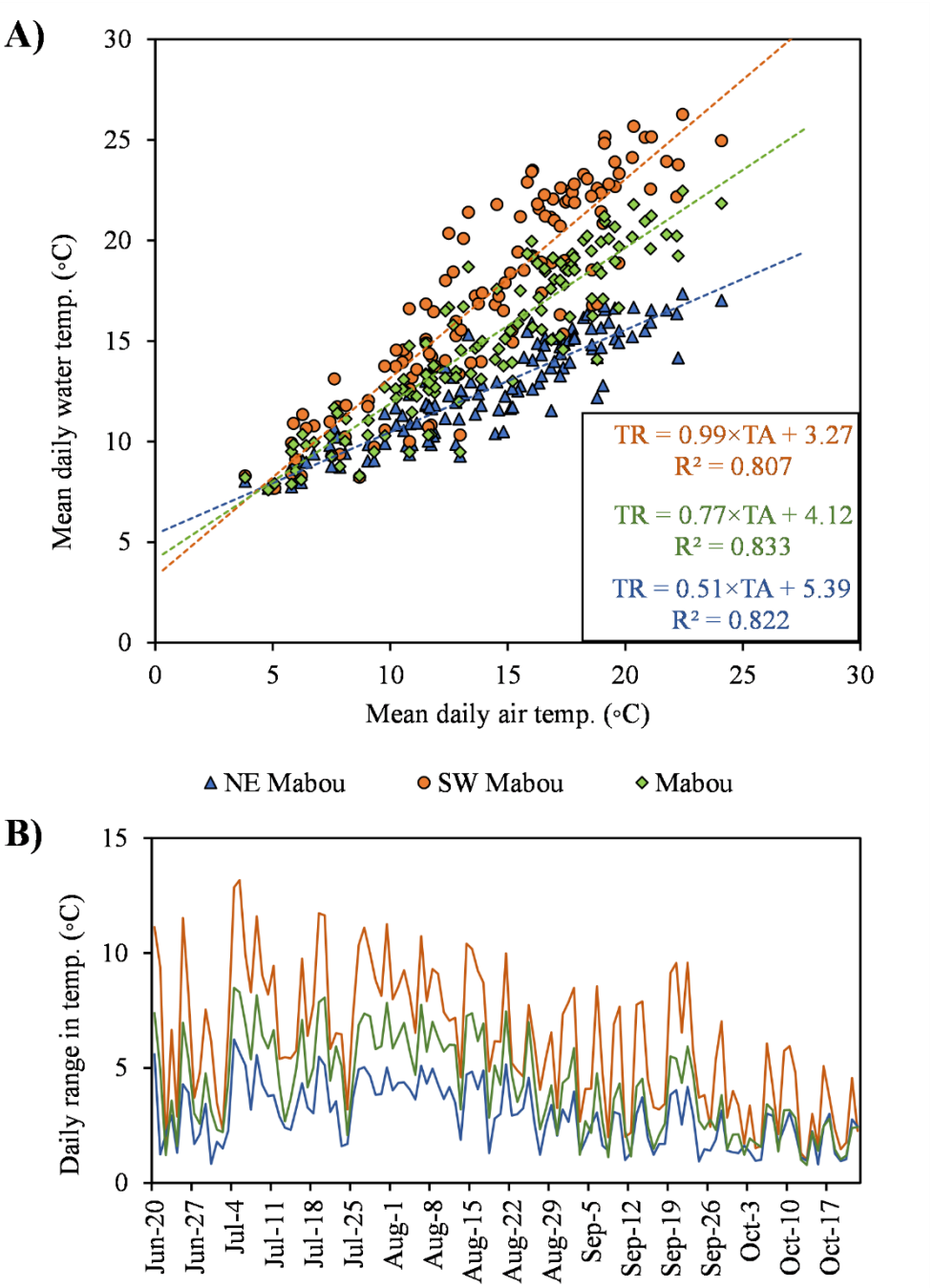

Figure 20: A) Simple regression models of stream temperatures for the Mabou, NE Mabou, and SW Mabou Rivers; and B) daily variations in water temperature for the Mabou, NE Mabou, and SW Mabou Rivers.

2.3.5 Seepage Meters

The seepage meter results are presented in Figure 21, and the summary of measured SGD fluxes are given in Table 5. The results are presented in Darcy fluxes for individual tidal cycles in addition to a storm surge lasting two tidal cycles. The mean fluxes observed at the different seepage meter stations varied by an order of magnitude. The maximum observed flux was 2.2×10^{-2} m d^{-1} (seepage meter 2) and the minimum was 3.1×10^{-4} m d^{-1} (seepage meter 3). Some sites showed strong variability between tidal cycles, which can be attributed to asymmetrical tides and potentially recharge following a precipitation event during tidal cycle 3 (Figure 21). Due to the storm surge, sampling was not possible; therefore, the storm data were collected over two tidal cycles and were excluded from the statistics. The mean Darcy flux and standard deviation for SGD among the four locations was $7.6\times10^{-3} \pm 6.9\times10^{-3}$. The large standard deviation (91% of mean flux) indicates strong heterogeneity in SGD; however, given the broad range of possible *K* values in such a heterogenous environment, which can be orders of magnitude different within the same sediment type, this variation in SGD is reasonable.

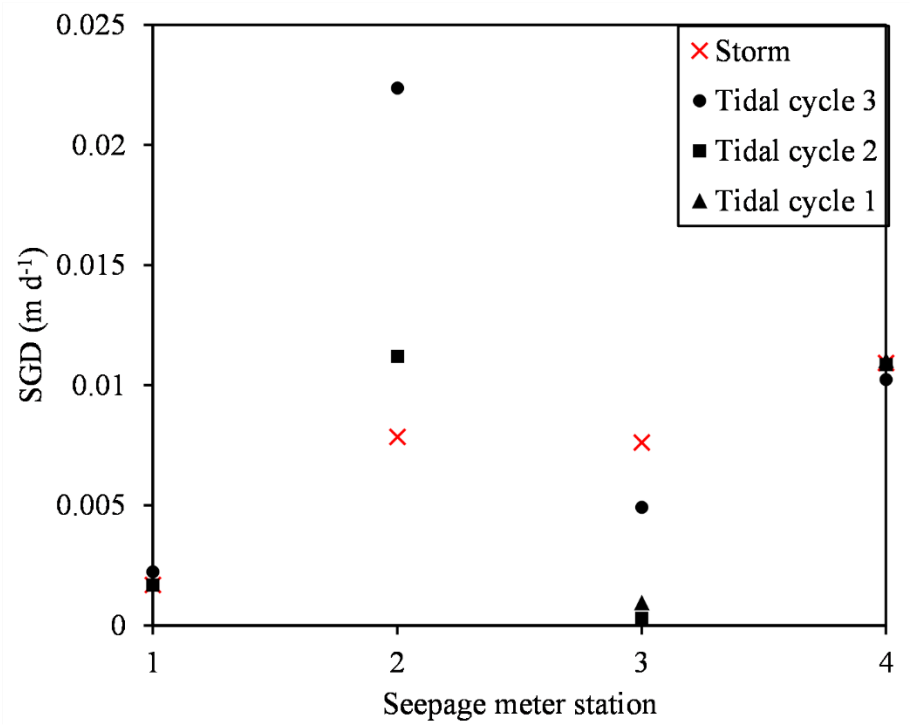

Figure 21: Seepage meter results over the three-tidal cycles (measured after each cycle) in addition to storm data (measured following two-tidal cycles)

Table 5: Summary of SGD results from the seepage meter study.

Seepage meter	Average SGD [m d^{-1}]
1	$1.9\times10^{-3} \pm 3.1\times10^{-4}$
2	$1.4\times10^{-2} \pm 7.6\times10^{-3}$
3	$3.5\times10^{-3} \pm 3.4\times10^{-3}$
4	$1.1\times10^{-2} \pm 3.6\times10^{-4}$
All seepage meters	$7.4\times10^{-3} \pm 6.0\times10^{-3}$

2.3.6 Water Balance

The precipitation and hydrometric data, along with the hydrograph analysis were used to estimate the evapotranspiration, runoff, and recharge for the Mabou River and NE Mabou River watersheds. Table 6 presents the water balance components over the field season in addition to estimates for the off-season. Surface runoff and groundwater

discharge were calculated by normalizing the respective discharge estimates [m^3 yr^{-1}] with the drainage area [m^2]. Due to the uncertainty associated with the extrapolation of seasonal data, only results from the field-season will be discussed in this section. The off-season and annual estimates are intended for model calibration (Section 3.2.3.3). The Q_G/P ratios provide insight into recharge conditions; the NE Mabou watershed was the most groundwater dominant, with an estimated recharge coefficient (assumed equal to Q_G/P) of 45% compared to 23% in the Mabou River watershed. *ET* was calculated by subtracting streamflow ($Q_R + Q_G$) from *P*. The estimated *ET* was 15% higher in the Mabou River watershed compared to the NE Mabou River watershed, and both *ET* estimates are within the potential *ET* (*PET*) over the field season calculated by the Penman – Monteith equation (0.425 m; Appendix I).

Table 6: Water balance for the Mabou River and NE Mabou River watersheds segmented into seasonal and annual periods. Off-season Q_G (Jan. 1 - May 5, 2019, Oct. 22 - Dec. 31, 2019) was estimated (est.) based on temporal patterns observed in Nova Scotia watersheds (Appendix I).

	P [m]	Q_R [m]	Q_G [m]	ET [m]	Q_R/P [%]	Q_G/P [%]	BFI
Mabou River							
Field-season	0.65	0.18	0.15	0.32	27	23	0.46
Off-Season (est.)	*0.87*	*0.34*	*0.31*	*0.22*	*39*	*36*	*0.48*
Annual (est.)	*1.52*	*0.52*	*0.46*	*0.54*	*33*	*30*	*0.47*
NE Mabou River							
Field-season	0.65	0.14	0.29	0.22	21	45	0.68
Off-season (est.)	*0.87*	*0.31*	*0.46*	*0.11*	*35*	*53*	*0.60*
Annual (est.)	*1.52*	*0.45*	*0.75*	*0.33*	*28*	*50*	*0.63*

2.4 DISCUSSION & CONCLUSION

2.4.1 Groundwater – Surface Water Interactions

2.4.1.1 Ocean – Aquifer Interactions

The head observations in coastal piezometers in addition to the FFT analysis provides insight into the connectivity between the coastal aquifer and ocean (Figure 17; Figure 18; Figure 19). Limited propagation of tidal signals indicates that the coastal aquifer has low-diffusivity and connectivity with the harbour; however, the two systems are hydraulically connected as displayed by the rapid increase in head when Lindy lower was inundated during a post-tropical storm (Figure 17). This limited tidal influence on the aquifer may result in a relatively small upper saline plume due to tidal forcing (Robinson et al., 2006), and thus a narrow coastal mixing zone (CMZ) between the fresh and saline groundwater. The location and geometry of the CMZ is typically dependent on fresh recharge, *K*, tidal range, and sea level, such that the width has been reported to vary from <1 m to kilometers (Robinson et al., 1998; Slomp and Van Cappellen, 2004; Robinson et al., 2006). It is also conceivable that the relatively low-*K* and steep hydraulic gradient compared to other coastal aquifers would affect the landward extent of the CMZ. For instance, a steep gradient would limit the horizontal extent of infiltration due to gradient reversals during high tides (Figure 22). In addition to the lack of tidal influence, freshwater conditions observed at Lindy lower and Lindy upper suggest that the CMZ does not extend significantly beyond the intertidal zone; however, the seaward extent is unknown. Modelling and field studies of strongly confined coastal aquifers yield mixing zones on the scale of kilometers during periods of transgression (Groen et al., 2000; Kooi et al., 2000; Kooi and Groen, 2001). Presumably, in such circumstances, the coastline transgression is

more rapid than saline recharge or diffusion, resulting in a lagging saltwater wedge. In the Mabou Harbour drainage basin, *K* for the local glacial sediments and shallow bedrock (Appendix IV) are within two orders of magnitude suggesting that the shallow bedrock aquifer is not strongly confined; therefore, it is unlikely that there is disequilibrium between the saltwater interface and the current coastline location resulting in a relatively narrow CMZ.

The relatively low magnitude of SGD observed in the harbour, relative to values cited in the literature (Taniguchi et al., 2002), indicates a low degree of ocean – aquifer connectivity in Mabou Harbour. The higher magnitude SGD fluxes reported in the literature may be due to research bias towards coastlines with conditions facilitating greater SGD fluxes; therefore, this study may be more applicable to coastal watersheds in low-permeability environments. It is also plausible that the decreased aquifer connectivity and response to tidal cycles would result in a disproportionately small amount of circulated seawater due to the reduced effect of tidal pumping. Future research could focus on the effects of low-permeability environments on SGD processes, such as tidal pumping.

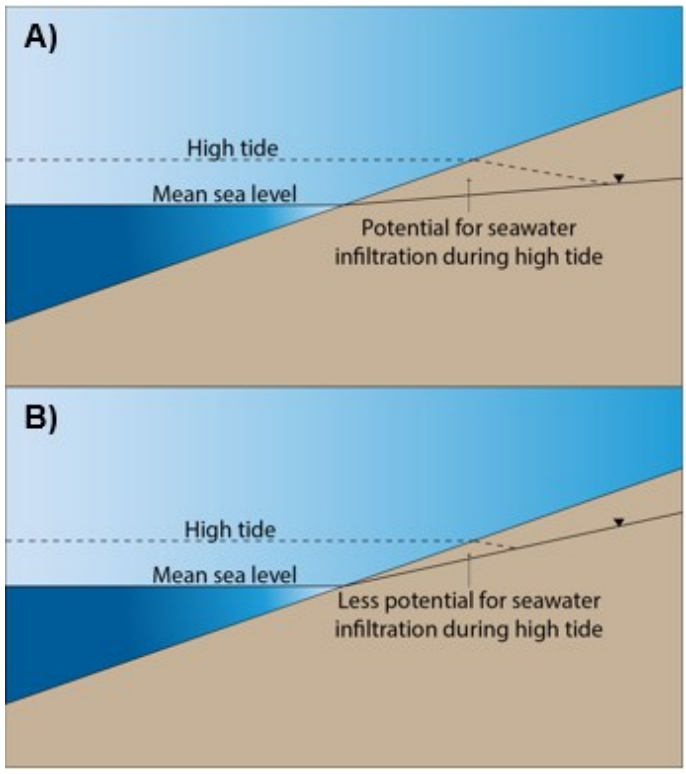

Figure 22: Potential effects of hydraulic gradient on seawater infiltration and landward migration during high tide gradient reversals. A) Shallow hydraulic gradient; B) steep hydraulic gradient, such as observed in Mabou. Low hydraulic conductivity in the coastal aquifer would also impact the landward infiltration of seawater during high tide.

2.4.1.2 Stream – Aquifer Interactions

Both the Mabou and NE Mabou Rivers displayed strong stream-aquifer connectivity, due to the permeable alluvial material in the fluvial valleys. The head-observations from floodplain piezometers, relative to stream stage, offers insight into the groundwater dynamics during high and low streamflow periods. Piezometer and hydrometric data also yield insight into aquifer response during precipitation events. The data from the Mabou River suggests that bank storage occurs during high streamflow events and within close proximity to riverbanks. Alternatively, the data from NE Mabou River exhibited increasing hydraulic gradients and elevated piezometer heads relative to

stage, which suggests that bank storage, if any is minimal. Overall, bank storage within the drainage basin appears to be narrow, thus having a limited impact on river nutrient levels.

Allen et al. (2010) categorized aquifer-stream systems into two types, direct recharge-driven and stream-driven. Direct recharge-driven systems are those in which groundwater is recharged solely by precipitation, and groundwater discharges into streams predominantly during periods of low flow. In stream-driven systems, groundwater exchange between aquifer and streams is bilateral and depends on stream stage. Major streams/rivers are often categorized as stream-driven (Allen et al., 2010). Although the NE Mabou and Mabou Rivers are major streams within the drainage basin, they behave more as direct-recharge driven systems likely due to their incised geomorphology. For instance, a deeply incised river would be surrounded by highlands with aquifers elevated relative to the river. Conversely, the data for the Mabou river does suggest that indirect recharge from the river occurs during high streamflows. A possible implication of direct-recharge driven aquifer systems in the Mabou Harbour drainage basin is that the denitrification associated with bank storage could be limited.

Both the thermal and hydrometric data indicate that the NE Mabou River is the most groundwater-dominated, followed by the Mabou River and SW Mabou River. One limitation of the thermal analysis is that the reach for the NE Mabou River is smaller than the Mabou and SW Mabou Rivers, which could have an impact on the comparative analysis of groundwater dominance. For instance, groundwater discharge becomes less dominant downstream from headwaters where streamflow is greater and exposed to a greater degree of meteorological conditions (Caissie, 2006). There may be other variables responsible for

the thermal regime of the SW Mabou River that are not related to groundwater contribution. For example, the shallow and wide fluvial channel would result in greater river temperatures (Mosley, 1983), presumably due to efficient heat transfer between the lower atmosphere and river surface; however, the comparative study of simple regression models does agree with the more quantitative evaluation of normalized baseflows.

2.4.2 Implications for Contaminant Transport

Water quality sampling (Appendix II) has indicated that groundwater is impacted by agricultural activities and potentially point sources of pollution, such as wastewater treatment and septic systems. Furthermore, the high *E. coli* and total coliform levels detected in the Farm Spring at baseflow conditions (Appendix II, Table A11) suggest that GSIs may play a role in microbial contamination of surface water bodies. Similarly, *E. coli* and total coliform loads of variable concentrations have been detected in the major rivers, with the maximum *E. coli* load sampled at baseflow conditions in the SW Mabou River; however, the possibility of the contaminant source being introduced directly into the stream network should not be ignored.

The temporal variations in GSIs may impact contaminant levels in surface water bodies. For instance, bank storage influences contaminant levels, particularly nutrients, within watercourses (Duff and Triska, 1990; Triska et al., 1993). For instance, bank storage increases residence time within riparian zones that support natural denitrification processes (Rassam, 2008). Groundwater sampling from the NE Mabou riparian zone shows that the shallow groundwater is relatively low in dissolved oxygen (25% DO), in comparison to the other groundwater samples, and high in dissolved organic carbon (DOC; Appendix II),

which acts as the primary electron donor in the reduction of nitrate (Tesoriero et al., 2000). It should be noted that groundwater sampling followed a recharge event that may have temporarily increased DO in the shallow groundwater. Anoxic conditions, possibly due to the oxidation and decay of organic material, combined with high organic carbon content, are ideal for rapid denitrification (Tesoriero et al., 2000). The extent and residence time of bank storage, however, has implications for nitrate levels. Nitrification occurs in the aerobic zone of the riparian banks nearest the stream, and denitrification occurs deeper into the riparian zone where conditions are anaerobic (Shuai et al., 2017). The shallow penetration of bank storage observed in the Mabou and NE Mabou Rivers, with limited residence time, may not support denitrification as the infiltrated river water may not spend sufficient time in the anaerobic zone of the floodplain. Therefore, the limited amount of bank storage in the Mabou and NE Mabou river-aquifer systems suggests that this nitrate buffering process may be ineffective in this drainage basin.

The chemical conditions and residence time within CMZs will also influence the denitrification of discharging groundwater (Slomp and Van Cappellen, 2004). As suggested by the local conditions at the Lindy station, both the aquifer and the seawater in Mabou Harbour are oxic, and nitrate may transport more conservatively while phosphorus would be largely removed (Slomp and Van Cappellen, 2004). The resulting nitrate to phosphorus ratio of the associated discharge may be high. Furthermore, the relatively small saline upper plume and narrow mixing zone associated with limited tidal influence (Robinson et al., 2007) may further reduce residence time and thus the efficacy of any denitrification occurring in the mixing zone. A higher ratio of fresh/saline SGD, due to the potentially reduced effectiveness of tidal pumping, may result in less dilution of

contaminant loads entering the shallow marine environment. Greater nutrient concentrations may have larger impacts on local scales, especially if the water column is not well-mixed.

REFERENCES: CHAPTER 2

Abarca, E., Karam, H., Hemond, H. F., & Harvey, C. F. (2013). Transient groundwater dynamics in a coastal aquifer: The effects of tides, the lunar cycle, and the beach profile. *Water Resources Research, 49*(5), 2473-2488.

Allen, D. M., Whitfield, P.H., & Werner, A. (2010). Groundwater level responses in temperate mountainous terrain: Regime classification and linkages to climate and streamflow. *Hydrological Processes, 24*, 3392–3412.

Arnold, J. G., Allen, P. M., Muttiah, R., & Bernhardt, G. (1995). Automated base flow separation and recession analysis techniques. *Groundwater, 33*(6), 1010-1019.

Arnold, J. G., & Allen, P. M. (1999). Automated methods for estimating baseflow and ground water recharge from streamflow records. *Journal of the American Water Resources Association, 35*(2), 411-424.

Barr, S. M., White, C. E., Fisher, B. E., McKinnon, J. S., Barras, A. L., & Hapgood, D. S. (2017). *DP ME 433, version 1, 2017. Digital geological data generated as part of the bedrock geological mapping compilation project for Cape Breton Island, Nova Scotia.* Nova Scotia Department of Natural Resources, Geoscience and Mines Branch.

Brodie, R. S., & Hostetler, S. (2005). A review of techniques for analysing baseflow from stream hydrographs. *Proceedings of the NZHS-IAH-NZSSS 2005 conference* (Vol. 28). Auckland New Zealand.

Butler Jr, J. J. (2019). *The design, performance, and analysis of slug tests* (2nd Edition). CRC Press. Boca Raton, FL.

Caissie, D. (2006). The thermal regime of rivers: A review. *Freshwater biology, 51*(8), 1389-1406.

Cann, D. B., MacDougall, J. I., & Hilchey, J. D. (1963). Soil survey of Cape Breton Island Nova Scotia. Canada Department of Agriculture and Nova Scotia Department of Agriculture and Marketing.

Di Baldassarre, G., & Claps, P. (2011). A hydraulic study on the applicability of flood rating curves. *Hydrology Research, 42*(1), 10-19.

Domeneghetti, A., Castellarin, A., & Brath, A. (2012). Assessing rating-curve uncertainty and its effects on hydraulic model calibration. *Hydrology and Earth System Sciences, 16*(4), 1191.

Domenico, P. A., & Schwartz, F. W., (1990). *Physical and Chemical Hydrogeology*. John Wiley & Sons, New York.

Duff, J. H., & Triska, F. J. (1990). Denitrifications in sediments from the hyporheic zone adjacent to a small forested stream. *Canadian Journal of Fisheries and Aquatic Sciences, 47*(6), 1140-1147.

Dugdale, S. J., Malcolm, I. A., Kantola, K., & Hannah, D. M. (2018). Stream temperature under contrasting riparian forest cover: Understanding thermal dynamics and heat exchange processes. *Science of The Total Environment, 610*, 1375-1389.

Duque, C., Russoniello, C. J., & Rosenberry, D. (2020). History and evolution of seepage meters for quantifying flow between groundwater and surface water: Part 2–Marine settings and submarine groundwater discharge. *Earth-Science Reviews*, 103168.

Ferris, J. G. (1952). *Cyclic fluctuations of water level as a basis for determining aquifer transmissibility* (No. Note 1). US Geological Survey Ground Water Notes.

Frigo, M., & Johnson, S. G. (1998). FFTW: An adaptive software architecture for the FFT. *Proceedings of the 1998 IEEE International Conference on Acoustics, Speech and Signal Processing, ICASSP'98 (Cat. No. 98CH36181)* (Vol. 3, pp. 1381-1384). IEEE.

Groen, J., Velstra, J., & Meesters, A. G. C. A. (2000). Salinization processes in paleowaters in coastal sediments of Suriname: Evidence from δ37Cl analysis and diffusion modelling. *Journal of Hydrology, 234*(1-2), 1-20.

Han, P. F., Wang, X. S., Wan, L., Jiang, X. W., & Hu, F. S. (2019). The exact groundwater divide on water table between two rivers: A fundamental model investigation. *Water, 11*(4), 685.

Hannula, S. R., Esposito, K. J., Chermak, J. A., Runnells, D. D., Keith, D. C., & Hall, L. E. (2003). Estimating ground water discharge by hydrograph separation. *Groundwater, 41*(3), 368-375.

Hiscock, K., & Bense, V. F. (2014). *Hydrogeology: Principles and practice* (Second ed.). Chichester, West Sussex, UK: Hoboken, New Jersey: John Wiley & Sons.

Hvorslev, M. J. (1951). *Time lag and soil permeability in ground-water observations* (No. 36). Waterways Experiment Station, Corps of Engineers, US Army.

Jacob, C. E. (1950). Flow of groundwater. In H. Rouse (Ed.), *Engineering hydraulics* (pp. 321–386). Hoboken, NY: John Wiley & Sons.

Johannes, R. E. (1980). The ecological significance of the submarine discharge of groundwater. *Marine Ecology Progress Series*, 365-373.

Kelleher, C., Wagener, T., Gooseff, M., McGlynn, B., McGuire, K., & Marshall, L. (2012). Investigating controls on the thermal sensitivity of Pennsylvania streams. *Hydrological Processes, 26*(5), 771-785.

Kooi, H., Groen, J., & Leijnse, A. (2000). Modes of seawater intrusion during transgressions. *Water Resources Research*, *36*(12), 3581-3589.

Kooi, H., & Groen, J. (2001). Offshore continuation of coastal groundwater systems; predictions using sharp-interface approximations and variable-density flow modelling. *Journal of Hydrology, 246*(1-4), 19-35.

Lee, D. R. (1977). A device for measuring seepage flux in lakes and estuaries. *Limnology and Oceanography*, *22*(1), 140–147.

Macan, T. T. (1958). The temperature of a small stony stream. *Hydrobiologia, 12*(2-3), 89-106.

Mackey, A. P., & Berrie, A. D. (1991). The prediction of water temperatures in chalk streams from air temperatures. *Hydrobiologia, 210*(3), 183-189.

Mau, D. P., & Winter, T. C. (1997). Estimating ground-water recharge from streamflow hydrographs for a small mountain watershed in a temperate humid climate, New Hampshire, USA. *Groundwater, 35*(2), 291-304.

Mayer, T. D. (2012). Controls of summer stream temperature in the Pacific Northwest. *Journal of Hydrology, 475*, 323-335.

Michael, H. A., Lubetsky, J. S., & Harvey, C. F. (2003). Characterizing submarine groundwater discharge: A seepage meter study in Waquoit Bay, Massachusetts. *Geophysical Research Letters*, *30*(6).

Mosley, M. P. (1983). Variability of water temperatures in the braided Ashley and Rakaia rivers. *New Zealand Journal of Marine and Freshwater Research, 17*(3), 331-342.

Nathan, R. J., & McMahon, T. A. (1990). Evaluation of automated techniques for base flow and recession analyses. *Water Resources Research, 26*(7), 1465-1473.

Nova Scotia Department of Environment. (2018). *1:10,000 watersheds for Nova Scotia*.

Nova Scotia Department of Lands and Forestry. (2020). *Nova Scotia topographic database*.

Parker, B.B. (2007) *Tidal analysis and prediction*. Silver Spring, MD, NOAA NOS Center for Operational Oceanographic Products and Services (NOAA Special Publication NOS CO-OPS 3).

Petersen-Øverleir, A. (2004). Accounting for heteroscedasticity in rating curve estimates. *Journal of Hydrology, 292*(1-4), 173-181.

Rantz, S. E. (1982). *Measurement and computation of streamflow* (Vol. 2175). US Department of the Interior, US Geological Survey.

Rassam, D. W., Pagendam, D. E., & Hunter, H. M. (2008). Conceptualisation and application of models for groundwater-surface water interactions and nitrate attenuation potential in riparian zones. *Environmental Modelling and Software*, *23*(7), 859–875.

Rivard, C., Paniconi, C., Gauthier, M. J., François, G., Sulis, M., Camporese, M., Larocque, M., & Chaumont, D. (2008). A modeling study of climate change impacts on recharge and surface–groundwater interactions for the Thomas Brook catchment (Annapolis Valley, Nova Scotia). In *Proceedings of GeoEdmonton, Canadian Geotechnical Society–International Association of Hydrogeologists–Canadian National Chapter Joint Annual Conference, Edmonton, Canada*.

Rivard, C., Paradis, D., Paradis, S., Bolduc, A., Morin, R. H., Liao, S., Pullan, S., Gauthier, M. J., Trepanier, S., Blackmore, A., Spooner, I., Deblonde, C., Fernandes, R., Castonguay, S., Hamblin, T., Michaud, Y., Drage, J., & Paniconi, C. (2012). Canadian groundwater inventory: Regional hydrogeological characterization of the Annapolis-Cornwallis Valley aquifers. *Geological Survey of Canada, Bulletin, 598*.

Rivard, C., Lefebvre, R., Paradis, D. (2014). Regional recharge estimation using multiple methods: An application in the Annapolis Valley, Nova Scotia (Canada). *Environmental Earth Sciences, 71*, 1389-1408.

Robinson, C., Gibbes, B., & Li, L. (2006). Driving mechanisms for groundwater flow and salt transport in a subterranean estuary. *Geophysical Research Letters, 33*(3).

Robinson, C., Li, L., & Barry, D. A. (2007). Effect of tidal forcing on a subterranean estuary. *Advances in Water Resources*, *30*(4), 851-865.

Robinson, M., Gallagher, D., & Reay, W. (1998). Field observations of tidal and seasonal variations in ground water discharge to tidal estuarine surface water. *Groundwater Monitoring & Remediation, 18*(1), 83-92.

Service Nova Scotia and Municipal Relations (Service NS). (2003). Enhanced digital elevation model, Nova Scotia, Canada. Service Nova Scotia and Municipal Relations, Registry and Information Management Services, Nova Scotia, Canada.

Shuai, P., Cardenas, M. B., Knappett, P. S., Bennett, P. C., & Neilson, B. T. (2017). Denitrification in the banks of fluctuating rivers: The effects of river stage amplitude, sediment hydraulic conductivity and dispersivity, and ambient groundwater flow. *Water Resources Research, 53*(9), 7951-7967.

Slomp, C. P., & Van Cappellen, P. (2004). Nutrient inputs to the coastal ocean through submarine groundwater discharge: Controls and potential impact. *Journal of Hydrology, 295*(1–4), 64–86.

SLR Consulting. (2015). *Proposed Black Point Quarry project Guysborough County, Nova Scotia: Hydrogeological technical report*.

Smith, K. (1981). The prediction of river water temperatures/prédiction des températures des eaux de rivière. *Hydrological Sciences Journal, 26*(1), 19-32.

Sophocleous, M. (2002). Interactions between groundwater and surface water: The state of the science. *Hydrogeology Journal, 10*(1), 52-67.

Stea, R. R., Conley, H., Brown, Y., & Fisher, B. E., (2006). *DP ME 36, Version 2, 2006. Digital version of Nova Scotia Department of Natural Resources map ME 1992-3, Surficial geology map of the province of Nova Scotia, 1:500 000*. Nova Scotia Department of Natural Resources, Mineral Resources Branch.

Taniguchi, M., Burnett, W. C., Cable, J. E., & Turner, J. V. (2002). Investigation of submarine groundwater discharge. *Hydrological Processes, 16*(11), 2115-2129.

Tesoriero, A. J., Liebscher, H., & Cox, S. E. (2000). Mechanism and rate of denitrification in an agricultural watershed: Electron and mass balance along groundwater flow paths. *Water Resources Research, 36*(6), 1545-1559.

Todd, G. K., (1995). Groundwater flow in relation to the flooding stream. *Proceedings of the American Society of Civil Engineers, 81*(628), 20-28.

Torgersen, C. E., Faux, R. N., McIntosh, B. A., Poage, N. J., & Norton, D. J. (2001). Airborne thermal remote sensing for water temperature assessment in rivers and streams. *Remote Sensing of Environment, 76*(3), 386-398.

Trglavcnik, V., Morrow, D., Weber, K. P., Li, L., & Robinson, C. E. (2018). Analysis of tide and offshore storm-induced water table fluctuations for structural characterization of a coastal island aquifer. *Water Resources Research, 54*, 2749–2767.

Triska, F. J., Duff, J. H., & Avanzino, R. J. (1993). The role of water exchange between a stream channel and its hyporheic zone in nitrogen cycling at the terrestrial—aquatic interface. In *Nutrient dynamics and retention in land/water ecotones of Lowland, Temperate Lakes and Rivers* (pp. 167-184). Springer, Dordrecht.

Türker, Y. (1969). *Short term variation of runoff-rainfall ratios in Nova Scotia IHD watersheds*. Dalhousie University.

Wang, S. L., Chen, C. T. A., Huang, T. H., Tseng, H. C., Lui, H. K., Peng, T. R., Kandasamy, S., Zhang, J., Yang, L., Gao, X., Lou, J. Y., Kuo F. W., Chen, X. G., Ye, Y., & Lin, Y. J. (2018). Submarine groundwater discharge helps making nearshore waters heterotrophic. *Scientific Reports, 8*(1), 1-10.

Wolanski, E., & Elliot, M. (2015). *Estuarine ecohydrology – An introduction* (2nd Edition). Elsevier.

Younger, P. L. (1993). Simple generalized methods for estimating aquifer storage parameters. *Quarterly Journal of Engineering Geology, 26*, 7-135

Zwieniecki, M. A., & Newton, M. (1999). Influence of streamside cover and stream features on temperature trends in forested streams of western Oregon. *Western Journal of Applied Forestry, 14*(2), 106-113.

Chapter 3: Numerical Modelling of Regional - Scale Groundwater-Surface Water Interactions and Flow Paths

3.1 Introduction

Numerical groundwater models are powerful hydrogeological tools that provide insight into the dynamics and functioning of a groundwater system. Prior to the 1950's, analytical methods were the primary tool for solving hydraulic problems, but it was realized that something needed to be developed to address how a groundwater system would respond to stresses on a large-scale (Bredehoeft, 2002). Currently, there is a variety of mathematical models, each with their own benefits and disadvantages. The greatest advantage of modern groundwater modelling systems is that they facilitate quantitative analysis of groundwater systems, including interpretive, predictive, and hindcasting applications (Anderson, 2015a). Furthermore, models are also versatile regarding scale, dimensions, and processes. A disadvantage of groundwater models is that they often fail to capture the heterogeneity and anisotropy inherent in groundwater systems. Some model developers overparameterize models in an attempt to capture geological complexities (Voss 2011a; Voss 2011b), which may result in a better fit to field observations but a poor representation of the dynamics of the groundwater system.

Numerical groundwater models are also becoming an increasingly popular method for assessing groundwater-surface water interactions (GSIs and Fleckenstein et al., 2010; Scibek et al., 2007; Bailey et al., 2016; Russoniello et al., 2016). This is particularly true when variations on larger spatiotemporal scales are of interest (e.g., Scibek et al., 2007;

Bailey et al., 2016). Numerical models can also be used to investigate the relationships between nutrient transport and topographical characteristics of riparian zones (Schilling et al., 2006). Groundwater flow models also offer insight into the flow paths and residence times of discharging groundwater, which can have profound effects on nutrient and microbial concentrations, respectively.

In this study, a simplified three-dimensional, steady-state groundwater flow model was constructed to analyze spatiotemporal trends in flow paths and GSIs. The resulting flow paths, residence times, and spatial distribution of groundwater discharge were then used to further evaluate harbour contamination risks via groundwater-borne nutrient and microbial contaminants. The significance of direct and indirect groundwater discharge on harbour water quality were evaluated.

3.2 METHODOLOGY

3.2.1 Conceptual Model

The development of a conceptual model is imperative to the modelling process and is used to inform model construction and evaluation, as well as interpretation (Tóth, 1970). This section outlines the conceptual model for the Mabou Harbour drainage basin based on literature review, field data and observations, secondary data, and the analysis of geographical information system (GIS) data (e.g., SNSMR, 2003; Stea et al., 2006; Barr et al., 2018; Nova Scotia Department of Environment, 2018; Drage and McKinnon, 2019; Nova Scotia Department of Lands and Forestry, 2020).

The local groundwater regime is expected to dominate the system due to the steep relief within the drainage basin and extensive surface water network (Tóth, 1963). Intermediate and deep groundwater flow regimes will discharge into the larger, deeply incised rivers as baseflow and into the harbour as submarine groundwater discharge (SGD; Figure 1; Figure 23). Recharge is expected to be primarily controlled by the overburden type (Healy and Scanlon, 2010), which is highly heterogeneous in the drainage basin. The overburden will effectively store the infiltrated water while the bedrock is recharged, and the excess will discharge into local watercourses. For longer periods (i.e., year[s]), this change in storage will be negligible and recharge to the groundwater system is discharged as baseflow or SGD. Increased recharge will occur in the coarse surficial sediments found in the region, such as alluvium, colluvium and residuum (Stea et al., 2006), where infiltration and storage are greater. Karst features, which are prevalent in the Mabou Harbour drainage basin (Baechler and Broehner, 2014; Drage and McKinnon, 2019), may

also influence recharge to bedrock aquifers, and recharge coefficients (Allocca, et al., 2014). Fine-grained, low-*K* glacial sediments dominate the landscape surface (Stea et al., 2006; Figure 5), confining the fractured bedrock aquifers. The overburden is discontinuous or thinned in areas where outcropping occurs (Stea et al., 2006). Fracturing is expected to be extensive due to the site's location within the Hollow fault – Aspy fault zone (Baechler, 2015). Secondary permeability, due to fracturing and karstification, will dominate the bulk hydraulic conductivity (*K*) in the shallow bedrock and be less pervasive with depth (Jiang et al, 2009; Rempe and Dietrich, 2014). Coarse surficial sediments will be predominantly located on alluvial plains in the highlands and lowland valley bottoms, and colluvium at the toe of steep slopes (Grant, 1994). These coarse sediments will act as discharge zones for deeper aquifers facilitating lateral flow to the rivers (Speiran, 2010). The benthic sediments of the harbour likely consist of organic mud, in addition to silt, and clay, resulting in a reduced SGD flux. This conceptual model generally agrees with others for fractured bedrock aquifers (e.g., Banks et al., 2009; Welch and Allen, 2014) and coastal watersheds found in the literature (e.g., Barazzuoli et al., 2008; Han et al., 2012).

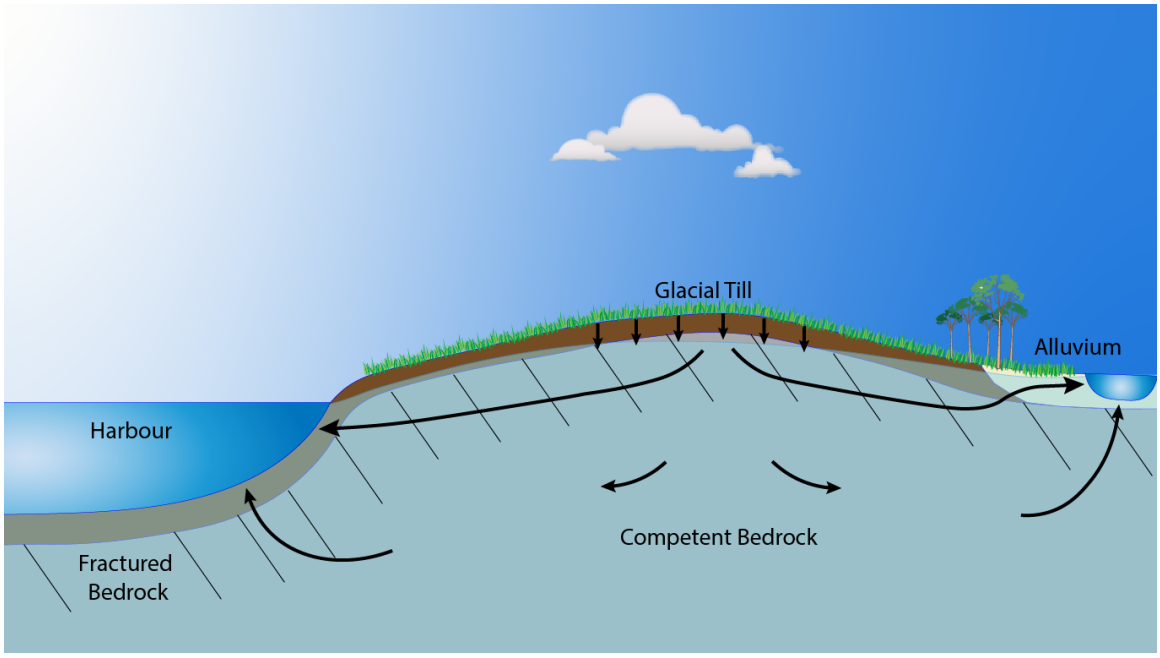

Figure 23: A conceptual model of the groundwater system where majority of flow occurs in shallow bedrock and alluvial aquifers.

3.2.2 Model Development

A steady state, three-dimensional groundwater flow model was constructed using a combination of ArcMap™ (ESRI, 2016), MODFLOW (Harbaugh, 2005; Niswonger et al., 2011), and ModelMuse™ (Winston, 2020) software. ModelMuse™ is an open-source graphical user interface created by the U.S. Geological Survey (USGS). The groundwater flow model is built on a simplified geological model derived from bedrock and surficial geology maps.

3.2.2.1 Governing Equation

Variable-density models are typically employed in coastal groundwater models (e.g., Thompson et al., 2006; Watson et al., 2010; Webb and Howard, 2011); however, given that the contaminants under investigation are terrestrially sourced, this study is only

concerned with fresh SGD (FSGD). The governing equation for the simulation of three-dimensional flow of constant-density groundwater is:

$$\frac{\partial}{\partial x}\left(K_x \frac{\partial h}{\partial x}\right) + \frac{\partial}{\partial y}\left(K_y \frac{\partial h}{\partial y}\right) + \frac{\partial}{\partial z}\left(K_z \frac{\partial h}{\partial z}\right) + W = S_S \frac{\partial h}{\partial t} \quad (6)$$

where K_x, K_y, K_z are hydraulic conductivity (K) in the x,y,z directions [m d^{-1}], respectively, h is head [m], W is the volumetric flux per unit volume of sources/sinks [d^{-1}], and S_S is specific storage [m^{-1}] (Psilovikos, 2006). Simply put, the left-hand side of the equation represents negative divergences of fluxes and a source/sink term while the right-hand side represents transient storage effects.

3.2.2.2 Model Selection

MODFLOW-NWT (Niswonger et al., 2011), a Newton-Raphson formulation of MODFLOW-2005 (Harbaugh, 2005), was the code selected for this modelling exercise. MODFLOW-2005 is a USGS open-source finite difference numerical groundwater model (Harbaugh, 2005) that has been widely used for a variety of groundwater related investigations (Prommer et al., 2003; Langevin et al., 2006; Lautz and Siegel, 2006; Brunner et al., 2010). MODFLOW-NWT was created to improve the abilities of MODFLOW when applied to unconfined aquifers and GSIs by solving issues associated with non-linearities of the unconfined groundwater flow equation, which are associated with drying and rewetting of cells (Niswonger et al., 2011). MODFLOW-2005 employs the Picard method to solve nonlinear equations related to unconfined aquifers and non-linear boundary conditions (Niswonger et al., 2011). The Picard method is an iterative process of solving non-linear equations where a solution is approximated and used in the subsequent iteration, thereby increasing accuracy. MODFLOW-NWT is used with the

Upstream Weighting Package (UPW) to calculate the discretized groundwater-flow equation (Niswonger et al., 2011). UPW differs from other approaches in how it calculates intercell conductance for cells with temporally variable transmissivity in addition to allowing dry cells to remain active (Niswonger et al., 2011).

3.2.2.3 Model Domain

The extents of the model domain were based on the boundaries of the Mabou Harbour drainage basin, covering an area of 363.2 km^2 (Section 1.2). The domain extents are assumed to delineate the groundwater divide, defined as the interface between groundwater basins through which no lateral groundwater-flow occurs. This method assumes that the water table resembles a subdued replica of the topography within most of the drainage basin (Tóth, 1963; Haitjema and Mitchel-Bruker, 2005); therefore, the groundwater divide approximately coincides with the drainage basin. This is a commonly applied approach in groundwater modelling (Hiscock and Bense, 2014; Han et al., 2019) as there is generally insufficient data to properly delineate the groundwater divide. The vertical extents of the domain range from the highest elevation within the watershed, 330 masl, down to 200 mbsl, which is sufficiently deeper than the assumed groundwater systems in Nova Scotia (~150 m; Kennedy et al., 2010).

The domain was created using ArcMap™ software to combine the pertinent secondary watersheds provided by the Nova Scotia Department of Environment (2018) in conjunction with the drainage area delineated by the Department of Natural Resources for use by CBP and IVFA (n.d.). The catchments surrounding the harbour lack major watercourses and were combined to create the harbour subcatchment.

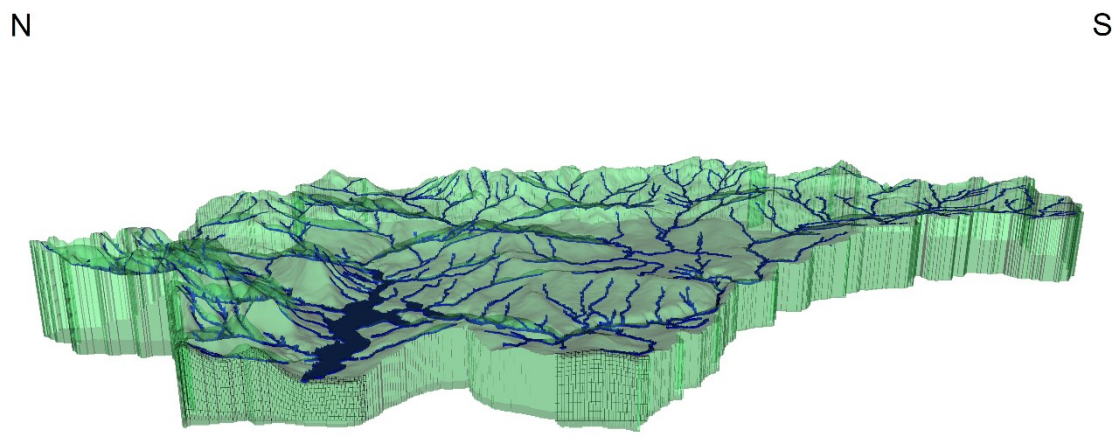

Figure 24: Modflow-NWT domain for the Mabou Harbour drainage basin.

3.2.2.4 Hydrostratigraphic Units

Mabou Harbour has a diverse and complex geology due to its location within an orogenic belt and a variety of depositional environments (Baechler et al., 2019). The convoluted and extremely heterogeneous geology was separated into 11 hydrostratigraphic units (HSUs) to simplify the model and to avoid over-parameterization. The Geological Mapping for Cape Breton Island (Barr et al., 2017) in addition to the Surficial Geology Map of the Province of Nova Scotia (Stea et al., 2006) were used to create the HSUs using ArcMap™. For this exercise, geologic boundaries were considered to be vertical. This simplification is justified by the generally moderate to steeply dipping orientations of the bedrock. This simplification introduces error in the situation of a slightly dipping bedrock, particularly at depth; however, the conceptual model predicts that shallow groundwater flow will be dominant and deep groundwater flow will be limited. Furthermore, the

geologic boundaries presented in maps are inherently uncertain and are generally subject to professional interpretation.

As presented in Figure 25, bedrock HSUs were formed by combining similar lithostratigraphic units based on the primary and secondary lithology from Barr et al. (2017). If the age and location of similar lithostratigraphic groups were comparable, it was assumed that the degree of deformation experienced would also be similar. Deformation, particularly brittle deformation, is an important control on secondary permeability and influences both *K* and *K* anisotropy (Welch and Allen, 2014). When available, bedrock *K* approximations derived from the Nova Scotia Well Logs Database (herein NSWLD; Appendix IV) were also considered when combining lithostratigraphic units. For instance, there were occurrences where lithology and age were similar between two geologic units, but the *K* values disagreed. In this situation the geologic units were separated into two distinct HSUs due to their differences in hydraulic properties. The resulting HSUs from this exercise are presented in Table 7 and Figure 26.

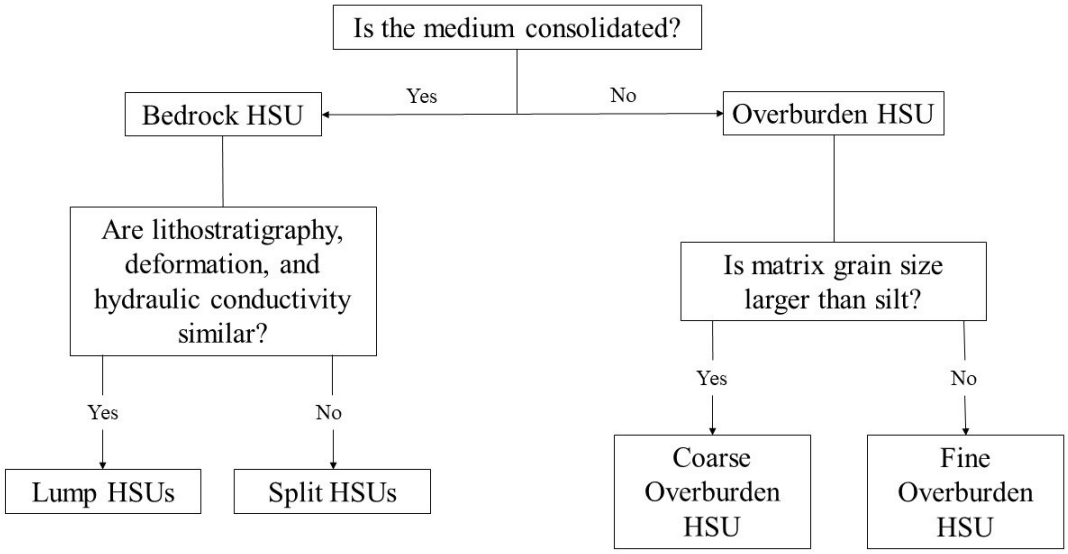

Figure 25: Flowchart for defining hydrostratigraphic units.

Table 7: Bedrock HSUs separated into Siliciclastic and Non-Siliciclastic.

Siliciclastic	Non-Siliciclastic
Sandstone 1	Crystalline
Sandstone 2	Limestone
Sandstone & Siltstone	Metacarbonate
Siltstone	Gypsum & Anhydrite
Mudstone	

The sandstone and siltstone HSU were not divided into two distinct groups due to the siltstone being intercalated within the sandstone (Barr et al., 2017). Metamorphic and igneous rock of various compositions were combined into the crystalline HSU due to their similarities in hydraulic properties as noted in regional reports (Kennedy et al., 2009; SLR Consulting, 2014) and the broader literature (Domenico and Schwartz, 1990). Metacarbonates were exempt from the crystalline HSU because although they are

metamorphic and have undergone recrystallization removing void-space, they are still carbonates and are thus susceptible to dissolution, which may result in different hydraulic properties due to karstification. Although many lithostratigraphic units within the domain contain intercalated carbonates or evaporites, only those units where this rock type was described as a primary lithology (Barr et al., 2017) were added to the limestone or gypsum and anhydrite HSUs. The prevalence of carbonates and evaporites as either a primary or secondary lithology in the sedimentary rock should be considered when evaluating the optimized *K* estimates following the calibration process, as karst features may be present.

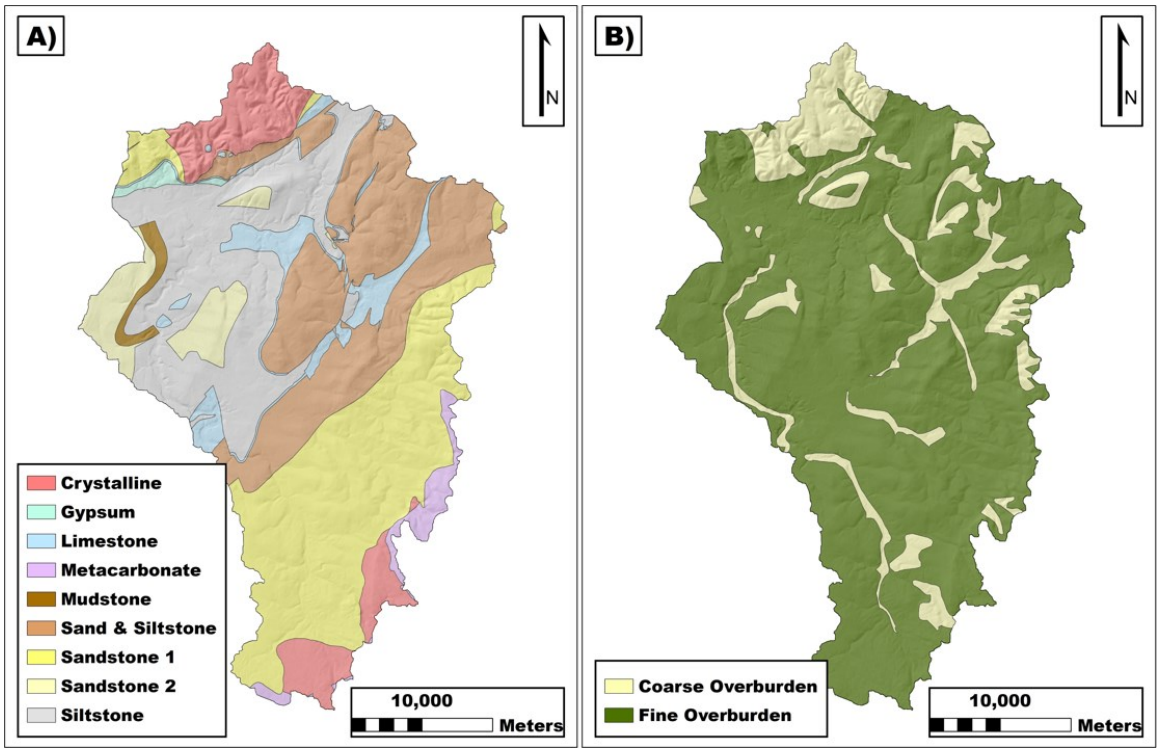

Figure 26: Hydrostratigraphic units of the Mabou Harbour drainage basin. A) Bedrock hydrostratigraphic units; B) overburden hydrostratigraphic units.

Each bedrock HSU was further separated into three hydrostratigraphic layers (HSLs) to capture the decay in *K* with depth that has been extensively observed (Louis,

1974; Manning and Ingebritsen, 1999; Maxwell and Kollet, 2008) yet rarely accounted for in regional groundwater studies (Jiang et al., 2009). This phenomenon is also exhibited by the estimated bedrock *K* values derived from the NSWLD (Figure 27). The three HSLs are shallow bedrock, intermediate bedrock, and deep bedrock.

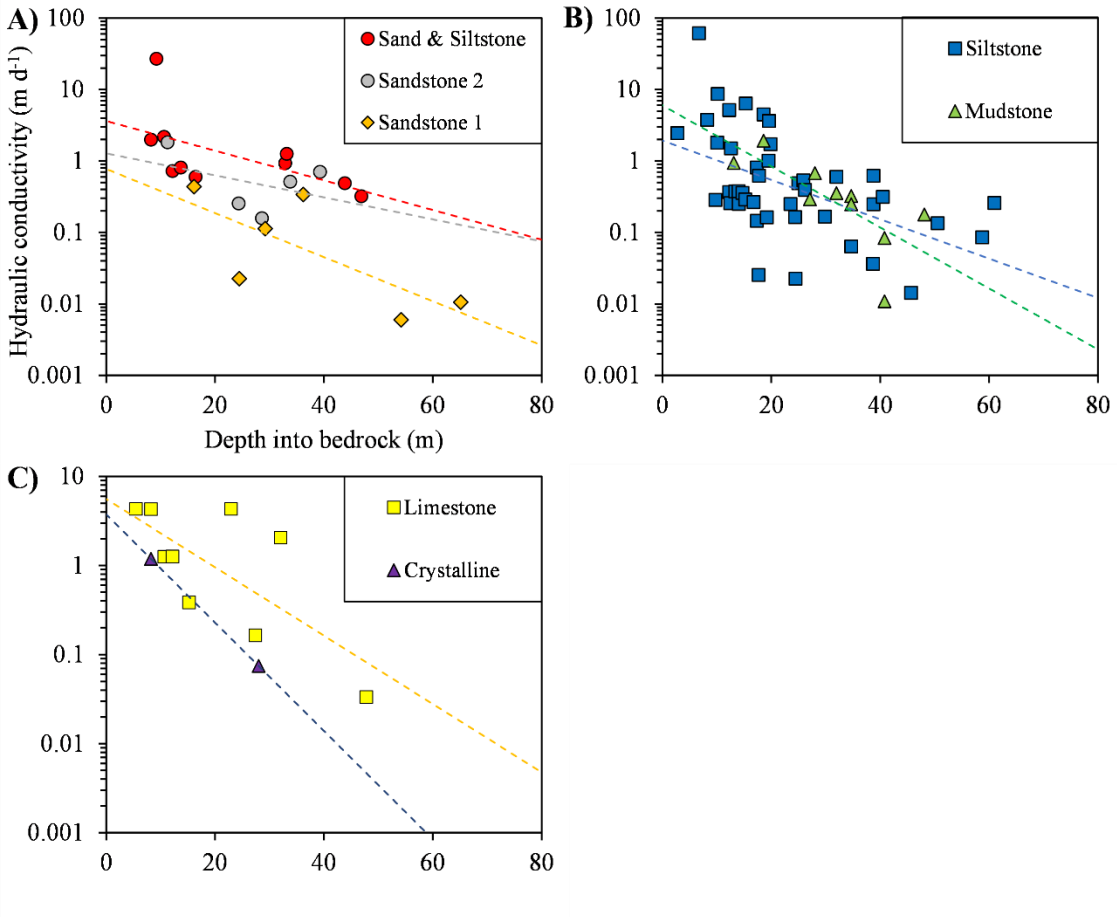

Figure 27: Hydraulic conductivity vs. depth into bedrock: A) sandstone HSUs; B) siltstone and mudstone HSUs; and C) crystalline and carbonate HSUs.

The overburden HSUs were defined by separating all surficial geology units from Stea et al. (2006) into either fine or coarse overburden based on grain size of the matrix (Figure 25). Surficial geology units were filtered into these two HSUs based on their map

unit label (Table 8). The resulting HSUs are displayed in Figure 26. Three of the unit labels required interpretation prior to allocating to HSUs, including marine deposits, organic deposits, and bedrock with till veneer. In the context of Mabou Harbour, marine deposits refer to West Mabou Beach, which consists of medium-grained sand and was therefore allocated into the coarse-grained deposits. Organic deposits were assigned to the fine overburden HSU. Soils of Cape Breton Island (Cann et al., 1963) indicates that the organic deposits within the domain have a saturated K of <1 m d^{-1} below 60 cm depth. Although the reliability of these K measurements is unknown, the organic content was stated to be 39-43%, and it was assumed that fine sediments constitute the remainder of the bulk volume given that organics generally accumulate in low energy environments, such as wetlands or bogs. Bedrock with till veneer was also assigned to the fine overburden HSU as Stea et al. (2006) described the unit as "overlain by a thin, discontinuous veneer of till". Stony till plain was assigned to the fine overburden despite being described as having a sandy matrix, as it is assumed to have a considerable silt content mixed in with the sand based on field observations.

Table 8: Coarse overburden and fine overburden HSUs and the corresponding surficial geology units taken from the Surficial Geology Map of the Province of Nova Scotia (Stea et al., 2006).

Coarse Overburden	Fine Overburden
Colluvial deposits	Bedrock (with till veneer)
Glaciofluvial deposits (Kames and Eskers)	Silty drumlin
Residuum	Silty till plain
Alluvial deposits	Stony till plain
Marine deposits	Organic deposits

3.2.2.5 Mesh Discretization

MODFLOW-NWT uses a finite difference mesh and does not allow for unstructured grid or quadtree refinement. Refinement is possible with a finite difference mesh; however, the reduced grid-spacing is extended to the edges of the domain. Given the extensive fluvial network within the domain, a simpler approach was to assign a ubiquitous grid-size of 50 m. A convergence analysis indicated that a cell size of 50×50 m is sufficiently small to simulate the GSIs at the regional scale for the relevant boundary conditions while remaining coarse enough to achieve model efficiency. This cell size is similar, if not more refined than other numerical groundwater models applied to regional groundwater studies (e.g., Ghoraba et al., 2013; Morgan et al., 2019). The mesh was rotated 12 degrees from north to run perpendicular to the shortest-axis of the domain, minimizing the number of cells required and improving model efficiency. All cells in the grid that lay outside the drainage basin were set to inactive resulting in a total of 1,783,560 active cells.

3.2.2.5.1 Vertical Discretization

The mesh was vertically discretized into 11 layers. The first layer, representing the overburden, was discretized as a single layer of variable thickness determined by the formula:

$$Min[(1.029z - 9.7), (z - 1)] \quad (7)$$

where z is the surface elevation [m] based on the DEM (SNSMR, 2003) with an accuracy and resolution of ~10 m and 20 m, respectively. This formula reflects the regression equation representing the relationship between surface and bedrock elevation (Figure 28), which was derived from historic well logs in the NSWLD. This coefficient of determination shows that 98.4% of the variability in the elevation of the bedrock surface can be explained by the topographic elevation. Only well logs within the domain that had depth-to-bedrock data were used in this analysis. The above equation suggests that the overburden thickness is greater in low-altitude regions, which is consistent with erosional and depositional theory stating that erosion generally occurs at topographic highs and deposits in lower regions or basins. At the maximum elevation (330 masl) and minimum elevation (16 mbsl) within the harbour, the overburden thickness is 0.1 m and 10.2 m, respectively. The *z – 1* component of equation 7 is implemented in circumstances where the overburden bottom becomes too close to the model top resulting in an overburden thickness of 1 m, thereby improving model convergence.

There may be some error in using the above equation to generalize the overburden thickness throughout the domain. For instance, Stea et al. (2006) shows areas within the domain where surficial geology was labelled as bedrock with thin veneer; however, well logs within these regions report till depth ranging from 0.91 – 8.93 m with a mean of 5.13

m (n=13), which is consistent with the predicted values from the equation (5.44-5.79 m, $\bar{x}$=5.47 m, n=13). This suggests that although "bedrock with thin veneer" is associated with outcropping, the area is generally overlain by glacial till.

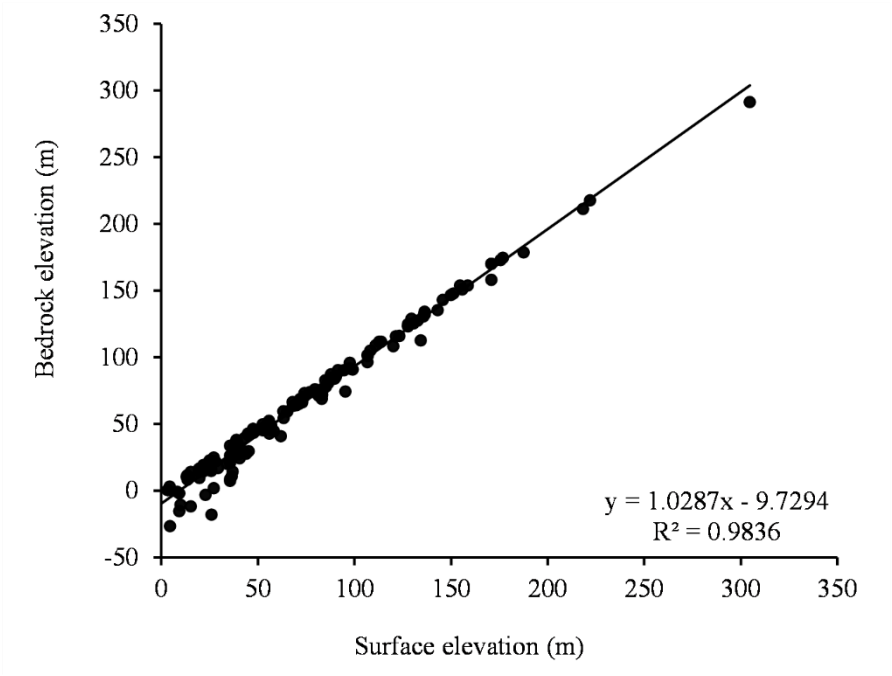

Figure 28: Linear relationship between bedrock and surface elevation. Data sourced from the Nova Scotia Well Logs Database.

The second HSL, representing shallow bedrock, was discretized by two layers immediately underlying the overburden. The bottom of the shallow bedrock layer was determined as overburden bottom – 20m. These layers were created to capture the phenomenon that hilly landscapes are generally characterized by overburden underlain by weathered bedrock, which may extend tens of meters (Rempe and Dietrich, 2014). Similarly, Chandra et al. (2019) found that the weathered zone in a suite of crystalline rocks were ~20 – 40 m in thickness. Creating a distinct group of layers containing weathered bedrock permits separate parameterization from the relatively competent bedrock in the

intermediate bedrock HSL. This is supported by the elevated *K* estimated for wells completed in the top ~20 m of the bedrock (Figure 27). Furthermore, Figure 27 shows that all upper outliers are located within this depth. It is assumed that any karstification that is present in the domain will be represented by the shallow bedrock layers as individual karst features are generally shallower than 10 m and are often densely clustered (Ford, 2015).

The third HSL, representing intermediate bedrock, was discretized by four layers of 20 m thickness immediately underlying the shallow bedrock bottom. The bottom of the intermediate bedrock was determined as overburden bottom – 100m. This depth will adequately capture the deepest of wells completed within the domain. The intermediate bedrock will capture the hydraulic properties of relatively competent bedrock that has experienced less physical and chemical weathering, and thus a reduced *K*.

The fourth and final HSL, representing deep bedrock, was discretized by 5 layers of variable thickness immediately underlying the intermediate bedrock. The bottom of the deep bedrock was determined as 200 mbsl and is thicker in the high-altitude regions and thinnest underneath Mabou Harbour. The purpose of this group of layers is to again allow for parameterization of what is assumed to be the least hydraulically conductive bedrock within the domain. Little flow is expected to occur in this region. It is also expected that fractures decrease in frequency and density with depth, and thus a reduction in fracture connectivity, which controls the capability of fractures to act as conduit for groundwater flow (Cook, 2003).

3.2.2.6 Boundary Conditions

3.2.2.6.1 Model Boundary

Neumann boundary conditions (specified flux) were applied to the extents of the model domain. As previously discussed in Section 3.2.2.3, the groundwater divide coincides with the lateral extents of the model domain. For the purpose of this study, the groundwater divide has been defined as the interface that separates groundwater basins through which no lateral groundwater flow occurs; thus, a no-flow boundary condition was applied to all lateral extents. The no-flow boundary condition was also applied to the bottom of the domain, where groundwater flow is greatly diminished due to the decrease in K with depth (Jiang et al., 2009). The upper boundary of the domain received a specified flux boundary condition, to represent recharge, with the magnitude depending on the overburden HSU. This specified flux boundary condition was not applied to cells within the harbour domain.

3.2.2.6.2 Harbour

A General-Head Boundary Package (Harbaugh et al., 2000) was applied to Mabou Harbour with the head set to 0 m. Given that a steady state model was used for this exercise, the transient tidal conditions of harbour levels were ignored and only the mean ocean head, of h=0 m was considered. The domain of the harbour was created using ArcMap™ by reclassifying the DEM (Service NS, 2003) and bathymetry data from the AGRG (2017) so that only cells with elevation ≤ 0 masl were displayed. A general outline was delineated based on the reclassified DEM, and all cells contained by this boundary were deemed to have a head equal to 0 m.

The General-Head Boundary Package is similar to a constant head (Dirichlet) boundary condition in that negative or positive fluxes to the cell are proportional to the difference between head in the cell and the reference head of the boundary condition (Winston, 2020). The difference is that the General-Head Package introduces a conductance parameter, which is essentially a measure of connectivity between the water feature and the aquifer. Conductance is controlled by a bed of sediments at the base of the water body and is represented by the equation (Winston, 2020):

$$Conductance = \frac{AK}{M} \tag{8}$$

where A equals the area of the boundary condition's interface within a cell [m^2], which is automatically calculated by ModelMuse™; K is the hydraulic conductivity of the bed [m d^{-1}], which in theory is primarily controlled by K_z of the bed; and M is the thickness of the bed [m]. The thickness of the benthic sediments was estimated to be 1 m, and the K was liberally set to equal the underlying overburden such that SGD is not impeded.

In contrast to other boundary conditions used during this model exercise, the General-Head Boundary Package does not limit the flux as the head gradient increases, which must be considered in situations where the head gradient becomes very high (Waterloo Hydrogeologic, 2019).

3.2.2.6.3 Watercourses

There is a large concentration of watercourses within the Mabou Harbour Drainage Basin, and these were separated into four main groups, the Mabou River, NE Mabou River, SW Mabou River, and harbour streams. These groups were further subdivided into rivers

and tributaries using ArcMap™ (ESRI, 2016) and the Nova Scotia Topographic Database (Figure 29; Department of Lands and Forestry, 2020). Dense groupings of first order streams in Department of Lands and Forestry (2020) were reduced to single watercourses to achieve a resolution more suitable for the model grid.

The Mabou, NE Mabou, and SW Mabou Rivers were assigned the River Package (Harbaugh et al., 2000), which is essentially a constant head boundary condition that falls under three scenarios allowing either river gain or loss: 1) the head within the cell is greater than the river stage; 2) the head within the cell is between the river stage and the river bottom; and 3) the head within the cell is below the bottom of the river (Winston, 2020). Under the first scenario, there will be a negative flux (i.e., water will flow from the aquifer into the river). Under the second scenario, there will be a positive flux (i.e., water will flow from the river into the aquifer) at a variable rate depending on the gradient between the cell head and the river stage. Under the third scenario, which is a disconnected stream, there will be a positive flux at a constant rate. A limitation for the River Package is that in the situation where river stage exceeds the head within the cell, the aquifer recharge could be over-simulated as the code assumes endless water resources in the river, which is not realistic for low-order or ephemeral streams but is reasonable for perennial rivers such as the three considered in this study.

Similar to the General-Head Boundary Package, the River Package requires a conductance parameter in addition to setting the river stage and river bottom elevations. In the context of a linear object, such as a river, the conductance is represented by the following equation (Winston, 2020):

$$Conductance = \frac{K_R l w}{M} \quad (9)$$

where l [m] is the length of the river within the cell, which is automatically calculated by ModelMuse^{TM}, w [m] is the width of the river, K_R [m d^{-1}] is the K of the riverbed, and M [m] is thickness of the riverbed sediments, respectively. River stage was set to be 0.6 m below the top of the domain for the Mabou/Mull (i.e., Mull River turns into the Mabou River), and SW Mabou rivers, and 0.3 m for the NE Mabou River. These measurements are consistent with cut bank depths observed in the field. River bottom elevations were set to be 0.4 m below river stage for the Mabou/Mull, and SW Mabou Rivers, and 0.3 m for the NE Mabou River. These depths agree with stage measurements observed during stream gauging operations at near-baseflow conditions.

The tributaries for each of the three rivers, in addition to the coastal streams, were assigned the Drain Package (Harbaugh et al., 2000). Unlike the River Package, the Drain Package only simulates gaining stream conditions. The Drain Package was selected for these watercourses because it was assumed that there would be inadequate baseflow to supply aquifer recharge as these are generally lower order or ephemeral streams. This approach avoids the exaggerated recharge that may be associated with the River Package. Some of the tributaries, particularly for the Mabou River, are 3rd order streams and likely do have enough baseflow to supply losing sections; therefore, the sensitivity of this boundary condition selection was tested (Section 3.2.4).

Watercourse width and bed thickness varied throughout the drainage basin but were required for the conductance parameter in both the River and Drain packages. To

approximate the width of the different watercourses, the measurement tool in Google Earth™ was used mid-reach. The resulting widths are displayed in Table 9. Although the Mull river turns into the Mabou river at the confluence with Shea Brook, widths were measured independently for accuracy. There was little information to use for the approximation of the bed thickness; therefore, an arbitrary value of 0.25 m was assigned; however, it is unlikely to have a significant influence on GSIs as *K* controls most of the variability in the conductance parameter.

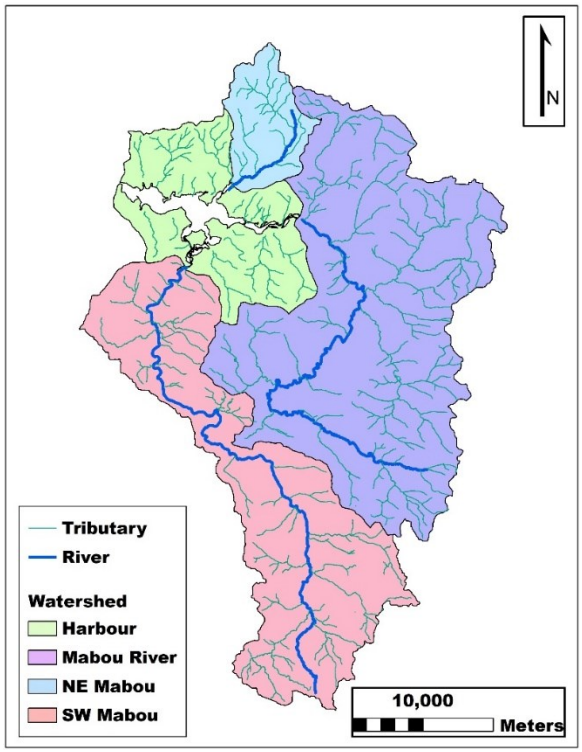

Figure 29: Major rivers of Mabou Harbour, their tributaries, and their corresponding catchments. Catchment delineations were derived from Nova Scotia Department of Environment (2018) and a shapefile created by the Department of Natural Resources for CBP and IVFA (n.d.). Watercourses were adapted from Department of Lands and Forestry (2020) as described in Section 3.2.2.6.3.

Table 9: Conductance variables for the river and drain boundary conditions..

Watercourse	Width [m]	Bed thickness [m]
SW Mabou River	30	0.25
Mabou River	20	0.25
Mull River	10	0.25
NE Mabou River	3	0.25
Tributaries	1	0.25
Coastal Streams	1	0.25

3.2.2.7 Parameterization of Hydraulic Properties

An individual *K* parameter was created for every HSL of each HSU to account for changes in hydraulic properties with depth. *K* represents the bulk *K* of large elementary volumes (>2,500 m^3). The *K* – anisotropy parameter was created to represent the anisotropy throughout the drainage basin controlled by the orientation of the geological structures. Much of the sedimentary rock are dipping less than 45°, thus a lower anisotropy could suggest depositional features, such as grain orientation or clay interbedding, and a higher anisotropy could suggest vertically oriented geologic features such as faulting or vertically oriented bedding. Given the variable orientations throughout the domain, this parameter will not represent the anisotropy within the individual HSUs but will perhaps provide perspective on the prevalence and significance of faulting or clay interbedding throughout the domain.

3.2.3 Model Calibration

The objective of model calibration is to refine the parameterization of the numerical groundwater flow model to closely match observations from field studies. It is assumed that the resulting model will adequately represent the natural flow regimes of the drainage

basin, including the spatial patterns of GSIs. The calibration methodology used was a combination of automated calibration, facilitated by the PEST Model – Independent Parameter Estimation (PEST) software (Doherty and Hunt, 2010), and manual calibration guided by intuition. Simulated values were calibrated to static water levels and baseflow estimates.

PEST is a computer-based software that uses regularized inversion, which is the combined use of numerical methods and many parameters to determine optimal parameter values and combinations. Regularized inversion is gaining popularity as an approach for reducing calibration difficulties and to transfer field observations to the parameters used in a numerical groundwater model (Doherty and Hunt, 2010). The PEST calibration process is iterative because the sensitivities of model outputs to parameters are not linear and vary as the parameters change. Every iteration begins with the calculation of a Jacobian matrix, which has a column for each parameter and a row for each observation (Figure 30 and Watermark Numerical Computing [WNC], 2020). The minimum number of model runs required to solve the Jacobian matrix is equal to the number of parameters. Following calculation, the matrix can be used to refine the parameter values. PEST uses the objective function to determine the model's quality of fit and will select the iteration with a combination of parameter values that minimizes the residuals.

	Parameters		
Model Observations	$\partial o_1/\partial b_1$	$\partial o_1/\partial b_2$	$\partial o_1/\partial b_3$
	$\partial o_2/\partial b_1$	$\partial o_2/\partial b_2$	$\partial o_2/\partial b_3$
	$\partial o_3/\partial b_1$	$\partial o_3/\partial b_2$	$\partial o_3/\partial b_3$

Figure 30: Format of the Jacobian matrix where o_i is the model-generated i^{th} observation and b_i is the i^{th} parameter value. Figure notation adapted from South Florida Water Management District (n.d.).

Manual calibration was conducted following PEST calibration and was only accepted if there was either an improvement to, or a negligible affect on RMSE. The shallow bedrock of sandstone 1 and crystalline HSUs were manually calibrated in response to an elevated water table between head observation points and drains. The shallow bedrock of the limestone was also manually increased to better represent the HSU at the expense of increased error on a few peripheral wells.

3.2.3.1 Selection of Parameter Ranges

There were 24 parameters adjusted throughout the calibration process that fall under the general categories of *K*, *K*-anisotropy, conductance, and recharge. The upper and lower bounds for *K* in the shallow bedrock were based on the range of estimates derived from the NSWLD and the Driscoll method (1986; Appendix IV). This assumes that the calibration bounds contain the mean bulk *K* for the elementary volume. The bounds for the intermediate and deep bedrock are generally based on the ranges presented by Domenico & Schwartz (1990). Due to the absence of well logs within the gypsum and anhydrite HSU,

the range was based completely on the literature (Domenico & Schwartz, 1990) with the exception that the upper bound was increased by two orders of magnitude to account for the karst geology suggested by the numerous sinkholes observed in satellite imagery (ESRI, 2018). *K* ranges for the fine and course overburden were based on approximate ranges for glacial till and alluvium, respectively, and were obtained from the literature and online resources (Domenico & Schwartz, 1990; Green et al., 2004; StructX, 2020).

The unitless conductance bounds were arbitrarily set from 1 to 10,000 to provide PEST with full flexibility. The conductance parameters essentially act as multipliers of overburden *K* within the cells that River or Drain Packages are located. This assumes that *K* can only be greater than the overburden which is supported by field observations where streambeds were composed of coarser sediment than surrounding stream bank materials.

The vertical anisotropy parameter, which is the ratio between K_z and K_x, was limited to the range of 0.05 – 5. It is generally assumed in hydrogeology that this ratio is 0.1 – 0.5 for alluvial materials and as low as 0.01 if clay layers are present (Todd, 1980). Conversely, in fault zones, K_z can be several orders of magnitude higher than K_x (Anderson and Bakker, 2008).

Calibration ranges for groundwater recharge coefficients in coarse and fine overburden were set to 20 – 70%, and 10 – 30%, respectively, to allow for flexibility in the calibration process. Kennedy et al. (2010) estimated that average bedrock recharge coefficient for this region was 21%. The water balance derived from field studies suggest

that recharge is 23% – 36% during the field season, depending on the surficial geology (Section 2.3.6).

3.2.3.2 Calibration to Static Water Levels

Static water levels for 88 wells from the Nova Scotia Groundwater Atlas were used to calibrate the hydraulic properties and functioning of the HSUs. Static water levels reflect the head measurements taken at the time of well development. Proper methodology for measuring static water levels is to measure prior to and during the well test to determine drawdown (Government of Ontario, 2019); however, static water level is less important to water supply drillers, so the correct procedures may not always be followed. If measured shortly after pumping, water levels may be underestimated. Given the regional scale and large relief of the domain, inconsistencies in static water level measurements will be negligible to model results, provided that error is on the scale of a few meters.

Residuals between observed and simulated water levels were weighted based on georeferencing precision. Given the large relief within the domain, particularly in the areas near the harbour where wells are concentrated, uncertainty in the location of a static water observation can result in erroneous calculation of residuals, thus a greater weight was allocated to static water observations with greater georeferencing precision. To quantify the relationship between statistical weight and geospatial precision, the precision was normalized to the maximum georeferencing error resulting in statistical weights from 1 to 11, corresponding to errors of 1,130 – 15 m as reported by the NSWLD. The magnitude of georeferencing error depends on the method. For instance, the smallest error is associated

with GPS recorded locations, whereas the largest errors are based on the centroid of UTM grids.

3.2.3.3 Calibration to Baseflow Observations

Calibration to static water levels alone is generally ineffective without prior knowledge of recharge magnitudes and preferably spatial patterns. Doing so results in equifinality of model parameters as any given combination that follows the same recharge/*K* ratio can yield the same piezometric surface (Hill and Osterby, 2003). To eliminate this issue, baseflow observations were introduced to condition the calibration of recharge.

As discussed in Section 2.2.1, only seasonal hydrometric data could be gathered during 2019 due to river-ice conditions; consequently, propagation of seasonal data was based on patterns observed in watersheds with similar BFI, geology, topography, and climate conditions (Appendix I). A source of uncertainty in this model is that although baseflow is useful in the assessment of recharge conditions (Hiscock and Bense, 2014), it may actually comprise of a combination of both interflow and recharge (Rivard et al., 2014). Therefore, it should be acknowledged that the use of hydrograph analysis, as a means of estimating the groundwater component of streamflow, may overestimate recharge.

3.2.4 Sensitivity Analysis

To better understand the uncertainty associated with model construction and parameterization, sensitivity analyses were performed on several different variables to

determine their influence on head and baseflow observations. The analyzed variables were overburden thickness, boundary condition selection, conductance, and the calibrated parameters. PEST automatically tests the sensitivity of calibrated parameters. The sensitivity value is based on the magnitude of the vector for the Jacobian Matrix column relating to the parameter (WNC, 2020; Figure 30). To complete the analyses of the remaining variables, overburden thickness, boundary conditions, and conductance parameters were altered independently and then evaluated. The decision to allocate all tributaries as Drain Package boundary conditions was tested by switching Glendyer Brook, a major tributary to the Mabou River, to the River Package.

3.2.5 Harbour Flushing Rate Estimates

To better constrain the contributions of direct and indirect groundwater discharge to the total harbour volume, the water balance from model results was used to estimate the flushing rate of the harbour using the following equation:

$$T_R = \frac{V}{Q_F + Q_S} \tag{10}$$

where T_R is the flushing rate [d], Q_F is the freshwater input [$m^3\ d^{-1}$], and Q_S is tidal flushing [$m^3\ d^{-1}$], which is defined as the intertidal volume [m^3] divided by the tidal period [d]. This method assumes that: evapotranspiration (*ET*) has negligible impact on precipitation falling directly into the harbour due to mixing; and the system experiences negligible changes in storage. The intertidal volume was calculated using the mean tidal amplitude (Appendix III) and harbour area. A first order estimate of the total volume of freshwater constituents within the harbour was then estimated by multiplying the discharge rate by the flushing rate. For comparison, the freshwater fraction method (Ketchum, 1950) is applied to salinity

data recorded by conductivity loggers installed in the harbour from June 19 – August 28, 2019 (Appendix II):

$$f = \frac{S_o - S_H}{S_o} \tag{11}$$

where f is the freshwater fraction [unitless], S_o is the salinity of the ocean endmember [ppt], and S_H is the salinity of the harbour [ppt]. The maximum salinity measured was used to represent S_o yielding a value of 27.06 ppt, which is consistent with regional reports (29.42 ppt; Petrie et al., 1996). The freshwater fraction was then applied to the harbour volume to determine the freshwater volume and then divided by the freshwater discharge to estimate the flushing rate.

3.2.6 Particle Tracking

MODPATH 7 (Version 7.2.001; Pollock, 2017), a particle tracking program for MODFLOW, was used to track flow paths and to estimate residence times and linear velocities. Particle tracking is a common method of evaluating residence or travel times within a three-dimensional groundwater flow model (Anderson et al., 2015a). To analyze the capture zones of surface water bodies within the domain, a single particle was allocated to the centre of each cell that corresponds to either General-Head Boundary, Drain, or River Package boundary conditions for backward-tracking. Particle movement was incrementally observed to identify recharge locations. Output time points were set to 50 days, annually for the first 5 years, and then for 5-year increments until 40 years was achieved. To estimate groundwater velocities from the Darcy flux, effective porosities of 5% were assigned to crystalline, limestone, and gypsum bedrock while the remaining HSUs were assigned 25%

based on the literature (McWhorter and Sunada, 1977; Freeze and Cherry, 1979; Domenico and Schwartz, 1997; Stephens et al., 1998).

3.3 RESULTS

3.3.1 Calibrated Parameters

The optimized parameter values from the calibration process are presented in Table 10. The calibrated *K* parameters are generally closer to the upper limit of the expected range, particularly for the shallow bedrock HSUs. Vertical anisotropy was calibrated to a ratio of 0.97 (K_z/K_x). Figure 31 displays agreement between the calibrated *K* and *K* values derived from well-log data for shallow and intermediate bedrock. Deep bedrock values were excluded due to the lack of field data at greater depths.

River conductance corresponds to a riverbed *K* of 4.8 and 296 m d^{-1} for cells that reside in the fine and coarse overburden, respectively. Drain conductance corresponds to a streambed *K* of 36.48 m d^{-1} in the fine overburden and 2.2×10^3 m d^{-1} in the coarse overburden. These values generally agree with those reported in the literature for riverbeds and alluvial sand and gravel (Domenico and Schwartz, 1990; Duwelius, 1996; StructX, 2020).

Calibrated recharge rates within the fine and coarse overburden were 377 and 852 mm yr^{-1}, respectively. With an estimated annual precipitation of 1,519 mm (ECCC climate IDs: 8200828 and 8204495), the recharge coefficients are approximately 25% and 56% for the fine and coarse overburden, respectively. Recharge within the bounds of the granitoid bedrock of the southern hills of the domain, an insensitive area lacking observational data

and agriculture, was lowered to 151 mm yr^{-1} (~60% decrease) in response to the simulated water table exceeding the model top. This recharge rate is comparable to those reported for granitoid bedrock in Guysborough County, Nova Scotia (SLR Consulting, 2015). Recharge was lowered rather than increasing *K* to unreasonable levels. The water table is expected to be shallow in the southern hills due to the low hydraulic conductivity, which would limit the drainage.

Table 10: Calibrated parameters and expected limits

	Calibrated value	Lower limit	Upper limit
Horizontal hydraulic conductivity [m d^{-1}]			
Sand & siltstone			
Shallow	1.3	2.6×10^{-1}	4.3
Intermediate	2.1×10^{-1}	8.6×10^{-6}	5.2×10^{-1}
Deep	8.2×10^{-3}	8.6×10^{-6}	5.2×10^{-1}
Sandstone 1			
Shallow	4.6×10^{-1}	1.1×10^{-2}	6.2×10^{-1}
Intermediate	1.7×10^{-2}	2.6×10^{-5}	6.2×10^{-1}
Deep	1.7×10^{-3}	2.6×10^{-5}	6.2×10^{-1}
Sandstone 2			
Shallow	3.0×10^{-1}	1.6×10^{-1}	1.8
Intermediate	1.0×10^{-1}	2.6×10^{-5}	5.2×10^{-1}
Deep	6.6×10^{-5}	2.6×10^{-5}	5.2×10^{-1}
Siltstone			
Shallow	1.5	1.4×10^{-2}	8.7
Intermediate	2.1×10^{-3}	8.6×10^{-6}	1.2×10^{-1}
Deep	7.4×10^{-5}	8.6×10^{-6}	1.2×10^{-3}
Mudstone			
Shallow	1.6×10^{-1}	1.1×10^{-2}	1.9
Intermediate	2.0×10^{-2}	5.0×10^{-9}	1.2×10^{-1}
Deep	5.0×10^{-5}	5.0×10^{-9}	1.2×10^{-3}
Crystalline			
Shallow	1.5×10^{-1}	7.4×10^{-2}	4.5
Intermediate	1.9×10^{-3}	3.0×10^{-9}	6.0×10^{-1}
Deep	1.6×10^{-3}	3.0×10^{-9}	6.0×10^{-1}
Metacarbonate			

	Calibrated value	Lower limit	Upper limit
Shallow	4.4	3.0×10^{-4}	6.1×10^{1}
Intermediate	7.7×10^{-2}	2.0×10^{-5}	2.0×10^{-1}
Deep	7.1×10^{-3}	2.0×10^{-5}	2.0×10^{-1}
Limestone			
Shallow	8.0×10^{-1}	3.0×10^{-2}	6.1×10^{1}
Intermediate	3.2×10^{-3}	8.6×10^{-5}	5.2×10^{-1}
Deep	1.4×10^{-4}	8.6×10^{-5}	5.2×10^{-1}
Gypsum & anhydrite			
Shallow	1.7	3.5×10^{-8}	1.7×10^{-3}
Intermediate	9.6×10^{-4}	3.5×10^{-8}	1.7×10^{-3}
Deep	7.7×10^{-5}	3.5×10^{-8}	1.7×10^{-3}
Overburden			
Fine	1.2×10^{-1}	1.0×10^{-7}	1.7×10^{-1}
Coarse	7.4	1.5×10^{-1}	2.1×10^{1}
Conductance (multiplier)			
River package	4.0×10^{1}	1	1.0×10^{4}
Drain package	3.04×10^{2}	1	1.0×10^{4}
Anisotropy (K_z/K_x)			
Vertical anisotropy	0.97	0.05	5
Recharge [m yr^{-1}]			
Fine overburden	0.377	0.145	0.435
Coarse overburden	0.852	0.29	1.015

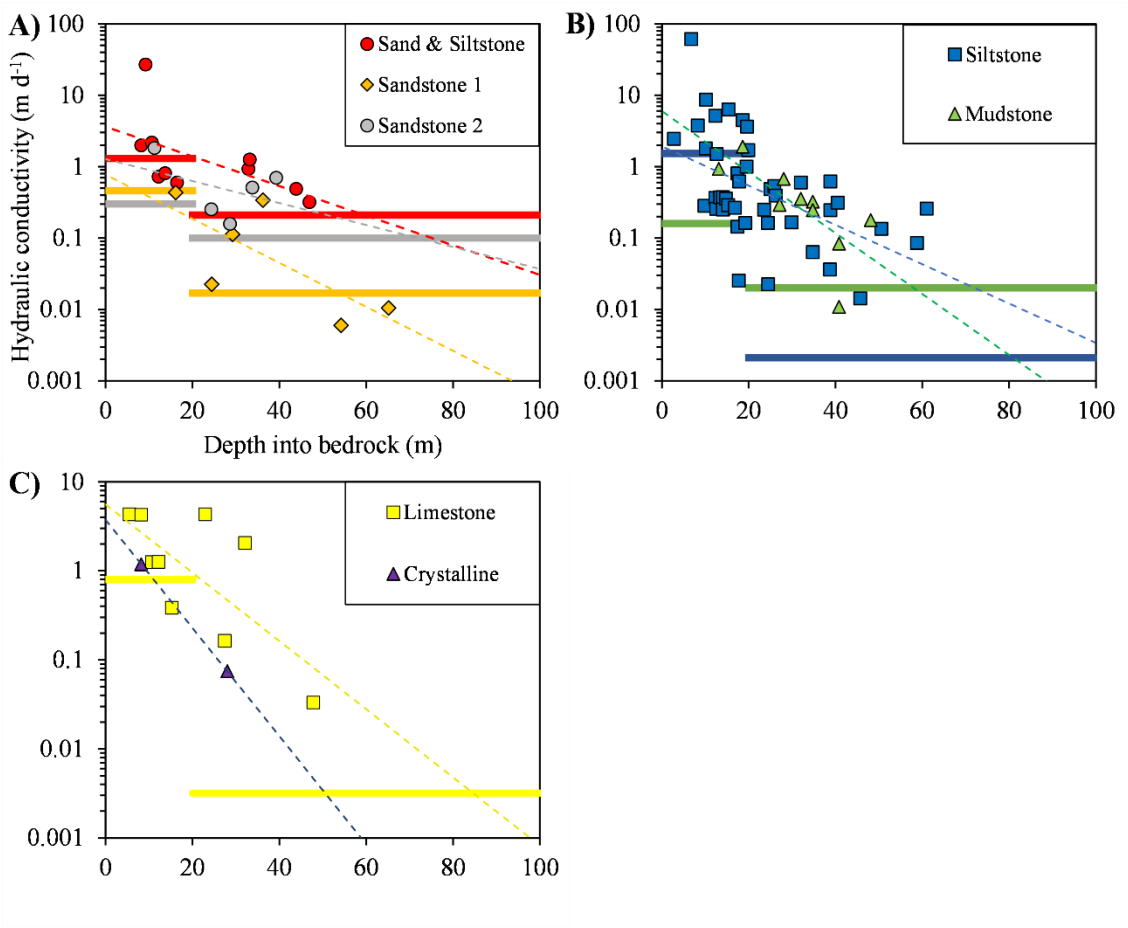

Figure 31: Calibrated shallow and intermediate bedrock hydraulic conductivities compared to well-log data. The thick solid lines indicate calibrated values and are horizontal because they were applied to depth-ranges. The dashed lines indicate the regression lines of well-log data. All lines and data points are colour coordinated to represent the appropriate HSU.

3.3.2 Sensitivity Analyses

PEST automatically records parameter sensitivities during the calibration phase, which are displayed on a logarithmic scale for each *K*, conductance, and recharge-related parameter (Figure 32). Sensitivity values are based on the magnitude of the vector for the Jacobian Matrix column relating to the parameter (Figure 30 and WNC, 2020). Recharge parameters were the most sensitive, generally followed by K_x and conductance. Fine overburden recharge was the most sensitive parameter, probably due to the proportion of

area this boundary condition occupies. In general, shallow bedrock hydraulic conductivities are the most sensitive K_x parameters, followed by intermediate bedrock and lastly, the deep bedrock. Head and baseflow simulations exhibited negligible sensitivities to vertical anisotropy and river conductance. Manual sensitivity analyses proved that these parameters do have an affect on results, but generally require alteration of at least an order of magnitude. The generally low sensitivity of deep bedrock K_x parameters, which are overall similar in magnitude, suggest that the simplification of geological contacts will have little impact on the head distribution in upper layers and the GSIs.

Manual sensitivity analyses were performed for overburden thickness, boundary condition selection, and harbour conductance. Results show that overburden thickness, within a reasonable range, exhibited little impact on simulated head distribution and baseflow. Similarly, assignment of Glendyer Brook as a River Package, rather than Drain Package, resulted in a similar total flux between the aquifer and the stream. Conversely, the model results are sensitive to the conductance parameter of the harbour. For instance, when conductance was reduced by an order of magnitude (i.e., 90% reduction) harbour SGD was reduced by 19% and baseflow in the coastal streams increased 20%. Presumably, with a reduced connectivity between coastal aquifer and ocean, groundwater will more readily discharge into watercourses where bed sediments are more permeable.

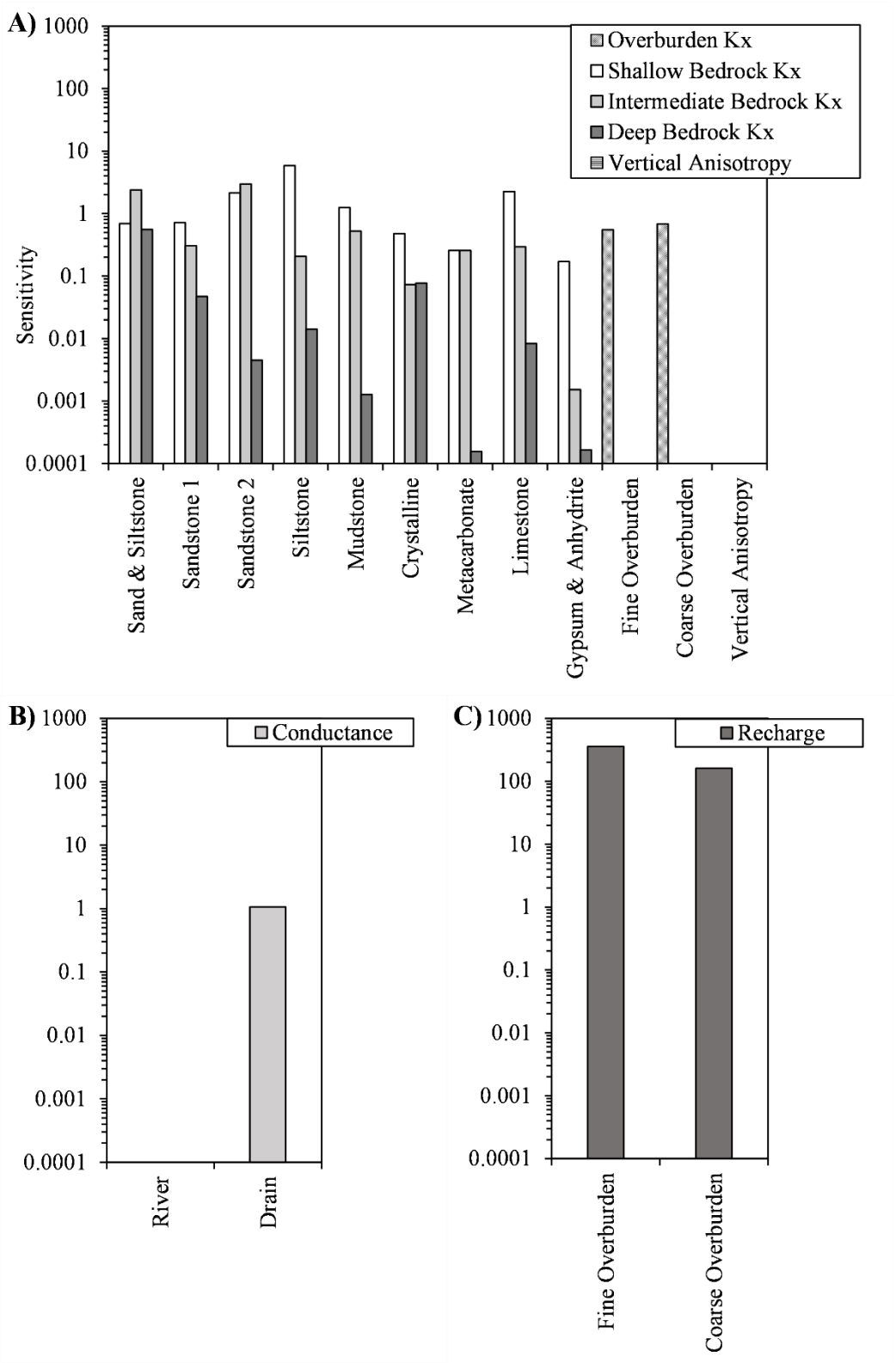

Figure 32: Parameter sensitivities to head and baseflow observations: A) hydraulic conductivity related parameters; B) conductance parameters; C) recharge parameters.

3.3.3 Model Statistics

Statistical measures were used to evaluate model fit, including mean residual, mean absolute residual, normalized root mean squared error (RMSE), and correlation coefficients (Table 11). These measures are often employed in the evaluation of numerical groundwater flow models (Anderson et al., 2015b). The complete report of measured and simulated head values, and their associated residuals are presented in Appendix V. The normalized RMSE is an effective measure of agreement between simulated and measured conditions (Anderson et al., 2015b). The RMSE essentially measures how well a model performs by analyzing residuals. Normalizing the RMSE to the full range of observations contextualizes the statistical evaluation to the conditions of the model. Normalized RMSE less than 10% are often considered to be acceptable in a groundwater model (Anderson et al., 2015b).

Table 11: Model statistics based on head observations. Observation group numbers increase with spatial accuracy. MR, MAR, RMSE, NRMSE, and CC respectively stand for mean residual, mean absolute residual, root mean square error, normalized root mean square error, and correlation coefficient. RMSE, NRMSE, and CC are only available on an integrated basis (all head observations).

Observation Group	n	MR	MAR	RMSE	NRMSE	CC
Head 1	22	2.71	6.17			
Head 2	38	1.90	8.32			
Head 3	1	-0.74	0.74			
Head 4	1	-0.13	0.13			
Head 8	13	4.90	6.80			
Head 9	3	-2.14	4.38			
Head 10	2	5.79	11.08			
Head 11	8	2.56	4.64			
All head observations	88	1.91	6.97	8.99	3.5%	0.985

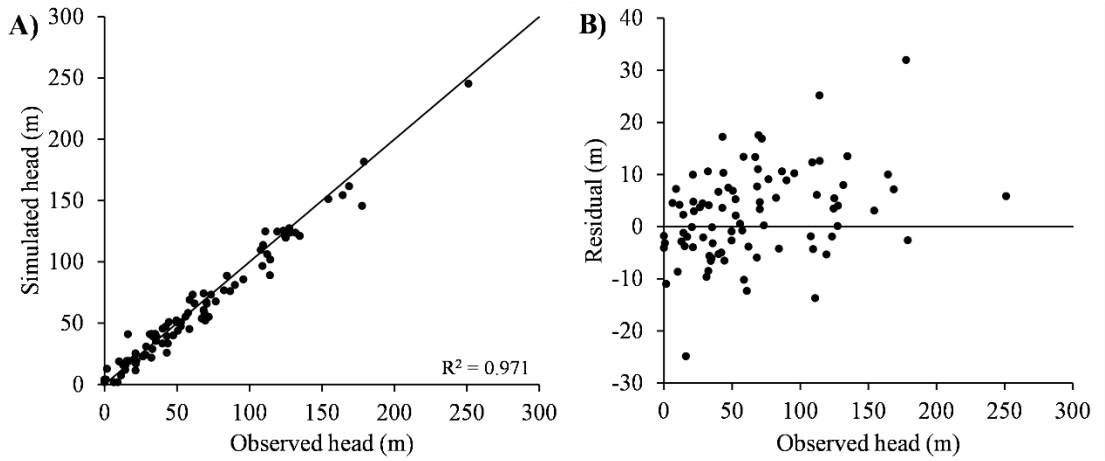

Figure 33: A) Simulated head vs observed head with a 1:1 line; B) residual vs observed head.

The mean residual for all head observations was 1.91 m indicating an overall equal spread around the identity line with a slight bias for positive residuals. Figure 33 shows a good fit to observations with a positive bias (Figure 33a), particularly at high elevations (>130m) as displayed in Figure 33b. This spread could be improved by calibrating the sandstone 1 and crystalline HSUs of the northern highlands separately from the south. The mean absolute residual is 6.97 m, which may be explained partially by georeferencing precision, the uncertainty associated with the ~10 m accuracy and 20 m resolution DEM, and the interpolation of the DEM on a 50 m mesh. The RMSE is 8.99 and the normalized RMSE is 3.6%, which is well within the threshold for adequate model performance (10%). The correlation coefficient of 0.985 indicates a strong positive relationship between observed and simulated heads.

3.3.4 Water Balance

The water balance for the groundwater flow model is presented in Table 12. Recharge accounted for the majority of the inflow to the groundwater system, followed by rivers. The recharge coefficient throughout the domain was approximately 30% (average of 452 mm yr^{-1}). Recharge coefficients for shallow bedrock and intermediate bedrock were 29% and 8%, respectively. Negligible inflow occurred from the harbour, as transient (e.g., tide-induced circulation) and variable-density conditions were ignored for this exercise. Drains accounted for the largest proportion of outflow, followed by rivers and then general-head boundary nodes (i.e., SGD). SGD accounted for 3.9% of groundwater discharge in the drainage basin (Table 13). According to freshwater discharge estimates (Appendix I), SGD is approximately 2% of river discharge into the harbour. Model results were also used to assess how groundwater discharge is partitioned between direct and indirect pathways on the subcatchment scale, rather than the full drainage basin. Based on model results, a liberal estimate of how much groundwater discharge is partitioned into SGD (Figure 1) within the harbour subcatchment is 30%, assuming that SGD is completely derived from local and intermediate groundwater flow. This is equivalent to approximately 14% of river flow (Appendix I). The SGD estimates on either scale are comparable to proportions presented in the literature. For example, Polemio and Limoni (2006) estimated that direct groundwater discharge into marine environments is ~6% of river discharge. Luijendijk et al. (2020) used spatially resolved global models to determine that near-coast discharge and SGD account for 0.2 – 26% of recharge in coastal watersheds. Furthermore, it is expected that indirect groundwater discharge would dominate over direct groundwater discharge in the harbour due to the elevated water table throughout the majority of the domain (Figure 34 and Russoniello et al., 2016).

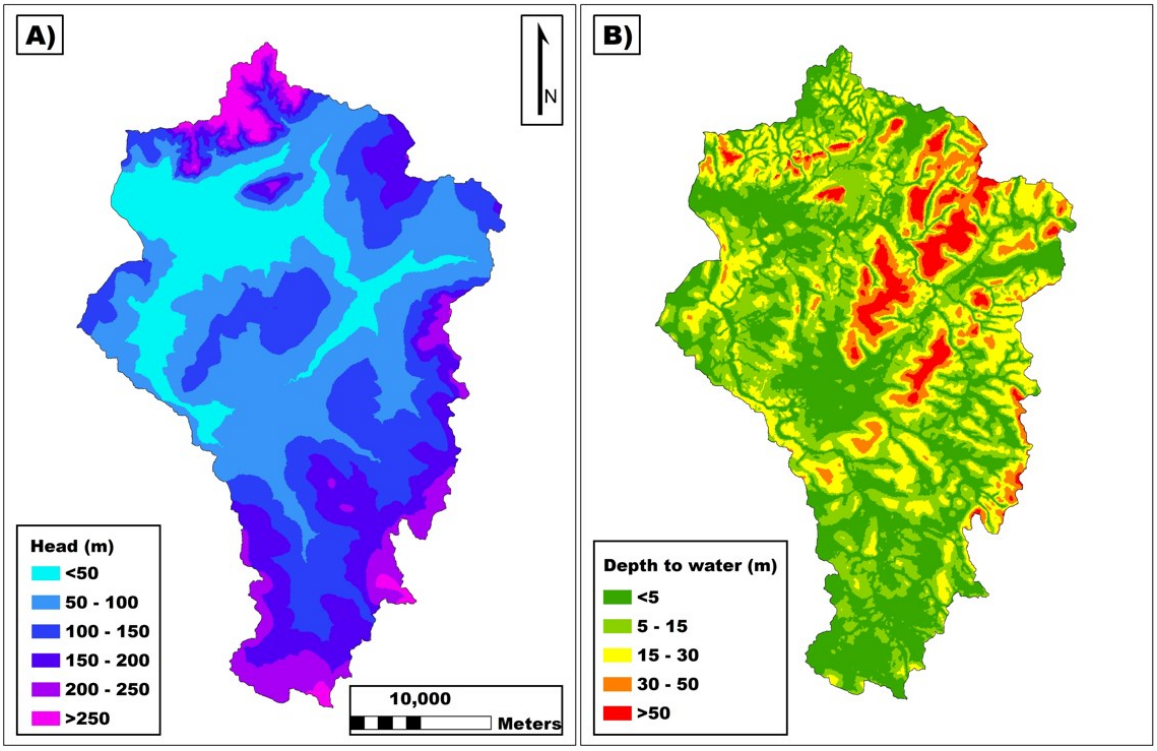

Figure 34: A) Head distribution from model results; B) depth to water table based on model results.

Table 12: Model water balance presenting inflows and outflows for the different boundary conditions.

	Inflow		Outflow	
	[$m^3 d^{-1}$]	[%]	[$m^3 d^{-1}$]	[%]
Rivers	136,653	23.3	242,642	41.4
Drains	0	0	326,424	55.7
General-head boundary	16	0	17,463	3.0
Recharge	449,860	76.7	0	0
Total flow	586,529	100.0	586,529	100.0

The normalized groundwater discharge of major surface water bodies is presented in Table 13. Total baseflow and SGD fluxes are normalized to the area of the corresponding watershed [m^2], such that the dominance of groundwater discharge in each water system can be evaluated. The rivers display a hierarchy of baseflow dominance in the order of NE Mabou River, followed by Mabou River, then SW Mabou River, which is consistent with the hydrograph analysis (Section 2.3.1) and their thermal regimes (Section 2.3.4). Prior to conditioning the baseflow, a version of the model with a single recharge parameter was calibrated exclusively to static water levels to evaluate the trends in GSIs without any guidance. This model iteration (results not shown) produced the same hierarchy indicating that certain subcatchments were more dominated by groundwater discharge due to factors other than recharge. The groundwater discharge within the harbour watershed is separated into harbour streams and harbour FSGD, based on the liberal assumption that all FSGD was recharged in the harbour subcatchment. The combined normalized flux for the harbour subcatchment is similar to the Mabou River (0.451 m yr^{-1}).

Table 13: Normalized groundwater discharge for the different subcatchments. Note that the harbour subcatchment is segmented into baseflow and FSGD.

	Area		Total flux		Norm. flux
	[km^2]	*[%]*	*[$m^3\ yr^{-1}$]*	*[%]*	*[$m\ yr^{-1}$]*
Mabou River	175.0	48.2	7.76×10^7	47.3	0.443
SW Mabou River	116.2	32.0	4.65×10^7	28.3	0.400
NE Mabou River	21.0	5.8	1.91×10^7	11.7	0.750
Harbour streams	50.9	14.0	1.46×10^7	8.9	0.314
Harbour FSGD	50.9	14.0	6.37×10^6	3.9	0.137
Total	363.2	100.0	1.64×10^8	100.0	0.452

Zonal budgets for the HSLs are presented in Table 14. Overburden and shallow bedrock are important aquifers in the drainage basin that account for the vast majority of groundwater flow (91.8%). This is supported by the abundance of drilled wells completed in shallow bedrock, and high yielding dug wells in coarse overburden. Coarse sediments disproportionately accounted for 44% of the flux from shallow bedrock into overburden, although they only account for 17% of the area. In general, there is more bedrock discharge occurring in areas with coarse overburden, which is consistent with expectations for the study site. Local and possibly intermediate flow regimes dominate the domain as only 7.6% and 0.6% of groundwater flow occurs in the intermediate and deep bedrock, respectively. Kennedy et al. (2010) suggested that groundwater systems are relatively shallow in Nova Scotia and the majority of the flow occurs in the upper 150 m. This agrees with model results, which indicate that 99.4% of flow occurs in the upper 100 m of bedrock. These results indicate that a no-flow boundary condition could safely be applied at a bedrock depth of 100 m to simplify the model in any future work. This also supports the simplification of vertical bedrock contacts used during model construction as deeper bedrock is relatively unimportant to groundwater flow.

Table 14: Zonal budgets for hydrostratigraphic layers

Zone	Total Outflow [$m^3\ yr^{-1}$]	Flow [%]
Overburden	1.00×10^6	59.9
Shallow Bedrock	5.34×10^5	31.9
Intermediate Bedrock	1.28×10^5	7.6
Deep Bedrock	1.07×10^4	0.6
All Zones	1.68×10^6	100.0

3.3.5 Groundwater – Surface Water Interactions

Figure 35a presents the estimated flux per unit length of the watercourse. The mean and standard deviation for river and drain groundwater discharge fluxes per unit length are 1.6 m^2 d^{-1} ± 9.9 and 1.3 m^2 d^{-1} ± 1.5, respectively. These numbers do not account for watercourse width, which ranges from 1 m for streams up to 30 m for the SW Mabou River. The mean groundwater discharge flux for drains likely represents the upper bound as some low order streams in high density networks were removed to better suit a 50m model grid resolution. The larger standard deviation in river flux is the result of variable widths in addition to both losing and gaining reaches being included. The discharge means are comparable to ranges presented in the literature (Duff et al., 2000). Certain reaches of tributaries exhibit parallel flow channels (Sophocleous, 2002), whereas the larger, more incised streams correspond to a more perpendicular flow path through the alluvial plain. Areas of heavy river loss in the SW Mabou River correspond with segments where the river is located close to the valley wall and may be the result of the lack of precision in the DEM interpolation onto a 50 m^2 grid.

Figure 35b presents the FSGD Darcy flux in the harbour. FSGD ranges from -0.003 to 0.123 m d^{-1} with a mean and standard deviation of 0.002 m d^{-1} ± 0.006. The highest fluxes are generally on the order of ~0.010 m d^{-1} and occur where hydraulic gradients are steepest or in areas that correspond with coarse overburden. The majority of the simulated FSGD occurs within 50 – 100 m of the shoreline, which is consistent with the literature (Taniguchi et al., 2002; Sawyer et al., 2016). Figure 36 presents the comparison between modelled SFGD within 50 m of the shoreline relative to observed SGD fluxes during the seepage meter study. For instance, the mean and standard deviation for simulated FSGD

and observed SGD within 50 m of the shoreline are 7.6×10^{-3} ± 0.0096 and 7.6×10^{-3} ± 0.0069, respectively. Furthermore, the upper range of simulated SFGD is less than the upper range for SGD, which is expected as FSGD will always be less than or equal to SGD. The model results yield SGD rates that are lower than what is generally published in the literature; however, Taniguchi et al. (2002) found that rates less than 0.100 m d^{-1} are most common. It is plausible that there is a bias in SGD research towards coastlines with greater fluxes as these are locations where SGD is more important. Other studies in the Arctic and Baltic Seas report SGD estimates less than 1 mm d^{-1} (Deming et al., 1992; Piekarek-Jankowska, 1996); however, the different recharge or permafrost conditions may complicate comparisons.

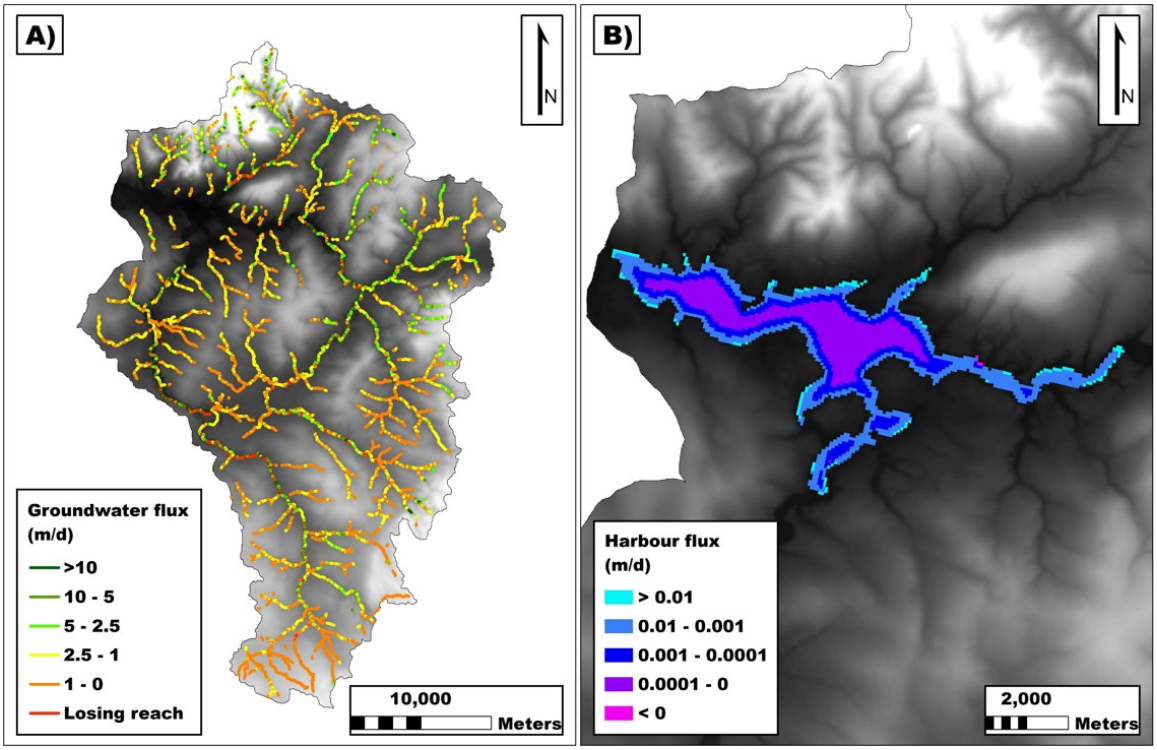

Figure 35: Groundwater - surface water interaction model results. A) River and drain groundwater fluxes; and B) harbour fluxes. A positive flux indicates groundwater discharge from aquifer.

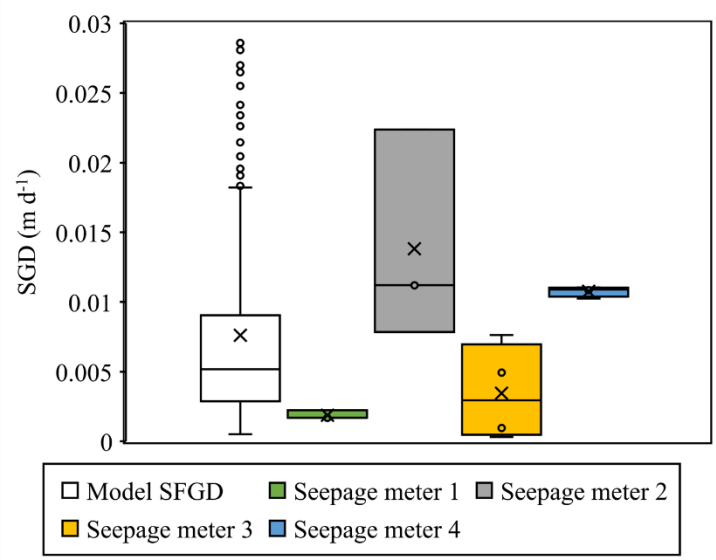

Figure 36: Box plots presenting distributions of modelled SFGD (within 50 m of shoreline) vs SGD measured during the seepage meter study.

3.3.6 Harbour Flushing Rate

When evaluating the importance of groundwater contributions to the harbour's water quality, the volume and flushing rate of the harbour must be considered. The flushing rate tells you approximately how long it takes for the volume of the harbour to replace itself; therefore, it offers insight into the contributions of direct and indirect groundwater discharge to the total harbour volume. Based on a spline-interpolation of bathymetric data, provided by AGRG (2017), the harbour volume is approximately 2.84×10^{7} m^3. Based on the precipitation record and the assumption that the *ET* rate was consistent between the Mabou River, SW Mabou River, and harbour subcatchments, the freshwater discharge into the harbour during 2019 was 1.02×10^{6} m^3 d^{-1} (Appendix I). Additionally, approximately 3.89×10^{6} m^3 of tidal water is introduced during each tidal cycle (Appendix III); therefore, the flushing rate of Mabou Harbour is ~3.3 days. By multiplying the groundwater discharge rates (direct and indirect) and the flushing rate, first-order approximations of the

contributions to the total harbour volume were calculated. Indirect groundwater discharge from the Mabou, SW Mabou, and NE Mabou Rivers contributed to approximately 2.5%, 1.5%, and 0.6% of the total harbour volume over the 3.3-day period, respectively. The contribution of the harbour streams and FSGD constituents to the harbour volume are 0.5% and 0.2%. In total, groundwater discharge (4.5×10^5 m^3d^{-1}) accounts for ~5.3% of the total harbour volume at any given time, with 5.1% attributed to indirect groundwater discharge. The total daily freshwater discharge corresponds to a contribution of 11.4% of the total harbour volume over a 3.3-day period. Furthermore, the groundwater contributions to harbour volume would not differ greatly under baseflow conditions, as the greatest variable in the flushing rate is the intertidal volume rather than freshwater discharge.

The freshwater fraction method (Ketchum, 1950) suggests that the freshwater fraction is 32% of the harbour volume. Given the estimated freshwater discharge during 2019, a flushing rate of 9 days would be required to achieve this freshwater fraction. This flushing rate corresponds to respective groundwater-derived contributions to the harbour volume of 6.7%, 4.0%, 1.7%, 1.3%, and 0.6% for the Mabou River, SW Mabou River, NE Mabou River, harbour streams, and FSGD. The total groundwater contribution to the harbour volume would be 14.3% given the longer flushing rate. The discrepancy between the freshwater fractionation and water budget methods might suggest that the harbour is not well-mixed and that there is a vertical salinity gradient/stratification. Stratification would overstate the freshwater component in the freshwater fraction method, and thus overestimate the flushing rate and groundwater contributions to harbour volume. The correlation between salinity minimums and low tide when the conductivity logger is closest to the surface (Appendix II, Figure A2) supports that the water column in the harbour may

be stratified. The stratification appears to increase following precipitation and high streamflow events (Figure A3).

3.3.7 Particle Tracking

The 20-year flow paths and 5-year recharge locations for Mabou Harbour, as predicted by the model, are presented in Figure 37. Agricultural zones were identified using the Agriculture Land Identification Project shapefile (EAT, 2018). The estimated residence time of SGD recharged in agricultural zones is generally less than 20 years. The predominant flow path for groundwater in the harbour valley is through the shallow bedrock, with very little lateral flow taking place in the overburden. Within five years, the majority of agricultural zones were reached by the backward particle tracking, especially on the northern flanks of the harbour where the gradient is the steepest. Tile drainage, where present, may reduce the residence time of agricultural groundwater prior to transport to the harbour; however, this was not assessed by the model.

Lateral flow within the domain primarily occurs in the shallow bedrock, particularly in areas where the bedrock is overlain by the less hydraulically conductive fine overburden. Conversely, when coarse overburden is present, flow generally occurs through the highly permeable alluvial, colluvial, and residuum deposits. In the broader floodplains, shallow-bedrock-groundwater discharges into the coarse overburden before continuing laterally towards the watercourse. Results show that the high-K of coarse overburden coupled with a steep hydraulic gradient (>3%) in the fluvial valleys can achieve flow rates of greater than 4 m d^{-1} (i.e., particles travel more than 200 m over the ~50 d survival time of faecal coliform bacteria). This is particularly true in regions where fractured crystalline

bedrock, with low effective porosity, coincides with steep gradients and coarse overburden (e.g., NE Mabou River subcatchment). In the steeper fluvial valleys, flow occurs predominantly through the shallow bedrock before discharging into the overburden of the floodplains, as predicted by the conceptual model. Overall, the mean and standard deviation for 50-day travel distance within fluvial valleys was 14 m ± 32 based on particle tracking results. The high standard deviation indicates the high variability between 50-day travel distances. Lateral travel distances from SGD discharge zones associated with fine overburden (vast majority of the harbour) were generally negligible over the 50-day period as the groundwater flow path is largely vertical through the fine sediments.

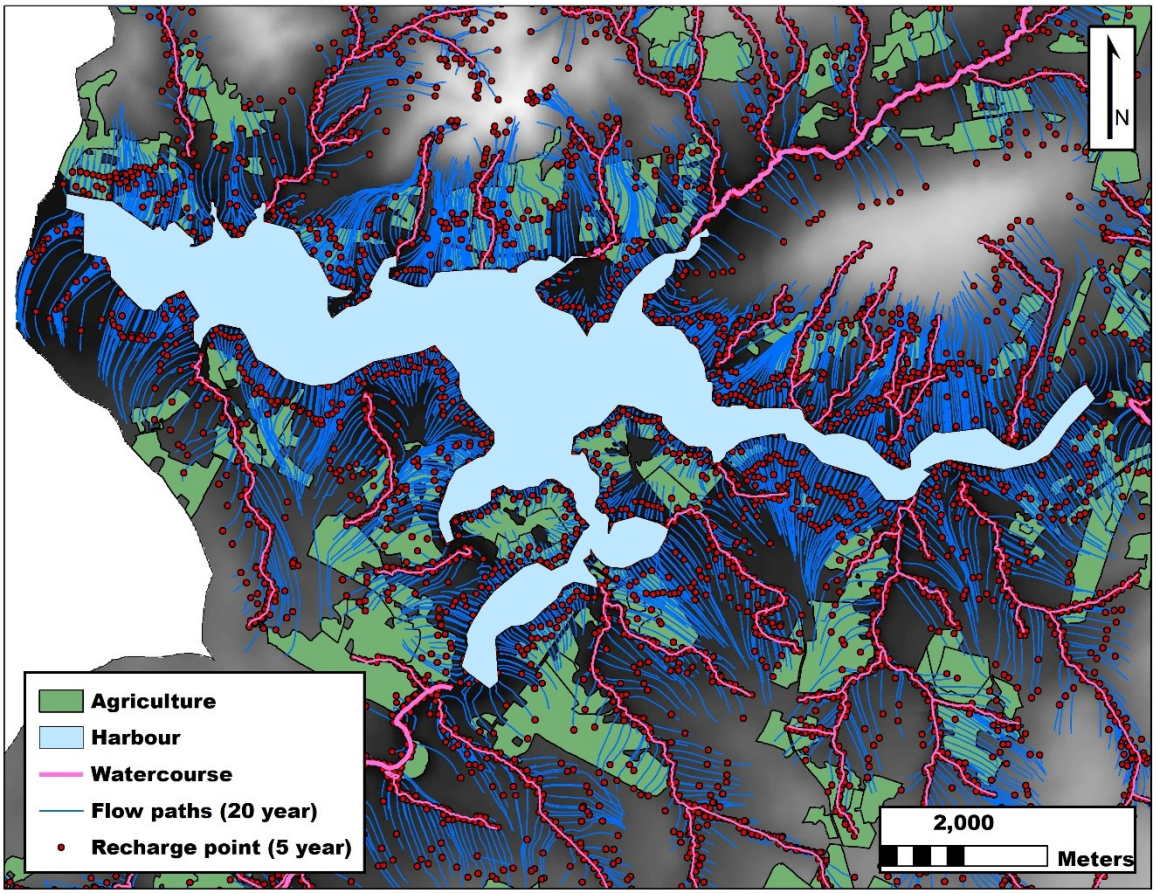

Figure 37: 20-year flow paths and 5-year recharge points surrounding Mabou Harbour. Recharge points represent the extent of particle back-tracking from surface water bodies over a 5-year period. Agricultural zones are indicated in green (EAT, 2018).

3.4 DISCUSSION & CONCLUSION

3.4.1 Calibration Results

The calibration results exhibited a decay of *K* with depth that is consistent with the conceptual model and the *K*-depth relationships presented by the well tests (Figure 27). The most rapid decrease in *K* generally occurs between the shallow and intermediate bedrock suggesting that secondary permeability will dominate in the shallow bedrock but will be less important with depth. The relatively high vertical anisotropy for the domain (0.97) indicates that vertically oriented geologic structures, such as fractures, are prevalent in the watershed.

Overall, the calibrated *K* values for the overburden and shallow bedrock are at the upper end of the expected range; however, the shallow bedrock HSUs agree with pumping tests for municipal wells and *K* estimates based on well tests (Appendix IV). Although relatively high, the overburden *K* values are consistent with those reported for unconsolidated Quaternary sediments and glacial till within the region (Cann et al., 1963; Rivard et al., 2008; Rivard et al., 2012; SLR Consulting, 2015). The high-*K* values in the shallow bedrock layers of gypsum and anhydrite, sandstone and siltstone, and limestone HSUs suggest areas of karstification that corroborate the delineation of these features on the Karst Risk Map of Nova Scotia (Drage and McKinnon, 2019).

3.4.2 Water Balance and Harbour Flushing Rate

The water balance from model results shows that indirect groundwater discharge dominates on the scales of the harbour subcatchment and the full drainage basin; however,

direct groundwater discharge is much more important within the harbour subcatchement. The model results agree well with the water balance derived from field data. For instance, the simulated baseflows for the Mabou and NE Mabou Rivers were within 1% of the results generated from baseflow separation. The Mabou and NE Mabou River baseflows were calibrated to baseflow separation results, and therefore, model results were influenced by field observations; however the model predicted that the SW Mabou River would be the least groundwater-dominated without any guidance from field observations during the calibration phase. These results are consistent with results from hydrograph and stream temperature analyses (Sections 2.3.1 and 2.3.3, respectively). Furthermore, the FSGD fluxes agree well with SGD measurements from the seepage meter study; however, seepage meter results could not be upscaled to reliably estimate the total SGD on a harbour scale for comparison. A source of uncertainty in the water balance is that water extraction from drilled wells were ignored. Extraction from such wells would redistribute water from the shallow and intermediate bedrock groundwater systems to surface water bodies; however, the municipal supply well VMa-P3 is currently approved for 396 m^3 d^{-1}, which is 0.09% of the estimated mean daily recharge to the groundwater system and would have a small impact on the drainage basin's water balance.

The calibrated recharge coefficients agree with those reported for watersheds with similar geology and climate conditions (Türker, 1969; Knott and Olimpio, 1986; Misstear et al., 2009), but are higher than other regional estimates (Kennedy et al., 2010; Rivard et al., 2014; SLR Consulting, 2015). The elevated recharge could be due to the large amount of coarse-grained sediments including alluvium, colluvium, and residuum in the drainage basin (17% of total overburden) that could facilitate a greater amount of infiltration.

Furthermore, many of the estimates for Nova Scotia focus on bedrock recharge, which will be lower than total recharge. Comparison of recharge coefficients with similar watersheds were attempted (i.e., River Inhabitants and MacLennan's Cross); however, streamflow exceeded precipitation indicating uncertainty in the historical climate data.

In addition to the water balance, the harbour flushing rate results suggests that groundwater contributes little to the total harbour volume. This low contribution of groundwater-derived freshwater suggests that groundwater may have limited influence on harbour water quality, particularly FSGD, assuming that the water column within the harbour is well mixed. Alternatively, the comparison of the water budget vs. freshwater fractionation methods for determining the harbour flushing rate suggests that the water column is stratified. The degree of stratification may have implications for the concentrations of groundwater-derived contaminants in the harbour. For instance, stratification would lead to higher concentrations of freshwater-borne contaminants at the surface. Therefore, impacted groundwater could have a greater influence on harbour water quality at the surface due to the limited amount of mixing throughout the water column.

3.4.3 Model Performance

Given the agreement between calibrated and observed *K* values, the overburden, shallow bedrock, and intermediate bedrock are considered to reasonably model the natural conditions within the domain, particularly in the HSUs associated with well-log data. Recharge conditions are reasonable given the geology and climate of the drainage basin. In some areas, particularly at toes of valley walls, the water table may exceed the surface

of the model, which could indicate that recharge is too large in local areas. In some cases, elevated water tables may be explained by missing streams from the model.

Model results agree well with field observations (Section 2.3). For instance, the hierarchy of groundwater contributions to the major rivers supports the results from hydrograph and stream temperature analyses (Sections 2.3.1 and 2.3.3, respectively). Local modelled hydraulic gradients agree well with corresponding field observations at NE Mabou River and Mabou River piezometer stations (1% vs. 1% and 2.5% vs. 2.7%, respectively). Conversely, the local hydraulic gradient at Lindy station differs (4.4% vs. 12%); however, this is likely attributed to the Lindy upper piezometer being completed in low-*K* sediments, which would increase the local head and hydraulic gradient determined through field methods. Additionally, the modelled FSGD within 50 m of the shoreline corroborates with seepage meter observations (Figure 36), such that field observations lie within the range of simulated results.

3.4.4 Nutrient Transport to the Mabou Harbour

Within the Mabou Harbour Drainage basin, the majority of agriculture resides upgradient and within short distances from groundwater discharge zones, such as watercourses or the harbour. Such conditions pose a risk for anthropogenic nutrients to enter the surface water network and thus contaminate Mabou Harbour. This risk is exacerbated by the ability for DIN to persist in groundwater over decades (Nolan et al., 1998).

As described in Section 1.1.3, riparian zones with shallow groundwater flow through organic rich sediments are effective nitrate buffers in coastal watersheds (Haycock and Pinay, 1993; Gold et al., 2001; Burt et al., 2002; Rassam et al., 2008) and will herein be referred to as effective riparian zones. Model results can be used to predict locations where effective riparian zones could exist (i.e., depth to water table <1 m). Figure 38 displays the common riparian conditions exhibited within the drainage basin. As displayed in Figure 38a, one set of conditions is where agriculture is in close proximity to a major river but is separated by a deeply incised valley wall. There is no effective riparian zone in this environment as the groundwater follows a deeper flow path, and thus limited denitrification can occur (Figure 39). In support of this conceptual model, Schilling et al. (2006) found that nitrate concentrations in riparian groundwater are greatest near incised streams with deeper water tables. As displayed in Figure 38b, the most effective riparian zones exist in the broader floodplains, which agrees with conceptual models from the literature (e.g., Rassam et al., 2006). Unfortunately, these zones are often used for agriculture as the fertile floodplain soils are desirable for farming. It is also common in agricultural regions to clear riparian forests and install drainage tiles or ditches to improve drainage and lower the water table (Hallberg, 1987; Zucker and Brown, 1998).

The residence time of the majority of groundwater recharged in agricultural zones immediately surrounding the harbour is less than 20 years, and nitrate contamination can persist for decades. Therefore, there is a risk of nutrient contamination in Mabou Harbour via SGD. Furthermore, water quality data provided by the Department of Energy and Mines presented elevated nitrate concentrations in a well located within an agricultural zone along the shore of the harbour. The nitrate concentrations were greater than the mean of non-

impacted wells (2.5 mg L^{-1} and 0.17 mg L^{-1}, respectively) suggesting that the aquifer beneath the agricultural zone has been impacted by anthropogenic activities.

It is possible that impacted SGD is more concentrated in nutrients relative to groundwater-derived baseflow given that flow paths from agricultural fields to the harbour predominantly occur in shallow bedrock, bypassing the shallow denitrification zones. In the study area, however, SGD fluxes are much less than baseflow, and therefore it may not disproportionately contribute to harbour contamination. Furthermore, the coastal mixing zone (CMZ), which was not considered in the numerical model, will likely influence the nutrient load to the harbour, regardless of the flow path.

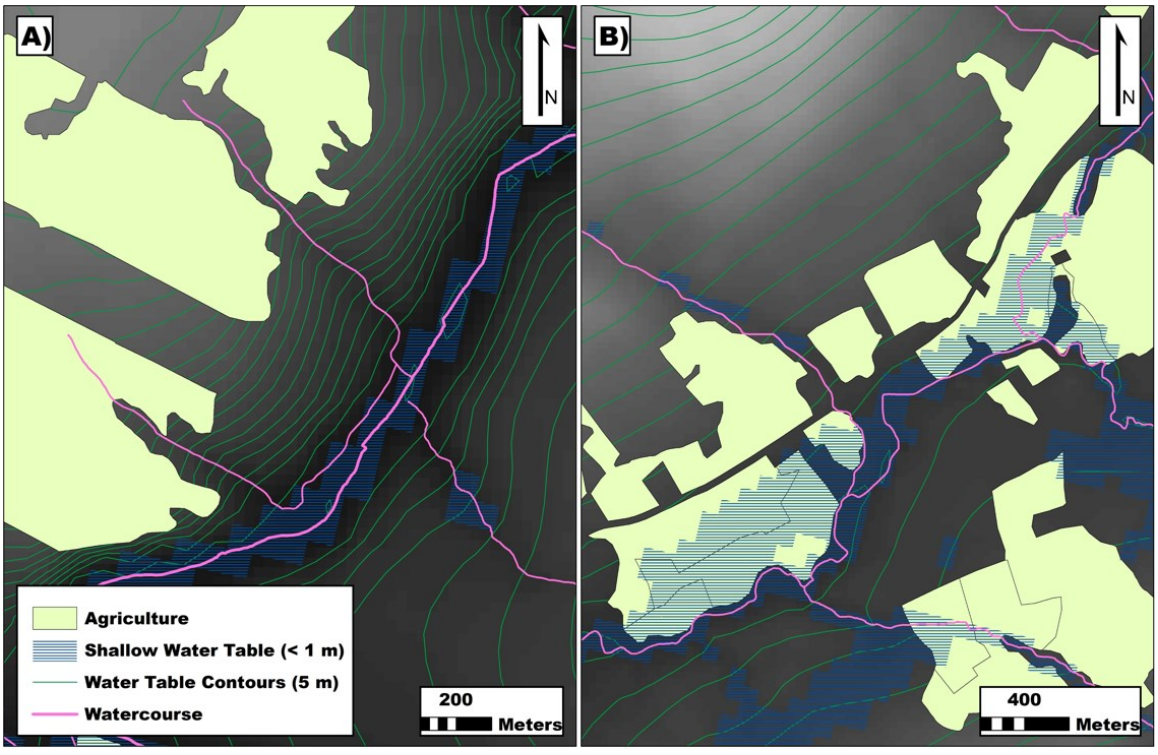

Figure 38: Areas where effective riparian zones may exist in relation to topography. A) Deeply incised fluvial valley of SW Mabou River; B) low-relief floodplains within the Mabou River subcatchment. Agriculture locations provided by EAT (2018). Watercourses were adapted from Department of Lands and Forestry (2020) as described in Section 3.2.2.6.3.

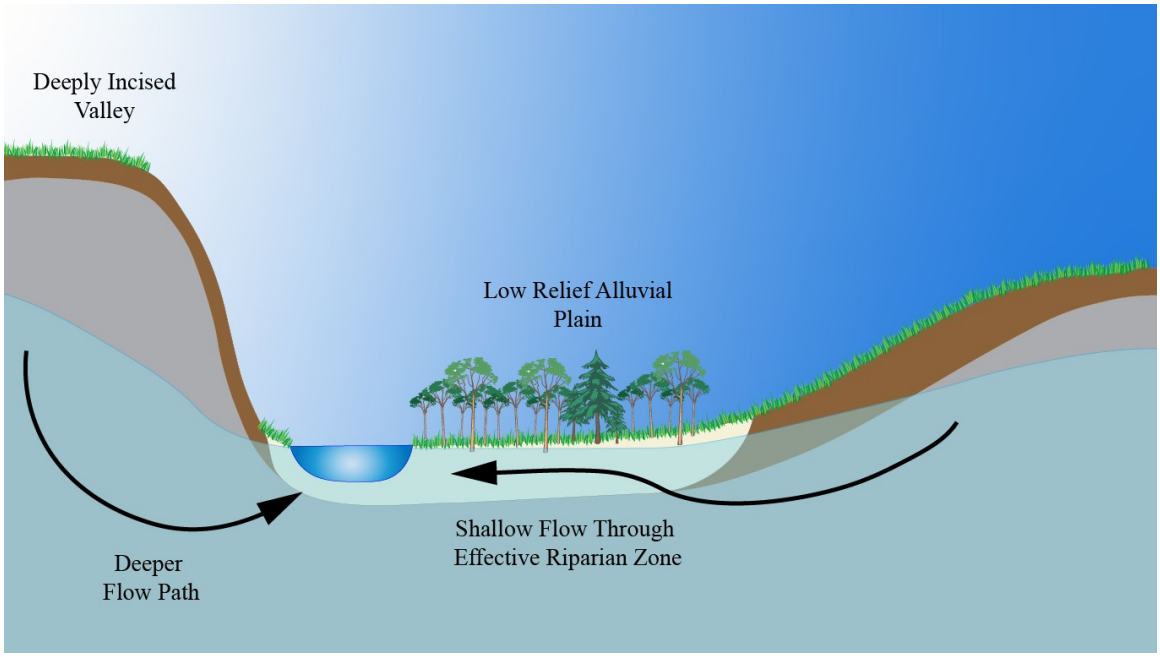

Figure 39: A conceptual model of shallow flow through the permeable sediments of an alluvial plain (effective riparian zone), which is often associated with the extensive denitrification of groundwater. Conversely, deeply incised valleys follow deeper flow paths through shallow bedrock that bypass effective riparian zones.

3.4.5 Microbial Transport to the Harbour

Pathogenic bacteria, such as some strains of *E. coli*, are often assumed to attenuate to safe levels within meters of flow through porous medium; however, travel distances of hundreds of meters under ideal conditions have been reported (Martin & Noonan, 1977; Harvey, 1989; Sinton, 1997). Because ~55 days is the approximate survival time of *E. coli* and other coliform pathogens in groundwater (McFeters et al., 1974; Keswick et al., 1982; Bitton et al., 1983; Pekdeger & Matthess, 1983; Dowd & Pillai, 1997; Taylor et al., 2004), 50 – day travel distances were analyzed to liberally identify risk areas for microbial contamination of surface water via groundwater discharge while neglecting other naturally attenuating processes such as mechanical filtration, adsorption, and decay. Model results show that the greatest 50-day travel distances occur in areas with high-*K* and hydraulic

gradients steeper than 1.5%. A risk map for areas that support rapid advection to surface water bodies was constructed by isolating the intersection of partially saturated coarse overburden, and moderate to high hydraulic gradients (Figure 40). Moderate and highly advective zones correspond to cells with hydraulic gradients between 1.5 – 3% and greater than 3%, respectively (Figure 40). High risk areas for rapid groundwater advection predominantly occur in the riparian zones of fluvial valleys where soils may be saturated and enriched in organics. Such conditions were identified as a positive influence on *E. coli* survival (Tate, 1978). It should be noted that the risk map predicts areas where rapid advection is possible; however, further characterization of the shallow aquifer would be required to determine if conditions are suitable for bacteria transport. A limitation of the risk map is that it does not account for preferential flow paths, such as fracture flow. Fractured bedrock with low effective porosity can support extremely rapid advective transport of bacteria (Champ & Schroeter, 1988; McKay, 1993; McKay, 1999).

Quick release pathways for groundwater coinciding with areas of manure application are also a risk for microbial harbour contamination via indirect groundwater discharge. Quick release pathways include springs, drainage ditches, and tile-drains intersecting or immediately adjacent to manure-spread fields. Tile drains in such environments often exceed drinking and recreational water standards (Warnemuende & Kanwar, 2000). Similarly, Howell et al. (1995) observed that springs in an agriculturally intensive watershed frequently exceeded primary contact water standards. Within the drainage basin, approximately 17 km of streams lie within 5 m of agricultural fields corresponding to a daily flux of approximately 11,000 m^3. Additionally, there is greater than 3 km of major rivers within 5 m of agriculture and an estimated daily flux of greater

than 6,000 m^3. These estimates are derived from GIS - shapefiles (EAT, 2018; Nova Scotia Department of Lands and Forestry, 2020) and are subject to geospatial inaccuracies in stream locations and farm borders. Given the high bacterial load of a sampled harbour stream (Appendix II; Table A11), these springs are possible contributors to the episodic bacteria contamination of the harbour. Furthermore, springs are often used as a source of drinking water in the Mabou Harbour drainage basin and may be falsely perceived to be of high quality.

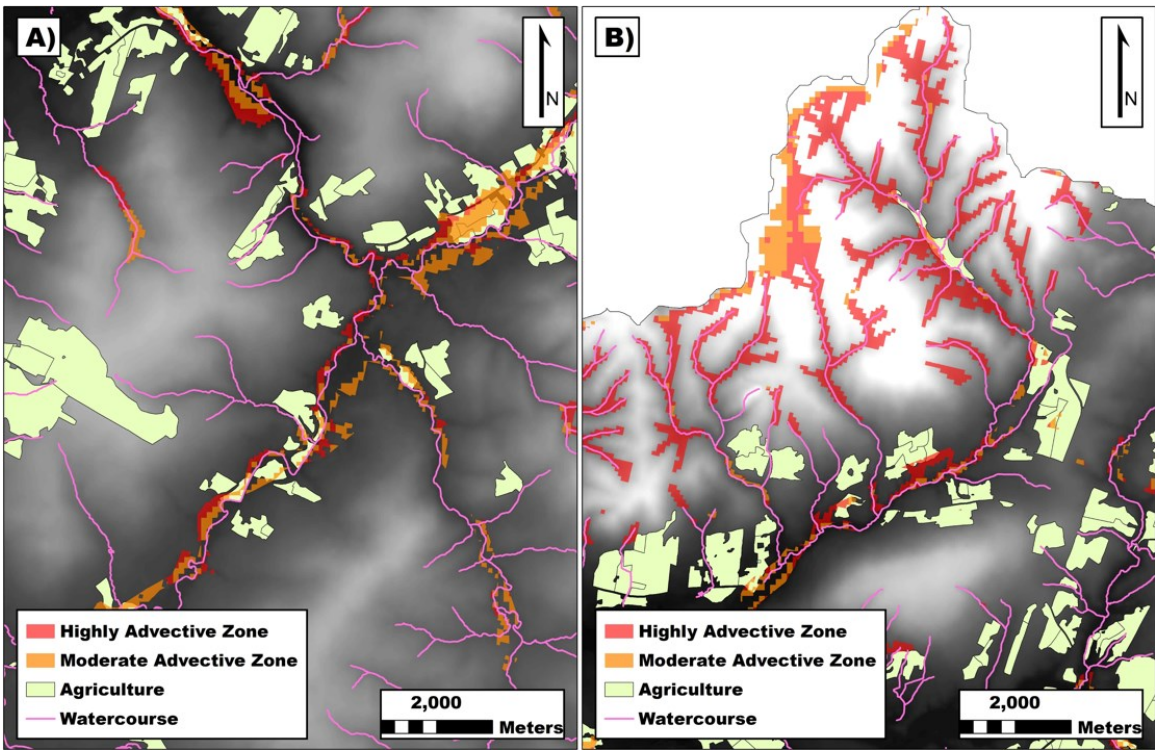

Figure 40: Risk maps for zones supporting rapid advection to surface water bodies (full map in Figure A7). A) The majority of moderate and highly advective zones exist in fluvial valleys (figure is focused on Mabou River watershed); and B) the majority of the highly advective zones are located in the Mabou Highlands of the NE Mabou River watershed. Agriculture shapefile provided by EAT (2018). Watercourses were adapted from Department of Lands and Forestry (2020) as described in Section 3.2.2.6.3.

REFERENCES: CHAPTER 3

Applied Geomatics Research Group. (2017). *Topo-bathymetric lidar research for aquaculture and coastal development in Nova Scotia: Final report*. Technical report, NSCC Middleton, NS.

Allocca, V., Manna, F., & De Vita, P. (2014). Estimating annual groundwater recharge coefficient for karst aquifers of the southern Apennines (Italy). *Hydrology and Earth System Sciences, 18*(2), 803-817.

Anderson, E. I., & Bakker, M. (2008). Groundwater flow through anisotropic fault zones in multiaquifer systems. *Water Resources Research, 44*(11).

Anderson, M. P. Woessner, W. W., & Hunt, R. J. (2015a). *Applied Groundwater Modeling—Simulation of Flow and Advective Transport.* Academic Press, Inc., San Diego, CA.

Anderson, M. P., Woessner, W. W., Hunt, R. J. (2015b). Assessing performance. In Anderson, M. P., Woessner, W. W., Hunt, R.J. (Eds.), *Applied Groundwater Modeling—Simulation of Flow and Advective Transport*: Academic Press, Inc., San Diego, Calif., pp. 375-436.

Baechler, F. (2015). The geology and hydrogeology of faults on Cape Breton Island, Nova Scotia, Canada: An overview. *Atlantic Geology, 51*, 242-268.

Baechler, F., & Broehner, R. (2014). Karst geology and hydrogeology of Cape Breton Island, Nova Scotia: An overview. *Canadian Journal of Earth Sciences*, *51*(7), 701–714.

Baechler, F. E., Cross, H. J., & Baechler, L. (2019). The geology and hydrogeology of springs on Cape Breton island, Nova Scotia, Canada: An overview. *Atlantic Geology*, *55*, 137–161.

Bailey, R. T., Wible, T. C., Arabi, M., Records, R. M., & Ditty, J. (2016). Assessing regional-scale spatio-temporal patterns of groundwater–surface water interactions using a coupled SWAT-MODFLOW model. *Hydrological Processes*, *30*(23), 4420–4433.

Banks, E. W., Simmons, C. T., Love, A. J., Cranswick, R., Werner, A. D., Bestland, E. A., Wood, M., & Wilson, T. (2009). Fractured bedrock and saprolite hydrogeologic controls on groundwater/surface-water interaction: A conceptual model (Australia). *Hydrogeology Journal, 17*(8), 1969-1989.

Barazzuoli, P., Nocchi, M., Rigati, R., & Salleolini, M. (2008). A conceptual and numerical model for groundwater management: A case study on a coastal aquifer in southern Tuscany, Italy. *Hydrogeology Journal, 16(*8), 1557-1576.

Barr, S. M., White, C. E., Fisher, B. E., McKinnon, J. S., Barras, A. L., & Hapgood, D. S. (2017). *DP ME 433, version 1, 2017. Digital geological data generated as part of the bedrock geological mapping compilation project for Cape Breton Island, Nova Scotia.* Nova Scotia Department of Natural Resources, Geoscience and Mines Branch.

Bitton, G., Farrah, S. R., Ruskin, R. H., Butner, J., & Choum, Y. J. (1983). Survival of pathogenic and indicator organisms in ground water. *Groundwater, 21*(4), 405–410.

Bitton, G., & Harvey, R. W. (1992). Transport of pathogens through soils and aquifers. *Environmental Microbiology*, *19*, 103-123.

Bredehoeft, J. D. (2002). The water budget myth revisited: Why hydrogeologists model. *Groundwater, 40*(4), 340-345.

Brunner, P., Simmons, C. T., Cook, P. G., & Therrien, R. (2010). Modeling surface water-groundwater interaction with MODFLOW: Some considerations. *Groundwater, 48*(2), 174-180.

Burt, T. P., Bates, P. D., Stewart, M. D., Claxton, A. J., Anderson, M. G., & Price, D. A. (2002). Water table fluctuations within the floodplain of the River Severn, England. *Journal of Hydrology, 262*, 1-20.

Cape Breton Partnership & The Inverness/Victoria Federation of Agriculture. (n.d.). Water resources program report: Mabou Harbour watershed. Prepared for: Nova Scotia Federation of Agriculture.

Cann, D. B., MacDougall, J. I., & Hilchey, J. D. (1963). Soil survey of Cape Breton Island Nova Scotia. Canada Department of Agriculture and Nova Scotia Department of Agriculture and Marketing.

Champ, D. R. and Schroeter, J. (1988). Bacterial transport in fractured rock - A field-scale tracer test at the chalk river nuclear laboratories. *Water Science and Technology 20*, 81–87.

Chandra, S., Auken, E., Maurya, P. K., Ahmed, S., & Verma, S. K. (2019). Large scale mapping of fractures and groundwater pathways in crystalline hardrock by AEM. *Scientific Reports, 9*(1), 1-11.

Cook, P. G. (2003). *A guide to regional groundwater flow in fractured rock aquifers*. Seaview Press, Henley Beach, South Australia.

Deming, D., Sass, J. H., Lachenbruch, A. H., & De Rito, R. F. (1992). Heat flow and subsurface temperature as evidence for basin-scale ground-water flow, North Slope of Alaska. *Geological Society of America Bulletin, 104*(5), 528–542.

Doherty, J. E., and Hunt, R. J. (2010). *Approaches to highly parameterized inversion—A guide to using PEST for groundwater-model calibration*. US Geological Survey Scientific Investigations Report 2010–5169.

Domenico, P. A., & Schwartz, F. W., (1990). *Physical and chemical hydrogeology*. John Wiley & Sons, New York.

Domenico, P. A., & Schwartz, F. W. (1997). *Physical and chemical hydrogeology* (2nd Edition). New York: Wiley.

Dowd, S. E., & Pillai, S. D. (1997). Survival and transport of selected bacterial pathogens and indicator viruses under sandy aquifer conditions. *Journal of Environmental Science and Health, 32*(8), 2245-2258.

Drage, J., & McKinnon, J. S., (2019). *DP ME 494, Version 1, 2019, Digital version of karst risk map of Nova Scotia.* Nova Scotia Department of Energy and Mines, Geological Survey Division.

Driscoll, F. G. (1986). *Groundwater and wells*. Johnson Division, St. Paul, Minn.

Duff, J. H., Toner, B., Jackman, A. P., Avanzino, R. J., & Triska, F. J. (2000). Determination of groundwater discharge into a sand and gravel bottom river: A comparison of chloride dilution and seepage meter techniques. *Internationale Vereinigung für theoretische und angewandte Limnologie: Verhandlungen, 27*(1), 406-411.

Duwelius, R. F. (1996). *Hydraulic conductivity of the streambed, east branch Grand Calumet River, nothern Lake County, Indiana*. US Geological Survey. Report 96-4218.

Environment and Agriculture Technology Research Group of the Nova Scotia Community College. (2018). *Agricultural land identification project*. Nova Scotia Community College.

ESRI. (2016). ArcGIS. Version 10.5.0.6491. Desktop: Release 10. Redlands, CA: Environmental Systems Research Institute.

ESRI. (2018). *World Imagery*. Updated Dec. 4, 2018. https://www.arcgis.com/home/item.html?id=2a060171c43e44888911e0d89145fd0c

Fleckenstein, J. H., Krause, S., Hannah, D. M., & Boano, F. (2010). Groundwater-surface water interactions: New methods and models to improve understanding of processes and dynamics. *Advances in Water Resources*, *33*(11), 1291–1295.

Ford, D. C. (2015). *Karst landform*. The Canadian Encyclopedia. Retrieved from: https://thecanadianencyclopedia.ca/en/article/karst-landform#:~:text=The%20most%20widespread%20surface%20karst,referred%20to%20as%20limestone%20pavement.

Freeze, A., & Cherry, J. (1979). *Groundwater*. Prentice-Hall, Englewood Cliffs, New Jersey.

Ghoraba, S. M., Zyedan, B. A., & Rashwan, I. M. H. (2013). Solute transport modeling of the groundwater for quaternary aquifer quality management in Middle Delta, Egypt. *Alexandria Engineering Journal, 52*(2), 197-207.

Gold, A. J., Groffman, P. M., Addy, K., Kellogg, D. Q., Stolt, M., & Rosenblatt, A. E. (2001). Landscape attributes as controls on ground water nitrate removal capacity of riparian zones. *Water Resources*, *37*(6), 1457–1464.

Government of Ontario. (2019). Chapter 10: Yield test. *Water supply wells: Requirements and best practices*. Ministry of the Environment, Conservation and Parks. Retrieved from: https://www.ontario.ca/document/water-supply-wells-requirements-and-best-practices/yield-test.

Grant, D. R. (1994). *Quaternary geology, Cape Breton Island, Nova Scotia*. Natural Resources Canada.

Green, J. M., Henkelman, K. K., & Caskey, R. M. (2004). *Hydraulic conductivity of near-surface alluvium in the vicinity of Cattlemans Detention basin, south Lake Tahoe, California*. US Geological Survey and US Department of the Interior.

Haitjema, H. M., & Mitchell-Bruker, S. (2005). Are water tables a subdued replica of the topography? *Groundwater, 43*(6), 781-786.

Hallberg, G. R. (1987). Nitrates in ground water in Iowa. F. M. D'Itri, L. G. Wolfson (Eds.), *Rural Ground Water Contamination*. Lewis Publishers, Chelsea, MI.

Han, D. M., Song, X. F., Currell, M. J., & Tsujimura, M. (2012). Using chlorofluorocarbons (CFCs) and tritium to improve conceptual model of groundwater flow in the South Coast Aquifers of Laizhou Bay, China. *Hydrological Processes, 26*(23), 2614-3629.

Han, P. F., Wang, X. S., Wan, L., Jiang, X. W., & Hu, F. S. (2019). The exact groundwater divide on water table between two rivers: A fundamental model investigation. *Water, 11*(4), 685.

Harbaugh, A. W. (2005). *MODFLOW-2005, the U.S. Geological Survey modular ground-water model: The ground-water flow process*. US Geological Survey Techniques and Methods 6-A16.

Harbaugh, A. W., Banta, E. R., Hill, M. C., & McDonald, M. G. (2000). *Modflow-2000, the U. S. geological survey modular ground-water model-user guide to modularization concepts and the ground-water flow process*. US Geological Survey: Open-file Report (00-92).

Harvey, R. W., George, L. H., Smith, R. L., & LeBlanc, D. R. (1989). Transport of microspheres and indigenous bacteria through a sandy aquifer: Results of natural and forced-gradient tracer experiments. *Environmental Science and Technology*, *23*(1), 51–56.

Haycock, N. E., & Pinay, G. (1993). Groundwater nitrate dynamics in grass and poplar vegetated riparian buffer strips during the winter. *Journal of Environmental Quality, 22*, 273-278.

Healy, R. W., & Scanlon, B. R. (2010). *Estimating groundwater recharge*. Cambridge UP, Cambridge.

Hill, M. C., & Osterby, O. (2003). Determining extreme parameter correlation in ground water models. *Ground water, 41*(4), 420-430.

Hiscock, K., & Bense, V. F. (2014). *Hydrogeology: Principles and practice* (Second ed.). John Wiley & Sons, New Jersey.

Howell, J.M., Coyne, M.S., & Cornelius, P. (1995). Fecal bacteria in agricultural waters of the Bluegrass Region of Kentucky. *Journal of Environmental Quality*, *24*(3), 411–419.

Jiang, X., Wan, L., Wang, X., Ge, S., & Liu, J. (2009). Effect of exponential decay in hydraulic conductivity with depth on regional groundwater flow. *Geophysical Research Letters, 36*(24).

Kennedy, G. W., Garroway, K. G. and Drage, J. M. (2009). Hydrogeology Program in Nova Scotia. In *Mineral Resources Branch, Report of Activities 2008*. Nova Scotia Department of Natural Resources, Report ME 2009-1, p. 53-60.

Kennedy, G. W., Garroway, K. G., & Finlayson-Bourque, D. S. (2010). Estimation of Regional Groundwater Budgets in Nova Scotia. In *Nova Scotia Department of Natural Resources, Mineral Resources Branch, Open File Illustration ME, 2*, 2010.

Keswick, B. H., Gerba, C. P., Secor, S. L., & Cech, I. (1982) Survival of enteric viruses and indicator bacteria in groundwater. *Journal of Environmental Science and Health, 17*(6), 903-912.

Ketchum, B. H. (1950). Hydrographic factors involved in the dispersion of pollutants introduced into tidal waters. *Journal of the Boston Society of Civil Engineers*, *37*, 296-314.

Knott, J. F., & Olimpio, J. C. (1986). *Estimation of recharge rates to the sand and gravel aquifer using environmental tritium, Nantucket Island, Massachusetts*. US Geological Survey: Water-Supply Paper 2297.

Langevin, C. D., & Guo, W. (2006). MODFLOW/MT3DMS–based simulation of variable-density ground water flow and transport. *Groundwater, 44*(3), 339-351.

Lautz, L. K., & Siegel, D. I. (2006). Modeling surface and ground water mixing in the hyporheic zone using MODFLOW and MT3D. *Advances in Water Resources, 29*(11), 1618-1633.

Louis, C. (1974). Rock hydraulics. In L Muller (Ed.), *Rock mechanics.* Springer, New York, pp. 299– 387.

Luijendijk, E., Gleeson, T., & Moosdorf, N. (2020). Fresh groundwater discharge insignificant for the world's oceans but important for coastal ecosystems. *Nature Communications, 11*(1).

Manning, C. E., & S. E. Ingebritsen (1999). Permeability of the continental crust: Implications of geothermal data and metamorphic systems, Reviews of *Geophysics, 37*, 127– 150.

Martin, G. N., & Noonan, M. J. (1977). *Effects of domestic wastewater disposal by land irrigation on groundwater quality of the Central Canterbury Plains*. Water and Soil Technical Publication No. 7, Ministry of Works and Development, Wellington, New Zealand.

Maxwell, R. M., & Kollet, S. J. (2008). Quantifying the effects of three-dimensional subsurface heterogeneity on Hortonian runoff processes using a coupled numerical, stochastic approach. *Advances in Water Resources, 31*(5), 807-817.

McFeters, G. A., Bissonnette, G. K., Jezeski, J. J., Thomson, C. A., & Stuart, D. G. (1974). Comparative survival of indicator bacteria and enteric pathogens in well water. *Journal of Applied Microbiology, 27*(5), 823-829.

McKay, L. D., Cherry, J. A., Bales, R. C., Yahya, M. T., & Gerba, C. P. (1993). A field example of bacteriophage as tracers of fracture flow. *Environmental Science & Technology, 27*(6), 1075-1079.

McKay, L., Fredericia, J., Lenczewski, M., Morthorst, J. & Klint, K. E. S. (1999). Spatial variability of contaminant transport in a fractured till, Avedore Denmark. *Nordic Hydrology, 30*, 333–360.

McWhorter, D. B., Sunada, D. K., & Sunada, D. K. (1977). *Ground-water hydrology and hydraulics*. Water Resources Publication.

Misstear, B.D.R., Brown, L., & Johnston, P.M. (2009). Estimation of groundwater recharge in a major sand and gravel aquifer in Ireland using multiple approaches. *Hydrogeology Journal*, *17*(3), 693–706.

Morgan, S. E., Allen, D. M., Kirste, D., Salas, C. J. (2019) Investigating the hydraulic role of a large buried valley network on regional groundwater flow. *Hydrogeology Journal, 27*, 2377-2397.

Niswonger, R. G., Panday, Sorab, & Ibaraki, M. (2011). *MODFLOW-NWT, a Newtonian formulation for MODFLOW-2005*. US Geological Survey Techniques and Methods 6-A37.

Nolan, B.T., Ruddy, B.C., Hitt, K.J., Helsel, D.R. (1998). A national look at nitrate contamination of ground water. *Water Conditioning and Purification, 39* (12), 76-79.

Nova Scotia Department of Environment. (2018). *1:10,000 watersheds for Nova Scotia*.

Nova Scotia Department of Lands and Forestry. (2020). *Nova Scotia topographic database*.

Pekdeger, A., & Matthess, G. (1983). Factors of bacteria and virus transport in groundwater. *Environmental Geology, 5*(2), 49–52.

Petrie, B. (1996). Temperature, salinity and sigma-t atlas for the Gulf of St. Lawrence. *Canadian Technical Report Hydrography and Ocean Sciences*, *178*, 256.

Piekarek-Jankowska. (1996). Hydrochemical effects of submarine groundwater discharge to the Puck Bay (Southern Baltic Sea, Poland). *Geographia Polonica, 67*, 103-120.

Polemio, M., & Limoni, P. (2006). *Groundwater pollution and risks for the coastal environment (southeastern Italy).* IAHS-AISH Publication. 477-486.

Pollock, D.W. (2017). *MODPATH v7.2.01: A particle-tracking model for MODFLOW*. US Geological Survey software release, 15 December 2017.

Prommer, H., Barry, D. A., & Zheng, C. (2003). PHT3D-A MODFLOW/MT3DMS based reactive multi-component transport model. *Groundwater, 42*(2), 247-257.

Psilovikos, Aris. (2006). Analysis of the governing partial differential equation of MODFLOW simulation model with two algorithms of backward differences. *Journal of Institute of Mathematics and Computer Sciences. Mathematics Series. 19.*

Rassam, D.W., Fellows, C., S., I., De Hayr, R., Hunter, H., & Bloesch, P. (2006). The hydrology of riparian buffer zones; Two case studies in an ephemeral and a perennial stream. *Journal of Hydrology*, *325*(1–4), 308–324.

Rassam, D. W., Pagendam, D. E., & Hunter, H. M. (2008). Conceptualisation and application of models for groundwater-surface water interactions and nitrate attenuation potential in riparian zones. *Environmental Modelling and Software*, *23*(7), 859–875.

Rempe, D. M., Dietrich, W. E. (2014). Bottom-up control on fresh-bedrock topography under landscapes. *Proceedings of the National Academy of Sciences of the United States of America, 111*(18), 6576-6581.

Rivard, C., Paniconi, C., Gauthier, M. J., François, G., Sulis, M., Camporese, M., Larocque, M., & Chaumont, D. (2008). A modeling study of climate change impacts on recharge and surface–groundwater interactions for the Thomas Brook catchment (Annapolis Valley, Nova Scotia). In *Proceedings of GeoEdmonton, Canadian Geotechnical Society–International Association of Hydrogeologists–Canadian National Chapter Joint Annual Conference, Edmonton, Canada*.

Rivard, C., Paradis, D., Paradis, S., Bolduc, A., Morin, R. H., Liao, S., Pullan, S., Gauthier, M. J., Trepanier, S., Blackmore, A., Spooner, I., Deblonde, C., Fernandes, R., Castonguay, S., Hamblin, T., Michaud, Y., Drage, J., & Paniconi, C. (2012). Canadian groundwater inventory: Regional hydrogeological characterization of the Annapolis-Cornwallis Valley aquifers. *Geological Survey of Canada, Bulletin, 598*.

Rivard, C., Lefebvre, R., Paradis, D. (2014). Regional recharge estimation using multiple methods: An application in the Annapolis Valley, Nova Scotia (Canada). *Environmental Earth Sciences, 71*, 1389-1408.

Russoniello, C. J., Konikow, L. F., Kroeger, K. D., Fernandez, C., Andres, A. S., & Michael, H. A. (2016). Hydrogeologic controls on groundwater discharge and nitrogen loads in a coastal watershed. *Journal of Hydrology, 538*, 783–793.

Sawyer, A. H., Michael, H. A., & Schroth, A. W. (2016). From soil to sea: The role of groundwater in coastal critical zone processes. *Wiley Interdisciplinary Reviews: Water*, *3*(5), 706–726.

Schilling, K. E., Li, Z., & Zhang, Y. (2006). Groundwater-surface water interaction in the riparian zone of an incised channel, Walnut Creek, Iowa. *Journal of Hydrology*, *327*(1-2), 140-150.

Scibek, J., Allen, D. M., Cannon, A. J., & Whitfield, P. H. (2007). Groundwater-surface water interaction under scenarios of climate change using a high-resolution transient groundwater model. *Journal of Hydrology*, *333*(2–4), 165–181.

Service Nova Scotia and Municipal Relations. (2003). *Enhanced digital elevation model, Nova Scotia, Canada*. Service Nova Scotia and Municipal Relations, Registry and Information Management Services, Nova Scotia, Canada.

Sinton, L. W., Finlay, R. K., Pang, L., & Scott, D. M. (1997). Transport of bacteria and bacteriophages in irrigated effluent into and through an alluvial gravel aquifer. *Water, Air, and Soil Pollution*, *98*(1–2), 17–42.

SLR Consulting. (2015). *Proposed Black Point Quarry project Guysborough County, Nova Scotia: Hydrogeological technical report*.

Sophocleous, M. (2002). Interactions between groundwater and surface water: The state of the science. *Hydrogeology Journal, 10*(1), 52-67.

South Florida Water Management District (n.d.). *Module 13: PEST Introduction*. Retrieved from: https://www.sfwmd.gov/sites/default/files/documents/ rsm_module_13.pdf

Speiran, G. K. (2010). Effects of groundwater-flow paths on nitrate concentrations across two riparian forest corridors. *Journal of the American Water Resources Association*, *46*(2), 246–260.

Stea, R. R., Conley, H., Brown, Y., & Fisher, B. E., (2006). *DP ME 36, version 2, 2006. Digital version of Nova Scotia Department of Natural Resources map ME 1992-3, surficial geology map of the province of Nova Scotia, 1:500 000*. Nova Scotia Department of Natural Resources, Mineral Resources Branch.

Stephens, D. B., Hsu, K. C., Prieksat, M. A., Ankeny, M. D., Blandford, N., Roth, T. L., Kelsey, J. A., & Whitworth, J. R. (1998). A comparison of estimated and calculated effective porosity. *Hydrogeology Journal, 6*(1), 156-165.

StructX. (2020). *Hydraulic conductivity ranges of various soil types*. Retrieved from: https://structx.com/Soil_Properties_007.html.

Taniguchi, M., Burnett, W. C., Cable, J. E., & Turner, J. V. (2002). Investigation of submarine groundwater discharge. *Hydrological Processes, 16*(11), 2115-2129.

Tate, R. L. (1978). Cultural and environmental factors affecting the longevity of Escherichia coli in histosols. *Applied and Environmental Microbiology,* 35, 925-929.

Taylor, R., Cronin, A., Pedley, S., Barker, J., & Atkinson, T. (2004). The implications of groundwater velocity variations on microbial transport and wellhead protection–Review of field evidence. *FEMS Microbiology Ecology, 49*(1), 17-26.

Thompson, C., Smith, L., Roudrajit, M. (2006). Hydrogeological modeling of submarine groundwater discharge on the continental shelf of Louisiana. *Journal of Geophysical Research, 12*.

Todd, D. K. (1980). *Groundwater hydrology* (2nd Edition). John Wiley & Sons, New York.

Tóth, J. (1963). A theoretical analysis of groundwater flow in small drainage basins. *Journal of Geophysical Research, 68*(16), 4795–4812.

Tóth, J. (1970). A conceptual model of the groundwater regime and hydrogeologic environment. *Journal of Hydrology, 10*(2), 164-176.

Türker, Y. (1969). *Short term variation of runoff-rainfall ratios in Nova Scotia IHD watersheds*. Dalhousie University.

Voss, C. I. (2011a). Editor's message: Groundwater modeling fantasies—Part 1, adrift in the details. *Hydrogeology Journal*, *19*(7), 1281-1284.

Voss, C. I. (2011b). Editor's message: Groundwater modeling fantasies—Part 2, down to earth. *Hydrogeology Journal*, *19*(8), 1455-1458.

Warnemuende, E., & Kanwar, R. (2002). Effects of swine manure application on bacterial quality of leachate from intact soil columns. *Transactions of the ASAE, 45*(6), 1849.

Waterloo Hydrogeologic. (2019). *Visual MODFLOW Flex 6.1: Boundary conditions theory*. Retrieved from https://www.waterloohydrogeologic.com/help/vmod-flex/index.html?vm_about_boundary_conditions____t.htm.

Watermark Numerical Computing. (2020). *PEST Model-independent parameter estimation user manual part 1: PEST, SENSAN and Global Optimisers.*

Watson, T. A., Werner, A. D., & Simmons, C. T. (2010). Transience of seawater intrusion in response to sea level rise. *Water Resources Research, 46*(12).

Webb, M. D., & Howard, K. W. (2011). Modeling the transient response of saline intrusion to rising sea-levels. *Groundwater, 49(4)*, 560-569.

Welch, L. A., & Allen, D. M. (2014). Hydraulic conductivity characteristics in mountains and implications for conceptualizing bedrock groundwater flow. *Hydrogeology Journal, 22*(5), 1003-1026.

Winston, R. B. (2020). *ModelMuse Version 4.3.* US Geological Survey Software Release.

Zucker, L. A., & Brown, L. C. (1998). *Agricultural drainage: Water quality impacts and subsurface drainage studies in the Midwest* (Vol. 871). Ohio State University Extension.

Chapter 4: CONCLUSION

The purpose of this thesis was to investigate the spatial patterns of groundwater-surface water interactions (GSIs) within a coastal drainage basin and evaluate the potential risks associated with direct and indirect groundwater discharge on nitrate and microbial contamination of a natural harbour. In this study, direct and indirect groundwater discharge are used to describe to the mechanisms through which groundwater reaches a natural harbour. Direct groundwater discharge is defined as submarine groundwater discharge (SGD) within the harbour, and indirect groundwater discharge is groundwater discharged into fluvial systems draining into the harbour. Mabou Harbour, on Cape Breton Island, NS was selected as the study site. Mabou Harbour has high agricultural density, potentially contributing to nitrate and microbial groundwater contamination, and a history of persistent bacterial contamination resulting in episodic harbour closures.

Within this study, a combination of field methods and modelling was employed. Stilling wells, thermal sensors, and floodplain piezometers were installed to characterize GSIs within the Mabou rivers, and to analyze their spatiotemporal patterns. Hydrograph analyses and thermal regimes of the major rivers were interpreted to compare the groundwater dominance between the rivers. Similarly, coastal zone piezometers and seepage meters were employed to characterize the ocean–aquifer interactions and spatiotemporal patterns. Fast Fourier transform (FFT) analysis was applied to harbour and piezometer hydrographs to analyze connectivity between the harbour and the coastal aquifer. Seepage meters were installed at four locations around the perimeter of the harbour

to capture large-scale heterogeneity in geological and hydrogeological conditions. The flushing rate of the harbour was calculated using the water budget and freshwater fractionation methods.

A simplified, steady state, three-dimensional groundwater flow model was constructed using MODFLOW-NWT to investigate groundwater flow paths and residence times in addition to the spatial distribution and fluxes of GSIs on a regional scale. In an attempt to capture the relatively complex geological framework of the drainage basin, nine bedrock hydrostratigraphic units (HSUs) were created based on primary and secondary lithology, in addition to hydraulic properties where available. The bedrock HSUs were further subdivided into three hydrostratigraphic layers (HSLs) to capture the decay of K in relation to depth. Two overburden HSUs were created based on matrix grain size and additionally functioned as the primary recharge zones. The model was calibrated to baseflow observations from the field and static water levels from the Nova Scotia Well Logs Database (NSWLD; n=88) using PEST. Model results were validated by the seepage meter analysis. Model results were then used to identify hydrogeological and geomorphological conditions associated with a risk of groundwater-borne contaminant transport to surface waters.

4.1 Ocean – Aquifer Interactions

FFT analysis, applied to data from coastal piezometers, suggests that direct groundwater discharge should be limited due to a low connectivity between the coastal aquifer and the harbour. Although connectivity is limited, aquifer responses to semi-diurnal

tidal signals and storm surges (during a post-tropical storm) observed in the nearest well indicate that the coastal aquifer is hydraulically connected to the harbour. The limited tidal influence on the aquifer may result in a relatively small upper saline plume, and thus a narrow mixing zone between the fresh and saline groundwater. Furthermore, groundwater chemistry in the nearest well suggests that the mixing zone is constrained to the intertidal zone.

Both the field methods and numerical modeling indicate that direct groundwater discharge to the harbour, in the form of fresh SGD (FSGD), is minor compared to indirect groundwater discharge. The seepage meter results yielded a mean and standard deviation of 7.6×10^{-3} m d^{-1} ± 0.0069. Similarly, simulation results yielded a mean and standard deviation of 7.6×10^{-3} m d^{-1} ± 0.0096 for FSGD within 50 m of the coastline. Model results indicate that FSGD accounts for a minor proportion of groundwater discharge in the drainage basin (3.9%), corresponding to 6.37×10^{6} m^{3} yr^{-1}. It is assumed that there is limited intermediate or regional groundwater flow that contributes to FSGD. This is supported by the zonal budgets, which indicate that the local groundwater flow regime through the overburden and shallow bedrock dominates within the drainage basin (91.8% of groundwater flow). Assuming negligible intercatchment flow to the harbour (i.e., regional groundwater flow), the majority of SGD can be assumed to have originated within the harbour subcatchment, which covers 13% of the drainage basin. A liberal estimate of direct groundwater discharge within the harbour subcatchment is 30% of total subcatchment groundwater discharge.

4.2 STREAM – AQUIFER INTERACTIONS

There is strong stream – aquifer connectivity in the Mabou and NE Mabou fluvial valleys due to the presence of permeable alluvial materials. The Mabou and NE Mabou Rivers are direct-recharge driven stream-aquifer systems, presumably due to deeply incised geomorphologies and high-water tables. Based on field data, limited bank storage occurs along the major rivers. The NE Mabou River data exhibited negligible bank storage over a distance of 1 m, and the Mabou River showed bank storage only during the highest streamflow event over a distance of 2.5 m. This suggests that major streams within the drainage basin displaying incised geomorphologies are direct-recharge driven, and thus receive limited bank storage, which limits potential for attenuation of nitrate.

The numerical model predicts that 96.1% of groundwater discharge enters the harbour indirectly as groundwater-derived baseflow. This is likely due to the prevalence of local regime groundwater flow (91.8% of groundwater flow) in addition to elevated water tables, which has been shown to promote a dominance of indirect groundwater discharge in coastal watersheds (Russoniello et al., 2016). Thermal and hydrometric data indicate that the NE Mabou River is the most groundwater-dominated river, followed by the Mabou and SW Mabou Rivers. This hierarchy of groundwater contributions between the major rivers is corroborated by model results. The model results predict that the mean and standard deviation for groundwater discharge into rivers and tributaries (per unit length) are 1.6 m^2 d^{-1} ± 9.9 and 1.3 m^2 d^{-1} ± 1.5, respectively.

4.3 POTENTIAL FOR HARBOUR CONTAMINATION

There are several potential sources for microbial and DIN contamination of aquifers within the drainage basin, including manure application, septic systems, fertilizers, and raw sewage disposal systems predating regulation. Given the prevalence of agriculture (30.8 km^2 or 8.5% of the drainage basin), it is considered to be the primary non-point source of nitrate and microbial contaminants introduced to the groundwater system. Furthermore, the majority of the agriculture within the drainage basin resides upgradient and within short distances from groundwater discharge zones, such as watercourses or the harbour.

Given that the vast majority of groundwater discharge entering the harbour comes from groundwater-derived baseflow, indirect groundwater discharge is the more probable vector for groundwater-borne contaminants to enter the harbour. Based on model results and the spatial distribution of agricultural sites, the majority of the agricultural recharge will enter the harbour indirectly as groundwater-derived baseflow through surface watercourses contributing to a greater contaminant load. Indirect groundwater discharge is also the more probable vector for groundwater-borne contaminants on the harbour subcatchment scale. For instance, although the predominant source of FSGD is assumed to be recharge from within the harbour subcatchment, the subcatchment's groundwater is largely drained by streams (conservatively estimated at >60%).

Flushing rates calculated from data collected during the instrumented field season indicate that groundwater-derived freshwater contributes little to the total harbour volume; however, further investigation is required to determine if groundwater discharge can have

significant local impacts on harbour quality. For instance, conductivity data revealed stratification of fresh and saline water in the harbour. Stratification is most intense following heavy precipitation and streamflow events. The degree of stratification may have implications for the concentrations and pervasiveness of groundwater-derived contaminants throughout the water column.

Water quality sampling and secondary data indicates that groundwater within the drainage basin is impacted by non-point and point sources. Furthermore, groundwater-surface water interactions (GSIs) may impact microbial concentrations within surface water bodies. Model results suggest that direct groundwater discharge poses little risk for groundwater-borne bacterial contaminants to enter the harbour. Model results also show that rapid advection with greater lateral transport distances is generally associated with indirect groundwater discharge. Under ideal conditions (i.e., rapid advective transport, coarse sediments, and short residence times), bacteria have been observed travelling hundreds of meters laterally in the phreatic zone (Martin & Noonan, 1977; Harvey, 1989; Sinton, 1997). Although it is difficult to assess the risk of faecal coliform bacteria transport on a regional scale, areas in which great advective transport distances occur within the short survival rate of most coliform pathogens can be identified. This method excludes the naturally attenuating processes that affect bacterial concentrations, such as mechanical filtration, 1st order decay, and adsorption. Further characterization of the shallow aquifer would be required to evaluate risk of microbial transport. Model results indicate that rapid groundwater advection and short residence times predominantly occur in the riparian zones of fluvial valleys. Furthermore, riparian soils may be saturated and enriched in organics supporting *E. coli* survival (Tate, 1978). Quick release pathways are also a risk for

microbial harbour contamination via indirect groundwater discharge. For instance, given the abundance of streams within close proximity to agriculture, and the high coliform concentrations observed in the field (600 CFU 100 mL^{-1}; Appendix II), such streams are possibly contributing significantly to bacteria contamination in the harbour. A limitation of the model is that it does not account for terrestrial coastal groundwater discharge (i.e., seepage faces along the bluffs and beaches) as a quick release pathway between agriculture and the harbour. Furthermore, other faecal pathogens, such as viruses, have a greater transport potential than bacteria in the saturated zone.

Results indicate that the harbour may be at risk of nitrate contamination via indirect groundwater discharge. Many of the watercourses within the drainage basin display incised geomorphology. Particle tracking shows that groundwater flow to deeply incised rivers predominantly occurs through shallow bedrock with deeper water tables. This relatively deeper flow path may allow nitrates to transport more conservatively prior to discharge. Model results predict that majority of effective riparian zones occur on alluvial plains; however, such riparian zones are often altered and exploited for agricultural purposes which may reduce efficacy of denitrification and add nutrients by way of manure or fertilizer. Furthermore, the limited amount and shallow penetration of bank storage in the Mabou and NE Mabou river-aquifer systems suggests that nitrate buffering processes associated with bank storage may be limited in this drainage basin.

Although direct groundwater discharge only contributes marginally to the total volume of the harbour, it is probable that it is impacted to some degree by agricultural activities. For instance, it was assumed that the Harbour subcatchment is the main

contributor of FSGD into the harbour and has the greatest density of agricultural coverage (20.5%); therefore, the risk of direct groundwater-borne harbour contamination should not be ignored. According to particle tracking results, a large portion of the groundwater that was originally recharged in agricultural zones and discharges as SGD has a residence time of less than 20 years. Given the persistence of nutrients over decades (Nolan et al., 1988), there is risk for direct groundwater discharge to contribute to nitrate levels in the harbour, particularly if crop-type and farm practices include nitrogen-rich fertilizers; however, residence times predicted by the model are likely too long to support microbial transport.

The geometry and redox conditions of the coastal mixing zone (CMZ) also play a role in the risk of nitrate contamination via direct groundwater discharge. The potentially small upper saline plume and narrow mixing zone, due to limited ocean-aquifer connectivity and tidal influence, may further reduce the residence time and efficacy of any denitrification associated with the biogeochemical processes hosted by the CMZ. Furthermore, the oxic conditions of the seawater and shallow groundwater would suggest that nitrate may transport more conservatively through the CMZ as little denitrification occurs in mixing zones between oxic groundwater and oxic seawater (Slomp and Van Cappellen, 2004).

4.4 HYPOTHESES CONCLUSIONS

The results and conclusions within this thesis partially falsify the following hypothesis:

iii) provided SGD is adequately large, direct groundwater discharge will be associated with a risk for nitrate contamination, and possibly microbial contamination provided residence times are sufficiently short.

For instance, the model results suggest that residence times of SGD, excluding extreme conditions (i.e., karst or extensive fracture flow), exceed the survival rate of most faecal coliform bacteria; however, it should be noted, that other faecal microorganisms, such as viruses, may have a greater transport potential through the saturated zone. The field and modelling results do suggest that nitrates may transport relatively conservatively to the harbour via direct groundwater discharge.

Furthermore, the results and conclusions support the following hypotheses:

i) indirect groundwater discharge is the dominant mechanism for groundwater to enter the harbour; and

ii) indirect groundwater discharge is associated with the greatest risk for groundwater-borne contaminants to enter the harbour due to a presumably larger contribution relative to SGD.

Model results suggest that 96.1% of groundwater discharge that enters the harbour does so as indirect groundwater discharge. Indirect groundwater discharge drains a greater proportion of agriculturally-based groundwater, and therefore likely contributes a greater contaminant load in comparison to direct groundwater discharge. Additionally, results

suggest that indirect groundwater discharge is associated with risks for both nitrate and microbial contamination. Furthermore, the contribution of direct groundwater discharge to the total harbour volume is relatively insignificant, and therefore, the influence on harbour water quality may be limited.

4.5 RESEARCH SIGNIFICANCE

This thesis provides a valuable case study regarding SGD and its potential impacts on coastal contamination in Canada, where there is a notable gap in research (Bobba et al., 2011). Additionally, little emphasis has been placed on SGD in low-permeability environments (Taniguchi et al., 2019), such as the till-dominated landscape of Mabou Harbour. Therefore, results will help broaden the understanding of SGD in glacial sediments where there is currently a bias towards more permeable materials such as glacial outwash. Given the vast amounts of Canadian coastlines dominated by glacial till and derivative sediments, this study yields a more realistic representation of how groundwater discharge is partitioned between direct and indirect pathways in such environments. The results of this thesis also have direct relevance for understanding pathways for groundwater-borne contaminants in major contaminated sites in Nova Scotia (e.g., Sydney Tar Ponds, and Boat Harbour). In regard to recent GSI research, there appears to be a gap in regional scale GSIs and their contributions to the ocean (e.g., Russoniello et al., 2016). Therefore, this case study may improve the understanding of how groundwater discharge is partitioned between direct and indirect pathways to the ocean.

Natural harbours are commonplace for rural agricultural communities in the Canadian Maritimes; therefore, the results and conclusions of this study may offer insight into the GSIs and associated contaminant risks within coastal drainage basins throughout the region and improve land-use planning. For instance, emphasis could be placed on maintaining riparian forests along major water courses in agricultural watersheds. This study may also act as the foundation for future work regarding groundwater-related water quality issues in Mabou Harbour. Contamination risks have been identified for the different groundwater pathways, and the spatial distribution of areas or conditions associated with these risks have been identified through numerical modelling. Furthermore, the connections made between geomorphology, hydrogeology, and contamination risks can be applied to many regions as both high and low relief conditions are considered in this study.

4.6 Recommendations for Future Work

Regarding the ongoing investigation of microbial contamination within the Mabou Harbour drainage basin, some recommendations for future work are provided below. Water sampling for faecal coliform bacteria should continue in the harbour and major watercourses to constrain microbial sources. Additionally, the high-risk areas for rapid advective transport may possibly be used to guide or corroborate with future sampling. Local characterization of shallow aquifers in areas supporting rapid advection would be required to determine if conditions are suitable for bacteria transport. Investigation into unique hydrogeological conditions, such as karst or fracture flow where the effective porosity is limited should be considered before completely ruling out the contribution of SGD to harbour faecal coliform bacteria levels. Such conditions could support the rapid

transport of faecal pathogens from manure spread fields to the harbour via direct groundwater discharge (Shinn et al., 1994; Paul et al., 1997). Similarly, macropore modelling may show that groundwater is transmitted through the glacial till more rapidly then suggested by the equivalent continuum approach (i.e., applying a bulk K to the entire model cell) used in this study (e.g., Christiansen, 2004). Sampling of groundwater discharge from quick release pathways should be considered as previous results have shown that total faecal coliform and *E. coli* levels can be high (Appendix II). This is especially true when considering that the Harbour subcatchment presents the greatest agricultural coverage and contains many of such streams discharging directly into the harbour that would not be captured by sampling the major rivers.

Regarding nitrate contributions to the harbour, the model results from this study may be used as the foundation for future field and modelling based research. Geomorphological characteristics associated with hydrogeological conditions that support more conservative transport of nitrate have been identified. Similarly, regions where riparian zones supporting extensive denitrification have been predicted by model results. The results of this study could be used to identify and focus local-scale investigations of high or low risk areas. Future work should include reactive transport, with macropore capabilities, and perhaps on a smaller scale to allow further grid refinement (e.g., Conan et al., 2003; Christiansen, 2004; Lee et al., 2006). Further groundwater sampling in riparian zones, CMZs, and agricultural areas along various flow paths could better characterize the denitrification processes that are occurring or are absent in the drainage basin (e.g., Tesoriero et al., 2000).

REFERENCES: CHAPTER 4

Bobba, A., Chambers, G., & Wrona, P. (2012). Submarine groundwater discharge (SGWD): An unseen yet potentially important coastal phenomenon in Canada. *Natural Hazards, 60*(3), 991-1012.

Christiansen, J. S., Thorsen, M., Clausen, T., Hansen, S., & Refsgaard, J. C. (2004). Modelling of macropore flow and transport processes at catchment scale. *Journal of Hydrology, 299*(1-2), 136-158.

Conan, C., Bouraoui, F., Turpin, N., de Marsily, G., & Bidoglio, G. (2003). Modeling flow and nitrate fate at catchment scale in Brittany (France). *Journal of Environmental Quality, 32*(6), 2026-2032.

Harvey, R. W., George, L. H., Smith, R. L., & LeBlanc, D. R. (1989). Transport of microspheres and indigenous bacteria through a sandy aquifer: Results of natural and forced-gradient tracer experiments. *Environmental Science and Technology*, *23*(1), 51–56.

Lee, M. S., Lee, K. K., Hyun, Y., Clement, T. P., & Hamilton, D. (2006). Nitrogen transformation and transport modeling in groundwater aquifers. *Ecological Modelling, 192*(1-2), 143-159.

Martin, G. N., & Noonan, M. J. (1977). *Effects of domestic wastewater disposal by land irrigation on groundwater quality of the Central Canterbury Plains*. Water and Soil Technical Publication No. 7, Ministry of Works and Development, Wellington, New Zealand.

Nolan, B.T., Ruddy, B.C., Hitt, K.J., & Helsel, D.R. (1998). A national look at nitrate contamination of ground water. *Water Conditioning and Purification, 39* (12), 76-79.

Paul, J. H., Rose, J. B., Jiang, S. C., Zhou, X., Cochran, P., Kellogg, C., Kang, J. B., Griffin, D., Farrah, S., & Lukasik, J. (1997). Evidence for groundwater and surface marine water contamination by waste disposal wells in the Florida Keys. *Water Resources*, *31*(6), 1448–1454.

Russoniello, C. J., Konikow, L. F., Kroeger, K. D., Fernandez, C., Andres, A. S., & Michael, H. A. (2016). Hydrogeologic controls on groundwater discharge and nitrogen loads in a coastal watershed. *Journal of Hydrology, 538*, 783–793.

Shinn, E. A., Reese, R. S., & Reich, C. D. (1994). *Fate and pathways of injection-well effluent in the Florida Keys.* US Geological Survey, Open-File Report.

Sinton, L. W., Finlay, R. K., Pang, L., & Scott, D. M. (1997). Transport of bacteria and bacteriophages in irrigated effluent into and through an alluvial gravel aquifer. *Water, Air, and Soil Pollution*, *98*(1–2), 17–42.

Slomp, C. P., & Van Cappellen, P. (2004). Nutrient inputs to the coastal ocean through submarine groundwater discharge: Controls and potential impact. *Journal of Hydrology*, *295*(1–4), 64–86.

Taniguchi, M., Dulai, H., Burnett, K. M., Santos, I. R., Sugimoto, R., Stieglitz, T., Kim, G., Moosdorf, N., Burnett, W. C. (2019). Submarine groundwater discharge: Updates on its measurement techniques, geophysical drivers, magnitudes, and effects. *Frontiers in Environmental Science*, *7*, 1–26.

Tate, R. L. (1978). Cultural and environmental factors affecting the longevity of Escherichia coli in histosols. *Applied and Environmental Microbiology,* 35, 925-929.

Tesoriero, A. J., Liebscher, H., & Cox, S. E. (2000). Mechanism and rate of denitrification in an agricultural watershed: Electron and mass balance along groundwater flow paths. *Water Resources Research, 36*(6), 1545-1559.

REFERENCES

Applied Geomatics Research Group. (2017). *Topo-bathymetric lidar research for aquaculture and coastal development in Nova Scotia: final report*. Technical report, NSCC Middleton, NS.

Anderson Jr, W. P., & Emanuel, R. E. (2010). Effect of interannual climate oscillations on rates of submarine groundwater discharge. *Water Resources Research, 46*(5).

Abarca, E., Karam, H., Hemond, H. F., & Harvey, C. F. (2013). Transient groundwater dynamics in a coastal aquifer: The effects of tides, the lunar cycle, and the beach profile. *Water Resources Research, 49*(5), 2473-2488.

Allen, D. M., Whitfield, P.H., & Werner, A. (2010). Groundwater level responses in temperate mountainous terrain: Regime classification and linkages to climate and streamflow. *Hydrological Processes, 24*, 3392–3412.

Allen, R. G., Pereira, L. S., Raes, D., & Smith, M. (1998). Crop evapotranspiration-Guidelines for computing crop water requirements- FAO Irrigation and drainage paper 56. *FAO, Rome, 300*(9), D05109.

Allocca, V., Manna, F., & De Vita, P. (2014). Estimating annual groundwater recharge coefficient for karst aquifers of the southern Apennines (Italy). *Hydrology and Earth System Sciences, 18*(2), 803-817.

Amani, M., Mahdavi, S., Afshar, M., Brisco, B., Huang, W., Mohammad Javad Mirzadeh, S., White, L., Banks, S., Montgomery, J. & Hopkinson, C. (2019). Canadian wetland inventory using Google Earth Engine: The first map and preliminary results. *Remote Sensing*, *11*(7), 842.

Anderson, E. I., & Bakker, M. (2008). Groundwater flow through anisotropic fault zones in multiaquifer systems. *Water Resources Research, 44*(11).

Anderson, M. P. Woessner, W. W., & Hunt, R. J. (2015a). *Applied Groundwater Modeling—Simulation of Flow and Advective Transport.* Academic Press, Inc., San Diego, CA.

Anderson, M. P., Woessner, W. W., Hunt, R. J. (2015b). Assessing performance. In Anderson, M. P., Woessner, W. W., Hunt, R.J. (Eds.), *Applied Groundwater Modeling—Simulation of Flow and Advective Transport*: Academic Press, Inc., San Diego, Calif., pp. 375-436.

Arnold, J. G., Allen, P. M., Muttiah, R., & Bernhardt, G. (1995). Automated base flow separation and recession analysis techniques. *Groundwater, 33*(6), 1010-1019.

Arnold, J. G., & Allen, P. M. (1999). Automated methods for estimating baseflow and ground water recharge from streamflow records. *Journal of the American Water Resources Association, 35*(2), 411-424.

Baechler, F. (2015). The geology and hydrogeology of faults on Cape Breton Island, Nova Scotia, Canada: An overview. *Atlantic Geology*, *51*, 242.

Baechler, F., & Broehner, R. (2014). Karst geology and hydrogeology of Cape Breton Island, Nova Scotia: An overview. *Canadian Journal of Earth Sciences*, *51*(7), 701–714.

Baechler, F. E., Cross, H. J., & Baechler, L. (2019). The geology and hydrogeology of springs on Cape Breton island, Nova Scotia, Canada: An overview. Atlantic Geology, 55, 137–161.

Bailey, R. T., Wible, T. C., Arabi, M., Records, R. M., & Ditty, J. (2016). Assessing regional-scale spatio-temporal patterns of groundwater–surface water interactions using a coupled SWAT-MODFLOW model. *Hydrological Processes*, *30*(23), 4420–4433.

Banks, E. W., Simmons, C. T., Love, A. J., Cranswick, R., Werner, A. D., Bestland, E. A., Wood, M., & Wilson, T. (2009). Fractured bedrock and saprolite hydrogeologic controls on groundwater/surface-water interaction: A conceptual model (Australia). *Hydrogeology Journal, 17*(8), 1969-1989.

Barazzuoli, P., Nocchi, M., Rigati, R., & Salleolini, M. (2008). A conceptual and numerical model for groundwater management: A case study on a coastal aquifer in southern Tuscany, Italy. *Hydrogeology Journal, 16(*8), 1557-1576.

Barr, S. M., White, C. E., Fisher, B. E., McKinnon, J. S., Barras, A. L., & Hapgood, D. S. (2017). DP ME 433, version 1, 2017. Digital geological data generated as part of the bedrock geological mapping compilation project for Cape Breton Island, Nova Scotia. Nova Scotia Department of Natural Resources, Geoscience and Mines Branch.

Batu, V. (1998). *Aquifer hydraulics: a comprehensive guide to hydrogeologic data analysis.* John Wiley & Sons.

Beven, K., & Germann, P. (2013). Macropores and water flow in soils revisited. Water Resources Research, 49(6), 3071-3092.

Bitton, G., Farrah, S. R., Ruskin, R. H., Butner, J., & Choum, Y. J. (1983). Survival of pathogenic and indicator organisms in ground water. *Groundwater, 21*(4), 405–410.

Bitton, G., & Harvey, R. W. (1992). Transport of pathogens through soils and aquifers. *Environmental Microbiology, 19*, 103-123.

Bobba, A., Chambers, G., & Wrona, P. (2012). Submarine groundwater discharge (SGWD): An unseen yet potentially important coastal phenomenon in Canada. *Natural Hazards, 60*(3), 991-1012.

Boehm, A. B., Shellenbarger, G. G., & Paytan, A. (2004). Groundwater discharge: Potential association with fecal indicator bacteria in the surf zone. *Environmental Science and Technology*, *38*(13), 3558–3566.

Bokuniewicz, H. J. (1992). Analytical descriptions of subaqueous groundwater seepage. *Estuarie*, *15*, 458–464.

Bokuniewicz, H., Taniguchi, M., Ishitoibi, T., Charette, M., Allen, M., & Kontar, E. A. (2008). Direct measurements of submarine groundwater discharge (SGD) over a fractured rock aquifer in Flamengo Bay Brazil. *Estuarine, Coastal and Shelf Science, 76*(3), 466-472.

Bratton, J. F., Böhlke, J. K., Manheim, F. T., & Krantz, D. E. (2004). Ground water beneath coastal bays of the Delmarva Peninsula: ages and nutrients. *Ground Water*, *42*(7), 1021–1034.

Bredehoeft, J. D. (2002). The water budget myth revisited: Why hydrogeologists model. *Groundwater, 40*(4), 340-345.

Brodie, R. S., & Hostetler, S. (2005). A review of techniques for analysing baseflow from stream hydrographs. *Proceedings of the NZHS-IAH-NZSSS 2005 conference* (Vol. 28). Auckland New Zealand.

Brunke, M., & Gonser, T. (1997). The ecological significance of exchange processes between rivers and groundwater. *Freshwater Biology*, *37*(1), 1–33.

Brunner, P., Simmons, C. T., Cook, P. G., & Therrien, R. (2010). Modeling surface water-groundwater interaction with MODFLOW: Some considerations. *Groundwater, 48*(2), 174-180.

Burnett, W. C., & Dulaiova, H. (2003). Estimating the dynamics of groundwater input into the coastal zone via continuous radon-222 measurements, *Journal of Environmental Radioactivity, 69*(1-2), 21–35.

Burnett, W. C., Cable, J., & Corbett, D. (2003). Radon tracing of submarine groundwater discharge in coastal environments. In *Land and Marine Hydrogeology* (pp. 25–43).

Burnett, W. C., Bokuniewicz, H., Huettel, M., Moore, W. S., & Taniguchi, M. (2003b). Groundwater and pore water inputs to the coastal zone. *Biogeochemistry*, *66*(1), 3-33.

Burt, T. P., Bates, P. D., Stewart, M. D., Claxton, A. J., Anderson, M. G., & Price, D. A. (2002). Water table fluctuations within the floodplain of the River Severn, England. *Journal of Hydrology 262*, 1-20.

Butler Jr, J. J. (2019). *The design, performance, and analysis of slug tests* (2nd Edition). CRC Press. Boca Raton, FL.

Caissie, D. (2006). The thermal regime of rivers: A review. *Freshwater biology, 51*(8), 1389-1406.

Cann, D. B., MacDougall, J. I., & Hilchey, J. D. (1963*). Soil survey of Cape Breton Island Nova Scotia*. Canada Department of Agriculture and Nova Scotia Department of Agriculture and Marketing.

Cape Breton Partnership & The Inverness/Victoria Federation of Agriculture. (n.d.). *Water resources program report: Mabou Harbour watershed*. Prepared for: Nova Scotia Federation of Agriculture.

Champ, D. R. and Schroeter, J. (1988). Bacterial transport in fractured rock - A field-scale tracer test at the chalk river nuclear laboratories. *Water Science and Technology 20*, 81–87.

Chandra, S., Auken, E., Maurya, P. K., Ahmed, S., & Verma, S. K. (2019). Large scale mapping of fractures and groundwater pathways in crystalline hardrock by AEM. *Scientific Reports, 9*(1), 1-11.

Charette, M. A., & Sholkovitz, E. R. (2002). Oxidative precipitation of groundwater-derived ferrous iron in the subterranean estuary of a coastal bay. *Geophyical Research Letters*, *29*(10), 85.

Chase, M. E., Jones, S. H., Hennigar, P., Sowles, J., Harding, G. C. H., Freeman, K., Wells, P. G., Krahforst, C., Crawford, R., Pederson, J., & Taylor, D. (2001). Gulfwatch: Monitoring spatial and temporal patterns of trace metal and organic contaminants in the Gulf of Maine (1991–1997) with the blue mussel, Mytilus edulis L. *Marine Pollution Bulletin, 42*(6), 490-504.

Christiansen, J. S., Thorsen, M., Clausen, T., Hansen, S., & Refsgaard, J. C. (2004). Modelling of macropore flow and transport processes at catchment scale. *Journal of Hydrology, 299*(1-2), 136-158.

Church, T. M. (1996). An underground route for the water cycle. *Nature*, *380*(6575), 579-580.

Conan, C., Bouraoui, F., Turpin, N., de Marsily, G., & Bidoglio, G. (2003). Modeling flow and nitrate fate at catchment scale in Brittany (France). *Journal of Environmental Quality, 32*(6), 2026-2032.

Conant Jr, B., Robinson, C. E., Hinton, M. J., & Russell, H. A. (2019). A framework for conceptualizing groundwater-surface water interactions and identifying potential impacts on water quality, water quantity, and ecosystems. *Journal of Hydrology, 574*, 609-627.

Cook, P. G. (2003). *A guide to regional groundwater flow in fractured rock aquifers*. Seaview Press, Henley Beach, South Australia.

Deming, D., Sass, J. H., Lachenbruch, A. H., & De Rito, R. F. (1992). Heat flow and subsurface temperature as evidence for basin-scale ground-water flow, North Slope of Alaska. *Geological Society of America Bulletin, 104*(5), 528–542.

Desmarais, T. R., Solo-gabriele, H. M., & Palmer, C. J. (2002). Influence of soil on fecal indicator organisms in a tidally influenced subtropical environment. *Applied and Environmental Microbiology, 68*(3), 1165–1172.

Diaz, R. J., & Rosenberg, R. (2008). Spreading dead zones and consequences for marine ecosystems. *Science*, *321*(5891), 926–929.

Di Baldassarre, G., & Claps, P. (2011). A hydraulic study on the applicability of flood rating curves. *Hydrology Research, 42*(1), 10-19.

Doherty, J. E., and Hunt, R. J. (2010). *Approaches to highly parameterized inversion—A guide to using PEST for groundwater-model calibration*. US Geological Survey Scientific Investigations Report 2010–5169.

Domeneghetti, A., Castellarin, A., & Brath, A. (2012). Assessing rating-curve uncertainty and its effects on hydraulic model calibration. *Hydrology and Earth System Sciences, 16*(4), 1191.

Domenico, P. A., & Schwartz, F. W., (1990). *Physical and chemical hydrogeology*. John Wiley & Sons, New York.

Domenico, P. A., & Schwartz, F. W. (1997). *Physical and chemical hydrogeology* (2nd Edition). New York: Wiley.

Dowd, S. E., & Pillai, S. D. (1997). Survival and transport of selected bacterial pathogens and indicator viruses under sandy aquifer conditions. *Journal of Environmental Science and Health, 32*(8), 2245-2258,

Drage, J., & McKinnon, J. S., (2019). *DP ME 494, Version 1, 2019, Digital version of karst risk map of Nova Scotia.* Nova Scotia Department of Energy and Mines, Geological Survey Division.

Driscoll, F. G. (1986). *Groundwater and wells*. Johnson Division, St. Paul, Minn.

Duff, J. H., & Triska, F. J. (1990). Denitrifications in sediments from the hyporheic zone adjacent to a small forested stream. *Canadian Journal of Fisheries and Aquatic Sciences, 47*(6), 1140-1147.

Duff, J. H., Toner, B., Jackman, A. P., Avanzino, R. J., & Triska, F. J. (2000). Determination of groundwater discharge into a sand and gravel bottom river: A comparison of chloride dilution and seepage meter techniques. *Internationale Vereinigung für theoretische und angewandte Limnologie: Verhandlungen, 27*(1), 406-411.

Dugdale, S. J., Malcolm, I. A., Kantola, K., & Hannah, D. M. (2018). Stream temperature under contrasting riparian forest cover: Understanding thermal dynamics and heat exchange processes. *Science of The Total Environment, 610*, 1375-1389.

Duque, C., Russoniello, C. J., & Rosenberry, D. (2020). History and evolution of seepage meters for quantifying flow between groundwater and surface water: Part 2–Marine settings and submarine groundwater discharge. *Earth-Science Reviews*, 103168.

Duwelius, R. F. (1996). *Hydraulic conductivity of the streambed, east branch Grand Calumet River, northern Lake County, Indiana*. US Geological Survey. Report 96-4218.

Environment and Agriculture Technology Research Group of the Nova Scotia Community College. (2018). *Agricultural Land Identification Project*. Nova Scotia Community College.

ESRI. (2016). ArcGIS. Version 10.5.0.6491. Desktop: Release 10. Redlands, CA: Environmental Systems Research Institute.

ESRI. (2018). *World Imagery*. Updated Dec. 4, 2018. https://www.arcgis.com/home/item.html?id=2a060171c43e44888911e0d89145fd0c

Ferris, J. G. (1952). *Cyclic fluctuations of water level as a basis for determining aquifer transmissibility* (No. Note 1). US Geological Survey Ground Water Notes.

Findlay, S. (1995). Importance of surface-subsurface exchange in stream ecosystems: The hyporheic zone. *Limnology and Oceanography, 40*(1), 159-164.

Filip, Z., Kaddu-Mulindwa, D., & Milde, G. (1988). Survival of some pathogenic and facultative pathogenic bacteria in groundwater. *Water Science and Technology, 20*, 227-231.

Fleckenstein, J. H., Krause, S., Hannah, D. M., & Boano, F. (2010). Groundwater-surface water interactions: New methods and models to improve understanding of processes and dynamics. *Advances in Water Resources, 33*(11), 1291-1295.

Ford, D. C. (2015). *Karst landform*. The Canadian Encyclopedia. Retrieved from: https://thecanadianencyclopedia.ca/en/article/karst-landform#:~:text=The%20most%20widespread%20surface%20karst,referred%20to%20as%20limestone%20pavement.

Freeze, A., & Cherry, J. (1979). *Groundwater*. Prentice-Hall, Englewood Cliffs, New Jersey.

Frigo, M., & Johnson, S. G. (1998). FFTW: An adaptive software architecture for the FFT. *Proceedings of the 1998 IEEE International Conference on Acoustics, Speech and Signal Processing, ICASSP'98 (Cat. No. 98CH36181)* (Vol. 3, pp. 1381-1384). IEEE.

Fujita, K., Shoji, J., Sugimoto, R., Nakajima, T., Honda, H., Takeuchi, M., Tominaga, O., Taniguchi, M. (2019). Increase in fish production through bottom-up trophic linkage in coastal waters induced by nutrients supplied via submarine groundwater. *Frontiers in Environmental Science*, *7*, 1–10.

Garrison, G. H., Glenn, C. R., & McMurtry, G. M. (2003). Measurement of submarine groundwater discharge in Kahana Bay, O'ahu, Hawai'i. *Limnology and Oceanography*, *48*(2), 920–928.

Ghoraba, S. M., Zyedan, B. A., & Rashwan, I. M. H. (2013). Solute transport modeling of the groundwater for quaternary aquifer quality management in Middle Delta, Egypt. *Alexandria Engineering Journal, 52*(2), 197-207.

Gold, A. J., Jacinthe, P. A., Groffman, P. M., Wright, W. R., & Puffer, R. H. (1998). Patchiness in groundwater nitrate removal in a riparian forest. *Journal of Environmental Quality, 27*, 146-155.

Gold, A. J., Groffman, P. M., Addy, K., Kellogg, D. Q., Stolt, M., & Rosenblatt, A. E. (2001). Landscape attributes as controls on ground water nitrate removal capacity of riparian zones. *Water Resources*, *37*(6), 1457–1464.

Goss, M. J., Barry, D. A. J., & Rudolph, D. L. (1998). Contamination in Ontario farmstead domestic wells and its association with agriculture: 1. Results from drinking water wells. *Journal of Contaminant Hydrology, 32*(3–4), 267–293.

Government of Ontario. (2019). Chapter 10: Yield test. *Water supply wells: Requirements and best practices*. Ministry of the Environment, Conservation and Parks. Retrieved from: https://www.ontario.ca/document/water-supply-wells-requirements-and-best-practices/yield-test.

Grant, D. R. (1994). *Quaternary geology, Cape Breton Island, Nova Scotia*. Natural Resources Canada.

Green, J. M., Henkelman, K. K., & Caskey, R. M. (2004). *Hydraulic conductivity of near-surface alluvium in the vicinity of Cattlemans Detention basin, south Lake Tahoe, California*. US Geological Survey and US Department of the Interior.

Grimm, N. B., & Fisher, S. G. (1984). Exchange between interstitial and surface water: Implications for stream metabolism and nutrient cycling. *Hydrobiologia, 111*(3), 219-228.

Groen, J., Velstra, J., & Meesters, A. G. C. A. (2000). Salinization processes in paleowaters in coastal sediments of Suriname: Evidence from δ37Cl analysis and diffusion modelling. *Journal of Hydrology, 234*(1-2), 1-20.

Haitjema, H. M., & Mitchell-Bruker, S. (2005). Are water tables a subdued replica of the topography? *Groundwater, 43*(6), 781-786.

Hallberg, G. R. (1987). Nitrates in ground water in Iowa. F. M. D'Itri, L. G. Wolfson (Eds.), *Rural Ground Water Contamination*. Lewis Publishers, Chelsea, MI.

Han, D. M., Song, X. F., Currell, M. J., & Tsujimura, M. (2012). Using chlorofluorocarbons (CFCs) and tritium to improve conceptual model of groundwater flow in the South Coast Aquifers of Laizhou Bay, China. *Hydrological Processes, 26*(23), 2614-3629.

Han, P. F., Wang, X. S., Wan, L., Jiang, X. W., & Hu, F. S. (2019). The exact groundwater divide on water table between two rivers: A fundamental model investigation. *Water, 11*(4), 685.

Hannula, S. R., Esposito, K. J., Chermak, J. A., Runnells, D. D., Keith, D. C., & Hall, L. E. (2003). Estimating ground water discharge by hydrograph separation. *Groundwater, 41*(3), 368-375.

Harbaugh, A. W. (2005). *MODFLOW-2005, the U.S. Geological Survey modular ground-water model: The ground-water flow process*. US Geological Survey Techniques and Methods 6-A16.

Harbaugh, A. W., Banta, E. R., Hill, M. C., & McDonald, M. G. (2000). *Modflow-2000, the U. S. geological survey modular ground-water model-user guide to modularization concepts and the ground-water flow process*. US Geological Survey: Open-file Report (00-92).

Harvey, R. W., George, L. H., Smith, R. L., & LeBlanc, D. R. (1989). Transport of microspheres and indigenous bacteria through a sandy aquifer: Results of natural and forced-gradient tracer experiments. *Environmental Science and Technology*, *23*(1), 51–56.

Hayashi, M., & Rosenberry, D. O. (2002). Effects of ground water exchange on the hydrology and ecology of surface water. *Groundwater, 40*(3), 309-316.

Haycock, N. E., & Pinay, G. (1993). Groundwater nitrate dynamics in grass and poplar vegetated riparian buffer strips during the winter. *Journal of Environmental Quality, 22*, 273-278.

Health Canada (2012). *Guidelines for Canadian Recreational Water Quality, Third Edition*. Water, Air and Climate Change Bureau, Healthy Environments and Consumer Safety Branch, Health Canada, Ottawa, Ontario. Catalogue No H129-15/2012E.

Healy, R. W., & Scanlon, B. R. (2010). *Estimating groundwater recharge*. Cambridge UP, Cambridge.

Heiss, J. W., Ullman, W. J., & Michael, H. A. (2014). Swash zone moisture dynamics and unsaturated infiltration in two sandy beach aquifers. *Estuarine, Coastal and Shelf Science*, *143*, 20–31.

Hill, M. C., & Osterby, O. (2003). Determining extreme parameter correlation in ground water models. *Ground water, 41*(4), 420-430.

Hiscock, K., & Bense, V. F. (2014). *Hydrogeology: Principles and practice* (Second ed.). Chichester, West Sussex, UK: Hoboken, New Jersey: John Wiley & Sons.

Howell, J.M., Coyne, M.S., & Cornelius, P. (1995). Fecal bacteria in agricultural waters of the Bluegrass Region of Kentucky. *Journal of Environmental Quality*, *24*(3), 411–419.

Hu, C., Muller-Karger, F. E., & Swarzenski, P. W. (2006). Hurricanes, submarine groundwater discharge, and Florida's red tides. *Geophysical Research Letters*, *33*(11), 1–5.

Hvorslev, M. J. (1951). *Time lag and soil permeability in ground-water observations* (No. 36). Waterways Experiment Station, Corps of Engineers, US Army.

Hynes, H. B. N. (1983). Groundwater and stream ecology. *Hydrobiologia*, *100*(1), 93–99.

Jacob, C. E. (1950). Flow of groundwater. In H. Rouse (Ed.), *Engineering hydraulics* (pp. 321–386). Hoboken, NY: John Wiley & Sons.

Jamieson, R. C., Gordon, R. J., Sharples, K. E., Stratton, G. W., & Madani, A. (2002). Movement and persistence of fecal bacteria in agricultural soils and subsurface drainage water: A review. *Canadian Biosystems Engineering / Le Genie Des Biosystems Au Canada*, 44, 1–9.

Jiang, X., Wan, L., Wang, X., Ge, S., & Liu, J. (2009). Effect of exponential decay in hydraulic conductivity with depth on regional groundwater flow. *Geophysical Research Letters, 36*(24).

Johannes, R. E. (1980). The ecological significance of the submarine discharge of groundwater. *Marine Ecology Progress Series*, *3*, 365–373.

Johannes, R. E., & Hearn, C. J. (1985). The effect of subsurface groundwater discharge on nutrient and salinity regimes in a coastal lagoon off Perth, West Australia. *Estuarine Coastal and Shelf Science, 21*(6), 789–800.

Johnson, A. G., Glenn, C. R., Burnett, W. C., Peterson, R. N., & Lucey, P. G. (2008). Aerial infrared imaging reveals large nutrient-rich groundwater inputs to the ocean. *Geophysical Research Letters*, *35*(15), 1–6.

Kalbus, E., Reinstorf, F., Schirmer, M., & Measuring, M. S. (2006). Measuring methods for groundwater – surface water interactions: A review. *Hydrology and Earth System Sciences, 10*, 873-887.

Kelleher, C., Wagener, T., Gooseff, M., McGlynn, B., McGuire, K., & Marshall, L. (2012). Investigating controls on the thermal sensitivity of Pennsylvania streams. *Hydrological Processes, 26*(5), 771-785.

Kennedy, G. W., Garroway, K. G. and Drage, J. M. (2009). Hydrogeology Program in Nova Scotia. In *Mineral Resources Branch, Report of Activities 2008*. Nova Scotia Department of Natural Resources, Report ME 2009-1, p. 53-60.

Kennedy, G. W., Garroway, K. G., & Finlayson-Bourque, D. S. (2010). Estimation of Regional Groundwater Budgets in Nova Scotia. In *Nova Scotia Department of Natural Resources, Mineral Resources Branch, Open File Illustration ME, 2*, 2010.

Keswick, B. H., Gerba, C. P., Secor, S. L., & Cech, I. (1982) Survival of Enteric Viruses and Indicator Bacteria in Groundwater. *Journal of Environmental Science and Health, 17*(6), 903-912.

Ketchum, B. H. (1950). Hydrographic factors involved in the dispersion of pollutants introduced into tidal waters. *Journal of the Boston Society of Civil Engineers*, *37*, 296-314.

Knott, J. F., & Olimpio, J. C. (1986). *Estimation of recharge rates to the sand and gravel aquifer using environmental tritium, Nantucket Island, Massachusetts*. US Geological Survey: Water-Supply Paper 2297.

Kohout, F. A. (1966). Submarine springs: A neglected phenomenon of coastal hydrology. *Hydrology, 26*, 391-413.

Kohout, F. (1967). Groundwater flow and geothermal regime of Florida Plateau. *AAPG Bulletin*, *51*(10), 2165–2166.

Kooi, H., Groen, J., & Leijnse, A. (2000). Modes of seawater intrusion during transgressions. *Water Resources Research*, *36*(12), 3581-3589.

Kooi, H., & Groen, J. (2001). Offshore continuation of coastal groundwater systems; predictions using sharp-interface approximations and variable-density flow modelling. *Journal of Hydrology, 246*(1-4), 19-35.

Kottek, M., Grieser, J., Beck, C., Rudolf, B., & Rubel, F. (2006). World map of the Köppen-Geiger climate classification updated. *Meteorologische Zeitschrift, 6*(3), 259-263.

Krause, S., Hannah, D., Fleckenstein, J., & Krause, S. (2009). Hyporheic hydrology: Interactions at the groundwater-surface water interface. *Hydrological Processes, 23*(15), 2103-2107.

Kroeger, K. D., Swarzenski, P. W., Greenwood, W. J., & Reich, C. (2007). Submarine groundwater discharge to Tampa Bay: Nutrient fluxes and biogeochemistry of the coastal aquifer. *Marine Chemistry*, *104*(1–2), 85–97.

Langevin, C. D., & Guo, W. (2006). MODFLOW/MT3DMS–based simulation of variable-density ground water flow and transport. *Groundwater, 44*(3), 339-351.

LaRoche, J., Nuzzi, R., Waters, R., Wyman, K., Falkowski, P., & Wallace, D. (1997). Brown tide blooms in Long Island's coastal waters linked to interannual variability in groundwater flow. *Global Change Biology, 3*(5), 397-410.

Lautz, L. K., & Siegel, D. I. (2006). Modeling surface and ground water mixing in the hyporheic zone using MODFLOW and MT3D. *Advances in Water Resources, 29*(11), 1618-1633.

Lee, D. R. (1977). A device for measuring seepage flux in lakes and estuaries. *Limnology and Oceanography*, *22*(1), 140–147.

Lee, M. S., Lee, K. K., Hyun, Y., Clement, T. P., & Hamilton, D. (2006). Nitrogen transformation and transport modeling in groundwater aquifers. *Ecological Modelling, 192*(1-2), 143-159.

Lee, Y., Kim, G., Lim, W., & Hwangb, D. (2010). A relationship between Submarine groundwater-borne nutrients traced by Ra isotopes and the intensity of Dinoflagellate red-tides occurring in the southern sea of Korea. *Limnology and Oceanography*, *55*(1), 1–10.

Li, L., Barry, D. A., Stagnitti, F., & Parlange, J. Y. (1999). Submarine groundwater discharge and associated chemical input to a coastal sea. *Water Resources Research*, *35*(11), 3253–3259.

Louis, C. (1974). Rock hydraulics. In L Muller (Ed.), *Rock mechanics.* Springer, New York, pp. 299– 387.

Luijendijk, E., Gleeson, T., & Moosdorf, N. (2020). Fresh groundwater discharge insignificant for the world's oceans but important for coastal ecosystems. *Nature Communications, 11*(1).

Macan, T. T. (1958). The temperature of a small stony stream. *Hydrobiologia, 12*(2-3), 89-106.

Mackey, A. P., & Berrie, A. D. (1991). The prediction of water temperatures in chalk streams from air temperatures. *Hydrobiologia, 210*(3), 183-189.

Manning, C. E., & S. E. Ingebritsen (1999). Permeability of the continental crust: Implications of geothermal data and metamorphic systems, Reviews of *Geophysics, 37*, 127– 150.

Martin, G. N., & Noonan, M. J. (1977). *Effects of domestic wastewater disposal by land irrigation on groundwater quality of the Central Canterbury Plains*. Water and Soil Technical Publication No. 7, Ministry of Works and Development, Wellington, New Zealand.

Mau, D. P., & Winter, T. C. (1997). Estimating ground-water recharge from streamflow hydrographs for a small mountain watershed in a temperate humid climate, New Hampshire, USA. *Groundwater, 35*(2), 291-304.

Maxwell, R. M., & Kollet, S. J. (2008). Quantifying the effects of three-dimensional subsurface heterogeneity on Hortonian runoff processes using a coupled numerical, stochastic approach. *Advances in Water Resources, 31*(5), 807-817.

Mayer, T. D. (2012). Controls of summer stream temperature in the Pacific Northwest. *Journal of Hydrology, 475*, 323-335.

McFeters, G. A., Bissonnette, G. K., Jezeski, J. J., Thomson, C. A., Stuart, D. G. (1974). Comparative survival of indicator bacteria and enteric pathogens in well water. *Applied Microbiology, 27*(5):823-829.

McKay, L. D., Cherry, J. A., Bales, R. C., Yahya, M. T., & Gerba, C. P. (1993). A field example of bacteriophage as tracers of fracture flow. *Environmental Science & Technology, 27*(6), 1075-1079.

McKay, L., Fredericia, J., Lenczewski, M., Morthorst, J. & Klint, K. E. S. (1999). Spatial variability of contaminant transport in a fractured till, Avedore Denmark. *Nordic Hydrology, 30*, 333–360.

McWhorter, D. B., Sunada, D. K., & Sunada, D. K. (1977). *Ground-water hydrology and hydraulics*. Water Resources Publication.

Menning, D. M., Wynn, J. G., & Garey, J. R. (2015). Karst estuaries are governed by interactions between inland hydrological conditions and sea level. *Journal of Hydrology*, *527*, 718–733.

Menon, A. S. (1988). Molluscan shellfish and water quality problems in Atlantic Canada. *Toxicity Assessment, 3*(5), 679-686.

Michael, H. A., Lubetsky, J. S., & Harvey, C. F. (2003). Characterizing submarine groundwater discharge: A seepage meter study in Waquoit Bay, Massachusetts. *Geophysical Research Letters*, *30*(6).

Michael, H. A., Mulligan, A. E., & Harvey, C. F. (2005). Seasonal oscillations in water exchange between aquifers and the coastal ocean. *Nature*, *436*(7054), 1145–1148.

Michael, H., Post, V., Wilson, A., & Werner, A. (2017). Science, society, and the coastal groundwater squeeze. *Water Resources Research, 53*(4), 2610-2617.

Misstear, B.D.R., Brown, L., & Johnston, P.M. (2009). Estimation of groundwater recharge in a major sand and gravel aquifer in Ireland using multiple approaches. *Hydrogeology Journal*, *17*(3), 693–706.

Moore, W. S. (1999). The subterranean estuary: A reaction zone of ground water and sea water. *Marine Chemistry*, *65*(1–2), 111–125.

Moore, W. S. (2010). The effect of submarine groundwater discharge on the ocean. *Annual Review of Marine Science*, 2, 59-88.

Moore, W. S., & Church, T. M. (1996). Submarine groundwater discharge. *Nature, 382*(6587), 122-122.

Moore, W. S., Krest, J., Taylor, G., Roggenstein, E., Joye, S., & Lee, R. (2002). Thermal evidence of water through a coastal aquifer: Implications for nutrient fluxes. *Geophysical Research Letters, 29*(14), 49-1.

Moore, W. S., Sarmiento, J. L., & Key, R. M. (2008). Submarine groundwater discharge revealed by 228Ra distribution in the upper Atlantic Ocean. *Nature Geoscience*, *1*(5), 309–311.

Moosdorf, N., Stieglitz, T., Waska, H., Durr, H. H., & Hartmann, J. (2015). Submarine groundwater discharge from tropical islands: A review. *Grundwasser*, *20*, 53–67.

Morgan, S. E., Allen, D. M., Kirste, D., Salas, C. J. (2019) Investigating the hydraulic role of a large buried valley network on regional groundwater flow. *Hydrogeology Journal, 27*, 2377-2397.

Mosley, M. P. (1983). Variability of water temperatures in the braided Ashley and Rakaia rivers. *New Zealand Journal of Marine and Freshwater Research, 17*(3), 331-342.

Mulligan, A. E., Evans, R. L., & Lizarralde, D. (2007). The role of paleochannels in groundwater/seawater exchange. *Journal of Hydrology*, *335*(3–4), 313–329.

Nace, R. L. (1970). World hydrology: Status and prospects. *Symposium on World Water Balance*, *1*(92).

Nathan, R. J., & McMahon, T. A. (1990). Evaluation of automated techniques for base flow and recession analyses. *Water Resources Research, 26*(7), 1465-1473.

Nelson, W. M., Gold, A. J., & Groffman, P. M. (1995). Spatial and temporal variation in groundwater nitrate removal in a riparian forest. *Journal of Environmental Quality 24*, 691-699.

Niswonger, R. G., Panday, Sorab, & Ibaraki, M. (2011). *MODFLOW-NWT, a Newtonian formulation for MODFLOW-2005*. US Geological Survey Techniques and Methods 6-A37.

Nolan, B.T., Ruddy, B.C., Hitt, K.J., & Helsel, D.R. (1998). A national look at nitrate contamination of ground water. *Water Conditioning and Purification, 39* (12), 76-79.

Nova Scotia Department of Environment. (2018). *1:10,000 watersheds for Nova Scotia*.

Nova Scotia Department of Lands and Forestry. (2020). *Nova Scotia topographic database*.

Oberdorfer, J. A., Valentino, M. A., & Smith, S. V. (1990). Groundwater contribution to the nutrient budget of Tomales Bay, California. *Biogeochemistry, 10*(3), 199–216.

Paldor, A., Shalev, E., Katz, O., & Aharonov, E. (2019). Dynamics of saltwater intrusion and submarine groundwater discharge in confined coastal aquifers: a case study in northern Israel. *Hydrogeology Journal, 27*(5), 1611-1625.

Parker, B.B. (2007) *Tidal analysis and prediction*. Silver Spring, MD, NOAA NOS Center for Operational Oceanographic Products and Services (NOAA Special Publication NOS CO-OPS 3).

Patriarche, D., Castro, M.C. & Goovaerts, P. (2005). Estimating regional hydraulic conductivity fields—A comparative study of geostatistical methods. *Mathematical Geology, 37*, 587–613.

Paul, J. H., Rose, J. B., Jiang, S. C., Zhou, X., Cochran, P., Kellogg, C., Kang, J. B., Griffin, D., Farrah, S., & Lukasik, J. (1997). Evidence for groundwater and surface marine water contamination by waste disposal wells in the Florida Keys. *Water Resources*, *31*(6), 1448–1454.

Pekdeger, A., & Matthess, G. (1983). Factors of bacteria and virus transport in groundwater. *Environmental Geology, 5*(2), 49–52.

Petersen-Øverleir, A. (2004). Accounting for heteroscedasticity in rating curve estimates. *Journal of Hydrology, 292*(1-4), 173-181.

Petrie, B. (1996). Temperature, salinity and sigma-t atlas for the Gulf of St. Lawrence. *Canadian Technical Report Hydrography and Ocean Sciences*, *178*, 256.

Piekarek-Jankowska. (1996). Hydrochemical effects of submarine groundwater discharge to the Puck Bay (Southern Baltic Sea, Poland). *Geographia Polonica, 67*, 103-120.

Polemio, M., & Limoni, P. (2006). *Groundwater pollution and risks for the coastal environment (southeastern Italy).* IAHS-AISH Publication. 477-486.

Pollock, D.W. (2017). *MODPATH v7.2.01: A particle-tracking model for MODFLOW*. US Geological Survey software release, 15 December 2017.

Prommer, H., Barry, D. A., & Zheng, C. (2003). PHT3D-A MODFLOW/MT3DMS based reactive multi-component transport model. *Groundwater, 42*(2), 247-257.

Psilovikos, Aris. (2006). Analysis of the governing partial differential equation of MODFLOW simulation model with two algorithms of backward differences. *Journal of Institute of Mathematics and Computer Sciences. Mathematics Series. 19.*

Rantz, S. E. (1982). *Measurement and computation of streamflow* (Vol. 2175). US Department of the Interior, US Geological Survey.

Rassam, D.W., Fellows, C., S., I., De Hayr, R., Hunter, H., & Bloesch, P. (2006). The hydrology of riparian buffer zones; Two case studies in an ephemeral and a perennial stream. *Journal of Hydrology*, *325*(1–4), 308–324.

Rassam, D. W., Pagendam, D. E., & Hunter, H. M. (2008). Conceptualisation and application of models for groundwater-surface water interactions and nitrate attenuation potential in riparian zones. *Environmental Modelling and Software*, *23*(7), 859–875.

Reddy, K. R., Khaleel, R., & Overcash, M. R. (1981). Behavior and transport of microbial pathogens and indicator organisms in soils treated with organic wastes. *Journal of Environmental Quality*, *10*(3), 255-266.

Rempe, D. M., Dietrich, W. E. (2014). Bottom-up control on fresh-bedrock topography under landscapes. *Proceedings of the National Academy of Sciences of the United States of America, 111*(18), 6576-6581.

Rivard, C., Paniconi, C., Gauthier, M. J., François, G., Sulis, M., Camporese, M., Larocque, M., & Chaumont, D. (2008). A modeling study of climate change impacts on recharge and surface–groundwater interactions for the Thomas Brook catchment (Annapolis Valley, Nova Scotia). In *Proceedings of GeoEdmonton, Canadian Geotechnical Society–International Association of Hydrogeologists–Canadian National Chapter Joint Annual Conference, Edmonton, Canada*.

Rivard, C., Paradis, D., Paradis, S., Bolduc, A., Morin, R. H., Liao, S., Pullan, S., Gauthier, M. J., Trepanier, S., Blackmore, A., Spooner, I., Deblonde, C., Fernandes, R., Castonguay, S., Hamblin, T., Michaud, Y., Drage, J., & Paniconi, C. (2012). Canadian groundwater inventory: Regional hydrogeological characterization of the Annapolis-Cornwallis Valley aquifers. *Geological Survey of Canada, Bulletin, 598*.

Rivard, C., Lefebvre, R., Paradis, D. (2014). Regional recharge estimation using multiple methods: An application in the Annapolis Valley, Nova Scotia (Canada). *Environmental Earth Sciences, 71*, 1389-1408.

Robinson, C., Gibbes, B., & Li, L. (2006). Driving mechanisms for groundwater flow and salt transport in a subterranean estuary. *Geophysical Research Letters, 33*(3).

Robinson, C., Li, L., & Barry, D. A. (2007). Effect of tidal forcing on a subterranean estuary. *Advances in Water Resources*, *30*(4), 851–865.

Robinson, C. E., Xin, P., Santos, I. R., Charette, M. A., Li, L., & Barry, D. A. (2018). Groundwater dynamics in subterranean estuaries of coastal unconfined aquifers: Controls on submarine groundwater discharge and chemical inputs to the ocean. *Advances in Water Resources*, *115*, 315–331.

Robinson, M., Gallagher, D., & Reay, W. (1998). Field observations of tidal and seasonal variations in ground water discharge to tidal estuarine surface water. *Groundwater Monitoring & Remediation, 18*(1), 83-92.

Russoniello, C. J., Konikow, L. F., Kroeger, K. D., Fernandez, C., Andres, A. S., & Michael, H. A. (2016). Hydrogeologic controls on groundwater discharge and nitrogen loads in a coastal watershed. *Journal of Hydrology, 538*, 783–793.

Sanford, W. E., & Pope, J. P. (2013). Quantifying groundwater's role in delaying improvements to Chesapeake Bay water quality. *Environmental Science and Technology*, *47*(23), 13330–13338.

Santos, I. R., Burnett, W. C., Chanton, J., Mwashote, B., Suryaputra, N. A., Dittmar, T., … Suryaputra, I. G. N. A. (2008). Nutrient biogeochemistry in a Gulf of Mexico subterranean estuary and groundwater- derived fluxes to the coastal ocean. *Limnology and Oceanography*, *53*(2), 705–718.

Santos, I. R., Burnett, W. C., Dittmar, T., Suryaputra, I. G. N. A., & Chanton, J. (2009). Tidal pumping drives nutrient and dissolved organic matter dynamics in a Gulf of Mexico subterranean estuary. *Geochimica et Cosmochimica Acta*, *73*(5), 1325–1339

Santos, I. R., Eyre, B. D., & Huettel, M. (2012). The driving forces of porewater and groundwater flow in permeable coastal sediments: A review. *Estuarine, Coastal and Shelf Science*, *98*, 1–15

Sawyer, A. H., Michael, H. A., & Schroth, A. W. (2016). From soil to sea: The role of groundwater in coastal critical zone processes. *Wiley Interdisciplinary Reviews: Water*, *3*(5), 706–726.

Schafer, C. T. (1973). Distribution of foraminifera near pollution sources in Chaleur Bay. *Water, Air, and Soil Pollution, 2*(2), 219-233.

Schilling, K. E., Li, Z., & Zhang, Y. (2006). Groundwater-surface water interaction in the riparian zone of an incised channel, Walnut Creek, Iowa. *Journal of Hydrology*, *327*(1-2), 140-150.

Scibek, J., Allen, D. M., Cannon, A. J., & Whitfield, P. H. (2007). Groundwater-surface water interaction under scenarios of climate change using a high-resolution transient groundwater model. *Journal of Hydrology*, *333*(2–4), 165–181.

Service Nova Scotia and Municipal Relations. (2003). Enhanced digital elevation model, Nova Scotia, Canada. Service Nova Scotia and Municipal Relations, Registry and Information Management Services, Nova Scotia, Canada.

Shinn, E. A., Reese, R. S., & Reich, C. D. (1994). *Fate and pathways of injection-well effluent in the Florida Keys.* US Geological Survey, Open-File Report.

Shinn, E. A., Reich, C. D., & Hickey, T. D. (2002). Seepage meters and Bernoulli's revenge. *Estuaries*, *25*(1), 126–132.

Shuai, P., Cardenas, M. B., Knappett, P. S., Bennett, P. C., & Neilson, B. T. (2017). Denitrification in the banks of fluctuating rivers: The effects of river stage amplitude, sediment hydraulic conductivity and dispersivity, and ambient groundwater flow. *Water Resources Research, 53*(9), 7951-7967.

Shum, K. T. (1992). Wave-induced advective transport below a rippled water-sediment interface. *Journal of Geophysical Research*, *92*(C1), 789–808.

Siah, A., Pellerin, J., Amiard, J. C., Pelletier, E., & Viglino, L. (2003). Delayed gametogenesis and progesterone levels in soft-shell clams (Mya arenaria) in relation to in situ contamination to organotins and heavy metals in the St. Lawrence River (Canada). *Comparative Biochemistry and Physiology Part C: Toxicology & Pharmacology, 135*(2), 145-156.

Simmons, R. C., Gold, A. J., and Groffman, P. M. (1992). Nitrate dynamics in riparian forests: Groundwater studies. *Journal of Environmental Quality, 21,* 656-665.

Sinton, L. W., Finlay, R. K., Pang, L., & Scott, D. M. (1997). Transport of bacteria and bacteriophages in irrigated effluent into and through an alluvial gravel aquifer. *Water, Air, and Soil Pollution*, *98*(1–2), 17–42.

Slomp, C. P., & Van Cappellen, P. (2004). Nutrient inputs to the coastal ocean through submarine groundwater discharge: Controls and potential impact. *Journal of Hydrology*, *295*(1–4), 64–86.

SLR Consulting. (2015). *Proposed Black Point Quarry project Guysborough County, Nova Scotia: Hydrogeological technical report*.

Small, C., & Nicholls, R. J. (2003). A global analysis of human settlement in coastal zones. *Journal of Coastal Resources*, *19*, 584–599.

Smith, K. (1981). The prediction of river water temperatures/prédiction des températures des eaux de rivière. *Hydrological Sciences Journal, 26*(1), 19-32.

Smith, M. S., Thomas, G. W., White, R. E., & Ritonga, D. (1985). Transport of Escherichia coli through intact and disturbed soil columns. *Journal of Environmental Quality, 14*, 87-91.

Sophocleous, M. (2002). Interactions between groundwater and surface water: The state of the science. *Hydrogeology Journal, 10*(1), 52-67.

South Florida Water Management District (n.d.). *Module 13: PEST Introduction*. Retrieved from: https://www.sfwmd.gov/sites/default/files/documents/ rsm_module_13.pdf

Speiran, G. K. (2010). Effects of groundwater-flow paths on nitrate concentrations across two riparian forest corridors. *Journal of the American Water Resources Association*, *46*(2), 246–260.

Starr, R. C. and Gillham, R. W. (1993). Denitrification and organic carbon availability in two aquifers. *Groundwater,* 31, 934 - 947.

Stea, R. R., Conley, H., Brown, Y., & Fisher, B. E., (2006). *DP ME 36, version 2, 2006. Digital version of Nova Scotia Department of Natural Resources map ME 1992-3, surficial geology map of the province of Nova Scotia, 1:500 000*. Nova Scotia Department of Natural Resources, Mineral Resources Branch.

Stephens, D. B., Hsu, K. C., Prieksat, M. A., Ankeny, M. D., Blandford, N., Roth, T. L., Kelsey, J. A., & Whitworth, J. R. (1998). A comparison of estimated and calculated effective porosity. *Hydrogeology Journal, 6*(1), 156-165.

StructX. (2020). *Hydraulic conductivity ranges of various soil types*. Retrieved from: https://structx.com/Soil_Properties_007.html.

Tait, D. R., Erler, D. V., Santos, I. R., Cyronak, T. J., Morgenstern, U., & Eyre, B. D. (2014). The influence of groundwater inputs and age on nutrient dynamics in a coral reef lagoon. *Marine Chemistry*, *166*, 36–47.

Taniguchi, M. (2002). Tidal effects on submarine groundwater discharge into the ocean. *Geophysical Research Letters*, *29*(12).

Taniguchi, M., Burnett, W. C., Cable, J. E., & Turner, J. V. (2002). Investigation of submarine groundwater discharge. *Hydrological Processes, 16*(11), 2115-2129.

Taniguchi, M., Dulai, H., Burnett, K. M., Santos, I. R., Sugimoto, R., Stieglitz, T., Kim, G., Moosdorf, N., Burnett, W. C. (2019). Submarine groundwater discharge: Updates on its measurement techniques, geophysical drivers, magnitudes, and effects. *Frontiers in Environmental Science*, *7*, 1–26.

Tate, R. L. (1978). Cultural and environmental factors affecting the longevity of Escherichia coli in histosols. *Applied and Environmental Microbiology,* 35, 925-929.

Taylor, R., Cronin, A., Pedley, S., Barker, J., & Atkinson, T. (2004). The implications of groundwater velocity variations on microbial transport and wellhead protection–review of field evidence. *FEMS Microbiology Ecology, 49*(1), 17-26.

Tesoriero, A. J., Liebscher, H., & Cox, S. E. (2000). Mechanism and rate of denitrification in an agricultural watershed: Electron and mass balance along groundwater flow paths. *Water Resources Research, 36*(6), 1545-1559.

Thompson, C., Smith, L., Roudrajit, M. (2006). Hydrogeological modeling of submarine groundwater discharge on the continental shelf of Louisiana. *Journal of Geophysical Research, 12*.

Todd, D. K. (1980). *Groundwater hydrology* (2nd Edition). John Wiley & Sons, New York.

Todd, G. K., (1995). Groundwater flow in relation to the flooding stream. *Proceedings of the American Society of Civil Engineers, 81*(628), 20-28.

Tóth, J. (1962). A theory of groundwater motion in small drainage basins in central Alberta, Canada. *Journal of Geophysical Research, 67*(11), 4375-4388.

Tóth, J. (1963). A theoretical analysis of groundwater flow in small drainage basins. *Journal of Geophysical Research, 68*(16), 4795-4812.

Tóth, J. (1970). A conceptual model of the groundwater regime and the hydrogeologic environment. *Journal of Hydrology, 10*(2), 164-176.

Torgersen, C. E., Faux, R. N., McIntosh, B. A., Poage, N. J., & Norton, D. J. (2001). Airborne thermal remote sensing for water temperature assessment in rivers and streams. *Remote Sensing of Environment, 76*(3), 386-398.

Trglavcnik, V., Morrow, D., Weber, K. P., Li, L., & Robinson, C. E. (2018). Analysis of tide and offshore storm-induced water table fluctuations for structural characterization of a coastal island aquifer. *Water Resources Research, 54*, 2749–2767.

Triska, F. J., Duff, J. H., & Avanzino, R. J. (1993). The role of water exchange between a stream channel and its hyporheic zone in nitrogen cycling at the terrestrial—aquatic interface. In *Nutrient dynamics and retention in land/water ecotones of Lowland, Temperate Lakes and Rivers* (pp. 167-184). Springer, Dordrecht.

Türker, Y. (1969). *Short term variation of runoff-rainfall ratios in Nova Scotia IHD watersheds*. Dalhousie University.

Valiela, I., Collins, G., Kremer, J., Lajtha, K., Geist, M., Seely, B., Brawley, J., & Sham, C. H. (1997). Nitrogen loading from coastal watersheds to receiving estuaries: New method and application. *Ecological Applications*, *7*(2), 358–380.

Valiela, I., Costa, J., Foreman, K., Teal, J. M., Howes, B., & Aubrey, D. (1990). Transport of groundwater-borne nutrients from watersheds and their effects on coastal waters. *Biogeochemistry, 10*(3), 177–197.

Voss, C. I. (2011a). Editor's message: Groundwater modeling fantasies—Part 1, adrift in the details. *Hydrogeology Journal*, *19*(7), 1281-1284.

Voss, C. I. (2011b). Editor's message: Groundwater modeling fantasies—Part 2, down to earth. *Hydrogeology Journal*, *19*(8), 1455-1458.

Warnemuende, E., & Kanwar, R. (2002). Effects of swine manure application on bacterial quality of leachate from intact soil columns. *Transactions of the ASAE, 45*(6), 1849.

Wang, S. L., Chen, C. T. A., Huang, T. H., Tseng, H. C., Lui, H. K., Peng, T. R., Kandasamy, S., Zhang, J., Yang, L., Gao, X., Lou, J. Y., Kuo F. W., Chen, X. G., Ye, Y., & Lin, Y. J. (2018). Submarine groundwater discharge helps making nearshore waters heterotrophic. *Scientific Reports, 8*(1), 1-10.

Waterloo Hydrogeologic. (2019). *Visual MODFLOW Flex 6.1: Boundary conditions theory*. Retrieved from https://www.waterloohydrogeologic.com/help/vmod-flex/index.html?vm_about_boundary_conditions____t.htm.

Watermark Numerical Computing. (2020). *PEST Model-independent parameter estimation user manual part 1: PEST, SENSAN and Global Optimisers.*

Watson, T. A., Werner, A. D., & Simmons, C. T. (2010). Transience of seawater intrusion in response to sea level rise. *Water Resources Research, 46*(12).

Webb, M. D., & Howard, K. W. (2011). Modeling the transient response of saline intrusion to rising sea-levels. *Groundwater, 49(4)*, 560-569.

Welch, L. A., & Allen, D. M. (2014). Hydraulic conductivity characteristics in mountains and implications for conceptualizing bedrock groundwater flow. *Hydrogeology Journal, 22*(5), 1003-1026.

Windom, H. L. (1992). Contamination of the marine environment from land-based sources. *Marine Pollution Bulletin*, 25(1-4), 32-36.

Winter, T. C., Harvey, J. W., Franke, O. L., & Alley, W. M. (1998). *Ground water and surface water: A single resource* (Vol. 1139). US Geological Survey Circular 1139.

Winston, R. B. (2020). *ModelMuse Version 4.3.* US Geological Survey Software Release.

Woessner, W. W. (2000). Stream and fluvial plain ground water interactions: Rescaling hydrogeologic thought. *Ground Water*, *38*(3), 423-429.

Wolanski, E., & Elliot, M. (2015). *Estuarine ecohydrology – An introduction* (2nd Edition). Elsevier.

Wroblicky, G. J., Campana, M. E., Valett, H. M., & Dahm, C. N. (1998). Seasonal variation in surface-subsurface water exchange and lateral hyporheic area of two stream-aquifer systems. *Water Resources Research, 34*(3), 317-328.

Xu, C. Y., & Singh, V. P. (2002). Cross comparison of empirical equations for calculating potential evapotranspiration with data from Switzerland. *Water Resources Management, 16*(3), 197-219.

Yates, M. V., Gerba, C. P., & Kelley, L. M. (1985). Virus persistence in groundwater. *Applied and Environmental Microbiology*, *49*(4), 778-781.

Yau, V. M., Schiff, K. C., Arnold, B. F., Griffith, J. F., Gruber, J. S., Wright, C. C., Wade, T. J., Burns, S., Hayes, J. M., McGee, C., Gold, M., Cao, Y., Boehm, A. B., Weisberg, S. B., & Colford, J. M. (2014). Effect of submarine groundwater discharge on bacterial indicators and swimmer health at Avalon Beach, CA, USA. *Water Research, 59*, 23–36.

Younger, P. L. (1993). Simple generalized methods for estimating aquifer storage parameters. *Quarterly Journal of Engineering Geology, 26*, 7-135

Younger, P. L. (1996). Submarine groundwater discharge. *Nature*, *382*, 121–122.

Zekster, I. S., Ivanov, V. A., & Meskheteli, A. V. (1973). The problem of direct groundwater discharge to the seas. *Journal of Hydrology*, *20*, 1–36.

Zektser, I. S., & Loaiciga, H. A. (1993). Groundwater fluxes in the global hydrologic cycle: Past, present and future. *Journal of Hydrology, 144*(1-4), 405-427.

Zektster, I. S., & Everett, L. G. (2000). *Groundwater and the environment: Applications for the global community.* CRC Press, Boca Raton.

Zucker, L. A., & Brown, L. C. (1998). *Agricultural drainage: Water quality impacts and subsurface drainage studies in the Midwest* (Vol. 871). Ohio State University Extension.

Zwieniecki, M. A., & Newton, M. (1999). Influence of streamside cover and stream features on temperature trends in forested streams of western Oregon. *Western Journal of Applied Forestry, 14*(2), 106-113.

APPENDIX I: HYDROGRAPH AND WATER BUDGET ANALYSIS

STREAM GAUGING DATA

Table A1: Stream gauging data for the Mabou, NE Mabou, and SW Mabou Rivers. Relative stage is in respect to the pressure logger within the stilling well. Mean depth is the average of station depths.

Date	Time (mid-test)	Relative stage [m]	Mean depth [m]	Q [m^3 s^{-1}]
Mabou River				
November 1, 2018	16:30	N/A	0.34	3.96
May 6, 2019	17:30	0.441	0.30	1.98
June 18, 2019	10:30	0.348	0.17	1.12
August 29, 2019	13:30	0.622	0.40	5.44
August 30, 2019	10:35	0.693	0.44	6.92
October 21, 2019	15:00	0.589	0.36	4.35
March 10, 2020	NA	0.491[a]	N/A	2.44
NE Mabou River				
November 1, 2018	13:00	N/A	0.41	0.901
February 2, 2019	16:50	N/A	0.37	0.466
May 6, 2019[b]	N/A	0.415	0.29	0.532
June 18, 2019	13:20	0.373[c]	0.28	0.39
August 28, 2019	10:30	0.571	0.50	1.83
August 29, 2019	17:05	0.419	0.33	0.642
October 21, 2019	17:00	0.470[d]	0.36	0.771
October 22, 2019	14:15	0.468[d]	0.33	0.659
March 10, 2020	N/A	0.384[a]	N/A	0.445
SW Mabou River				
November 1, 2018	15:15	N/A	0.32	2.59
May 6, 2019	13:35	N/A	0.30	1.16
June 18, 2019	08:34	N/A	0.36	0.821
August 29, 2019	10:29	N/A	0.47	4.57
October 22, 2019	08:53	N/A	0.33	2.11

Notes:
a = relative stage determined through surveying relative to piezometer
b = date discrepancy
c = rebar/stilling well corrected
d = relative stage determined manually in stilling well

ANALYSIS OF CAPE BRETON CATCHMENTS

To facilitate model calibration to baseflow, annual baseflow was estimated based on patterns observed in watersheds with similar BFI, geology, topography, and climate. Although precipitation, stream discharge, and baseflow to precipitation ratios can vary between years, the proportion of annual baseflow that occurs in the field season versus the off-season is consistent, regardless of differences in annual precipitation, and streamflow. Similarly, the BFI is generally not consistent between the field and off-seasons, but the ratio is similar between years.

To assist in the extrapolation of seasonal data for the Mabou and NE Mabou River, hydrometric data from Environment Canada was gathered for the River Inhabitants at Glenora (01FA001) and Middle River at MacLennan's Cross (01FF001), respectively. Both surrogate watersheds have similar geology, topography, climate, and BFI as their Mabou Harbour counterparts. Indian Brook at Indian Brook (01FE002) and Cheticamp River above Robert Brook (01FC002) were also analysed for temporal patterns but are not reported in this document as they were determined to not be relevant to the Mabou rivers.

Table A2: Hydrograph analysis results and water budget for Middle River at MacLennan' s Cross (2017-2018)

Precipitation [m^3]		Streamflow [m^3]		Baseflow [m^3]		BFI		Baseflow/Precipitation Ratio	
2017	2018	2017	2018	2017	2018	2017	2018	2017	2018
Field Season									
1.06E+08	1.35E+08	6.62E+07	9.01E+07	3.50E+07	4.52E+07	0.53	0.50	0.33	0.33
48.7%	48.6%	31.5%	33.8%	30.8%	33.2%	N/A	N/A	N/A	N/A
Off Season									
1.12E+08	1.43E+08	1.44E+08	1.76E+08	7.88E+07	9.10E+07	0.55	0.52	0.70	0.63
51.3%	51.4%	68.5%	66.2%	69.2%	66.8%	N/A	N/A	N/A	N/A
Total									
2.18E+08	2.79E+08	2.10E+08	2.66E+08	1.14E+08	1.36E+08	0.54	0.51	0.52	0.49

Table A3: Hydrograph analysis results and water budget for River Inhabitants at Glenora (2017-2018)

Precipitation [m^3]		Streamflow [m^3]		Baseflow [m^3]		BFI		Baseflow/Precipitation Ratio	
2017	2018	2017	2018	2017	2018	2017	2018	2017	2018
Field Season									
1.06E+08	1.35E+08	6.62E+07	9.01E+07	3.50E+07	4.52E+07	0.53	0.50	0.33	0.33
48.7%	48.6%	31.5%	33.8%	30.8%	33.2%	N/A	N/A	N/A	N/A
Off Season									
1.12E+08	1.43E+08	1.44E+08	1.76E+08	7.88E+07	9.10E+07	0.55	0.52	0.70	0.63
51.3%	51.4%	68.5%	66.2%	69.2%	66.8%	N/A	N/A	N/A	N/A
Total									
2.18E+08	2.79E+08	2.10E+08	2.66E+08	1.14E+08	1.36E+08	0.54	0.51	0.52	0.49

FRESHWATER INPUT ESTIMATES

Freshwater input to the harbour was approximated based on temporal trends observed in similar watersheds (Table A2 and Table A3). The freshwater input to the harbour was estimated on field-season, off-season, annual, and daily timescales (Table A4; Table A5; Table A6). Evapotranspiration (*ET)* in the SW and Harbour subcatchments were assumed to be equal to the Mabou River watershed.

Table A4: Estimation of freshwater input to the harbour during the field-season. The sea catchment represents precipitation that falls directly into the harbour. ET is based on temporal trends observed in Table A2 and Table A3.

Catchment	DA (m2)	P (m)	P (m3)	ET (%)	ET (m3)	Q (m3)
Mabou	1.75E+08	0.647	1.13E+08	0.501	5.67E+07	5.65E+07
SW	1.16E+08	0.647	7.52E+07	0.501	3.77E+07	3.75E+07
NE	2.55E+07	0.647	1.65E+07	0.334	5.51E+06	1.10E+07
Harbour	4.64E+07	0.647	3.00E+07	0.501	1.50E+07	1.50E+07
Sea	6.70E+06	0.647	4.33E+06	0.000	0.00E+00	4.33E+06

Table A5: Estimation of freshwater input to the harbour during the off-season. The sea catchment represents precipitation that falls directly into the harbour. ET is based on temporal trends observed in Table A2 and Table A3.

Catchment	DA (m2)	P (m)	P (m3)	ET (%)	ET (m3)	Q (m3)
Mabou	1.75E+08	0.871	1.52E+08	0.248	3.78E+07	1.15E+08
SW	1.16E+08	0.871	1.01E+08	0.248	2.51E+07	7.61E+07
NE	2.55E+07	0.871	2.22E+07	0.121	2.69E+06	1.95E+07
Harbour	4.64E+07	0.871	4.04E+07	0.248	1.00E+07	3.04E+07
Sea	6.70E+06	0.871	5.84E+06	0.000	0.00E+00	5.84E+06

Table A6: the annual and mean-daily estimates of freshwater input to the harbour based on Table A4 and Table A5. The sea catchment represents precipitation that falls directly into the harbour.

Catchment	Q_F [m3 yr-1]	Q_F [m3 d-1]
Mabou	1.71E+08	4.69E+05
SW	1.14E+08	3.11E+05
NE	3.05E+07	8.36E+04
Harbour	4.54E+07	1.24E+05
Sea	1.02E+07	2.79E+04
Total	3.71E+08	1.02E+06

PENMAN – MONTEITH EQUATION

The FAO Penman – Monteith equation was used to evaluate the reference crop evapotranspiration (ET_o) [mm d^{-1}], which represents the maximum amount of *ET* possible from a reference surface with unlimited water given the atmospheric conditions (Allen et al., 1998). The FAO Penman – Monteith equation, as presented by Allen et al. (1998), is as follows:

$$ET_o = \frac{0.408\Delta(R_n - G) + \gamma\left(\frac{900}{T + 273}\right)u_2(e_s - e_a)}{\Delta + \gamma(1 + 0.34u_2)} \quad (12)$$

where R_n is the net radiation [MJ m^{-2} d^{-1}], G is the soil heat flux density [MJ m^{-2} d^{-1}], e_s and e_a are the saturation and actual vapour pressures [kPa], (e_s – e_a) is the saturation vapour pressure deficit [kPa], u_2 is the wind speed at a height of 2 m [m s^{-1}], Δ is the slope vapour pressure curve [kPa °C^{-1}], and γ is the psychrometric constant [kPa]. The variable u_2 was estimated using the wind profile relationship discussed in Allen et al. (1998).

Net Radiation at the Crop Surface

Net radiation was calculated using the following equations from Allen et al. (1998):

$$R_n = R_{ns} - R_{nl} \quad (13)$$

$$R_{ns} = (1 - \alpha)R_s \quad (14)$$

where albedo (α) was assumed to be 0.25 to represent grass and forest cover. R_{nl} was calculated using the following equation (Allen et al., 2018):

$$R_{nl} = \sigma R_{ns} - R_{nl}\left(\frac{T_{max} + T_{Min}}{2}\right)\left(0.34 - 0.14\sqrt{e_a}\right)\left(1.35\frac{R_s}{R_{so}} - 0.35\right) \quad (15)$$

where R_{nl} is the net outgoing longwave radiation [MJ m^{-2} d^{-1}], σ is the Stefan Boltzmann constant [4.903×10^{-9} MJ K^{-4} m^{-2} d^{-1}], T_{max} and T_{min} are the maximum and minimum

temperatures [K], e_a is actual vapour pressure [kPa], R_s and R_{so} is solar and clear-sky radiation [MJ m^{-2} d^{-1}]. R_{so} can be determined from the following equation from Xu et al. (2002):

$$R_{so} = (0.75 + 2 \times 10^{-5} z) R_a \quad (16)$$

where z is elevation [m] and R_a is extraterrestrial radiation [MJ m^{-2} d^{-1}]. R_a can be calculated from the equation (Xu et al., 2002):

$$R_a = \frac{24(60)}{\pi} G_{sc} d_r [\omega_s \sin(\varphi) \sin(\delta) + \cos(\varphi) \cos(\delta) \sin(\omega_s)] \quad (17)$$

where G_{sc} is the solar constant [0.0820 MJ m^{-2} min^{-1}], d_r is the inverse relative distance between the Earth and the Sun, ω_s is the sunset hour angle, is the latitude [rad], and δ is the solar decimation. The variables d_r, ω_s, φ, and δ can be calculated using the following equations from Allen et al. (1998):

$$d_r = 1 + 0.033 cos\left(\frac{2\pi}{365} J\right) \quad (18)$$

$$\omega_s = \arccos[-tan(\varphi)\, tan(\delta)] \quad (19)$$

$$\delta = 0.409 sin\left(\frac{2\pi}{365} J - 1.39\right) \quad (20)$$

where J is the day number (i.e., number of days between December 31 and the date).

Vapour Pressures

The saturation and actual vapour pressures are calculated using the equations from Xu et al. (2002):

$$e_s(T_a) = 0.611 exp\left(\frac{17.27 T_a}{T_a + 237.3}\right) \quad (21)$$

$$e_a(T_d) = 0.611exp\left(\frac{17.27T_d}{T_d + 237.3}\right) \quad (22)$$

where T_a is the air temperature [°C] and T_d is the dew point temperature [°C].

Psychrometric Constant

The psychrometric constant (γ) can be calculated from the following equations presented by Xu et al. (2002):

$$\gamma = 0.00163\frac{P}{\lambda} \quad (23)$$

$$\lambda = 2.501 - (2.361 \times 10^{-3})T_a \quad (24)$$

where λ is the latent heat of vaporization [MJ kg^{-1}] and P is atmospheric pressure [kPa].

Assumptions with Penman – Monteith Equation

1. The air temperature reported by Environment Canada was representative of the air temperature at a height of 2 m.
2. The soil heat flux density is negligible on the diurnal basis (Allen et al., 1998).
3. An albedo of 0.25 is representative of the drainage basin.

Results

The results from the Penman-Monteith method are presented in Table A7. The field season had over double the *PET* (68% of annual *PET*) than the off season, which is consistent with water balance estimates (Section 2.3.6).

Table A7: Penman-Monteith results for the Mabou Harbour drainage basin during 2019.

ET [mm]		ET Ratio
2019 Field season	424.845	0.68
2019 Off season	200.925	0.32
2019 Annual	625.77	1

REFERENCES: APPENDIX I

Allen, R. G., Pereira, L. S., Raes, D., & Smith, M. (1998). Crop evapotranspiration-Guidelines for computing crop water requirements- FAO Irrigation and drainage paper 56. *FAO, Rome, 300*(9), D05109.

Xu, C. Y., & Singh, V. P. (2002). Cross comparison of empirical equations for calculating potential evapotranspiration with data from Switzerland. *Water Resources Management, 16*(3), 197-219.

APPENDIX II: WATER QUALITY SAMPLING

WATER CHEMISTRY AND PHYSICAL PROPERTIES

General water chemistry and physical properties were tested in the field using a YSI ProDSS handheld multiparameter water quality meter (YSI) for both surface water and groundwater samples. In the 2020 field campaign, a peristaltic pump was used to purge the well and continue pumping for a further 5-10 minutes. Following purging, the pump was used to fill the container to facilitate testing with the YSI.

The groundwater chemistry, observed in the different piezometers and a domestic well, are presented in Table A8 (Appendix II). The majority of the sampled groundwater is fresh with the exception of NE Mabou Harbour, which consistently exhibited slightly saline total dissolved solids (TDS). Furthermore, freshwater conditions were observed between 3.2 and 17.5 m from the regular hightide mark at depths of 0.935 and 1.185 m, respectively. All samples presented neutral to slightly basic pH. Sampling equipment and methodology used in 2019 may have added uncertainty to the dissolved oxygen (DO) analyte results. These issues were rectified in 2020 sampling was conducted using a peristaltic pump after purging continuously for 5-10 minutes. The 2020 DO results showed that the groundwater in the NE Mabou River piezometer is more anoxic than in the coastal aquifers. Furthermore, tap water from a coastal domestic well of unknown depth was oxic. The house water was left running to purge the lines; however, the DO may be less reliable considering the house uses a dug well.

Nitrate samples collected on October 9, 2020 does not indicate nitrate contamination in the major rivers (Table A 9). The samples were collected during the recession of an event flow, and thus may be diluted by surface runoff. Dissolved organic carbon (DOC) was high in the NE Mabou piezometer supporting the conceptual model that riparian zones on low relief alluvial plains host the conditions appropriate for heavy denitrification, including shallow groundwater flow, organic rich soil (high DOC), and lower DO.

Table A8: Summary of surface water and groundwater chemical and physical properties tested in the field (2019-2020). Analytes include specific conductivity (SC), salinity (Sal), total dissolved solids (TDS), pH, dissolved oxygen (DO), and temperature (T).

	SC [µS/cm]	Sal [psu]	TDS [mg L^{-1}]	pH	DO [% Sat]	DO [mg L^{-1}]	T [°C]
Surface water							
Mabou River							
February 19, 2019	306.9	N/A	N/A	7.76	116.0	16.96	-0.06
May 7, 2019	263.7	N/A	N/A	8.05	121.2	12.92	12.55
June 18, 2019	260.8	0.12	170	8.26	106.3	10.68	15.17
August 27, 2019	139.0	0.07	90	7.95	99.2	9.72	16.33
October 21, 2019	155.3	0.07	101	8.19	100.1	11.58	9.00
March 20, 2020	215.4	0.10	140	8.27	98.7	14.44	0.1
October 8, 2020	302.1	0.15	197	7.83	96.3	9.97	12.50
NE Mabou River							
February 18, 2019	274.5	N/A	N/A	7.16	101.5	14.85	-0.08
May 7, 2019	335.8	N/A	N/A	7.92	115.5	13.16	9.44
June 18, 2019	289.2	0.14	188	7.95	102.1	10.40	14.50
August 28, 2019	134.7	0.06	88	7.83	96.3	10.09	13.22
August 29, 2019	309.3	0.15	201	8.02	96.7	9.82	14.67
October 21, 2019	197.9	0.09	129	8.17	96.8	11.08	9.33
March 20, 2020	320.0	N/A	208	8.07	97.9	14.33	0.0
October 8, 2020	286.4	0.14	186	7.86	92.1	9.58	12.20
October 9, 2020	568.0	0.28	369	7.64	91.3	10.59	8.50
SW Mabou Harbour							
February 18, 2019	471	N/A	N/A	7.22	118.7	17.46	-0.02
May 6, 2019	264	N/A	N/A	8.05	121.2	12.92	12.55
June 18, 2019	784	0.39	509	7.72	93.1	8.97	17.06
August 29, 2019	309	0.15	201	7.83	96.4	9.79	14.61
October 22, 2019	415	0.20	270	8.51	95.5	11.93	5.83
October 8, 2020	1010	0.50	656	7.52	91.4	9.30	13.10
Mabou Harbour							
June 17, 2019	43,584	28.08	28330	8.08	115.7	10.14	13.44
Farm Spring							
October 23, 2019	487	0.24	316	8.23	92.6	10.85	8.39

	SC [µS/cm]	Sal [psu]	TDS [mg L^{-1}]	pH	DO [% Sat]	DO [mg L^{-1}]	T [°C]
Groundwater							
WWTP							
October 21, 2019	1060	0.53	689	7.62	63.2[a]	6.85[a]	11.67
Mabou River piezometer							
October 21, 2019	440	0.21	286	7.65	36.1[a]	3.81[a]	12.94
NE Mabou River piezometer							
October 21, 2019	1807	0.92	1174	7.23	60.8[a]	6.69[a]	10.83
October 9, 2020	2007	1.03	1307	7.27	24.8	2.70	10.50
Lindy lower							
October 21, 2019	989	0.49	643	7.94	70.2[a]	7.55[a]	11.94
October 9, 2020	600	0.22	292	7.45	66.1	7.13	9.90
Lindy well							
October 9, 2020	297	0.14	193	7.94	83[b]	8.57[b]	N/A
South harbour piezo							
October 22, 2019	625	0.31	406	7.84	48.4[a]	5.41[a]	10.33
October 8, 2020	320	0.15	208	7.65	81.5	8.00	N/A
Tile Drain							
October 22, 2019	530	0.26	345	8.07	91.4	10.01	11.28
SW Mabou River spring							
October 22, 2019	208	0.10	135	6.95	72.9	8.06	10.89

Notes:
a = uncertainty introduced through sampling method and equipment used
b = uncertainty inherent in well design. Dug wells may have a greater well volume and exposure to atmosphere

Table A 9: Nitrate and dissolved organic carbon (DOC) concentrations in the NE Mabou piezometer, major rivers, and farm spring. Nitrate samples from the harbour are not reported due to unusually high detection limits resulting from high salinity.

	Nitrate as N [mg L^{-1}]	DOC [mg L^{-1}]
NE Mabou piezometer		
October 9, 2020	0.20	4.6
NE Mabou River		
October 9, 2020	0.12	N/A
Mabou River		
October 9, 2020	0.14	N/A
SW Mabou River		
October 9, 2020	<0.05	N/A
Farm spring		
October 9, 2020	0.16	N/A

Harbour Salinity

Two Salt Water Conductivity/Salinity Data Loggers (HOBO; U24-002-C) were installed in the Mabou Harbour from June 19 – August 28, 2019 (Figure A1). The accuracies of the conductivity/salinity data loggers are either 3% or 50µS in low-salinity conditions (100-10,000 µS) and are substantially greater in waters with higher salinity variation in high-salinity conditions (5000-55,000 µS). A Virtuoso tidal logger (RBR), with an accuracy and resolution of ±0.05% and 0.001% of full scale, respectively, was also installed at the outer harbour location. The salinity trends for the conductivity loggers and relative sea levels are presented in Figure A2, presenting a strong correlation between minimum salinities and low tides. The lowest salinity minimums are correlated with high discharge streamflows in the Mabou River (Figure A3).

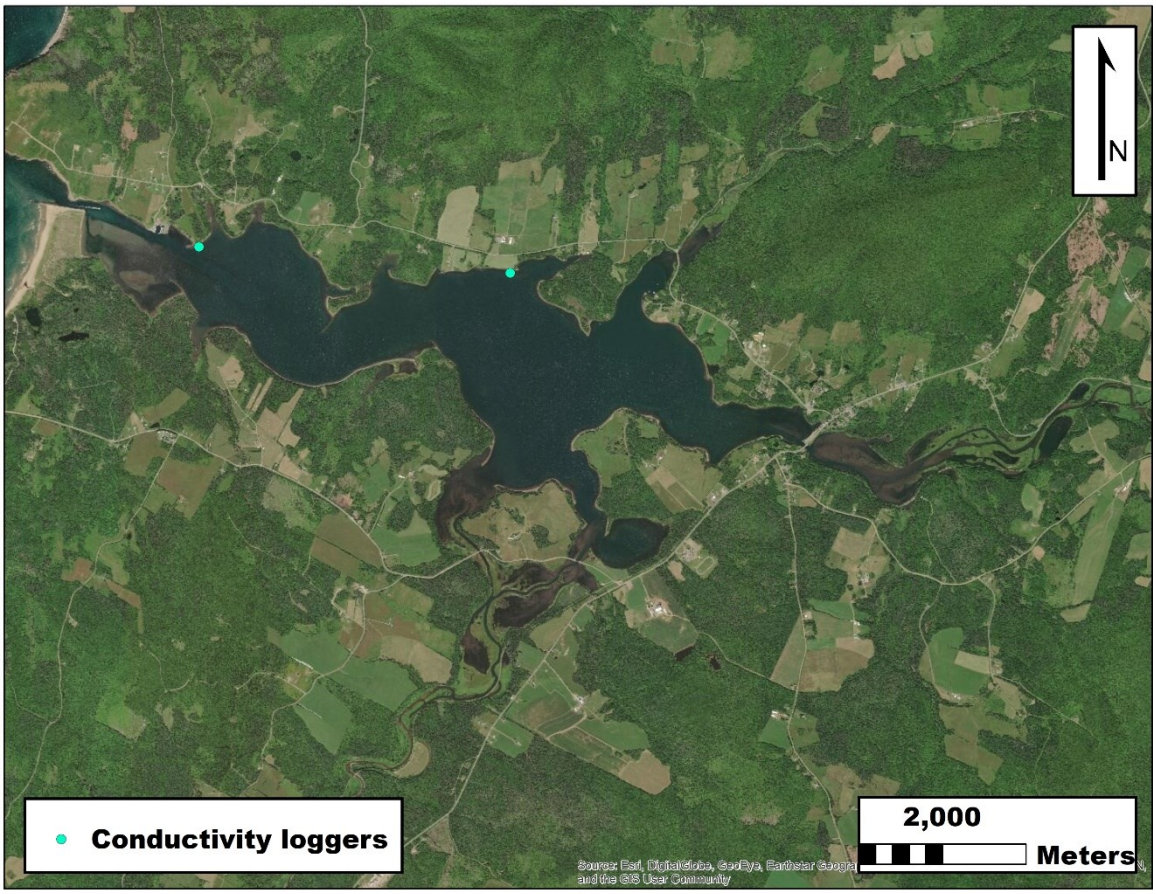

Figure A1: Conductivity loggers within the Mabou Harbour. The inner harbour is located to the east, and outer harbour is located to the west near the mouth of the harbour. Basemap sourced from ESRI (2018).

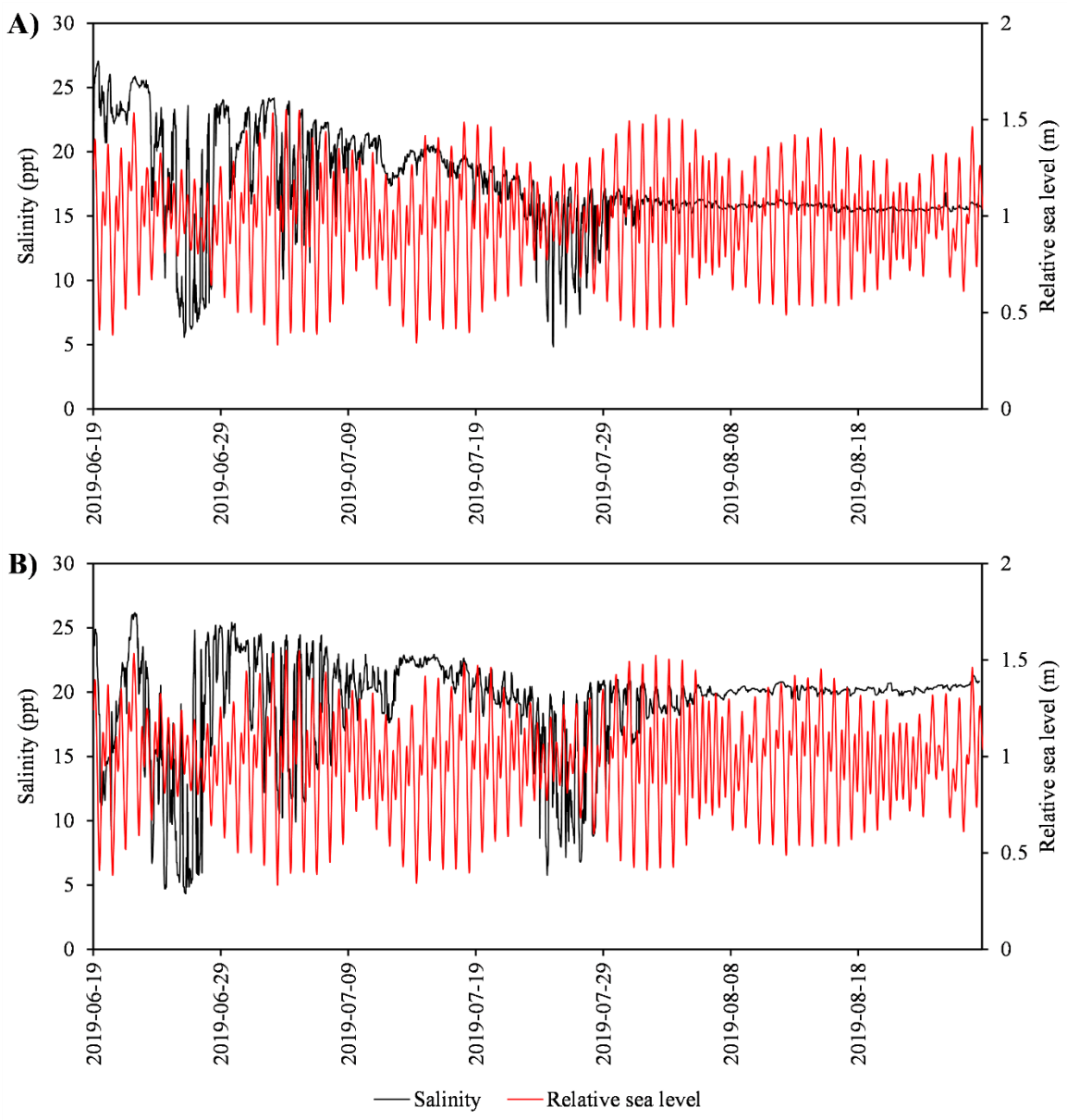

Figure A2: Harbour salinity and sea level relative to the Virtuoso tidal logger (RBR) at the outer harbour (A) and inner harbour (B) locations.

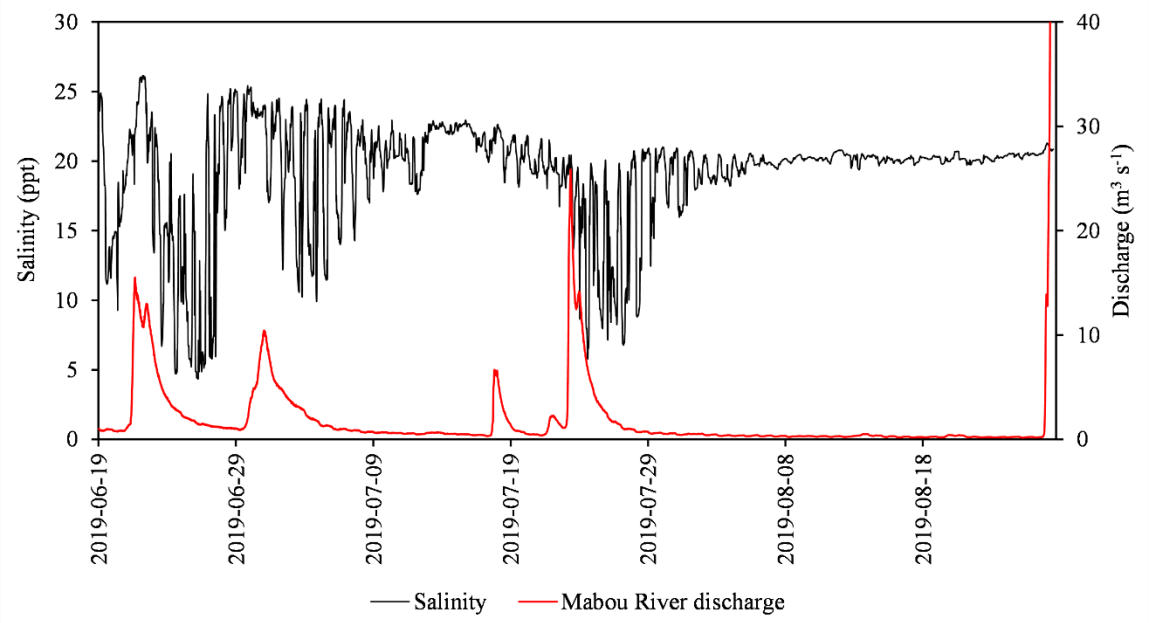

Figure A3: Salinity at the inner harbour location and Mabou River discharge. The lowest salinity minimums occur following major streamflow.

Table A 10: Mean and maximum salinities used in the freshwater fractionation method.

	Mean salinity [ppt]	Max salinity [ppt]
Outer harbour	17.4	27.06
Inner harbour	19.2	26.15

COLIFORM SAMPLING AND MICROBIAL SOURCE TRACKING

Bacteria testing and microbial source tracking (MST) in surface water and groundwater was conducted by Dr. Rob Jamieson's lab at Dalhousie University. The recreational water quality guidelines for *E. coli* (Health Canada, 2012) are ≤200 CFU 100 mL^{-1} (geometric mean from a minimum of 5 samples) or ≤400 CFU 100 mL^{-1} (single sample maximum concentration). The major rivers were the most frequently sampled, and the results exhibited highly variable microbial loads with maximum *E. coli* and other coliform levels reaching 70 and 400 CFU 100 mL^{-1}, respectively, in the SW Mabou River on October 1, 2020. Negligeable precipitation had occurred in the days leading up to sampling; therefore, baseflow conditions can be assumed. Groundwater from the WWTP presented *E. coli* and total coliform levels of 30 and 2800 CFU 100 mL^{-1}, respectively. A first-order tributary transecting agricultural operations on the northern shore was sampled on October 23, 2019, yielding an *E. coli* concentration of 400 100 mL^{-1} and 600 for total coliform. This sample is considered to represent baseflow conditions as the previously recorded precipitation event was three days prior; therefore, this sample may be representative of groundwater discharge sourced from livestock-bearing agricultural operations. Furthermore, manure is assumed to be the main source given that MST yielded 5.10 log gene copies 100 mL^{-1} of ruminant markers relative to 3.89 and 2.85 for human and avian, respectively. There is a residence and potentially a sceptic field nearby the spring, which could explain the human markers exhibited by the MST results.

Table A11: Coliform and microbial source tracking results from 2019-2020 (performed by Dr. Rob Jamieson's Lab)

	E. coli	Total coliform	Human markers	Avian markers	Ruminant markers
	[CFU 100 m L^{-1}]		[Log copies 100 m L^{-1}]		
Surface Water					
Mabou River					
February, 2019	3	160			
February, 2019	3	80			
May, 2019	<1	76	<1.1	1.26	2.98
October 1, 2020	9	220	<1.1	<1.1	1.51
NE Mabou River					
February, 2019	1	70			
February, 2019	2	40			
May, 2019	<1	11	2.22	<1.1	<1.1
October 1, 2020	12	210	2.75	<1.1	<1.1
SW Mabou River					
February, 2019	7	200			
February, 2019	4	160			
May 7, 2019	<1	2	<1.1	<1.1	1.55
October 1, 2020	70	400	<1.1	<1.1	<1.1
WWTP stream					
February, 2019	10	160			
February, 2019	10	240			
Farm Spring					
November, 2019	400	600	3.89	2.85	5.10
Groundwater					
WWTP piezometer					
November, 2019	30	2800	2.59	2.58	1.30
Tile drain					
November, 2019	10	600	<1.1	1.82	1.81

	E. coli	Total coliform	Human markers	Avian markers	Ruminant markers
	[CFU 100 m L^{-1}]		[Log copies 100 m L^{-1}]		
Lindy lower piezometer**					
November, 2019	1	600	<1.1	3.34	3.00

Notes:
** Sample possibly subjected to cross contamination from WWTP piezometer

REFERENCES: APPENDIX II

ESRI. (2018). *World Imagery*. Updated Dec. 4, 2018. https://www.arcgis.com/home/item.html?id=2a060171c43e44888911e0d89145fd0c

Health Canada (2012). *Guidelines for Canadian Recreational Water Quality, Third Edition*. Water, Air and Climate Change Bureau, Healthy Environments and Consumer Safety Branch, Health Canada, Ottawa, Ontario. Catalogue No H129-15/2012E.

APPENDIX III: TIDAL DATA

A Virtuoso tidal logger (RBR), with an accuracy and resolution of ±0.05% and 0.001% of full scale, respectively, was installed on a piece of rebar at the outer harbour station (Figure A1) from June 19 – October 22, 2019. The tidal summary statistics and tidal data for Mabou Harbour are presented in Table A12 and Figure A4, respectively. The tidal data exhibit mixed tidal cycles, such that semi-diurnal tides are asymmetrical (Figure A5). Tidal asymmetry is so strong at times that a diurnal signal dominates.

Table A12: Tidal statistics over the period of June 19 - August 28, 2019. The approximate area of the harbour was used to estimate tidal volumes.

Tidal statistics	Value
Mean tidal amplitude [m]	0.290397
Max tidal amplitude [m]	0.568846
Min tidal amplitude [m]	0.101957
Mean intertidal volume [m^3]	3,891,323
Max intertidal volume [m^3]	7,622,540
Min intertidal volume [m^3]	1,366,228

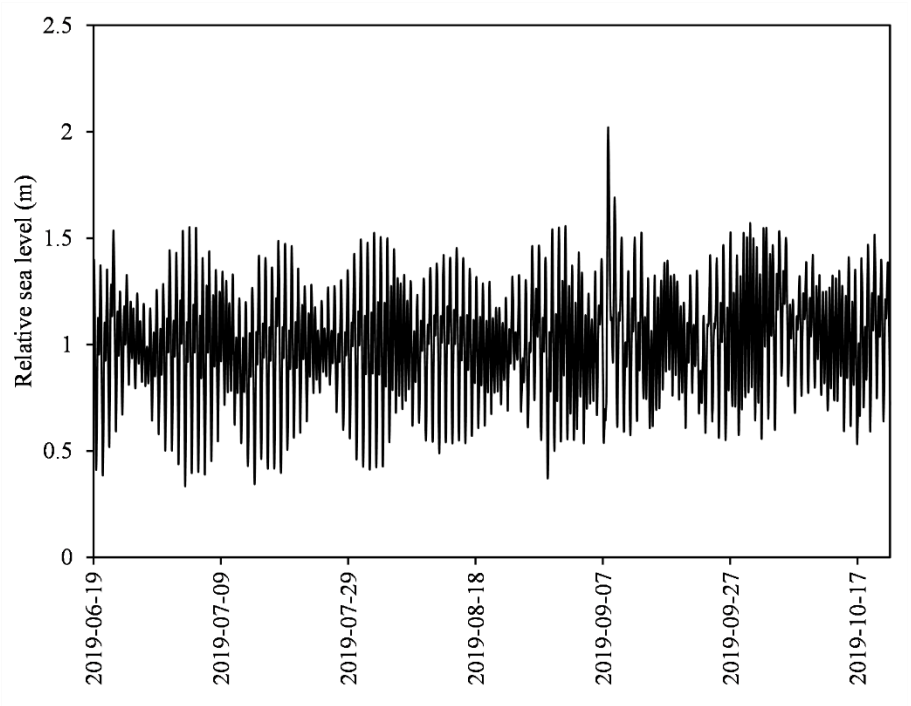

Figure A4: Sea level relative to RBR logger located at the outer harbour station.

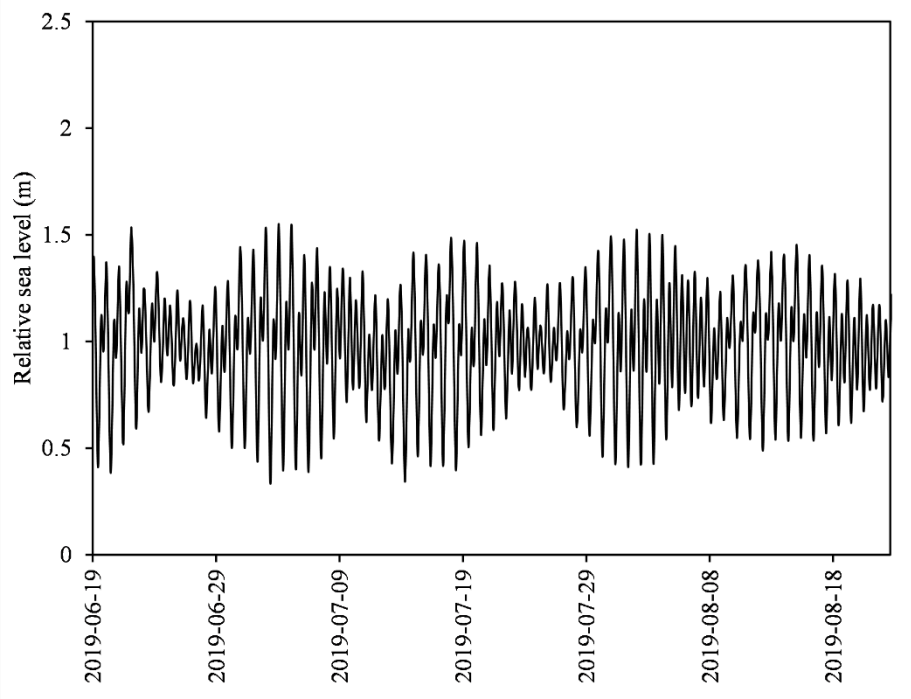

Figure A5: Expanded section of tidal series presenting mixed tidal cycles. Time-series represents sea level relative to the Virtuoso tidal logger (RBR) located at the outer harbour station.

APPENDIX IV: HYDRAULIC CONDUCTIVITY ESTIMATION

HVORSLEV METHOD

The Hvorslev method (1951) is a single-well test that can be applied to either slug or bail tests. This method estimates hydraulic conductivity based on well recovery as indicated at any point by drawdown (H) [m] and considers well geometry, such as standpipe radius (r_w) [m], and screen length (l_s) [m] and radius (R_s) [m]. H_o [m] represents the total drawdown at the beginning of the tests and H/H_o is the drawdown ratio, such that $H/H_o = 0$ at the beginning of the test. When H/H_o=0.37, the corresponding time is called the basic time lag (T_o) [d] and can be used to estimate K in the following simplified equation:

$$K = \frac{r_w^2 \ln\left(\frac{l_s}{r_s}\right)}{2LT_o} \tag{25}$$

The main variables and results from the Hvorslev method, which was applied to the Lindy lower and NE Mabou River piezometers, are displayed in Table A13.

Table A13: Main parameters and K estimates using the Hvorslev method.

	Lindy lower	NE Mabou #1	NE Mabou #2
H_o [m]	0.7806	0.9334	0.8692
T_o [d]	0.06398	0.003776	0.00168
L [m]	0.25	0.25	0.25
r_w [m]	0.0127	0.0127	0.0127
r_s [m]	0.0127	0.0127	0.0127
K [m d^{-1}]	0.015	0.25	0.57

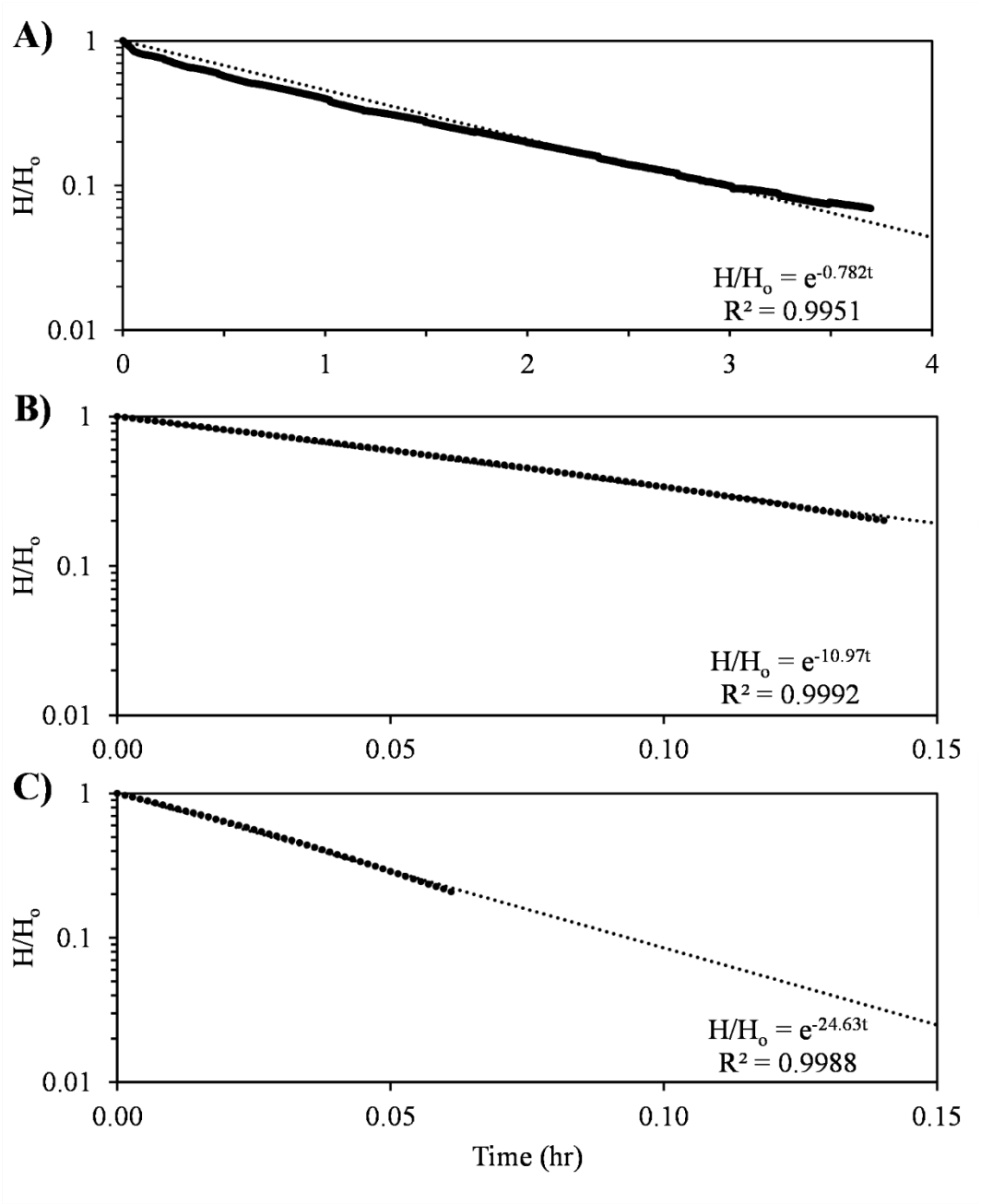

Figure A6: Drawdown ratio (H/Ho) vs time (hr) for the Lindy lower piezometer (A) and NE Mabou River piezometer (B and C).

JACOB EQUATION

The Jacob equation (1950) is used to estimate the propagation of a tidal signal in a confined aquifer using the following equation:

$$h(x,t) = H_o e^{\left(-x\sqrt{\frac{\pi}{Dp}}\right)} sin\left(\frac{2\pi t}{p} - x\sqrt{\frac{\pi}{Dp}}\right) \quad (26)$$

which can be further simplified to isolate the amplitude component of the sin-wave:

$$a = H_o e^{\left(-x\sqrt{\frac{\pi}{Dp}}\right)} \quad (27)$$

where $h(x,t)$ is the head within the aquifer [m], a is the signal amplitude within the aquifer [m], H_o is the amplitude of the tidal signal [m], x is the distance from the well to the sea, p is period [d], t is time [d] and D is hydraulic diffusivity [m^2 d^{-1}], which is equivalent to K/Ss.

A clean diurnal tidal signal was selected with strong asymmetry in the mixed signal, such that the diurnal signal dominated (2019-09-20 8:30 to 2019-09-21 10:00). Minimum and maximum heads within the harbour and aquifer are presented in Table A14. The parameters used in the K estimation are presented in Table A15. The use of Ss, rather than specific yield, as the storage parameter in Equation (27) is predicated on the assumption that the glacial till functions as a confined aquifer in terms of how it transmits tidal signals. For instance, it is assumed that water is released from compressibility rather than drainage. The specific storage parameter was based on the literature (Younger, 1993).

Table A14: Tidal signal data for the harbour (outer harbour station) and aquifer (Lindy Lower piezometer) during 2019-09-20 8:30 to 2019-09-21 10:00. Head is measured in meters above sea level (masl).

	Max head [masl]	Min head [masl]	Amplitude [m]
Aquifer	1.197	1.162	0.0175
Harbour	0.321	-0.396	0.3585

Table A15: Parameters used in Jacob equation to estimate K.

Jacob equation parameters	
x [m]	8.2
P [d]	1.06
Ho [m]	0.359
Ss [m^{-1}]	9.82×10^{-4}
D estimate [m^2 d^{-1}]	21.83
K estimate [m d^{-1}]	0.021

DRISCOLL METHOD

The Driscoll method (1986) utilizes common well test data that can be accessed from domestic well reports upon installation to estimate transmissivity (T; $m^2\ d^{-1}$). The method is based on specific capacity, which is defined as the yield per unit drawdown. Drawdown and average yield data for domestic wells in the Mabou Harbour drainage basin were collated from the Nova Scotia Well Logs Database (NSWLD). The following equation was used to estimate T:

$$T = \frac{1.385 * Y * 1.44}{s} \tag{28}$$

where Y is the average well yield, s is drawdown [m], 1.385 is the coefficient suggested by Batu (1998) for a confined aquifer divided by 1000 to represent $m\ d^{-1}$, and the coefficient of 1.44 is the conversion of the original equation from $m^3\ d^{-1}$ to liter per minute. Drawdown was assumed to be to the depth of the pump if stated, and the bottom of the well if not stated. Dug wells and wells under 5 m depth were removed as they do not represent bedrock conditions. To convert from T to K, the aquifer depth was set to equal the screened interval as proposed in the literature (e.g., Patriarche et al., 2005).

The occurrence of calibrated K values below what was expected given well test data (Figure 31) could possibly be explained by uncertainty in the Driscoll method of estimating K. When the Driscoll method was applied to two municipal wells with known hydraulic properties from pumping tests, the estimate was almost exactly one order of magnitude higher; however, it is unknown if the larger diameter casing for the municipal wells had a role to play.

Table A16: K and well construction data derived from the Nova Scotia Well Log Database. The Driscoll method (1987) was applied to determine K.

Well number	HSU	K [m d^{-1}]	Depth [m]	Casing [m]	Bedrock [m]	Depth into bedrock [m]
13627	Sandstone/Siltstone	6.0E-01	25.58	12.18	9.14	16.44
141296	Sandstone/Siltstone	4.9E-01	45.68	18.27	1.83	43.85
781187	Sandstone/Siltstone	2.0E+00	18.88	13.7	10.66	8.22
861538	Sandstone/Siltstone	7.3E-01	17.05	9.44	4.87	12.18
880773	Sandstone/Siltstone	8.1E-01	19.18	7.31	5.48	13.7
931776	Sandstone/Siltstone	9.3E-01	36.54	12.18	3.65	32.89
951062	Sandstone/Siltstone	2.7E+01	15.22	14.31	6	9.22
972538	Sandstone/Siltstone	2.2E+00	19.79	10.66	9.14	10.65
981886	Sandstone/Siltstone	3.2E-01	74.3	30.45	27.4	46.9
882161	Sandstone/Siltstone	1.3E+00	37.45	12.18	4.26	33.19
20581	Siltstone	1.6E-01	31.97	21.32	7.61	24.36
121284	Siltstone	3.6E-02	42.63	12.18	3.96	38.67
121294	Siltstone	5.2E+00	18.27	18.27	6	12.27
131172	Siltstone	6.0E-01	36.54	30.45	4.57	31.97
670267	Siltstone	3.6E+00	25.58	25.58	6	19.58
670284	Siltstone	3.8E+00	13.7	5.79	5.48	8.22
710346	Siltstone	3.8E-01	21.92	8.53	7.92	14
711511	Siltstone	2.5E-02	42.63	24.97	24.97	17.66
711512	Siltstone	2.4E+00	14.31	12.79	11.57	2.74
720110	Siltstone	1.3E-01	52.07	33.19	1.52	50.55
720793	Siltstone	1.8E+00	21.62	11.57	11.57	10.05
740297	Siltstone	6.1E+01	17.36	16.75	10.66	6.7
780862	Siltstone	6.2E-01	44.76	14.62	6	38.76
781188	Siltstone	2.5E-01	18.27	7.31	4.26	14.01
781295	Siltstone	2.3E-02	30.45	14.01	6	24.45
781296	Siltstone	2.5E-01	18.27	7.31	4.26	14.01
790202	Siltstone	4.9E-01	29.54	6.7	4.57	24.97
820775	Siltstone	8.1E-01	22.84	17.97	5.48	17.36
830053	Siltstone	5.3E-01	29.54	6.7	3.65	25.89
830648	Siltstone	1.5E+00	18.57	8.83	6	12.57
830658	Siltstone	3.7E-01	22.53	10.66	9.14	13.39
840870	Siltstone	6.2E-01	23.75	23.75	6	17.75
850800	Siltstone	1.6E-01	21.92	6.39	2.74	19.18
850806	Siltstone	3.7E-01	18.27	6.39	6	12.27
850807	Siltstone	2.7E-01	23.75	7.92	7	16.75
872129	Siltstone	3.1E-01	44.76	14.01	4.26	40.5
880777	Siltstone	3.9E-01	30.75	6.7	4.57	26.18
880779	Siltstone	1.4E-01	21.92	6.7	4.57	17.35
902182	Siltstone	1.4E-02	48.72	12.18	3.04	45.68
902307	Siltstone	2.5E-01	44.76	8.83	6	38.76
931324	Siltstone	2.6E-01	25.27	12.79	12.79	12.48
941493	Siltstone	8.7E+00	16.14	14.92	6	10.14

Well number	HSU	K [m d^{-1}]	Depth [m]	Casing [m]	Bedrock [m]	Depth into bedrock [m]
941632	Siltstone	1.0E+00	22.84	16.14	3.35	19.49
942510	Siltstone	2.5E-01	29.54	18.27	6	23.54
942576	Siltstone	2.8E-01	21.32	16.44	11.57	9.75
951083	Siltstone	6.3E+00	21.32	17.97	6	15.32
951089	Siltstone	8.5E-02	63.94	11.57	5.18	58.76
960578	Siltstone	1.7E+00	25.88	15.22	6	19.88
972860	Siltstone	1.7E-01	39.58	12.18	9.74	29.84
982247	Siltstone	6.4E-02	37.15	12.18	2.44	34.71
991037	Siltstone	2.6E-01	66.99	22.84	6	60.99
820756	Siltstone	2.9E-01	18.27	6.7	3.04	15.23
790225	Siltstone	4.5E+00	22.23	6.7	3.65	18.58
890934	Siltstone	3.6E-01	20.71	20.71	6	14.71
620130	Sandstone 2	2.5E-01	30.45	7.31	6.09	24.36
801215	Sandstone 2	5.1E-01	37.45	6.7	3.65	33.8
820770	Sandstone 2	7.0E-01	45.37	37.15	6.09	39.28
840002	Sandstone 2	1.8E+00	16.75	15.22	5.48	11.27
870905	Sandstone 2	1.6E-01	34.1	26.8	5.48	28.62
760155	Limestone	1.6E-01	28.93	19.79	1.52	27.41
781189	Limestone	4.3E+00	10.66	6.7	5.18	5.48
801210	Limestone	3.9E-01	18.27	7	3.04	15.23
801211	Limestone	1.3E+00	13.7	10.96	3.04	10.66
810904	Limestone	3.3E-02	53.29	26.8	5.48	47.81
840836	Limestone	4.3E+00	15.22	12.79	7	8.22
872131	Limestone	1.3E+00	14.62	6.39	2.44	12.18
951068	Limestone	2.1E+00	38.06	29.54	6	32.06
971410	Limestone	4.3E+00	28.93	14.31	6	22.93
1717	Sandstone 1	1.1E-01	30.45	6.09	1.22	29.23
781186	Sandstone 1	2.3E-02	30.45	14.01	6	24.45
850798	Sandstone 1	4.4E-01	21.32	17.05	5.18	16.14
882067	Sandstone 1	3.4E-01	40.8	32.89	4.57	36.23
962231	Sandstone 1	1.1E-02	67.6	12.18	2.44	65.16
13607	Sandstone 1	6.0E-03	62.12	12.18	7.92	54.2
21250	Mudstone	3.5E-01	37.15	12.18	5.18	31.97
21251	Mudstone	1.9E+00	22.23	12.18	3.65	18.58
760156	Mudstone	1.1E-02	44.76	20.1	3.96	40.8
771094	Mudstone	2.9E-01	37.45	13.4	10.35	27.1
882108	Mudstone	1.8E-01	52.37	13.4	4.26	48.11
882109	Mudstone	8.3E-02	44.76	12.18	3.96	40.8
882110	Mudstone	9.3E-01	14.31	6.09	1.22	13.09
882111	Mudstone	3.2E-01	37.15	12.79	2.44	34.71
902165	Mudstone	2.5E-01	37.15	12.18	2.44	34.71
952502	Mudstone	6.7E-01	43.85	18.27	15.83	28.02
790171	Crystalline	1.2E+00	21.92	14.92	13.7	8.22
921029	Crystalline	7.4E-02	30.45	8.22	2.44	28.01

Table A17: K statistics for shallow (0-20 m) and intermediate (20-100 m) bedrock in addition to the K for all depths. K values are based on Driscoll method (1986).

	Geometric Mean K ($m\ d^{-1}$)	Max K ($m\ d^{-1}$)	Min K ($m\ d^{-1}$)
Shallow bedrock			
Siltstone	8.7E-01	6.1E+01	2.5E-02
Sand & siltstone	1.9E+00	2.7E+01	6.0E-01
Sandstone 1	4.4E-01	4.4E-01	4.4E-01
Sandstone 2	1.8E+00	1.8E+00	1.8E+00
Mudstone	6.0E-01	1.9E+00	9.3E-01
Limestone	1.6E+00	4.3E+00	3.9E-01
Crystalline	1.2E+00	1.2E+00	1.2E+00
Intermediate bedrock			
Siltstone	1.6E-01	6.2E-01	1.4E-02
Sand & siltstone	6.5E-01	1.3E+00	3.2E-01
Sandstone 1	3.5E-02	3.4E-01	6.0E-03
Sandstone 2	3.5E-01	7.0E-01	1.6E-01
Mudstone	1.8E-01	6.7E-01	1.1E-02
Limestone	4.7E-01	4.3E+00	3.3E-02
Crystalline	7.4E-02	7.4E-02	7.4E-02
All depths			
Siltstone	4.6E-01	6.1E+01	1.4E-02
Sand & siltstone	1.2E+00	2.7E+01	3.2E-01
Sandstone 1	5.4E-02	4.4E-01	6.0E-03
Sandstone 2	4.8E-01	1.8E+00	1.6E-01
Mudstone	2.6E-01	1.9E+00	1.1E-02
Limestone	9.4E-01	4.3E+00	3.3E-02
Crystalline	3.0E-01	1.2E+00	7.4E-02

REFERENCES: APPENDIX IV

Batu, V. (1998). *Aquifer hydraulics: a comprehensive guide to hydrogeologic data analysis.* John Wiley & Sons.

Driscoll, F.G. (1986). Groundwater and wells. Johnson Division, St. Paul, Minn.

Hvorslev, M. J. (1951). *Time lag and soil permeability in ground-water observations* (No. 36). Waterways Experiment Station, Corps of Engineers, US Army.

Jacob, C. E. (1950). Flow of groundwater. In H. Rouse (Ed.), *Engineering hydraulics* (pp. 321–386). John Wiley & Sons, Hoboken, NY.

Patriarche, D., Castro, M.C. & Goovaerts, P. (2005). Estimating regional hydraulic conductivity fields—A comparative study of geostatistical methods. *Mathematical Geology, 37*, 587–613.

Younger, P. L. (1993). Simple generalized methods for estimating aquifer Storage parameters. *Quarterly Journal of Engineering Geology, 26*, 7-135.

APPENDIX V: CALIBRATION RESIDUALS

Table A18: Calibration residuals for the head observations derived from the Nova Scotia Well Log Database.

Head observation	Group	Measured [masl]	Modelled [masl]	Residual
mw1_850807	head1	17.1628	19.09647	-1.9336737
mw1_850798	head1	154.4019	151.3091	3.09284849
mw1_850806	head1	58.54699	45.15223	13.3947607
mw1_850800	head1	22.0428	19.09647	2.94632631
mw1_840002	head1	127.4684	127.3635	0.10486698
mw1_840836	head1	68.38878	60.70131	7.68747461
mw1_840870	head1	44.42598	50.96838	-6.5424038
mw1_830658	head1	15.3428	19.09647	-3.7536737
mw1_830649	head1	124.6118	121.1466	3.46516304
mw1_830648	head1	124.6118	121.1466	3.46516304
mw1_820756	head1	168.7656	161.6317	7.13393191
mw1_820775	head1	42.22928	47.21029	-4.9810128
mw1_810904	head1	1.720073	12.7342	-11.014123
mw1_801211	head1	0.8952251	4.079902	-3.1846771
mw1_801210	head1	0	4.079902	-4.0799022
mw1_790171	head1	125.03	119.5905	5.43952301
mw1_790202	head1	90.03925	81.15216	8.88708936
mw1_780862	head1	179.0468	181.6636	-2.6168047
mw1_781296	head1	134.6618	121.1466	13.515163
mw1_781188	head1	134.6618	121.1466	13.515163
mw1_781187	head1	95.85916	85.63205	10.2271104
mw1_781189	head1	21.71032	16.94881	4.76151324
mw2_120092	head2	164.4482	154.4518	9.996372
mw2_100005	head2	50.7	43.83311	6.86688538
mw2_21251	head2	52.78402	50.66867	2.11534553
mw2_21250	head2	49.73402	50.66796	-0.9339373
mw2_20581	head2	12.8628	15.71992	-2.8571211
mw2_13627	head2	52.67038	47.41356	5.25681723
mw2_981666	head2	251.1147	245.2801	5.83462493
mw2_982247	head2	127.822	123.7887	4.0333266
mw2_981669	head2	69.56318	52.02577	17.5374117
mw2_972538	head2	55.85515	55.31649	0.53865983
mw2_972860	head2	26.51084	22.79036	3.72047669
mw2_960578	head2	14.3928	15.59699	-1.2041906
mw2_962231	head2	108.9492	96.60939	12.3398097
mw2_951068	head2	40.06242	33.40113	6.66128551

Head observation	Group	Measured [masl]	Modelled [masl]	Residual
mw2_951083	head2	35.87437	39.08334	-3.2089735
mw2_951062	head2	69.03318	58.01505	11.0181348
mw2_941493	head2	49.66396	52.29972	-2.6357569
mw2_942510	head2	86.71553	76.1424	10.573135
mw2_942576	head2	28.83637	30.87994	-2.0435662
mw2_941632	head2	119.2843	124.6401	-5.3558443
mw2_931324	head2	33.44437	39.08334	-5.6389735
mw2_931776	head2	123.3948	125.2888	-1.8940489
mw2_921029	head2	114.17	89.00246	25.1675433
mw2_902307	head2	112.2291	106.1636	6.06548001
mw2_902182	head2	43.71917	33.42244	10.2967342
mw2_902165	head2	31.39	41.03358	-9.643577
mw2_882067	head2	177.69	145.7119	31.9781012
mw2_880779	head2	131.782	123.7869	7.9951424
mw2_880777	head2	111.0643	124.7997	-13.735444
mw2_880773	head2	60.9124	73.23534	-12.322944
mw2_882111	head2	16.16	41.03358	-24.873577
mw2_882110	head2	34.43	40.98755	-6.557545
mw2_882109	head2	35.04	41.10551	-6.0655107
mw2_882108	head2	32.61	41.10551	-8.4955107
mw2_872129	head2	42.96682	39.39197	3.57485223
mw2_870905	head2	114.378	101.7638	12.6142289
mw2_861538	head2	58.78638	69.01003	-10.223653
mw2_801215	head2	109.4864	113.7861	-4.2997481
mw3_80041	head3	57.59315	58.33302	-0.7398654
mw4_971410	head4	35.41045	35.53763	-0.1271782
mw8_771094	head8	76.80038	67.71717	9.08320928
mw8_760156	head8	32.37988	21.79046	10.5894232
mw8_760155	head8	43.04105	25.79854	17.2425099
mw8_740297	head8	10.11196	18.76595	-8.6539912
mw8_720110	head8	82.40318	76.86465	5.53853309
mw8_720793	head8	73.47038	73.22582	0.24455755
mw8_711510	head8	9.030836	1.808401	7.22243513
mw8_711511	head8	0	1.771492	-1.7714919
mw8_711512	head8	6.340836	1.783876	4.55696042
mw8_710346	head8	47.38652	39.93592	7.45059928
mw8_670267	head8	11.52	7.337677	4.18232347
mw8_670284	head8	21.35	11.39873	9.95127258
mw8_620130	head8	107.8308	109.7109	-1.8800841
mw9_882161	head9	68.33173	74.27236	-5.9406318
mw9_830053	head9	70.40502	67.03838	3.36663652

Head observation	Group	Measured [masl]	Modelled [masl]	Residual
mw9_790225	head9	62.18184	66.01738	-3.8355398
mw10_120450	head10	71.91917	55.04896	16.8702122
mw10_991037	head10	40.20609	45.48892	-5.2828321
mw11_141296	head11	32.98915	28.89716	4.09199233
mw11_131172	head11	14.28919	12.00093	2.28826398
mw11_121284	head11	70.48402	65.80176	4.68226219
mw11_121294	head11	21.36514	25.33521	-3.9700727
mw11_952502	head11	28.51547	24.06075	4.45472095
mw11_890934	head11	20.53137	20.60969	-0.0783178
mw11_781295	head11	84.44759	88.67354	-4.2259482
mw11_91578	head11	67.08514	53.73146	13.3536794

APPENDIX VI: RAPID ADVECTION RISK MAP

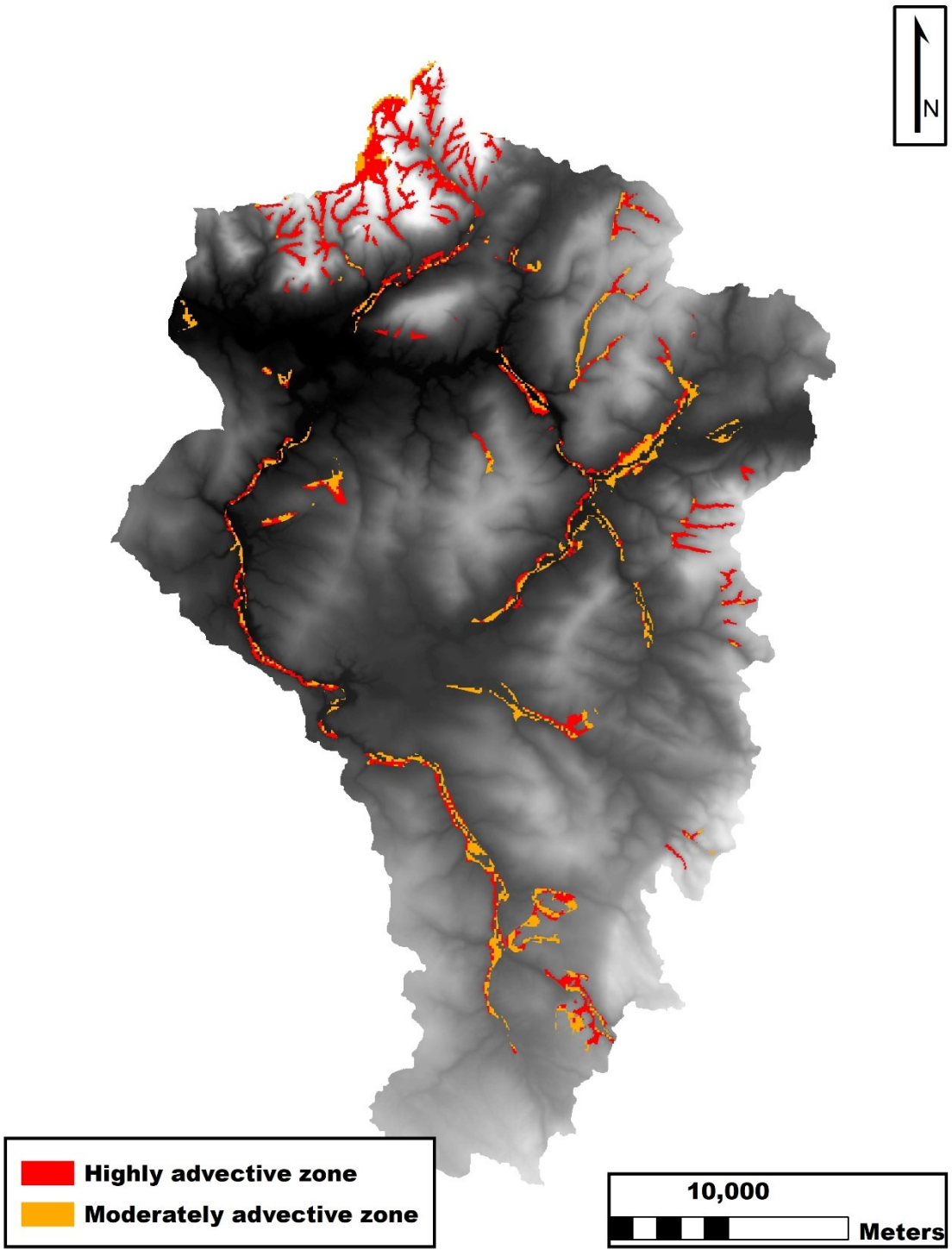

Figure A7: Risk map for zones supporting rapid advection to surface water bodies in the Mabou Harbour drainage basin.